

THE UNIVERSITY OF HULL

**Development Towards a Point-of-Care System
To Monitor Pregnancy and Fertility Biomarkers**

being a Thesis submitted for the Degree of

Doctor of Philosophy

in the University of Hull

by

Kevin John Wright

MChem

August 2015

Abstract

The aim of this thesis was to develop a point of care (POC) device that could monitor progesterone and oestriol in saliva. These hormones have a key role to play in both female fertility and pregnancy. Understanding the concentration of progesterone in the body is key to understanding a patient's fertility and pregnancy status. Combining progesterone and oestriol detection can give valuable insight into when labour may commence during pregnancy. This can be achieved by measuring the progesterone to oestriol ratio in saliva samples, throughout the pregnancy progesterone is the more dominant hormone but a few weeks before labour oestriol becomes the more dominant hormone. Saliva was chosen as the biological sample due to the ease of collection as well as it providing a better chemical understanding of the active hormonal concentrations compared to blood. Typical levels in saliva are $<31 \text{ pg mL}^{-1}$ rising to $>100 \text{ ng mL}^{-1}$ for progesterone and $0 - 5 \text{ ng mL}^{-1}$ for oestriol.

The work presented began with the design of a chemiluminescence immunoassay which could be translated onto a microfluidic device, this approach would provide both good sensitivity and selectivity. Chemiluminescence was chosen as a detection system due to the high sensitivities that can be achieved with simple instrumentation where a CCD camera could be used to also obtain spatial information. The CL assay involved the chemical immobilisation of the antibodies onto glass slides. Silanisation with (3-aminopropyl)triethoxysilane (APTES) in combination with a N-(3-dimethylaminopropyl)-N'-ethylcarbodiimide/N-hydroxysulfosuccinimide (EDC/sulfo-NHS) linker proved the most successful immobilisation method, with a LOD of $33 \pm 3 \text{ pg mL}^{-1}$ being achieved for progesterone in 10 mM phosphate buffered saline (PBS). This method however lacked reproducibility and did not transfer well on to polymer substrates or the microfluidic devices due to problems with the antibody immobilisation procedure.

Immobilisation of anti-progesterone was then investigated on a range of electrode surfaces (Au, glassy carbon and ITO). This immobilisation procedure involved electrochemically depositing nitrobenzene onto the electrode surface followed by an electrochemical reduction of the nitro groups to the corresponding amine. To allow electrochemical detection ferrocene was tagged to the anti-progesterone antibodies to give a redox tag. The antibodies were then immobilised through an EDC/sulfo-NHS linkage. This method proved to be successful and very reproducible. By tagging ferrocene onto the antibody a rigid structure was achieved during the immobilisation procedure allowing the ideal antibody orientation, this process also allowed quantification of the concentration of antibodies on the surface ($4.46 \times 10^{-7} \text{ mol m}^{-2}$). Electrochemical based immunoassays were successfully carried with a 15 min incubation time for progesterone giving LODs of 1 pg mL^{-1} for the gold and glassy carbon and 0.1 pg mL^{-1} for the ITO. The ITO performed better than the other materials due to the electrode being uniformly flat enabling more efficient surface modifications. The methodology was also translated for use with artificial saliva with a LOD of 1.7 pg mL^{-1} for progesterone.

Once the electrochemical immobilisation platform had been shown to be successful this was taken forward as a potential route to carry out a CL immunoassay. This novel approach utilised the oxidised ferrocene tag on the antibody as the catalyst for the luminol CL reaction. A static system was devised in which the antibodies had been immobilised on to ITO using the electrochemical approach and the CL reagents added by pipette, LODs of 2.35 and 2.54 pg mL^{-1} were obtained for progesterone and oestriol respectively in saliva after a 30 min incubation time. The static system could therefore be used as a POC device for these hormones meeting the aims of this thesis. The next step was then to start developing a more automated method within a flow cell. Initially the ITO electrode with the pre-prepared immobilised antibody and the oxidised ferrocene tag was incorporated into a microfluidic device. The CL immunoassay was successfully carried

out in the macrofluidic device although the LODs were an order of magnitude higher than those seen from the static system for both progesterone and oestriol in saliva due to the large volume of the flow cell. Finally the ITO electrode with pre-prepared immobilised antibody with the oxidised ferrocene tag was slotted into the microfluidic device that had been designed and measurement were made. There was however problems with the design and possible new designs are discussed.

Acknowledgments

I would like to thank my supervisors Professor Gillian Greenway and Dr. Jay Wadhawan for the opportunity to study the PhD and for all their help and guidance throughout, for all their kind words when experiments were not going well and maintaining their belief in me and for being there whenever I needed them. I would also like to thank them for the opportunities to attend various conferences throughout the last 4 years.

I would like to thank Professor Stephen Haswell, Dr. Giuseppe Benazzi, Dr. Nathan Brown, Dr. Gary Kipling, Dr. Mohammed Nasr Esfahani and Dr. Steve Clark for all their help and assistance with the microfluidic fabrication and experimentation, their help has been extremely appreciated.

I would also like to thank Dr. Thomas Varley, Dr. Yan Zhou, Dr. Amal Altalhi and Lee Partington for all their help and collaboration with the electrochemical investigations.

A great big thank you goes to the University of Hull for the funding for the project and for giving me the opportunity to carry out this research as well as the opportunity to be a teaching assistant for the last 4 years which has been a fantastic experience.

I would like to thank all of my friends for all their support, not only this year but throughout my educational career especially Dr. Kreshnik Hoxha who helped me a lot during all the difficult times, the rest of the analytical group for all their assistance and for making the work days even more enjoyable.

And finally I would like to dedicate this thesis to my family for all of their support throughout my educational career and for supporting all of my decisions and helping me when things have been difficult I would not have got this far without them.

Contents

ABSTRACT	I
ACKNOWLEDGMENTS	IV
LIST OF FIGURES AND TABLES	IX
ABBREVIATIONS	XIV
CHAPTER 1 INTRODUCTION	1
1.1 INTRODUCTION	1
1.2 BIOMARKERS INVOLVED IN FERTILITY AND PREGNANCY	1
1.2.1 <i>Female menstrual cycle</i>	2
1.2.2 <i>Hormones involved in pregnancy</i>	5
1.2.3 <i>Progesterone and oestriol</i>	7
1.2.4 <i>Current methods to monitor progesterone and oestriol</i>	9
1.3 DETECTING AND MONITORING PROGESTERONE AND OESTRIOL	9
1.3.1 <i>Progesterone and oestriol in saliva</i>	10
1.4 ANTIBODIES AND IMMUNOASSAYS	10
1.4.1 <i>Antibodies</i>	11
1.4.2 <i>Immunoassays</i>	12
1.4.3 <i>Antibodies used to carry out immunoassays</i>	20
1.5 ANTIBODY IMMOBILISATION METHODS.....	21
1.5.1 <i>Glass substrates for heterogeneous immunoassays</i>	22
1.5.2 <i>Plastic substrates for heterogeneous immunoassays</i>	31
1.5.3 <i>Other Substrates for heterogeneous immunoassays</i>	36
1.6 POINT-OF-CARE TESTING	39
1.6.1 <i>Lab-on-a-chip for POC</i>	40
1.6.2 <i>Microfluidics</i>	40
1.7 FABRICATING LOC SYSTEMS	41
1.7.1 <i>Substrates</i>	41
1.7.2 <i>LOC Fabrication</i>	42

1.7.3 <i>Microflow</i>	45
1.7.4 <i>Mixing of reagents</i>	46
1.7.5 <i>Detection methods on microfluidic chips</i>	49
1.8 CHEMILUMINESCENCE	52
1.8.1 <i>Molecules involved in chemiluminescence reactions</i>	63
1.8.2 <i>Chemiluminescence in microfluidic immunoassays</i>	69
1.8.3 <i>Chemiluminescence detection</i>	70
1.9 ELECTROCHEMISTRY	73
1.9.1 <i>Movement of ions towards the electrode</i>	73
1.9.2 <i>Electrochemical methods</i>	77
1.10 CONCLUSIONS.....	81
1.11 AIMS AND OBJECTIVES.....	82
CHAPTER 2 EXPERIMENTAL	83
2.1 REAGENTS.....	83
2.2 MATERIALS.....	84
2.3 INSTRUMENTATION	85
2.4 DESIGN OF THE MICROFLUIDIC DEVICE.....	86
2.5 INCLUSION OF ELECTRODES IN FLOW DEVICES	89
2.6 EXPERIMENTAL SETUP	91
2.7 CONCLUSIONS.....	92
CHAPTER 3 CHEMICAL PROCESS FOR ANTIBODY IMMOBILISATION	93
3.1 INTRODUCTION	93
3.2 EXPERIMENTAL PROCEDURES	94
3.2.1 <i>Evaluation of the CL detection method</i>	94
3.2.2 <i>Chemical immobilisation on glass slides</i>	94
3.2.3 <i>CL immunoassay using a plastic substrate</i>	98
3.3 RESULTS AND DISCUSSION.....	100
3.3.1 <i>Evaluation of the CL detection method</i>	100
3.3.2 <i>Optimising HRP as a chemiluminescence catalyst</i>	104

3.3.3 Chemiluminescence immunoassay on glass slides.....	106
3.3.4 CL immunoassay on a microfluidic device.....	117
3.3.5 CL Immunoassay on plastic substrates	121
3.4 CONCLUSION TO THE CHEMICAL IMMOBILISATION INVESTIGATION	125
CHAPTER 4 ELECTROCHEMICAL PROCESS FOR ANTIBODY IMMOBILISATION	126
4.1 INTRODUCTION	126
4.2 EXPERIMENTAL PROCEDURES	128
4.2.1 Synthesis of ferrocene tagged antibodies.....	128
4.2.2 Electrode modification	129
4.2.3 Antibody immobilisation and electrochemical immunoassay	132
4.2.4 Electrochemical immunoassay in artificial saliva	133
4.3 RESULTS AND DISCUSSIONS	134
4.3.1 Anti-progesterone labelling with ferrocene.....	134
4.3.2 Comparison of electrode materials for the electrochemical immunoassay.....	138
4.3.3 Optimising the ITO electrode for progesterone analysis in saliva.....	166
4.3.4 Electrochemical immunoassay of progesterone in artificial saliva.....	171
4.4 CONCLUSION TO THE ELECTROCHEMICAL IMMUNOASSAY INVESTIGATION	174
CHAPTER 5 DEVELOPMENT OF A CHEMILUMINESCENCE IMMUNOASSAY FOR PROGESTERONE AND OESTRIOL WITH AN ELECTROCHEMICAL IMMOBILISATION PROTOCOL.....	177
5.1 INTRODUCTION	177
5.2 EXPERIMENTAL PROCEDURES	179
5.2.1 Immobilisation of ferrocene tagged anti-progesterone onto an ITO electrode.....	179
5.2.2 Procedure for carrying out the CL immunoassay.....	180
5.2.3 CL immunoassay within a flow cell	181
5.2.4 CL immunoassay in the microfluidic device	182
5.3 RESULTS AND DISCUSSION.....	182
5.3.1 CL immunoassay for progesterone on the ITO electrode.....	185
5.3.2 CL immunoassay of progesterone and oestriol on the ITO electrode	189
5.3.3 Progesterone and oestriol immunoassay using the macroflow device.....	196

5.3.4 <i>Integrated microfluidic device</i>	201
5.4 CONCLUSION TO CL INVESTIGATION ON AN ELECTROCHEMICAL IMMOBILISATION PLATFORM	203
CHAPTER 6 CONCLUSIONS & FUTURE WORK.....	205
CHAPTER 7 REFERENCES.....	214
PRESENTATIONS.....	221

List of Figures and Tables

Figure Number	Page Number
1.1: Concentration profiles of four fertility biomarkers.	2
1.2: Structure of progesterone.	7
1.3: Structure of oestriol.	8
1.4: General antibody structure.	11
1.5: Schematic showing a homogeneous immunoassay.	13
1.6: Example of a heterogeneous competitive immunoassay.	15
1.7: Example of heterogeneous non-competitive immunoassay.	15
1.8: Schematic showing how an ELISA is carried out.	16
1.9: Schematic showing how APTES silanises a surface.	24
1.10: How glutaraldehyde is used as a crosslinker.	25
1.11: Mechanism of antibody attachment using EDC/sulfo-NHS.	26
1.12: Diagram showing the various antibody orientation possibilities.	29
1.13: Structure of PMMA	34
1.14: Schematic of the wet etching process in glass.	43
1.15: Flow profiles for parabolic and EOF.	45
1.16: Diagram showing how EOF operates.	46
1.17: Diagram showing the differences between laminar and turbulent flow.	47
1.18: Jablonski Diagram	52
1.19: Inner and outer sphere mechanism.	54
1.20: Energy profile showing transition state theory	54
1.21: How the change in reaction coordinate alters the required activation energy.	56
1.22: Non-adiabatic and adiabatic electron transfer diagrams.	57
1.23: Profile relating rate constant to the Gibbs free energy.	58
1.24: Parabolic profiles of various electron transfer pathways.	60
1.25: Electron transfer energy profile for a CL reaction.	62
1.26: Structure of lucigenin	63
1.27: Structure of 4-(2-succinimidylloxycarbonyl)phenyl-10-methylacridinium-9-carboxylate fluorosulfonate	64

1.28: Structure of luminol and isoluminol	65
1.29: Textbook mechanism for the luminol and peroxide reaction	66
1.30: Alternative intermediate for the luminol & peroxide reaction	67
1.31: Proposed mechanism with cobalt catalysis	68
1.32: Diagram of a photomultiplier tube	70
1.33: Operation of a charge coupled device.	72
1.34: Schematic representing the electrical double layer.	74
1.35: Example of an electrochemical immunoassay on a microfluidic device.	77
1.36: Cyclic voltammetric waveform.	79
1.37: Example of a cyclic voltammogram.	79
1.38: Square wave waveform.	80
2.1: Design of the glass microfluidic device.	88
2.2: Design of the polymer microfluidic device.	89
2.3: Photograph of the integrated macroflow device.	90
2.4: Design of the integrated microfluidic device.	90
2.5: Schematic of the microfluidic setup.	91
2.6: Schematic of an electrochemical experimental setup.	92
3.1: Holder for 1 x 1 cm squared chips.	96
3.2: Photograph of the microfluidic device.	97
3.3: Optimum camera exposure time.	101
3.4: How the CL signal is affected by luminol concentrations.	102
3.5: How the CL signal is affected by H ₂ O ₂ concentrations.	103
3.6: Optimisation of the luminol concentration when HRP is used.	104
3.7: Optimisation of the H ₂ O ₂ concentration when HRP is used.	105
3.8: Contact angle of a liquid droplet on a solid surface.	107
3.9: Contact angle studies on APTES functionalised glass.	107
3.10: Contact angle studies on GPTS functionalised glass.	108
3.11: Mechanism showing how glutaraldehyde can react with itself.	110
3.12: Fluorescence image of antibody immobilised onto APTES functionalised glass.	110
3.13: Fluorescence image of antibody immobilised on GPTS functionalised glass.	111

3.14: CL image of anti-progesterone bound with progesterone-HRP on APTES.	112
3.15: Calibration curve of progesterone.	113
3.16: Calibration curve of progesterone using a log scale.	113
3.17: Calibration curve showing the change in signal.	114
3.18: CL image of anti-progesterone bound with progesterone-HRP on GPTS.	115
3.19: Progesterone calibration curves using an ELISA based system.	116
3.20: UV-Vis spectrum of the microfluidic device.	118
3.21: CL image within the serpentine of the microfluidic device.	118
3.22: Microscope images showing the flow of dye and water.	119
3.23: Flow profile across reaction chamber to show efficient mixing.	120
3.24: CL image within the microfluidic device.	121
3.25: UV-Vis spectrum of PMMA.	122
3.26: Contact angle on PMMA modified with LiAlH_4 .	123
3.27: Contact angle on PMMA modified with NaOH.	123
3.28: CL image of progesterone-HRP on PMMA.	124
4.1: Schematic showing the molecular wire concept.	126
4.2: Resonance of the amide bond.	127
4.3: Schematic showing the ferrocene tagging to the antibody.	129
4.4: Diagram of the experimental setup of the ITO electrode.	130
4.5: Schematic of the electrode immobilisation process.	131
4.6: UV-Vis spectrums of ferrocene tagged anti-progesterone.	135
4.7: Calibration plots of ferrocene tagged anti-progesterone.	136
4.8: CV of nitrobenzene deposition onto Au.	138
4.9: Schematic showing the nitrobenzene deposition mechanism.	139
4.10: Alternate pathway for nitrobenzene deposition.	140
4.11: Nitrobenzene deposition on GC.	141
4.12: Nitrobenzene deposition on ITO.	142
4.13: CV of the nitro to amine reduction on Au.	143
4.14: Mechanism of the nitro to amine reduction.	144
4.15: Nitro to amine reduction on GC.	145
4.16: Nitro to amine reduction on ITO.	146

4.17: CVs of ferrocene tagged anti-progesterone at various scan rates on Au.	147
4.18: Plot of the peak current against the scan rate on gold.	148
4.19: Plot of $\frac{i_p}{\sqrt{v}}$ vs \sqrt{v} on gold.	149
4.20: CVs of ferrocene tagged anti-progesterone at various scan rates on GC.	150
4.21: Plot of peak current against scan rate on GC.	151
4.22: CVs of ferrocence tagged anti-progesterone at various scan rates.	152
4.23: Plot of peak current against scan rate.	153
4.24: Plot of $\frac{i_p}{\sqrt{v}}$ vs \sqrt{v} on ITO.	153
4.25: CVs after incubation with various concentrations of progesterone on Au	155
4.26: SWVs after incubation with various progesterone concentrations on Au.	156
4.27: Calibration plots of progesterone on Au.	158
4.28: CVs after incubation with various progesterone concentrations on GC.	159
4.29: SWVs after incubation with various concentrations of progesterone on GC.	160
4.30: Calibration plots of progesterone on GC.	161
4.31: CVs after incubation with various progesterone concentrations on ITO.	162
4.32: SWVs after incubation with various concentrations of progesterone on ITO	163
4.33: Calibration plots of progesterone on ITO.	164
4.34: CVs and SWVs after incubation at various incubation times.	166
4.35: Graphs showing the effect of incubation time on the peak currents and potentials from the CVs.	167
4.36: Graphs showing the effect of incubation time on the peak currents and potentials from the SWVs.	168
4.37: CV and SWVs after incubation with various concentrations of progesterone in artificial saliva.	172
4.38: Calibration plots of progesterone in artificial saliva.	173
4.39: Future electrode design.	174

5.1: Schematical concept of the CL immunoassay.	178
5.2: CV showing the oxidation of ferrocene.	183
5.3: Reaction scheme showing the ferrocene oxidation.	183
5.4: CL images showing the stability of the ferrocene catalysis.	184
5.5: Mechanism of the catalytic effect of ferrocene.	185
5.6: CL images before and after incubation with progesterone.	185
5.7: Optimisation of the luminol concentration.	187
5.8: Optimisation of the hydrogen peroxide concentration.	187
5.9: Graph to show the optimum camera exposure time.	188
5.10: Calibration plots of progesterone.	190
5.11: Calibration plots of oestriol.	192
5.12: Chart showing effects of interferences.	195
5.13: CL image within the macroflow device.	196
5.14: Graphs showing the optimum flow rates.	198
5.15: Calibration plots of progesterone within the macroflow device.	199
5.16: Calibration plots of oestriol within the macroflow device.	200
5.17: CL images within the microfluidic device.	202
6.1: Future design of an integrated microfluidic device.	213

Table Number	Page Number
1.1: ELISA protocol.	21
1.2: Diffusion times for small molecules.	48
4.1: Comparison of electrode materials.	165
4.2: Resistivity measurements across 4 ITO electrodes.	169
5.1: Possible interfering molecules	194

Abbreviations

Ab	Antibody
APTES	3-Aminopropyltriethoxysilane
CL	Chemiluminescence
CV	Cyclic voltammogram
EDC	N-(3-dimethylaminopropyl)-N'-ethylcarbodiimide
ELISA	Enzyme-Linked Immunosorbent Assay
GC	Glassy Carbon
GPTS	(3-glycidoxypropyl)trimethoxysilane
HRP	Horseradish Peroxidase
ITO	Tin-doped Indium Oxide
LOC	Lab-on-a-Chip
LOD	Limit of Detection
PBS	Phosphate Buffered Saline
PMMA	Poly(methylmethacrylate)
POC	Point-of-Care
Sulfo-NHS	N-Hydroxysulfosuccinimide
SWV	Square wave Voltammogram

Chapter 1 Introduction

1.1 Introduction

With an ever-growing rise in population, resulting in a greater strain on health services the development of point-of-care (POC) systems where patients can take greater control of their own health and well-being is required. This work aims to develop a system that can monitor progesterone and oestriol levels in saliva samples, as a route to investigate fertility issues as well as premature and/or spontaneous births. Current systems operate *via* simple lateral flow test strips which are not quantitative or complex methods in the laboratory that are time and reagent consuming. Point-of-care systems could deliver more information in comparison to the strips currently in use, while removing the complexity of current laboratory based systems.

1.2 Biomarkers Involved in Fertility and Pregnancy

A biomarker can be defined as a biological molecule that can be identified by the role that it plays in a biochemical process.

There are a number of different biomarkers that are involved in fertility and pregnancy, each of these have a key role in identifying a patient's fertility health status; this therefore identifies the probability of successful conception; followed by a successful pregnancy. Biomarkers that are involved during various stages of pregnancy can also give information on the health of the baby and mother as well as how the body is responding throughout the pregnancy.

What type of biomarkers are of interest?

Biomarkers come in a variety of different forms, these can be proteins, cells, hormones and others. Within this work hormones are of interest. Hormones are chemical messengers that trigger a certain response, these come in the form of amino acids, proteins and steroids.¹ It is these biomarkers that trigger a response during the menstrual cycle and throughout pregnancy; therefore it is necessary to look at each hormone involved and the individual role it plays.

1.2.1 Female menstrual cycle

The female menstrual cycle is on average a 28 day cycle where the uterus prepares to accept a fertilised egg, day 21 of the cycle is the point at which the highest probability of conception occurs. The cycle can be split into two stages; the follicular phase (days 1 – 14) and the luteal phase (days 15-28). Figure 1.1 shows a schematic of the entirety of the cycle and the key biomarkers involved at each stage.

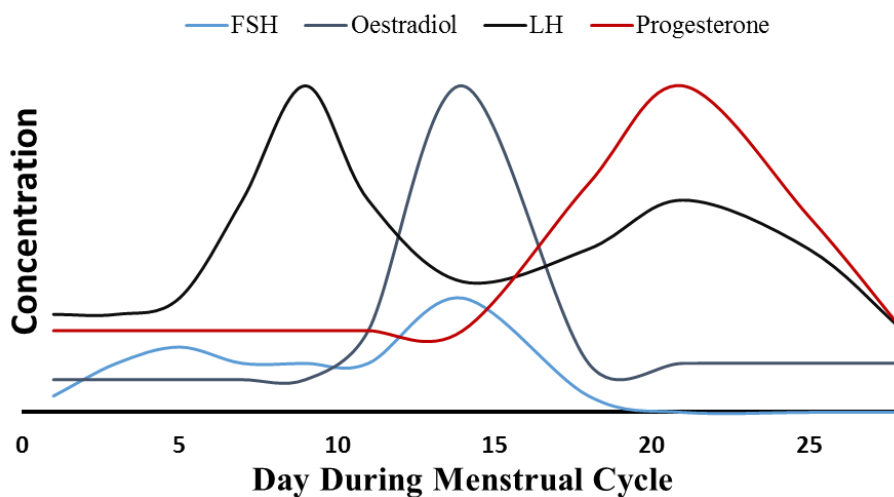


Figure 1.1: Schematic showing four of the key biomarkers involved during the menstrual cycle and their relative concentrations at each stage of the process, with days 1-14 representing the follicular phase, day 14 being the day of ovulation and days 15-28 showing the luteal phase.

From Figure 1.1 it is clear that at different stages of the cycle different biomarkers are dominant, each having a specific role to play. Understanding their concentrations can give clinicians important information on fertility and the probability that a mother can or cannot conceive. Each of these biomarkers are discussed in detail.

Follicle-stimulating hormone (FSH)

Follicle-stimulating hormone (FSH) is a protein that is secreted by the gonadotrophic cells found within the pituitary glands,² these glands are found within the brain. FSH stimulates the growth of ovarian follicles; causing the production of oestradiol which results in the maturation of an egg.³ These processes occur at the start of the cycle (days 1-7); after which the FSH levels subside until days 13-14 when FSH facilitates the release of the egg (ovulation).⁴

Oestradiol

Oestradiol (E2) is the most prominent of the oestrogen hormones found in women and has a very important role in female reproduction. It is mainly synthesised within the ovarian follicles themselves however synthesis can occur in other regions of the body.⁵ Oestradiol production causes the egg to grow and mature; towards the end of the follicular phase oestradiol sends signals to the pituitary gland to begin the production of luteinizing hormone (LH). Observing figure 1.1 oestradiol concentration is at its peak around days 8-10 this is to coincide with the egg creation, it can also be seen that the oestradiol concentration rises again around days 20-23 this is due to it having a shared role with progesterone in thickening the uterus lining to accept a fertilised egg.⁶

Luteinizing hormone (LH)

LH, like FSH, is produced from the gonadotrophic cells situated within the pituitary glands; it is this hormone that causes ovulation to occur by triggering the eggs release.⁷ LH concentrations peak on day 14 of the cycle and this is known as the ovulation period and point of highest probability of conception. Due to the specific role LH plays as well as its narrow time frame it is an ideal biomarker to be used to indicate ovulation and minimising error as to when/if it has occurred; for this reason current commercial tests measure this hormone as an ovulation indicator.

Progesterone

Progesterone has arguably the most significant role in the whole of the menstrual cycle, as this hormone only becomes dominant during the luteal phase (after ovulation) when it acts along with oestradiol to regulate the endometrium (inner-lining) of the uterus wall to accept a fertilised egg.⁸ Progesterone synthesis occurs as a consequence of egg release.³ Progesterone therefore is the hormone of choice to monitor for fertility; successful ovulation i.e. a high LH concentration does not necessarily mean successful conception. This can only be investigated through monitoring progesterone to determine the levels are where they should be, this would need to be carried out consistently over a number of days. Through knowing the progesterone concentration clinicians can get a great insight into the probability of conception being successful. Progesterone itself will be discussed in more detail in section 1.2.3.

1.2.2 Hormones involved in pregnancy

Just like in the menstrual cycle whereby there are numerous different hormones that have certain roles to play, the same applies to pregnancy where many different hormones are involved; an understanding of which is important. Here some of the key hormones involved are discussed.

Human chorionic gonadotropin

Human chorionic gonadotropin (hCG) is a protein that is released from the placenta after successful implantation of a fertilised egg. hCG levels are very high during the first trimester peaking at around weeks 10-11 before subsiding during the rest of the pregnancy.⁹ Due to the production of this hormone occurring at the early stages of pregnancy, current pregnancy tests operate by detecting this hormone in urine, with corresponding concentration levels giving an indication as to the time frame since conception.

hCG is involved in several processes during the first trimester, these include encouraging the continuing production of progesterone from the ovaries to maintain the lining of the uterus wall, helping to maintain a strong implantation of the foetus as well as an immunological role to protect both the mother and foetus.^{9, 10}

Progesterone

As stated in the previous section hCG causes the ovaries to maintain the production of progesterone during the first trimester, however once this period ceases progesterone synthesis occurs within the placenta itself; where this continues for the entirety of the pregnancy and this is known as the luteal-placental shift.¹¹ Its primary role is in maintaining the placental wall and keeping the foetus implanted, the concentration of progesterone remains high throughout the pregnancy. Progesterone in this context will also be investigated, understanding progesterone levels pre-pregnancy can give information about the likelihood of a successful conception and therefore successful pregnancy; carrying this through into the pregnancy can then give vital information about the state of the pregnancy with any issues being discovered at the earliest possible opportunity.

Oestriol

Oestriol (E3) is another of the three major oestrogen hormones, its role is largely illusive and therefore not readily studied.¹² However during pregnancy oestriol becomes an important biomarker mainly because it is synthesised by the foetus itself as well as the placenta.¹³ Knowing oestriol concentrations can give clinicians valuable information on the health and progression of the pregnancy. Understanding a mother's oestriol and progesterone levels gives an indication of when labour may occur which is explained fully in section 1.2.3.

1.2.3 Progesterone and oestriol

Having looked at the major biomarkers involved with fertility and pregnancy progesterone and oestriol were selected for monitoring. The relative concentrations of these hormones in the female can give valuable information to clinicians and expectant parents about their fertility and pregnancy status; including risks by predicting the onset of labour. Within the literature there is a consensus that knowing the progesterone/oestriol ratio can act as a tool to predicting premature births.¹⁴⁻¹⁶

Progesterone

Progesterone is a steroidal hormone that is synthesised from cholesterol within the corpus luteum. Figure 1.2 shows the structure of progesterone:

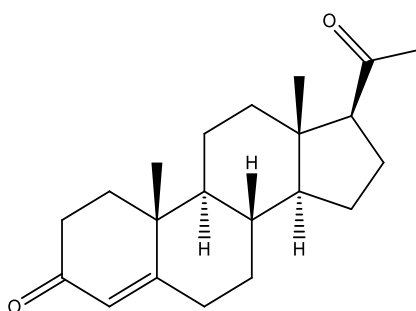


Figure 1.2: Structure of progesterone with a molecular weight of 314.46 g mol⁻¹.

The corpus luteum is a temporary structure found within the ovaries that is formed afresh during each menstrual cycle by the follicles that produce the egg. Should the egg not become fertilized the corpus luteum will stop progesterone synthesis resulting in the uterus wall breaking down during menstruation.³ Should the egg become fertilised hCG production from placenta triggers the corpus luteum to maintain progesterone production for the first trimester after which progesterone is synthesised by the placenta itself.³

As discussed in sections 1.2.1 and 1.2.2 progesterone has an important role in the menstrual cycle and pregnancy.¹⁷

Oestriol

Oestriol like progesterone is a steroidal hormone. This hormone however has very little activity during an average woman's lifetime, until she becomes pregnant; this hormone will then appear and have a substantial impact on the pregnancy as a whole and is regarded as a blueprint to show the health of both the mother and foetus. Figure 1.3 shows the structure of oestriol:

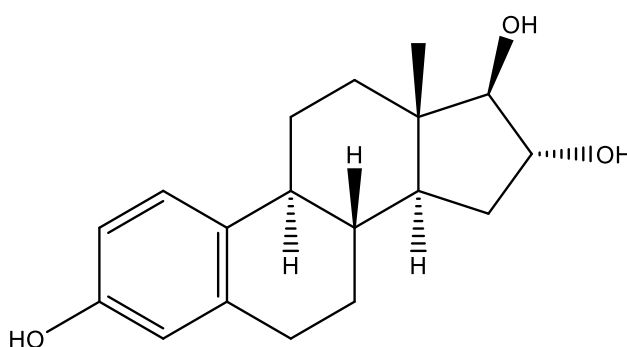


Figure 1.3: Structure of oestriol with a molecular weight of 288.39 g mol⁻¹.

Oestriol is synthesised in large amounts during pregnancy from 16-hydroxydehydroepiandrosterone sulfate. (16-OH DHEAS) this steroidal hormone originates from within the adrenal glands of the foetus itself; where within the placenta is converted into oestriol.¹⁸ Oestriol concentrations vary during pregnancy and knowing these concentrations can give warnings into potential problems such as Down's syndrome this is routinely measured through the triple test.¹⁹ Oestriol levels can also give valuable information as to when labour may commence due to a large increase in oestriol production around 3-5 weeks prior to labour and this is true for both preterm and term delivery.^{12, 20} It is viewed labour occurs as a consequence of oestriol becoming the more dominant hormone, with respect to its ratio to progesterone.^{12, 21}

1.2.4 Current methods to monitor progesterone and oestriol

Currently progesterone and oestriol are monitored through an ELISA blood test (discussed in section 1.4.2.3), the National Health Service will typically look at measuring progesterone to understand the fertility status of a patient, they warn however that this process can take a long time and that further tests may be required which can be stressful.²² Progesterone tests tend to be only carried out if the patient has a history of premature labour and/or miscarriage; a GP may then opt for a progesterone test and some form of treatment.²³ As mentioned oestriol is currently tested as an indicator for Down's syndrome however this requires a blood test and for reasons outlined later is not ideal and in this context the results have no bearing with respect to labour.^{12, 24}

So while there are current methods for testing for these hormones, the availability is rather limited and non-universal, therefore a system needs developing that can monitor these hormones through a route that is universally accessible.

1.3 Detecting and Monitoring Progesterone and Oestriol

Progesterone and oestriol can be found in all of the main bodily fluids that are used when conducting point of care analysis; saliva,¹⁵ blood²⁵ and urine.²⁶ Koka *et al.* investigated which of these fluids patients would prefer to donate for diagnostic purposes. 413 patients were surveyed and voted overwhelmingly that saliva would be preferential when it came to donating samples for analysis which is unsurprising.²⁷

1.3.1 Progesterone and oestriol in saliva

Saliva is a biological fluid that is secreted by the salivary glands found in the mouth, the fluid is 99.5% water, with the other 0.5% containing electrolytes, hormones, enzymes and other biological molecules.²⁸

In saliva progesterone and oestriol are found in a biologically active form, whereas in blood these hormones are found in the free biologically active form as well as the protein bound form which is chemically inactive.²⁹ Because of this serum analysis is not 100% reliable in understanding the patient's progesterone or oestriol status.

Unfortunately from a detection point of view, because there is only the free hormone in saliva the concentrations can therefore be 50-100 times lower than that found in blood;³⁰ with this in mind a sensitive methodology is required to measure these hormones quantitatively.

In saliva the typical range found for progesterone is $<31.4 \text{ pg mL}^{-1}$ during the follicular phase, rising to $>720 \text{ pg mL}^{-1}$ on day 21 of the cycle,⁸ during pregnancy these levels rise to greater than 100 ng mL^{-1} .^{15, 31} Oestriol has a concentration range of between 0 and 5 ng mL^{-1} during pregnancy.^{32, 33} Saliva typically has a pH of between 6.5 and 7.5 indicating saliva is slightly acidic in relation to the rest of the body.³⁴

1.4 Antibodies and Immunoassays

To detect and monitor progesterone and oestriol successfully in a sample at the low concentrations found a very specific technique is required. Immunoassays are ideal for this aim, this technique exploits the antibody-antigen interaction.

1.4.1 Antibodies

Antibodies are specific proteins generated in the body to combat pathogenic invaders known as antigens. Like all proteins, antibodies consist of amine and carboxylic acid groups and are often referred to as immunoglobulins (Ig) which can be split into different classes; all of which have different roles and fight different pathogens. The two main classes are the IgG and IgM, with the other three classes being referred to as IgA, IgD and IgE.³⁵ Within this work only IgG antibodies are of interest due to their uses in immunoassays and therefore only this class of antibody will be discussed.

IgG antibodies are found in all bodily fluids and are the most abundant of all the immunoglobulins, they are also the only antibody type that can cross the placenta from a mother to foetus. These antibodies are also the heaviest with their weights being ~150 kDa. Antibodies have a Y shaped structure where there are two heavy chains and two light chains (see Figure 1.4 for the general structure) where the heavy chain are made up of ~450 polypeptide residues and the light chains with ~215 polypeptide residues, with a disulphide bond linking the chains together.³⁶

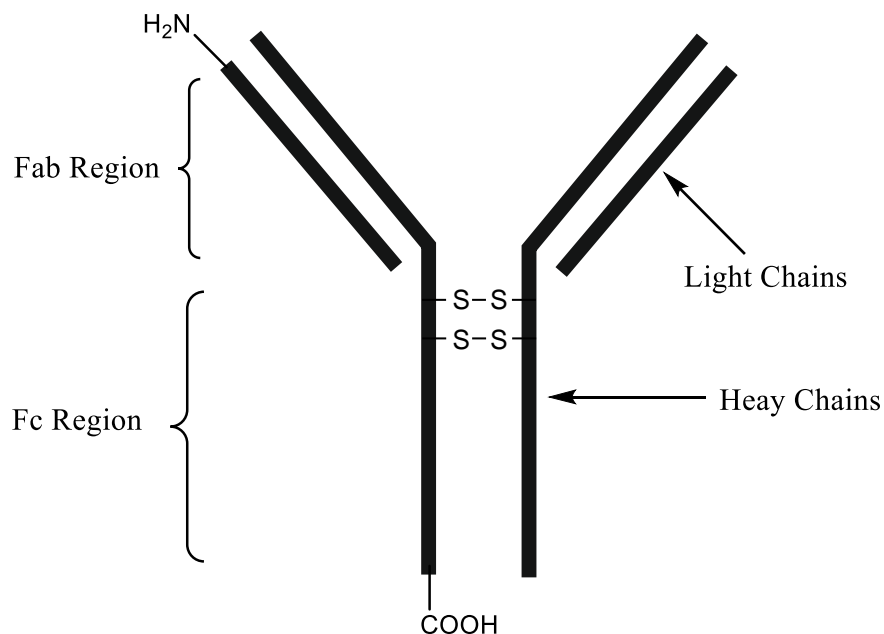


Figure 1.4: General structure of an IgG antibody.

The fragment antigen binding (Fab) region is the area at the top of the antibody where there are both the heavy and light chains, it is within this region that the paratope is located which is the area where the antigen becomes bound to the antibody. The paratope is described as the part of the antibody that recognises the epitope of the target antigen, like a lock and key. The fragment crystallisable (Fc) region is involved in making sure that the antibody generates an appropriate immune response by binding to certain Fc receptors.³⁷ Based on a protein chain that contains amino acids, within the Fc area acid groups are situated with the amine groups being found within the Fab region, however as the antibodies have various side chains these groups are situated all over the protein this is a general and simplistic description.³⁸

1.4.2 Immunoassays

Immunoassays can work for quantitative analysis or qualitative analysis, for this reason this technique has proved invaluable and is often used when researching into antibodies and their interaction with antigens. Immunoassays are generally studied with chemical labels either on the antibody or on the antigen which subsequently gives rise to a measurable signal once binding occurs (See section 1.4.2.4) but can be tag free in detection methods such as surface plasmon resonance.³⁹ Immunoassays can be split into two main classes and these are homogeneous and heterogeneous immunoassays.

1.4.2.1 Homogeneous immunoassays

Homogeneous immunoassays are those that occur in solution, where either the antigen or the antibody itself contains a label for analysis (see section 1.4.2.4). The main advantage with this form of immunoassay is the need to separate the free antigen from the antibody-antigen bound complex is unnecessary.⁴⁰

Akhavan-Tafti *et al.* successfully developed a chemiluminescence (see section 1.4.2.4) homogeneous immunoassay through a sandwich immunoassay, one antibody contained a horseradish peroxidase (HRP) label and the second antibody contained an acridan based label. Within their work they successfully detected interleukin-8 (IL-8) with a LOD of 0.64 pg mL^{-1} . These results were comparable to current commercial methods. The systems works as shown in figure 1.5 with a “trigger solution” that contains hydrogen peroxide and *p*-hydroxycinnamic acid, a combination of this solution along with HRP and an acridan complex is needed to give the CL signal. It was reasoned that the high sensitivity was achieved because as an immunological complex the acridan and HRP were in close proximity and thus in larger concentrations relative to each other compared to the bulk solution.⁴⁰

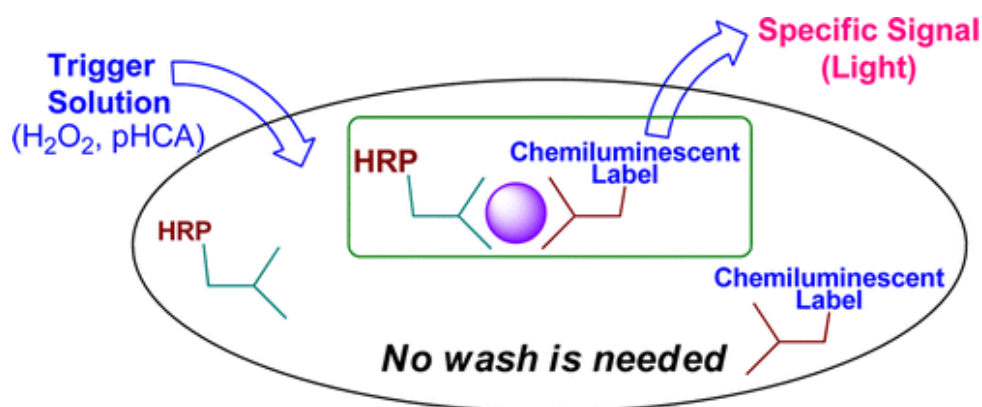


Figure 1.5: Schematic showing how this homogeneous immunoassay was conducted.

Reprinted with permission from H. Akhavan-Tafti, D. G. Binger, J. J. Blackwood, Y. Chen, R. S. Creager, R. de Silva, R. A. Eickholt, J. E. Gaibor, R. S. Handley, K. P. Kapsner, S. K. Lopac, M. E. Mazelis, T. L. McLernon, J. D. Mendoza, B. H. Odegaard, S. G. Reddy, M. Salvati, B. A. Schoenfelner, N. Shapir, K. R. Shelly, J. C. Todtleben, G. Wang and W. Xie, *JACS*, 2013, 135, 4191-4194. Copyright 2015.

However if you wish to measure more than one immunoassay response at a time (multiplexing) (which is required to monitor progesterone and oestriol) there needs to be a way of generating different responses from each of the hormone-antibody complexes. Chen *et al.* use quantum dots tagged to the antibodies to change the fluorescence response

from the antibodies to enable the detection of two viruses (Human Enterovirus 71 and Coxsackievirus B3) by emitting light at different wavelengths; this emission can then be quantified.⁴¹ However when dealing with molecules with similar structures such as steroidal hormones cross-reactivity can become an issue, therefore studies are needed so that false positives do not arise.⁴²

1.4.2.2 Heterogeneous immunoassays

Heterogeneous immunoassays involve immobilizing antibodies onto a solid surface, the antibody and antigen then interact at the “boundary layer”. In the same way as a homogeneous immunoassay, detection usually occurs through a label on either the antigen or antibody (see section 1.4.2.4). Once a sample is loaded and the antigen is given time to interact with the antibody (incubation time) the surface is washed to remove any unused antigen or interfering species from the sample. In homogeneous immunoassays the sample matrix will still be present and may affect the signal which can result in complex detection systems. Heterogeneous immunoassay detection can operate using general laboratory equipment or even smartphones through the possibility of spatial resolution.^{39,43} The method has the advantage of an increase in specificity and sensitivity towards its target compared with homogeneous immunoassays.⁴⁴ Care must be taken however in washing any antigen that has not bound to the antibody, to make sure the antigen does not adsorb onto the surface where antibodies are not bound this is combatted by blocking the surface that however adds further steps to the process.⁴⁵ Despite this, the need to develop a system that is very sensitive means this thesis will therefore focus on using heterogeneous immunoassays. How this can be carried out is explained in section 1.5.

1.4.2.3 Competitive and non-competitive immunoassays

Homogeneous and heterogeneous immunoassays can be further split into competitive and non-competitive immunoassays. A competitive immunoassay relies on a lower

concentration of antibodies on the solid surface. The target antigen and a tagged equivalence of the same antigen then compete for the limited number of antibody binding sites (Figure 1.6). Whereas a non-competitive immunoassay generally operates through a sandwich assay where the detection label is on a secondary antibody. The primary antibody binds to the target analyte and the secondary antibody then binds to primary antibody-antigen complex (Figure 1.7).

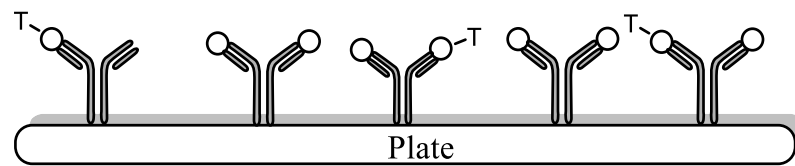


Figure 1.6: Example of a heterogeneous competitive immunoassay where T represents a label on the antigen.

Figure 1.6 shows a competitive heterogeneous immunoassay where the circle represents the antigen and the T represents a tag. During the incubation period the tagged antigen and free antigen (found in a sample) will compete for a limited number of available binding sites. During detection if the concentration of antigen in the sample was low, more tagged antigen would bind giving a larger signal; if the concentration in the sample was high then less tagged antigen would bind resulting in a lower signal. Therefore the signal is inversely proportional to the concentration within the sample.

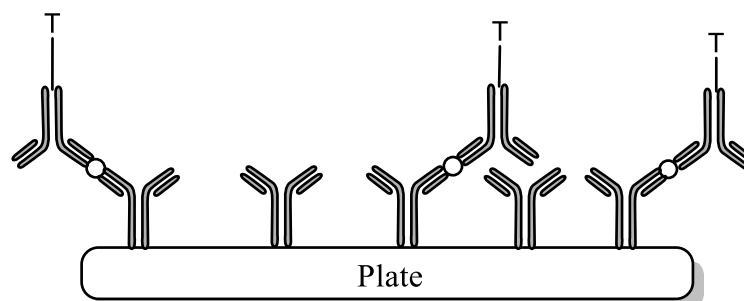


Figure 1.7: An example of a heterogeneous non-competitive “sandwich-assay” where T is the detection label on a secondary antibody.

Figure 1.7 shows an example of a non-competitive heterogeneous immunoassay, following incubation with the sample which enables the antigen to bind to the antibody, the tagged second antibody is added and the signal detected. In this case the signal is proportional to the concentration of the sample; i.e. more antigen in the sample results in more of the secondary antibody binding giving a larger signal.

The current hospital methods for measuring progesterone and oestriol levels are based on enzyme-linked immunosorbent assays (ELISA). ELISAs work by immobilising the antibodies into the individual wells, this typical through physical adsorption.⁴⁶ The antigen in the sample then binds to the pre-deposited antibody followed by the addition of a secondary antibody which is typically tagged with an enzyme, which can then catalyse a chemical reaction to give rise to a signal in the form of a colour change (Figure 1.8). The procedure can be used either to determine the concentration of an analyte in a given sample or simply the presence of the analyte. ELISAs generally operate within 96 well microtitre plates in which the antibody is immobilised at the bottom of the well.

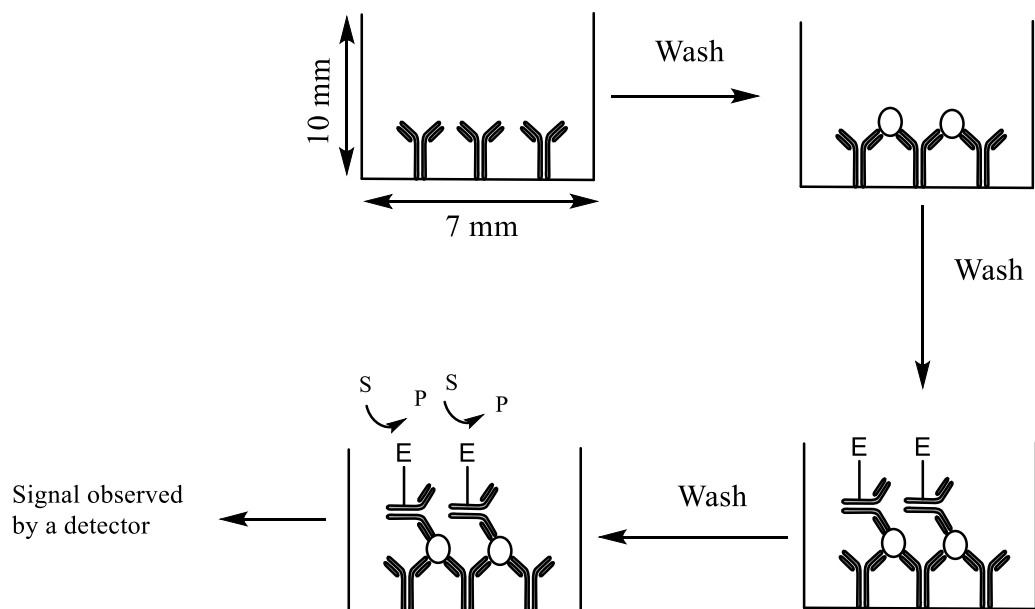


Figure 1.8: A non-competitive ELISA where in the first step the antibody is bound to the well, the sample is added where any antigen present will bind to the antibody, a secondary antibody with the detection tag is added which then binds to the antigen-antibody complex and a substrate is added to give rise to a detectable response.⁴⁷

ELISAs work well as they have good sensitivities, ranging typically from 0.1 ng mL^{-1} rising up to $>1 \text{ ng mL}^{-1}$ however there are problems, ELISAs are labour and time intensive.

1.4.2.4 Detection methods used in immunoassays

There are a variety of different detection methods that can be for immunoassays. Currently a lot of work has been conducted with the aim of detecting the point at which interaction happens between antibody and antigen. Traditionally chemical species have been added to the antigen or antibody which can result in a signal that can be detected. The most common tags are chemiluminescence, fluorescence, electrochemical and radio labels.

Label-free immunoassays

Label-free analysis is usually achieved by using surface plasmon resonance (SPR). This technique operates by measuring any changes to the surface interface. The antibody is immobilised on a gold surface and light is shone towards the gold surface and is refracted to a detector. Any changes to the surface i.e. a reaction of the antibody with its target, results in a change in the refracted light which can be measured.⁴⁸ Despite SPR being a very common technique used in laboratories, the technique itself has not been used extensively with respect to a clinical setting. The reasons for this is by using clinical samples such as blood, urine and saliva uncontrollable background signals can be observed due to non-specific binding. Therefore for this reason this technique will not be investigated.⁴⁹

A secondary form of a label free immunoassay is by using impedance; impedance is a technique where the resistivity of a system is measured compared to the frequency with respect to alternating current, with respect to direct current the resistance does not change with frequency. Within immunoassays the interaction between the antigen and antibody causes a change in the resistance of the electrode surface, this change can be plotted as a calibration. The technique was reviewed by Daniels and Pourmand where a number of benefits of the technique were mentioned with it being label free, does not exert the sensors to the harsh voltages and currents seen in other techniques. However drawbacks include a disagreement about the sensitivity due to interferences, which for the levels this work requires is not ideal and how easily a result can be distorted because of pH changes, ionic strength and others which for clinical applications it is hard to predict any changes within a sample.⁵⁰

Labelled immunoassays

Historically radioimmunoassay's were initially utilised to carry out sensitive immunoassays which involves the tagging of a radiolabel to the antibody or antigen, the most commonly used labels are iodine 125 (¹²⁵I) or tritium (³H), mainly due to their long half-lives of 60 days and 12.26 years for the iodine and tritium respectively. A scintillation counter is required to measure the radiation that is emitted, the procedure works by substituting any iodine species into the ¹²⁵I isotope so that the antigen is largely unchanged; by using the amount of radiation produced from the system a determination of the concentration of the antigen present in the original sample. This method works very well, however drawbacks include the need for expensive equipment, the dangers of working with radioactive material and extra expense caused by storing the material.⁵¹

With these drawbacks other labels have been researched with fluorescence labels being the most commonly used:

In this method the label is a fluorescent dye which emits radiation when irradiated by a strong light source such as a laser. (Full theory on how fluorescence operates in section 1.7.5). Fluorescence is commonly used in homogeneous immunoassays due to its sensitivity and the different properties that can be exhibited through the light that is emitted such as polarization.⁵² The draw back to using these labels is the requirement of a powerful external light source to provide the sensitivities needed which can be expensive.

Chemiluminescence (CL) labels remove the need for an external light source because the label itself takes part in a chemical reaction resulting in the emission of light, the theory of CL is discussed in section 1.8. The most common label used in chemiluminescence is horseradish peroxidase (HRP). HRP is an enzyme found in horseradish that can catalyse the breakdown of peroxide this enzyme is used due to the sensitivities that are possible as well as the ease to purchase antibodies tagged with HRP.³⁶ When used in combination with luminol light is emitted that can then be quantified. Other labels include the use of gold nanoparticles and a combination of these to aid multiplexing.⁵³ Without the need of a light source CL labels are very popular however care needs to be taken to ensure that no background light interferes with the measurements. These labels offer an opportunity to develop a system that is suitable for POC.

Another type of label are electrochemical labels which are redox active meaning they are readily oxidised and reduced this requires the use of an electrode. When a potential is applied to the system there is a point where the redox species is oxidised or reduced, when this happens there is a change in current and this current can then be measured to determine the concentration of analyte within the sample. This redox species can be tagged to the antibody or antigen or even be the analyte itself. There are many different tags used such as ferrocene,⁵⁴ gold nanoparticles,⁵⁵ and many others. These will be discussed fully in section 1.9. These differ to impedance which is label free because electrochemical

labels give extra sensitivity and are less prone to interferences, the sensitivities are on a similar level to those seen with CL which will be explained further in section 1.9.⁵⁰

1.4.3 Antibodies used to carry out immunoassays

When carrying out an immunoassay the class of antibodies used can make a huge difference. When the antibodies are purchased they are available in two forms monoclonal and polyclonal. As described previously when an antibody binds towards its target (which is usually a protein) there are a number of different sites that the antibody can bind to; these sites are called epitopes. Monoclonal antibodies target these sites specifically; whereas polyclonal antibodies are a mixture of all the different antibodies that can attack all the various epitopes on the antigen. Monoclonal antibodies are not found in humans naturally because when an infection occurs many different antibodies are produced to attack the entire structure of the pathogen and bind to all the epitopes.³⁶

In experimental work monoclonal antibodies, are better providing increased sensitivity and better reproducibility. With polyclonal antibodies every batch is different which makes it harder to get reproducibility and the required sensitivity between each batch. The production of monoclonal antibodies was first reported by Kohler and Milstein.⁵⁶ Whilst monoclonal antibodies are more specific, they are more expensive to produce which is a major disadvantage. When dealing with quantitative analysis use of monoclonal antibodies is preferable as an antigen can bind to multiple antibodies that target different regions and therefore is not a true reflection on the quantity present whereas monoclonal antibodies only target one region.

1.5 Antibody Immobilisation Methods

To carry out a successful heterogeneous immunoassay the antibodies need to be immobilised onto a solid surface. This section examines the methods available to immobilise the antibodies on different substrates.

ELISAs are usually carried out on 96 well plates are typically made from polystyrene as it is a cheap material to produce, that can be produced on a large scale, however there are many different types of substrates that can be used to carry out immunoassays and these are each described below. This method that has been used for many years due to its ease and sensitivity.³⁹ A typical assay ELISA can take in excess of 24 hours due to the number of steps and the large size of the wells.

The steps are shown in Table 1.1.

Competitive Immunoassay	Non-Competitive Immunoassay
Sample Preparation	Sample Preparation
Antibody Immobilization	Antibody Immobilization
Washing	Washing
Antigen Addition	Antigen Addition
Washing	Washing
Detection	Second Antibody Addition
	Wash
	Detection

Table 1.1: List of the protocol required to carry out an ELISA.

The wells of micro titre plates have various dimensions depending on the brand or application however the dimensions vary from 10 mm to 20 mm in depth and have a width of 5 mm to 15 mm. These dimensions indicate a significant amount of time is needed for the analytes to diffuse across the well and interact with the immobilised antibodies. Furthermore for the system to be useful and reliable the sample handling needs to be automated and the robotics required means that the systems have a high cost.³⁹ This can work fine for batch analysis of large numbers of samples in a hospital situation but for POC devices there is a need for immunoassays to be carried out at a faster rate that maintains the sensitivity of the protocol within the range required for that particular investigation without the use of expensive instrumentation.

1.5.1 Glass substrates for heterogeneous immunoassays

Immobilization of antibodies on to glass has been shown to be challenging.⁵⁷ Several factors need to be considered when identifying the best immobilization method for an antibody, with this in mind the following relates to the IgG form of antibodies used in this work.

Commercial functional group slides

It is possible to buy glass slides that already contain the desired functional groups, this approach is commonly used for convenience with a number of companies supplying these functionalised slides. Generally when using these slides the same chemistries can be applied as with those when using the silanised glass slides described in the next section; with the major difference being that these commercial slides have already been functionalised and are ready for the reaction with the antibodies, For example, Zheng *et al.*⁵⁸ utilised epoxide derivatised glass slides (Array it[®] (U.S)) where 500 $\mu\text{g mL}^{-1}$ of antibody was immobilised onto the surface and a sandwich immunoassay was carried out successfully. As these functionalised slides will have been rigorously tested; with all

preparations being carried out in a clean room environment, they should ensure reproducible results but all this comes at an added expense and in this work we need to immobilise the antibodies within specifically designed substrates.

1.5.1.1 Silanisation

Glass surfaces naturally contain hydroxyl groups on the surface, which make the surface hydrophilic, these groups need modifying to give functional groups that can interact with the antibody as well as making the surface more hydrophobic, the hydrophobicity is required to stop the antibody spreading. This can be achieved through silanisation of the glass surface but, for this to occur the glass surfaces needs to be sufficiently cleaned to allow the silane reagent to react with the surface and give a uniform monolayer, Crass *et al.* ⁵⁹ investigated the best method for cleaning microscope slides in preparation for silanisation and observed that a mixture of methanol and hydrochloric acid wash, followed by immersion in a bath in concentrated sulphuric acid gave the best results. There are various silanising reagents that can be used to immobilise antibodies onto the surface of a glass substrate, most silanising methods then rely on a cross-linker to link the antibody onto the surface. The antibodies can be spotted onto the prepared surface by use of an automated spotting machine that can accurately dispense a droplet of known volume of antibody onto the surface.

Immobilisation with (3-aminopropyl)-trimethoxysilane (APTMS) and (3-aminopropyl)-triethoxysilane (APTES)

APTMS and APTES are commonly used silanising reagents, APTES has an ethoxy group attached to the silicon compared to APTMS which has a methoxy group. Both of these reagents result in amine functionality on the glass surface as shown for APTES in Figure 1.9. These silanising reagents are commonly used compared to others due to the ability of the amine group to bind to the antibody through various routes.

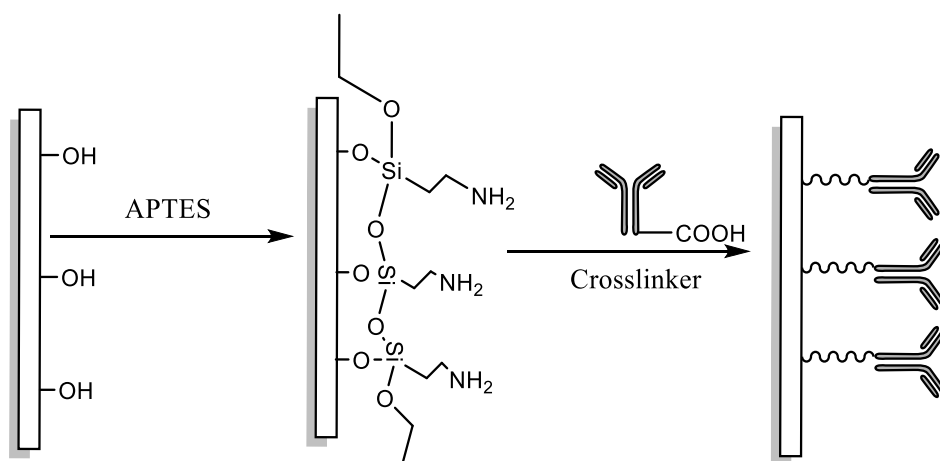


Figure 1.9: Schematic showing the silanisation process as well as the antibody immobilisation on glass, this example is with respect to APTES.

Within the literature there are many different ways to introduce these reagents onto a glass surface, ranging from using dry toluene as the base solvent (Akkoyun *et al.*⁶⁰), ethanol (Mendoza *et al.*⁶¹) or water with a pH adjustment to 3 with hydrochloric acid. (Glass, *et al.*⁶²) All three methods required thorough drying and curing of the slides, this needs to be carried out in an oven at an appropriate temperature for each solvent.

Cross linkers used with APTES

Glutaraldehyde is a dimer with two aldehyde groups at either end of the chain and therefore it can be used as a linker to enable immobilization of the antibody. As shown in Figure 1.10 one of the aldehyde groups can interact with the silanised glass surface while the other group can interact with the amines found on the antibody.

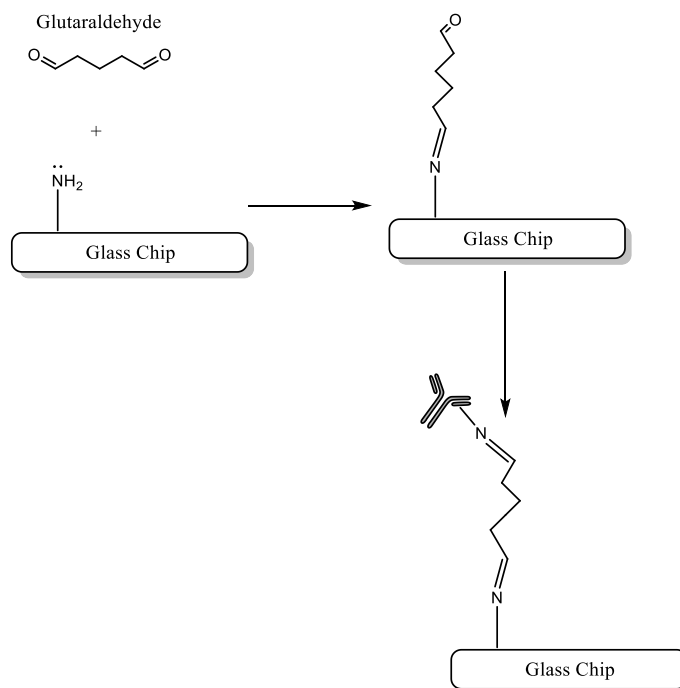


Figure 1.10: Schematic outlining the use of glutaraldehyde as a linker for antibody immobilisation on an amine derivatised glass surface.

However one major drawback with this method is described by Shriver-Lake *et al.*⁶³. Despite glutaraldehyde being universally utilised as a convenient linker there can be variations between batches of the reagent and when stored it can self-polymerise which has been shown to strongly effect reproducibility. It is therefore important to consider alternative linkers, such as N-(3-dimethylaminopropyl)-N'-ethylcarbodiimide (EDC) with N-hydroxysuccinimide (NHS). As shown in Figure 1.11 EDC is a carbodiimide which activates the acid groups on the antibody to form an o-acylisourea ester which can then interact with the amine groups on the APTES derivatized glass surface to form an amide bond enabling the antibody to be covalently bound to the surface. The o-acylisourea ester intermediate is unstable so NHS or its sulfinated derivatives are often added to create an NHS ester with stabilises the intermediate substantially. The antibody then reacts with the amine derivatised surface as discussed previously.

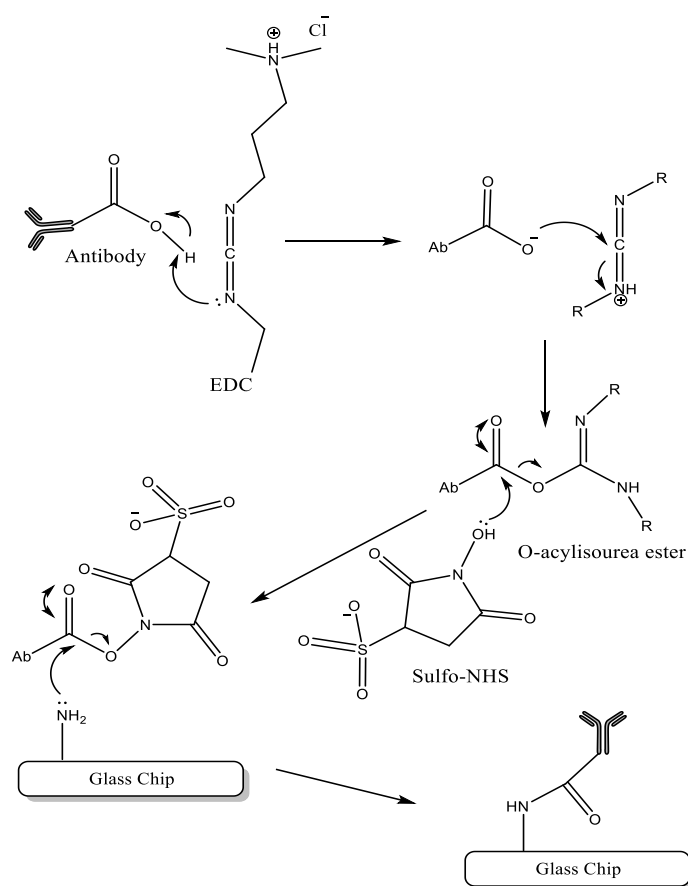


Figure 1.11: Schematic showing the mechanism of how EDC and sulfo-NHS immobilises antibodies onto the amine derivatised glass surface.

Akkoyn *et al.*⁶⁰ used these reagents to immobilise dextran *via* activation of the carboxymethyl groups on the silanized surface and then used these same reagents to activate the antibodies to bind to the immobilized dextran. However prior to adding the activated antibodies to the glass slide, there had to be an incubation time of 7 minutes with the (80/20 mM) solution of EDC and NHS to allow the activation to occur with the antibody prior to immobilization. There are many other ways that this principle has been applied, Mendoza *et al.* just used the NHS ester to interact with the amine group on the surface and the amine group of the antibody to form a linkage, this was carried out by using bis-sulfo-succinimidyl substrate (BS³).

(3-glycidoxypropyl)trimethoxysilane (GPTS)

GPTS, gives rise to an epoxide functional group on the glass surface instead of an amine. Mathias *et al.*⁶⁴ placed glass slides in a solution containing 2.5 % GPTS, 10 mM glacial acetic acid and ethanol for 1 hour and washed with ethanol and dried under nitrogen, the antibodies were spotted on the slides within a glycerol buffer consisting of 5 % glycerol in phosphate buffered saline (PBS) and left overnight at 4 °C, no further addition required. The benefit of this methodology was there was no requirement for linkers. Gering *et al.*⁶⁵ silanized the glass surface by refluxing the slides in a solution containing 73.5 mL of isopropanol and 1.5 mL of water. When the reflux temperature was reached, 130 µL of the GPTS was added and left to reflux for 15 minutes, after this the slides were immersed in pure isopropanol and left to air dry. The immobilization of the antibodies by this method is discussed further in section 3.3.3.

Mercaptopropyltrimethoxysilane (MPTS)

MPTS gives rise to thiol groups on the surface of the glass, Kusenezow *et al.*⁶⁶ describes many silanizing procedures including the ones above. They suggest that glass slides can be prepared with 10 mM acetic acid in ethanol and 1 % MPTS. With an acetic acid (10 mM) in ethanol wash. Experiments were carried out both by using a linker and without a linker, the linker used was a maleimido-R-N-succinimidylesters where the R represents various groups. It was observed that when $R = (\text{CH}_2)_2\text{NHCO}(\text{C}_6\text{H}_{10})\text{CH}_3$ was used more reproducible results were obtained compared to when the R group was an ethyl, propyl or cyclohexyl group. When the results obtained for MPTS were compared with APTES it was the APTES that gave significantly better results. They report that when no linker was used poorer results were observed. With respect to APTES when the R chain increased the signal observed was doubled whereas with the MPTS the improvement was less than double.

1.5.1.2 Poly-L-Lysine (PL)

Kusnezow *et al.*⁶⁶ looked at using PL as a route to modify glass surfaces, where the PL was physically adsorbed onto the glass. A solution was prepared by making a 0.01 % solution of PL in phosphate buffered saline (PBS) and baking it in an oven at 45 °C for 30 minutes. Prior to placing the slides in the oven, they were washed with water and ethanol. The results were not as good as those surfaces modified with APTES and GPTS, the slides themselves had a lower shelf-life in comparison to the other methods as well as a decrease in the sensitive of the corresponding immunoassays.

1.5.1.3 Streptavidin

Streptavidin is a protein that has a very high affinity towards biotinylated species this combination is known as one of the strongest non-covalent bonds in nature and for this reason it is commonly used in immunoassays. Jang *et al.*⁶⁷ used polyethyleneimine to coat glass slides along with glutaraldehyde. The slide was then incubated in streptavidin and immediately the biotinylated tagged antibody was placed onto the surface. The biotin tag had been added to the antibody using NHS-LC-LC-Biotin reagent in excess in dimethylsulfoxide (DMSO) for 1 hour at room temperature. The modified antibody was purified *via* dialysis and size exclusion chromatography. They resulted in sensitive results as the detection occurred through chemiluminescence however undergoing this methodology is expensive, which bearing in mind the cost of the reagents required anyway this is an issue when developing POC systems.

1.5.1.4 Antibody modification

Various ways have been investigated where the antibodies themselves are modified as a route for immobilising the antibodies onto the glass surface.

Splitting the antibody into two segments

There are some problems with the methods discussed previously. In particular there is little control of the orientation of the antibody on the surface. This can be seen in Figure 1.12 where the antibody is randomly orientated. The epitope region of the antibody is within the Fab region therefore for the greatest sensitivity it is key that this region has the greatest interaction with the sample and therefore ideally the immobilisation method should allow for orientation as shown in figure 1.12.

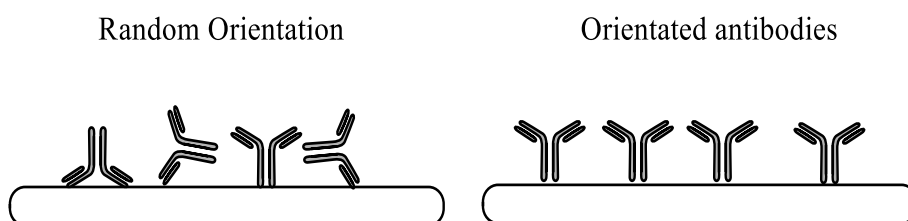


Figure 1.12: A scheme to show how antibodies can be orientated on a solid surface, there is no control however to make sure that antibodies are all orientated in the desired fashion shown.

To overcome this problem a commercial company provides a protocol (ThermoScientific™) for antibody immobilization onto glass surfaces, this protocol proposes antibody modification binding occurs through the sulphur groups on the antibody, similar to the use of mercaptosilane as discussed in section 1.5.1.1). In their method a maleimide linker was used that can then interact with the thiol groups present on the antibody. The protocol works by reducing the disulfide bonds to obtain thiol groups. This procedure was adapted from the bioconjugate techniques⁶⁸ which was carried out by breaking the disulfide bridges that bind the two parts of the antibody together with 2-mercaptoethylamine used to form the corresponding thiol. Once this step

has been accomplished, the antibodies need to be used immediately to minimise the reformation of the disulfide bonds. The benefit of this methodology is that the orientation of the antibody is controllable. However a major drawback arises from the need to break the antibody apart, which reduces the activity of the antibody impacting on the sensitivity of the immunoassay and therefore this method is not widely discussed in the literature.

Modification of carbohydrate groups on the antibody

Another way to immobilise the antibodies onto the surface is through their carbohydrate moieties, this is carried out *via* aldehyde bonding to a hydrazide derivatised surface. This approach was reported by Gerin *et al.*⁶⁵ where the glass surfaces were treated with an epoxysilane reagent, this was then hydrolysed under acidic conditions to give rise to a diol. The diol was then treated with periodic acid to form an aldehyde which was reacted with adipic acid dihydrazide to give a free hydrazide group which reacted with the antibody. To avoid any exposed hydrazide groups from interacting with any unreacted aldehyde groups on the surface these were reduced with sodium borohydride. The antibody was modified by agitating it in 20 mM sodium acetate buffer pH 5.0, 150 mM NaCl and 10 mM periodic acid, the reaction was stopped by the addition of ethylene glycol. Purification was carried out *via* dialysis; the antibodies were then sandwiched between two modified glass slides and contained at 4 °C.

This method enabled antibodies to remain intact and become immobilised onto the surface, allowing the activity and the sensitivity to be retained, however as this requires chemical modification of the antibody care is required, if the procedure is not carried out correctly this can alter the antibodies and affect how they operate, again for these reasons this is not a widely used technique as antibodies are expensive, it is not desirable to attempt to modify them in anyway if other methods are possible.

1.5.1.5 Glass beads

Glass beads are micrometre to millimetre sized beads that can be incorporated into a microfluidic device; using these beads provides a higher surface area than a glass slide which enables a greater interaction between the antibody and the bead surface. They can be modified in the same way as glass slides and the most general way of carrying this out is using APTES. For example Yoon Lee *et al.*⁶⁹ silanised glass beads with APTES using glutaraldehyde as a crosslinker to the antibody when the amine groups of the antibody interact with the aldehyde groups through a Schiff's base formation, the binding was enhanced by a reduction with sodium cyanoborohydride. Lates *et al.*⁷⁰ used the EDC/NHS linker however in this experiment the antigen itself was immobilized onto the beads rather than the antibody.

Glass beads can be incorporated into a microfluidic device by having chambers built within the microfluidic device that can hold the beads. Yoon Lee *et al.*⁶⁹ moulded chambers into PDMS and by using the beads in the chamber a greater amount of control was obtained. This included the ability to multiplex using spatial control, a major drawback to the use of glass beads is the manipulation of the beads within a sample this can be complex for these reasons glass beads are not heavily utilised.

1.5.2 Plastic substrates for heterogeneous immunoassays

1.5.2.1 Polystyrene

As mentioned previously in current laboratory practices immunoassays are normally carried out in polystyrene 96 well plates through an ELISA. Unlike the methods described for glass surfaces immobilization of the antibody typically occurs through physical adsorption where the antibody is prepared in a coating buffer. Scott⁷¹ used a coating buffer that consisted of 0.1 M glycine adjusted to pH 8.8 with sodium hydroxide, whereas Shi-Qi⁷² used a coating solution which is used to aid the antibody immobilization process and this consisted of a citrate salt buffer at pH 4.8, with Scott's⁷¹ method the coating

solution with the antibodies remained in the well either for two hours at room temperature or overnight at 4 °C, Shi-Qi⁷² also left the solution at 4 °C but they specify that this was for 18 hours.

As the antibodies are passively adsorbed onto the surface many parameters need to be optimised as the binding is based on Van der Waals forces which are weak intermolecular forces. Factors that affect binding include pH, the concentration of the antibody and its natural hydrophobicity. If the antibody is naturally hydrophobic, it will have a greater affinity to the hydrophobic polystyrene and adsorb to the surface better. It is also known that some antibodies can denature upon adsorption onto the polystyrene surface, with that covalent attachment can alternatively be used.³⁶

Dixit *et al.*⁷³ successfully covalently bound antibodies to polystyrene, polymethylmethacrylate (PMMA) and cyclic olefin copolymer (COC) and their results concluded that the results are independent to which substrate used. The method by which the antibodies were immobilized were as follows: A bottomless 96 well plate was used in which the bottom of the plate consisted of each of the polymers under investigation, each well was then in turn washed with ethanol and then 1% w/v KOH for 1 hour at 37 °C this was to form OH groups on the polymer surface. The surface was subsequently modified with APTES 2 % v/v at 80 °C for 1 hour and after a wash the antibody solution was added using EDC and Sulfo-NHS as a linker.

As mentioned previously EIA/ ELISA (Enzyme Immunoassays and Enzyme immunosorbent assays) are used every day in the laboratory due to their high sensitivity, despite the length of time required for an analysis to take place. Shi-Qi⁷² demonstrated for a specific experimental set up that the time taken from the addition of the first antibody into the well to when analysis can occur was in excess of three days, this large amount of

time required is overcome to some extent when operating in batch mode with 96 wells and thus 96 parallel assays occurring.

In contrast a POC system aims to deliver result in a short timescales. For these systems plastic materials or more practical for immobilization of the antibodies because it is feasible to fabricate low cost disposable devices, preventing cross contamination. Although polystyrene is favoured for 96 well plates it is not so suitable for microfluidic devices. Young *et al.*⁷⁴ described the complicated fabrication techniques required. Furthermore polystyrene is also susceptible to leaching of bioactive materials and for these reasons there has been work into using other polymers such as PMMA and COC.

1.5.2.1 PMMA

PMMA is frequently used for microfluidic devices as it is cheap to produce and easy to fabricate, the added benefit PMMA gives over COC is that surface modification is easier with several different approaches possible for antibody immobilization. Cheng *et al.*⁷⁵ described a PMMA device in which after thoroughly washing the PMMA surface with water it was dried under a stream of nitrogen and placed in a solution containing 16 g of lithium aluminium hydride (LiAlH_4) in 100 mL of diethyl ether for 24 hours which reduced the ester groups to alcohol groups (OH-R). This type of surface can then be further modified using the same methods as described previously for glass substrates. Goddard *et al.*⁷⁶ discusses numerous ways to modify PMMA surfaces which include using 10 M sodium hydroxide or 3 M sulphuric acid to hydrolyse the ester groups on the surface resulting in the formation of carboxylic acid group. With this type of modified surface a procedure outlined by Yang *et al.*⁷⁷ can be used for immobilization where the acid groups are activated using NHS to form the NHS ester. This is in the same way as discussed previously in which the surface was aminated by using polyoxypropylenediamine (Jeffamine) from this point various amounts of chemistries are

then available for different applications. Goddard *et al.*⁷⁶ and Brown *et al.*⁷⁸ also discuss a direct amination of the surface with ethylene diamine (1 M) in dimethyl sulfoxide.

A really common method for surface activation of polymers is outlined by Goddard⁷⁶ which involves surface plasma treatment. Commonly oxygen is used for the plasma where, under a large voltage, oxygen gas becomes a plasma and modifies the surface to make it hydrophilic and contain (OH-) groups, this method is widely used as it works for all different types of plastics and it avoids the need to use chemical techniques however there is much optimisation required when using this technique to find the right parameters best suited to enable the surface to be modified to an extent the antibody immobilization can take place. Figure 1.13 shows the structure of PMMA.

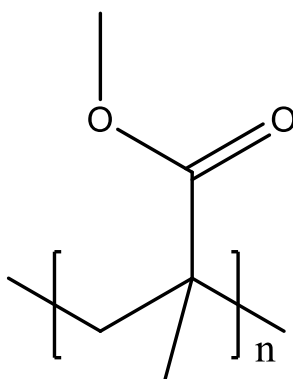


Figure 1.13: Structure of PMMA.

1.5.2.3 COC

Cyclic olefin copolymer is a hydrophobic polymer that is increasingly being used based on its compatibility with biological systems. This polymer does not however have functional groups available for covalent attachment of the antibody. For this reason there has been a lot of work into looking at the best way to modify this surface. Stachowiak *et al.*⁷⁹ investigated the process of photografting, a two-step process involving grafting hydrophilic polymers onto the polymer surface, the first step involved physically adsorbing a photoinitiator onto the surface. In the second step the microchip was placed

into a solution of the monomer followed by exposure to UV light. A major drawback of this method is that as the photoinitiator is only physically adsorbed there is a chance it can become desorbed from the surface. To combat this Stachowiak⁷⁹ covalently bound the initiator on the surface by flushing the device with the initiator followed by exposure to UV light, after which the monomer was flushed through the device and it was again exposed to UV light, after which the chip was ready to be used.

An alternative approach for surface activation is ozonolysis a process that is described by Diaz-Quijada *et al.*⁸⁰ this was achieved by placing the chips in an ozone generator for one hour where carboxylic acid groups formed. After the microchips were ready for further activation with EDC and NHS.

Finally the most common approach is the use of oxygen plasma in the same way as discussed for the PMMA. Raj *et al.*⁸¹ exposed COC slides to the oxygen plasma at 150 W for 15 minutes, they found any further exposure damaged the surface of the plastic which needs to be avoided. After exposure the slides were modified with 3 % APTES in methanol : water (95:5), and then the antibodies were bound to the surface using a succinimidyl-4-(N-maleimidomethyl)cyclohexane-1-carboxylate (sulfo-SMCC) the maleimide sub-unit can react with the amine groups on the substrate, allowing the antibodies thiol groups to react and bind to the surface.

1.5.3 Other Substrates for heterogeneous immunoassays

Gold

As a solid substrate, gold can work really well to bind antibodies by adsorption through their native thiol groups, this is known to be a very stable and favourable interaction on gold surfaces this is generally achieved by using a bifunctional linker with a thiol group present.⁸²

As with the surfaces previously described there are similarities as to how antibodies can be immobilized onto the surface of gold, Vashist *et al.*⁸³ modified the gold surface with APTES, EDC and a sulfo-NHS linker methodology. Gold however is an expensive material to use which for developing a POC device is not ideal, typically SPR is favoured as a detection method through the use of gold substrates. Another way to measure immunoassays on gold surfaces is through electrochemical means, where a shift in current or potential can be measured based on the addition of the antigen, Dou *et al.*⁵⁴ modified a gold electrode surface to have free amine groups on the surface, and in the same way as Vashist *et al.*⁸³ EDC and sulfo-NHS was used as a linker for the antibody to the gold surface. This antibody however was modified to contain a ferrocene tag to give an electrochemical response, Voltammetric measurements were taken to monitor the subsequent addition of the antigen and a change in current was observed. The results from this show great sensitivities with an LOD of 23 pg mL⁻¹ and strong reproducibility.

Gold can also be used without the need for electrochemical measurements; purely as an immobilisation substrate, there has been work into splitting the antibody in half to generate free thiol groups and as described previously (section 1.5.1) this has not been heavily utilised due to the complications in splitting the antibody and the loss of sensitivity.⁸²

The benefits of gold substrates for antibody immobilisation is the high degree of success this is outlined by the fact gold is typically used for SPR which as mentioned is one of the forefront techniques for carrying out immunoassays. However an issue is the expense that comes with using gold, the metal is expensive and when developing POC systems that would be disposable, gold does present economic challenges.

Silicon

Silicon is a material commonly used as a semiconductor, Yakovleva *et al.*⁸⁴ silanized silicon microchips with APTES and used glutaraldehyde as a linker, they also investigated using GPTS with a branched polyethylenimine (BPEI) covalently attached; to which glutaraldehyde can be adsorbed and bound to the antibodies. Linear polyethyleneimine (LPEI) was also investigated, but the GPTS system gave rise to the best results however they had stated the precision between assays was low, therefore it was determined that the use LPEIs covalently bound to the silicon surface was the best way to conduct this sort of research. Silicon however is very expensive to use for this reason this will not be discussed further.

Magnetic particles

Magnetic particles generally consist of a magnetic core usually iron based with a polystyrene coating, these particles can be purchased consisting of various functional groups based on the application that is being studied, they have a good advantage, that they can be controlled *via* magnetism which in a microfluidic system has great benefits; the particles themselves can remain in a set area of the device and not be influenced by the flow. Zhang *et al.*⁸⁵ used chitosan/Fe₃O₄ magnetic particles to generate an immunosensor, they prepared chitosan/Fe₃O₄ magnetic particles with glutaraldehyde as a linker to which the antibodies were added, this group used quantum dots, with electrogenerated chemiluminescence as a detection method, however other detection

methods can be used depending on what type of analysis is being carried out and the setup of the experiment.

Paper

This method is gaining in popularity as a low cost-simple substrate to carry out immunoassays; Yen *et al.* developed a lateral flow system based on paper based microfluidic system where antibodies containing various sizes of silver nanoparticles which will appear as different colours. Within this test Ebola, yellow fever and dengue can all be detected however the immobilisation process is not mentioned in the paper.⁸⁶

Liu *et al.* developed a paper based chemiluminescence immunoassay for the detection of cotinine, which is a metabolite of nicotine. Within this work chitosan was deposited into the detection chamber followed by glutaraldehyde as a linker, to which the antibodies were added; a competitive immunoassay ensured with HRP as the catalyst. A limit of detection of 5 ng mL^{-1} was achieved.⁸⁷ Mu *et al.* developed a chemiluminescence immunoassay on paper for the diagnosis of hepatitis C, through this work the antibodies were physically adsorbed to the paper surface.⁸⁸

Park *et al.* developed a paper microfluidic system where salmonella is quantified by using a smartphone, as a light source as well as a detector. The vast majority of modern day smartphones consist of a flash and a digital camera, this flash is sufficient as a light source and the camera acts a detector based on the amount of light absorbed.⁸⁹ Within this work the antibodies were immobilised onto polystyrene beads which through the channels etched into the paper could be manipulated. With a change in the absorption measured.

However there are some issues with paper based systems as reviewed by Yetisen *et al.* there are difficulties in guaranteeing sufficient washings throughout the analysis as well as their abilities to become commercial and profitability. The review also outlines a lot of

potential in the area and is and will continue to be one of the emerging technologies however due to their limitations this substrate will not be taken forward.⁹⁰

1.6 Point-of-Care Testing

Point-of-care (POC) systems operate based on the idea of providing a result as and when it is required within a short time frame at a place where the patient can obtain treatment or advice appropriately. Therefore a system by which the patient gives a sample and gets the result at the same time. James Nichols described POC as systems where the tests are carried out “where or near clinical care” is conducted⁹¹; this could be in the form of a doctor's surgery or within the hospital themselves. This has numerous advantages as it allows GP's to have a greater control over the health care of their patients as well as rapid diagnosis of issues.

Examples of where POC systems have become commercial are the lateral flow immunoassays; an example of which, is the ovulation test that mothers can use to give an indication as to whether or not they are ovulating, one of the common commercial products in the UK is produced by a company called Clearblue. The test is based on a urine sample where LH binds to pre-deposited antibodies on the surface. After which one of two readings can occur, either a blank circle to indicate ovulation has not occurred (no LH) or a smiley face to indicate ovulation has occurred (high LH). These tests are very popular due to the ease of use and rapid response.

POC can be carried out *via* many different ways and many new methods are being developed to allow diagnostics to occur on a smaller and more user friendly scale. These systems would preferably be able to detect several analytes at the same time the lab-on-a-chip (LOC) platform is ideal for enabling this to occur.

1.6.1 Lab-on-a-chip for POC

LOC are devices that incorporate multiple analytical steps on a chip that is no more than a few square centimetres in area, the device typically incorporates channels with micrometre dimensions. These systems work by manipulating the analyte and reagents through different stages such as pre-concentration, mixing and detection. This area of research is fairly new having taken shape within the last 20-30 years, the opportunities that can be achieved through this area makes it very attractive. This area is synonymous with POC however there are opportunities to carry out synthesis as well as other applications on a small device⁹². In this context developing a LOC system would allow the mixing of the saliva with another solution containing a labelled component, the mixture can therefore bind to the pre-immobilised antibodies, followed by CL detection. A key feature involved with these systems is microfluidics.

1.6.2 Microfluidics

Many LOC devices operate through microfluidics due to the sizes of the channels within the device. Microfluidics involves the movement of very small volumes of reagents; typically on the 10^{-6} – 10^{-18} litres range⁹³ through micro-channels that have dimensions of 10's rising to 100's of micrometres in width and depth. These channels can be designed based on the requirements of the system and what role the channel has within the system. The huge benefit of these volumes is the low sample and reagent requirement which can aid cost as well as speed up analysis.

1.7 Fabricating LOC Systems

1.7.1 Substrates

There are various different substrates that can be used to fabricate microfluidic devices, the substrate of choice depends very much on the required application of the system, what form of detection the system will take and the chemicals that are involved. Some of the main substrates include silicon, quartz and glass.⁹⁴ The benefits of these materials are they are chemically compatible, have good optical properties and ease of channel fabrication. Silicon is an ideal substrate when it comes to fabricating channels that are in the <100 nm region; however due to its electrical conductivity it is not suitable for systems that require the use electroosmotic flow (EOF) (see section 1.7.3). Silicon is also hydrophobic which can cause issues when it comes to fluid manipulation specifically when using the aqueous phase. Quartz on the other hand has excellent optical properties, allows the use of EOF and has a low thermal conductivity which can allow a greater control of the system. Fabrication in quartz is however challenging. To prepare a microchannel two quartz plates need to be thermally bound together at temperatures in excess of 1150 °C also quartz is very expensive.⁹⁵ Glass in various forms such as soda-lime, Pyrex and borosilicate are commonly used to fabricate microfluidic devices, glass is substantially cheaper than quartz and thermal bonding can occur at a more modest 600 °C.

In more recent times polymer has emerged onto the scene as an alternative way of developing microfluidic devices, several polymers have good optical properties (transparent down to 300 nm) and despite a large initial cost for the required equipment for fabrication (see section 1.7.2.3) polymer devices are cheap to fabricate, therefore can be disposable, which for a POC system is ideal where a one-time test is required. A few examples of polymers currently used are polymethylmethacrylate (PMMA), polydimethylsulfoxide (PDMS) and cyclic olefin copolymer (COC). A major drawback

however to the use of polymer substrates are that they are chemically incompatible with a number of organic solvents.

1.7.2 LOC Fabrication

Fabricating microfluidic systems can be achieved in different ways and the technique that would be used depends on the substrate, the accuracy of the channels that are required the equipment available to carry out the fabrication and time needed.

1.7.2.1 Fabrication in glass using wet etching

This process is one of the most common methods of fabricating a microfluidic device using glass or silicon as the substrate. McCreedy, showed that wet etching can be carried out by covering the glass or silicon with a chromium metallic layer over which a photoresist is spin coated and finally a mask which contains the design of the channels. Initially UV light penetrates the photoresist which imprints the channel design onto the surface of the device. The chromium layer is then removed using a metal etch after which the channels are etched into the substrate using an etching solution⁹⁶ (typically hydrofluoric acid). A diagram of this process can be seen in figure 1.13. When etching in glass it is important to note that the etching is isotropic resulting in the walls not being parallel, as the etch solution etches deeper this causes etching of the wall of the glass resulting in a non-uniform width across the channel.^{96, 97} This fabrication technique has an accuracy of a few microns.

The glass fabrication technique follows a route represented in figure 1.14:

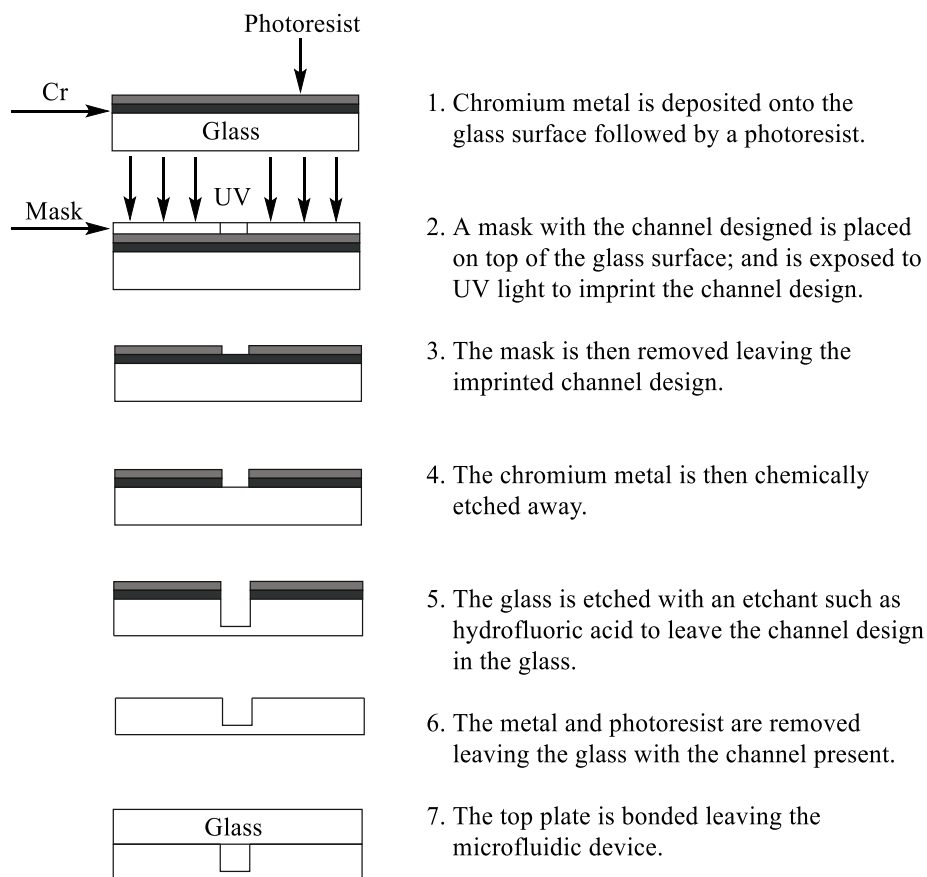


Figure 1.14: Schematic showing each process involved during the fabrication of a glass microfluidic device.

Bonding of glass chips

As shown in figure 1.14 the final stage involves the addition of a top plate to the base plate to create a closed environment, this binding typically occurs through thermal bonding (~550 °C) however within this work the antibodies will be immobilised onto the chip prior to bonding the glass plates together, therefore due to the high temperatures that are involved antibody destruction would result, an alternative method therefore is required.

1.7.2.2 Polymer fabrication

One of the most common ways to prepare polymers chips is through injection moulding. This technique allows mass scale manufacture of polymer microfluidic chips.⁹⁸ The principle behind it is the fabrication of a mould that contains the design of the microfluidic device which can therefore be used over and over again. However for each new chip design a new mould would need producing. Melted polymer pellets are injected into the mould at a high temperature and pressure; as it solidifies the polymer takes the shape of the device design.⁹⁹ The mould itself is typically made from a metal such as nickel due to the high pressures and temperatures involved.¹⁰⁰

The mould can be prepared in metals *via* the traditional photolithography technique discussed in section 1.7.2.1, where UV light can be used to map out the design of the microfluidic device. However instead of wet etching this process relies on electroplating to outline the channels.¹⁰⁰ However polymer fabrication is moving away from developing moulds through lithography and to using computer numerical control (CNC) this system works by programming a machine, for example a drill that can be used to fabricate a design into a metal such as aluminium.¹⁰¹ The use of CNC relies on a large initial cost for the machinery and software however after this initial outlay polymer devices can be produced on a large scale for very little cost, the resolution that is possible is very dependent on the equipment and drills purchased, however accuracy can be down to a few microns and is therefore comparable to glass fabrication.

1.7.3 Microflow

Manipulating fluids on such a small scale can have its challenges as parameters such as surface tension become more important.¹⁰² The way fluids are controlled through the microfluidic device stem from the chips design and the pumping method. Pumps are commonly used as a way to introduce fluids and control the rate at which the fluid moves around the device, this is known as pressure driven flow.^{96, 103}

Pressure driven flow is compatible with both aqueous and non-aqueous fluids, the flow required for the system is heavily dependent on the viscosity of the liquid as well as the devices geometry this parabolic flow (figure 1.15). Alternatively applying a voltage across the surface of a channel which is already charged, liquids can be moved by electroosmotic flow (EOF). EOF creates a plug flow profile see figure 1.15.¹⁰⁴

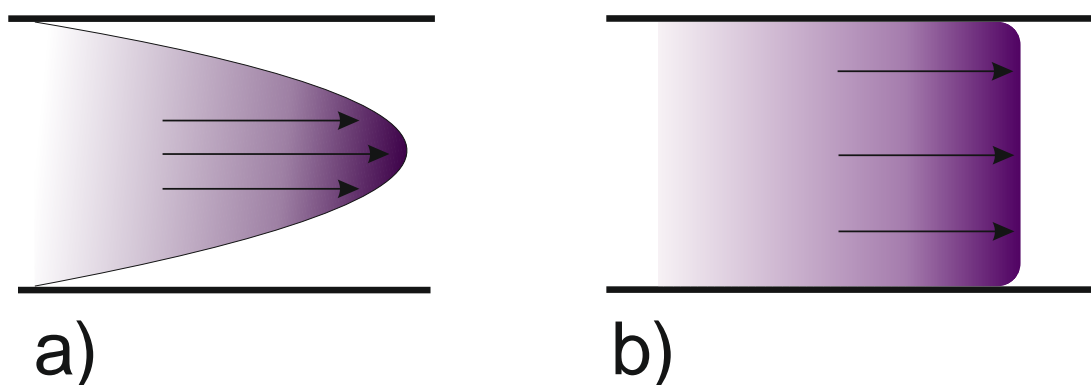


Figure 1.15: Flow profile for a) parabolic flow where the flow is faster within the middle of the stream due to friction from the channel edge and b) EOF showing a plug profile where the liquid flows universally across the channel.

EOF is the flow of liquid where, a potential is applied across the channel and with glass surfaces being negative, counter ions in the bulk solution will become attracted to the surface giving rise to the Stern layer with an electrical double layer as shown in figures 1.16 and figure 1.34. When an electrical field is applied, along with a DC potential across the channel this layer then migrates along the channel taking the bulk solution with it due to hydrogen bonding between the water molecules and the ions present in the solution.

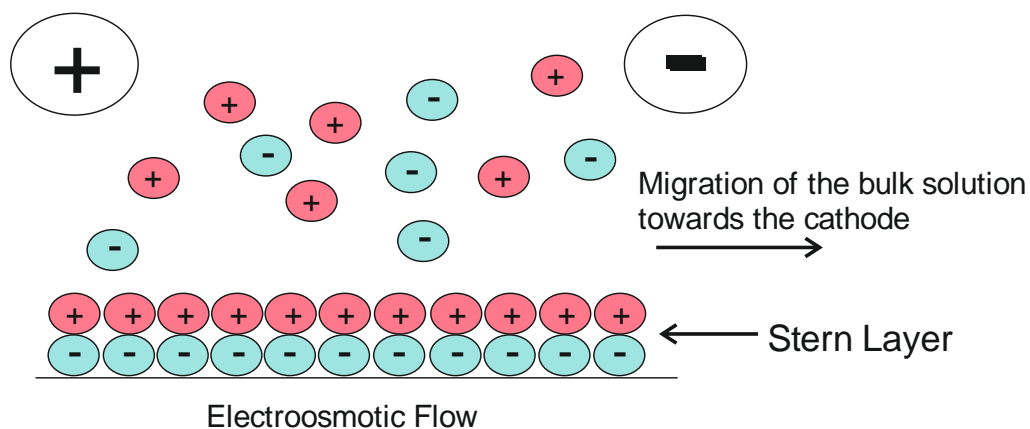


Figure 1.16: Schematic showing how EOF occurs where the negatively charged glass surface attracts the positively charged counter ions. Followed by migration of the bulk flow due to the electrical field.

Taking figure 1.15 where parabolic flow and plug flow are illustrated, the big difference between parabolic and plug flow, with parabolic flow the centre of the flow travels fastest this is due to frictional forces due to the walls of the channels. Whereas during plug flow which is controlled through a voltage the entirety of the flow travels at the same speed across the channel.

Chips that are designed to run *via* EOF generally contain reservoirs where the reagents are placed before any experimentation work is carried out. The flow rate can then be controlled by varying the voltage and from the current that is produced the flow rate can be determined.¹⁰⁵

1.7.4 Mixing of reagents

When carrying out reactions on a microfluidic device, rapid mixing of the reagents is necessary for a POC device. Due to the small channel sizes viscous forces are dominant which affects the flow and laminar flow is observed in these systems. Mixing relies on diffusion of the species across the channel; whereas in turbulent flow, flow is random and mixing occurs fairly easily in comparison.¹⁰⁶ Figure 1.17 shows both turbulent and laminar flow.

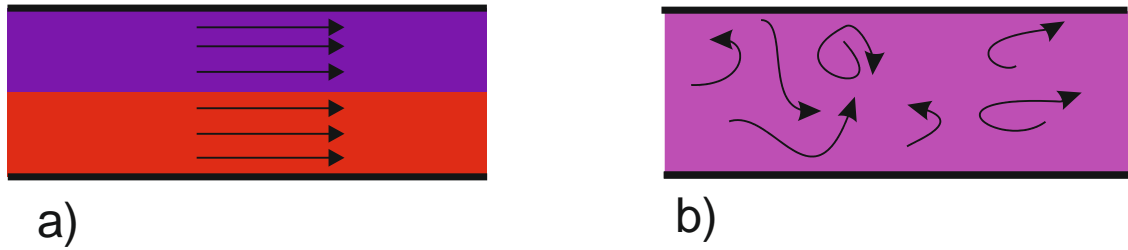


Figure 1.17: a) shows laminar flow where the red and blue represents two separate streams of liquid which will flow side by side, requiring diffusion to mix with b) showing turbulent flow which is largely random and allows mixing to occur at a faster rate.

The Reynolds number is used to determine whether or not flow will be laminar or turbulent.

$$R_e = \frac{\rho v L}{\eta} \quad (1.1)$$

Where: R_e is the Reynolds number, v is the velocity of the liquid (m s^{-1}), ρ is the density of the liquid (kg m^{-3}), η is the viscosity (Ns m^{-2}) and L is the channel diameter (m).

When the Reynolds number is <2000 then the flow is deemed to be laminar and when it is >3000 the flow is turbulent, between this range the system shows properties of both laminar and turbulent flow.¹⁰⁶

For example the Reynolds number is very low (1.5) when flowing water (density of 1000 kg m^{-3}) through a channel which has a typical width of $150 \text{ }\mu\text{m}$, a velocity of 1 cm s^{-1} and a viscosity of 0.001 Ns m^{-2} , therefore mixing relies significantly on diffusion. When it comes to designing the device it is necessary to know the diffusion coefficient of the species in question to determine the length of time for diffusion to occur from one side of the channel to the other. The diffusion coefficient of the species can be determined through Fick's first law on diffusion (Equation 1.2).

$$J = -D \frac{\partial[A]}{\partial x} \quad (1.2)$$

Where J is the flux of the material, D is the diffusion coefficient ($\text{cm}^2 \text{s}^{-1}$), [A] is the concentration of the species (mol L^{-1}) and x is the length of diffusion (m).

From this equation the Einstein-Smoluchowski equation is derived (equation 1.3).

$$X = \sqrt{2Dt} \quad (1.3)$$

Where X is the distance to be travelled (cm), D is the diffusion coefficient ($\text{cm}^2 \text{s}^{-1}$), and t is the time required (s).¹⁰⁷

The diffusion coefficient itself can also be calculated by using Stokes-Einstein's equation (equation 1.4):

$$D = \frac{k_B T}{6 \pi \eta r} \quad (1.4)$$

Where D is the diffusion coefficient ($\text{m}^2 \text{s}^{-1}$), k_B is Boltzmann's Constant ($1.38 \times 10^{-23} \text{ m}^2 \text{ kg s}^{-2} \text{ K}^{-1}$), T is the absolute temperature (K), η is the viscosity of the fluid (Pa.s) and r is the Stoke's radius of the molecule (m).

For most small molecules a typical diffusion coefficient is on the order of $10^{-10} \text{ m}^2 \text{ s}^{-1}$. So

Table 1.2 shows the calculated diffusion times at different distances.

Distance	Time to diffuse
10 mm	138 hrs
1 mm	83 mins
100 μm	50 s
10 μm	0.5 s
1 μm	5 ms

Table 1.2: Diffusion times of a small molecule across various distances.

Having calculated these values for small molecules, this data can be used to approximate the diffusion times for progesterone and oestriol which is useful in designing the chip as discussed in section 2.4.

1.7.5 Detection methods on microfluidic chips

Microfluidic devices have been developed for many different analytical applications, these can include but not limited to; bioanalysis,¹⁰⁸ pharmaceutical analysis^{109, 110}, clinical^{111, 112} and forensic applications.¹¹³ The wide variety of applications on microfluidic devices stems from the ability to design and use them to compliment a variety of detection methods. Electrochemical and spectrometric methods are most commonly used in conjunction with microfluidic devices for portable applications.¹¹⁴

Spectrometric detection

Spectrometric detection includes UV-Vis spectrometric, fluorescence and chemiluminescence methods.

Spectrophotometric detection in LOC

Spectrophotometric techniques are commonly used as a way to detect and quantify many different molecules, which is why this methodology is increasingly popular when using microfluidic devices. However generally when carrying out UV-Vis spectroscopy the cuvette used is typically 1 cm and incorporating this technique into a microfluidic device would normally reduce the dimensions of the detection cell, which through the Beer-Lambert Law (equation 1.5) causes a reduction in the path length, resulting in a substantial decrease in the sensitivity of the system.

$$A = \log \frac{I_0}{I} = \epsilon cl \quad (1.5)$$

Where A is the absorbance, I_0 is the initial intensity of light prior to absorption, I is the intensity of light after absorption, ϵ is the molar absorptivity coefficient ($\text{dm}^3 \text{mol}^{-1} \text{cm}^{-1}$), c is the concentration (mol dm^{-3}) and l is the path length (cm).

Another disadvantage to this method is the requirement of an external light source which can greatly influence the design of a microfluidic device, however research has been able to reduce the size of these light sources for example incorporating light-emitting diodes (LEDs) into the devices themselves.

Fu *et al.* developed an integrated microfluidic system where the quantification of methanol and sulfur dioxide was required. The integrated system used an LED that emitted light at 430 nm, this light was then picked up by a photodiode which when attached to a voltmeter read a voltage. This voltage was inversely proportional to the concentrations of methanol and sulfur dioxide with results being no more than 3.7 % different from those obtained *via* the normal spectrophotometric methods. The group also stated that the LED itself can be changed to emit a wavelength that is suitable for detecting other molecules.¹¹⁵ Other approaches include using fibre optics and a microspectrometer this would allow the device to be entirely portable which for a clinical setting is not essential but can allow clinicians to take devices with them when treating patients at home.

Nicolini *et al.* developed a way to increase the path length by modifying a surface to decrease its wettability resulting in the formation of droplets. Through this method the droplet that had formed increases the path length increasing the sensitivity of the system; which is an issue of microfluidic devices.¹¹⁶

Fluorescence

Fluorescence is a property that some molecules exhibit where they have the ability to absorb light at one wavelength and then emit light at another wavelength that is longer than the initial incident wavelength, these molecules are called fluorophores. The intensity of the fluorescence is described by equation 1.6:

$$I = kP_0c \quad (1.6)$$

Where I is the intensity of the incident light, c is the concentration of the emitting species (mol dm^{-3}), P_0 is the radiant power of the incident light and k is a constant.¹¹⁷ However limitations to this equation are that this only applies at very low concentrations of analyte, whereby at higher concentrations the inner filter effect can prevent accurate analysis of analytes in a solution. What the equation does tell us however is that the intensity of light is proportional to the radiant power; meaning we can analyse very low concentrations of analyte by using a powerful light source making it a very sensitive technique. However these light sources are not cheap.

The process of fluorescence is illustrated by the Jablonski diagram, (figure 1.18). This diagram shows that a species will absorb a photon which results in the excitation of an electron to an excited singlet state. This electron through internal conversion (IC) will relax to another excited singlet state. The electron can then undergo one of two options:

- The electron returns to its ground state emitting light through fluorescence (F) or chemiluminescence (CL) if the excited state is generated through a chemical reaction and not the absorption of a photon (section 1.8).
- Undergo intersystem crossing (ISC) to an excited triplet state. N.B. this process is spin forbidden, and then relax back to the ground state emitting light through phosphorescence.

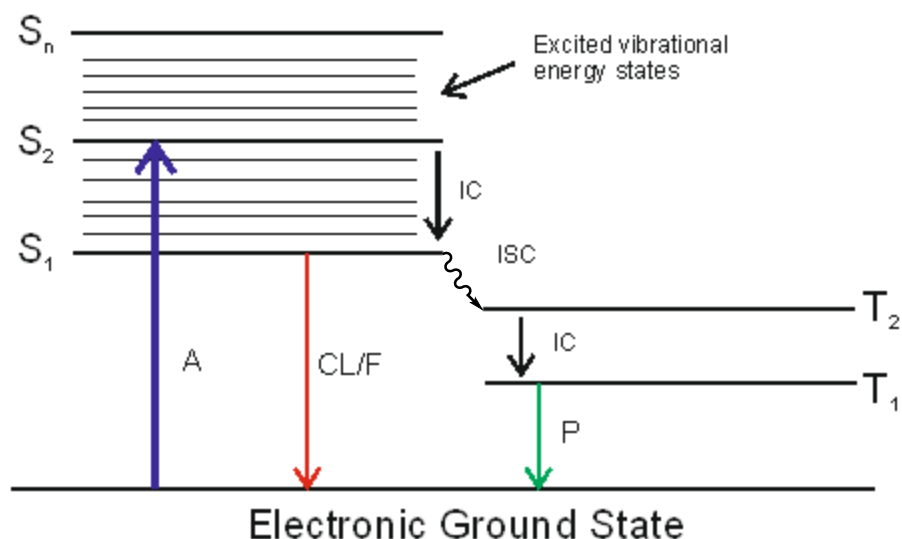


Figure 1.18: Jablonski diagram showing the excitation of an electron followed by the various routes this may take upon relaxation, where S and T represent the singlet and triplet states respectively, A is adsorption, CL/F is chemiluminescence and fluorescence respectively, P is phosphorescence, IC is internal crossing and ISC is intersystem crossing.

The high sensitivity of fluorescence means it is commonly used as a method for clinical applications generally through immunoassays.¹¹⁸

1.8 Chemiluminescence

Chemiluminescence (CL) is the emission of light resulting from a chemical reaction. It is similar to fluorescence however unlike fluorescence where the electron excitation occurs through the absorption of a photon, in CL the excitation is the result of a chemical reaction.

The efficiency of a CL reaction can be given by its quantum yield which is shown in equation 1.7.

$$\Phi_{CL} = \Phi_R \times \Phi_{ES} \times \Phi_F \quad (1.7)$$

Where Φ_R reflects the chemical yield of the chemical reaction, Φ_{ES} is the fraction of the product that enters the excited state and Φ_F is the fluorescence quantum yield.

There are cases however where the CL results from an energy transfer from the excited state to a fluorophore causing a secondary emission in this case the energy transfer efficiency (Φ_{ET}) as well as the fluorescence efficiency of the acceptor (Φ'_F) needs to be addressed. Equation 1.8 illustrates this.¹¹⁹

$$\Phi_{CL} = \Phi_R \times \Phi_{ES} \times \Phi'_F \times \Phi_{ET} \quad (1.8)$$

For a chemiluminescence reaction to occur an electron needs to be promoted to an excited state which unlike fluorescence where this excitation occurs from visible light in chemiluminescence it comes from the reaction itself; meaning that a large amount of energy is needed for this process typically (40-70 kcal mol⁻¹)¹¹⁹ therefore the reaction needs to be sufficiently exothermic for this to occur. These chemical reactions are typically redox reactions where one molecule is oxidised and another is reduced occurring through the transfer of an electron.

Electron transfer mechanisms

It is necessary to briefly look at how a redox reaction takes place as the electron transfer can occur through two mechanisms, the inner sphere and outer sphere. Electron transfer through the inner sphere mechanism relies on two reacting species sharing a ligand through which the electron is transferred, the outer sphere mechanism relies on the two reacting species being in close proximity to each other with the electron tunnelling between the two metal species. (Figure 1.19)

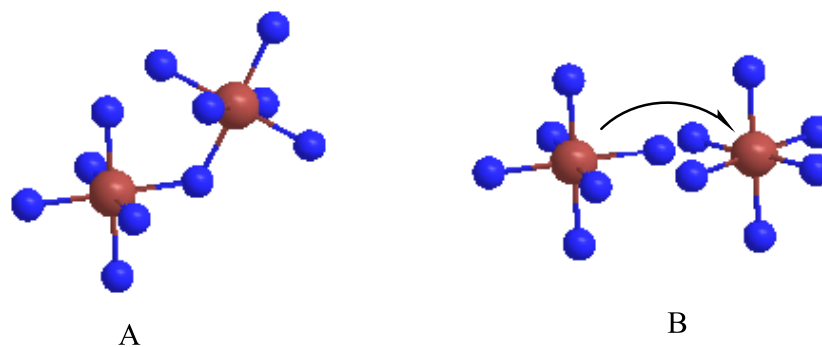


Figure 1.19: Mechanisms representing a) inner sphere and b) outer sphere electron transfer processes.

Figure 1.19a shows the bridging between the two metal centres where the electron transfer can take place, within figure 1.19b the arrow represent the electron transfer occurring through electron tunnelling between the two metal centres. In CL reactions the electron transfer occurs through the outer sphere mechanism.¹²⁰

Having examined the chemical process for electron transfer, the kinetics of the system needs exploring, for most chemical processes the reaction follows transition state theory which discusses how reactions takes place and states that the formation of the products is favoured over remaining as reactants, i.e. the products need to be lower in energy than the reactants (figure 1.20).

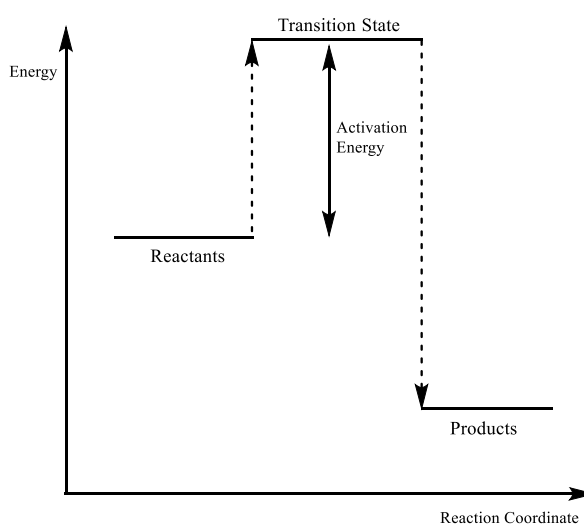


Figure 1.20: Energy profile for a typical chemical reaction.

Figure 1.20 shows that the reactants are higher in energy than the products, insinuating that the formation of the products are favourable. However as the figure shows the transition state is higher in energy still and therefore an activation barrier needs overcoming, this is known as the activation energy. What this means is that energy needs putting into the system to initiate the chemical reaction. Transition state theory is useful for reactions where bonds are broken and formed, this is not the case for electron transfer processes, for these scenarios Marcus theory outlines the relationship between transition states and activation energies required.¹²⁰

Marcus Theory

In 1956 Rudolph Marcus proposed a theory to show the rate of electron transfer, this theory shows the amount of energy that is required to enable an electron transfer to occur, the theory states that the activation energy (ΔG^\ddagger) is low when the reactants and products are similar in molecular geometry; with the activation energy being large when the reactants and products respective geometries are substantially different, this is shown by figure 1.21 where the greater change in the reaction coordinate (Δx) the larger the activation energy required:

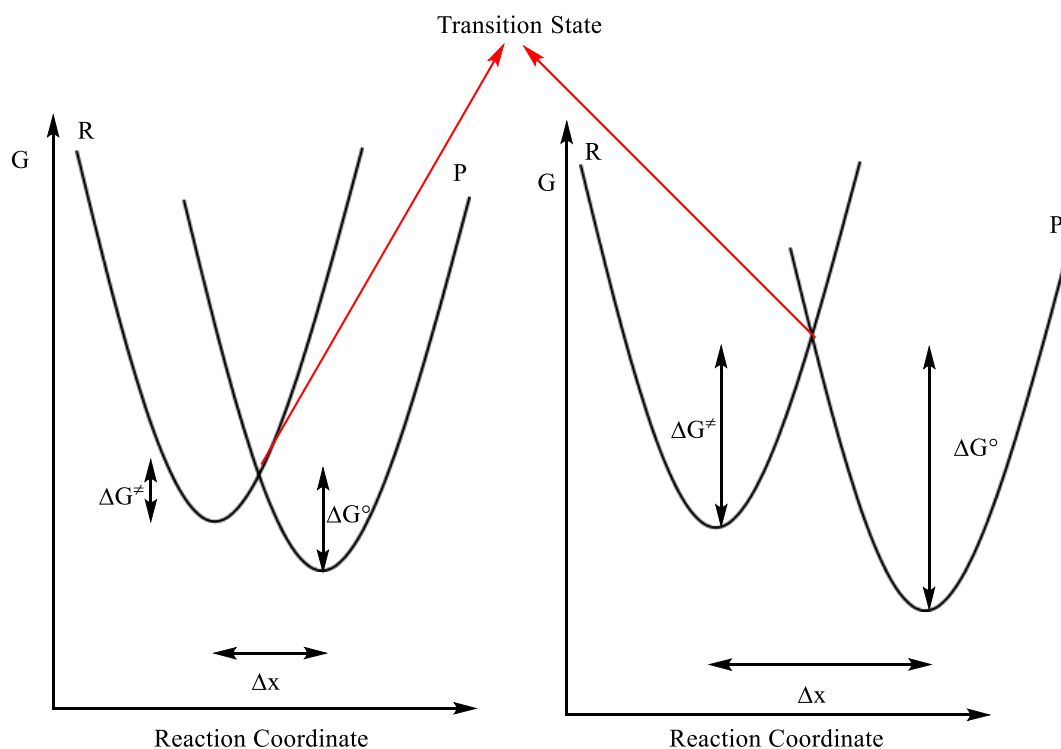


Figure 1.21: Schematic showing how the change in the reaction coordinate affects the activation energy required for successful electron transfer.

Figure 1.21 shows how the activation is affected by the reaction coordinate with a larger reaction coordinate resulting in a larger activation energy. These figures shows the systems as parabolic this is to follow Hook's Law which states that vibrational energy states are harmonic oscillators. The transition steps occur after a vertical increase in energy, this is caused by the Frank-Condon principle; which suggests that the electron transfer is so rapid that no nuclear configuration can take place.

The Marcus model followed on from previous work by Libby which shows that slow electron transfer kinetics is a result of solvation effects, where a reorganisation of the oxidised or reduced species needs to take place, this is due to the electrostatic interaction between the solvent molecules and the redox species.¹²¹ Marcus took this further, within his model the reorganisation is given by the term λ . His model expands to show the probability of electron transfer as well as the rate constant for this process as ΔG becomes more negative.

Marcus looked at the probability of electron transfer occurring which is due to the strength of the coupling between the electron donor and acceptor, he outlined two ways for this to occur which is adiabatic and non-adiabatic (figure 1.22).

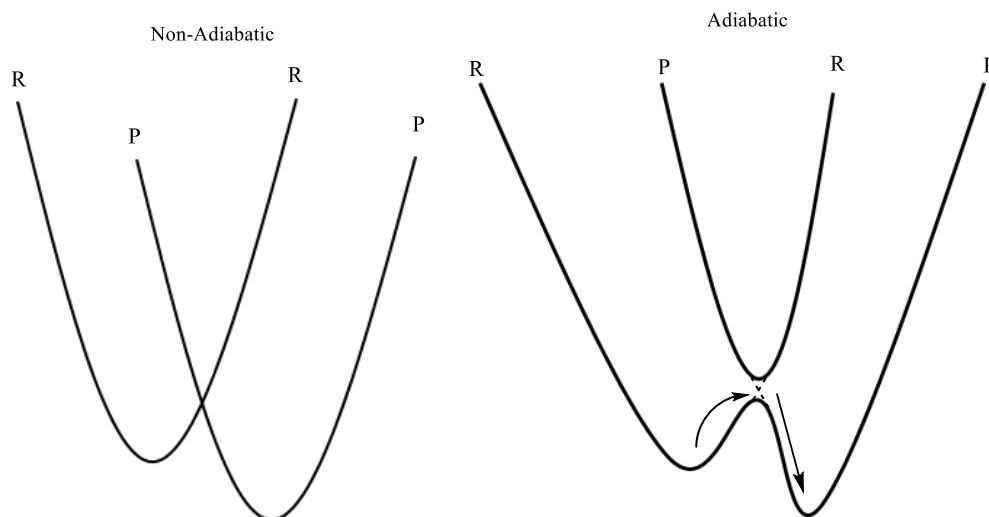


Figure 1.22: Schematic showing the parabolas for a non-adiabatic and adiabatic system.

Figure 1.22 shows parabolas for non-adiabatic and adiabatic systems, a non-adiabatic system involves a quantum jump between the two curves, an adiabatic system is one that is impassable to heat; i.e. no heat is generated or lost. With respect to electron transfer no quantum jump occurs instead the two curves form a continuum whereby the electron transfers smoothly between the two states.¹²²

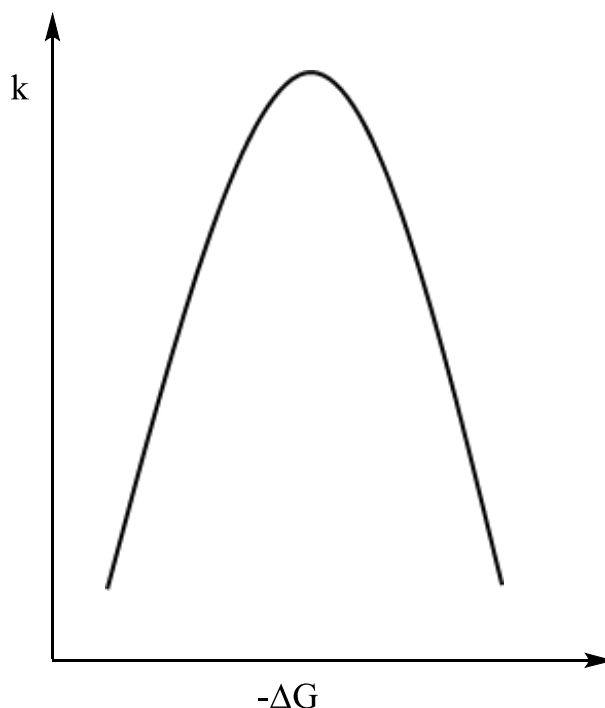


Figure 1.23: Schematic profile showing how the rate constant changes when the negative Gibb's free energy increases.

The key finding from Marcus was that the rate constant increases as the electron transfer becomes more exothermic, this is known as the normal region; what was of note which can be seen in figure 1.23 where at a certain point, as the electron transfer becomes more exothermic the rate constant decreases, this is known as the Marcus “inverted” region. At the tip of this bell curve the process is activation-less ($\Delta G^\ddagger=0$).

To assist in understanding the Marcus model it is necessary to look at Arrhenius' expression, this expression shows the relationship between the rate of reaction and the activation energies (Equation 1.9).

$$k = A \exp^{-\frac{E_a}{RT}} \quad (1.9)$$

Where: k is the reaction rate constant, E_a is the activation energy, R is the universal gas constant, T is the absolute temperature and A is a pre-exponential factor.

What the Arrhenius expressions tells us is that for large activation energies the rate constant will be small and for low activation energies the rate constant will be large which is indicative of a CL reaction where the system needs to be sufficiently exothermic to allow the excitation of the electron, typical 40-70 kcal mol⁻¹ is required.¹²³ However as figure 1.23 shows as the Gibbs energy gets more negative the rate constant decreases indicating that CL reactions take place in the Marcus “inverted” region.

Through the Marcus model there is an assumption that the reactant (R) and product (P) curves are parabolic and therefore follows:

$$\Delta G^\ddagger = \frac{(\lambda + \Delta G^o)^2}{4\lambda} \quad (1.10)$$

Figure 1.24 explains this equation graphically:

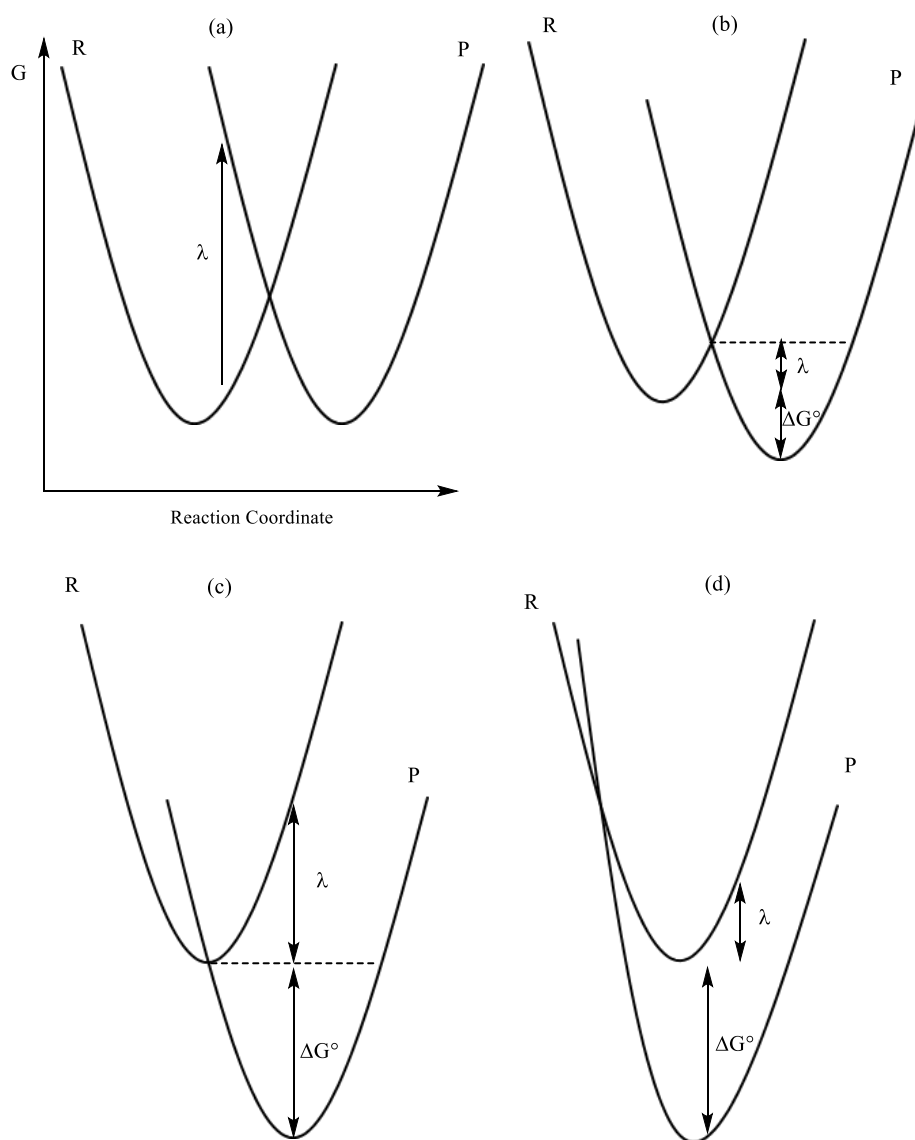


Figure 1.24: Parabolic profiles showing the different electron transfer pathways, where a) represents a scenario where the reaction is neither exothermic nor endothermic, b) the normal Marcus region, c) the activation-less region and d) the Marcus inverted region.

Figure 1.24a occurs when $\Delta G^\circ = 0$ and therefore ΔG^\ddagger is equal to $\lambda/4$, in profile (b) ΔG° is becoming negative resulting in a small λ and therefore a lower activation energy, this profile is a representation of the normal region. In (c) $\Delta G^\circ = \lambda$ this profile represents the top of the bell plot shown in figure 1.23, at this point the electron transfer is activation-less ($\Delta G^\ddagger=0$) and finally profile (d) shows the situation where ΔG° becomes so negative that the activation energy will start to increase, which is the Marcus inverted region.

Finally this can allow us to derive an expression to calculate the rate constant for a redox reaction which like Arrhenius relates energy to the rate constant however taking into account all the different parameters that affect electron transfer:

$$k_{ET} = k_{el} \nu_n \exp \left[\frac{-(\lambda - \Delta G^o)^2}{4\lambda k_B T} \right] \quad (1.11)$$

Where k_{ET} is the rate constant for the electron transfer, k_{el} is the electron transmission coefficient, ν_n is the vibrational frequency of the transition state, k_B is Boltzmann's constant and T is the absolute temperature.

This equation is known as the Marcus equation by taking the assumption that the curves are parabolic and combining with transition state theory.^{124, 125} CL reactions are observed within the Marcus inverted region and was reported as such in 1965.¹²⁶

Electron Transfer in CL reactions

Hercules describes the electron transfer process within chemiluminescent reactions particular well, they state that for a CL reaction to occur the system needs to favour the formation of the excited state rather than the ground state i.e. the excited intermediate has a lower activation energy than the straight formation of the ground state products (figure 1.25).

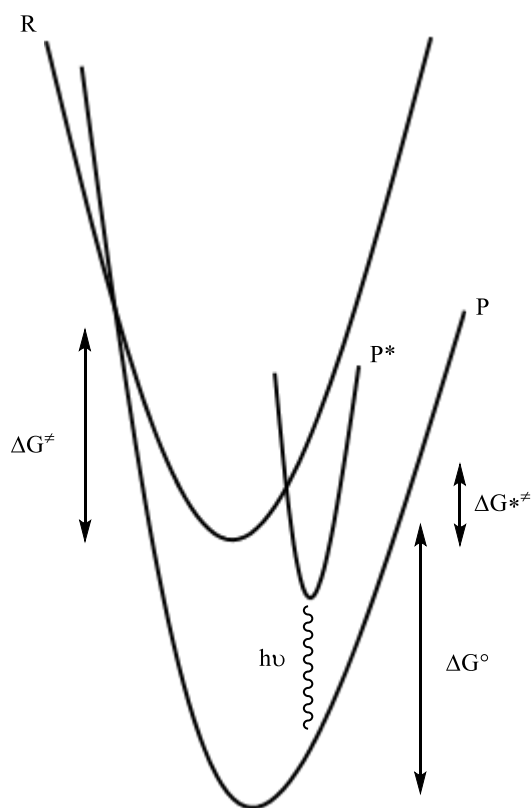


Figure 1.25: Energy profile showing the electron transfer processes for a chemiluminescence reaction.

For a CL reaction that gives off absolute light intensity the formation of the excited state needs to be favourable, as can be seen in the figure that the formation of the products is exothermic with respect to the formation of the ground state products and the excited state products, however the formation of the excited state products has a lower activation requirement and is therefore kinetically favoured, resulting in the formation of the excited state and subsequently the emission of light. CL reactions occur as an example of the inverted region because as the system becomes more exothermic more energy is then required to activate the formation of the ground state products.¹²⁷

Having explored the theory behind the phenomenon of chemiluminescence lets investigate the various molecules that can exhibit this.

1.8.1 Molecules involved in chemiluminescence reactions

1.8.1.1 Peroxyoxalates

Peroxyoxalates are oxalates that have been treated with hydrogen peroxide, this molecules when in contact with dyes emit light, with the dye that is used affecting the colour of the light that is emitted. It is through these molecules that glow sticks operate. These molecules operate where the light emission comes from the fluorophore and not from the products of a chemical reaction as is the case with luminol for example. As stated this allowed the emission of the light to be controlled by the fluorophore used in the reaction. Peroxyoxalates are not used with regards to immunoassay therefore they will not be discussed further.

1.8.1.2 Lucigenin and acridium esters

Lucigenin (10,10'-dimethyl-9,9'-bisacridinium dinitrate) (Figure 1.26) reacts in a similar fashion to that of luminol and undergoes oxidation using hydrogen peroxide or oxygen as oxidants however the light emitted is very intense especially when in the presence of transition metals such as cobalt (II) where a bright blue-green light is observed.

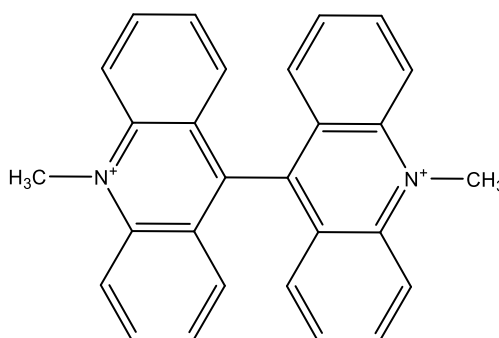


Figure 1.26: Structure of lucigenin.

From the figure we can see that lucigenin has the acridinium backbone this means a number of other molecules that are closely related to lucigenin can exhibit chemiluminescence properties. Weeks *et al.* successfully synthesised 4-(2-succindimidyloxycarbonylethyl)phenyl-10-methylacridinium-9-carboxylate fluorosulfonate see figure 1.27. ¹²⁸

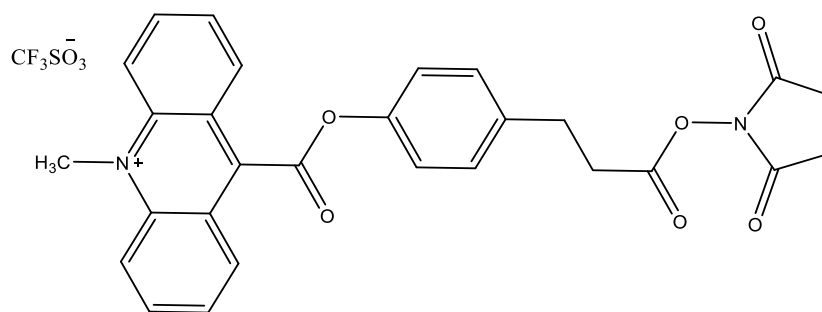


Figure 1.27: Structure of 4-(2-succindimidyloxycarbonylethyl)phenyl-10-methylacridinium-9-carboxylate fluorosulfonate synthesised by Weeks *et al.* ¹²⁸

Weeks used this molecule as a label tagged to an antibody that can then be used in immunoassays, which was very advantageous at the time when the majority of immunoassays relied on radio labels. These esters have the big advantage that they do not rely on an external oxidant such as hydrogen peroxide, however they rely on harsh basic conditions (pH 12-13) to give the optimum CL response. Also these esters are fairly unstable and within this basic environment and with oxygen the pseudo base can form that does not undergo any CL responses. ^{119, 128, 129}

1.8.1.3 Acylhydrazides

Luminol is one of the most familiar molecules that exhibit chemiluminescence and has been studied extensively since it was first reported by Albrecht in 1928. ¹³⁰ Luminol along with an oxidant, usually hydrogen peroxide under alkaline conditions produces light. This reaction can be enhanced by the use of catalysts, these include enzymes (that have already been mentioned for immunoassay detection) and metals, many of the 3d metals can act

as a catalyst such as copper, iron, manganese, iron and cobalt.¹¹⁹ Luminol is also unique in that within the aqueous phase it will emit light in the blue region of the electromagnetic spectrum, whereas in an aprotic solvent a yellow/green light is emitted.¹¹⁹

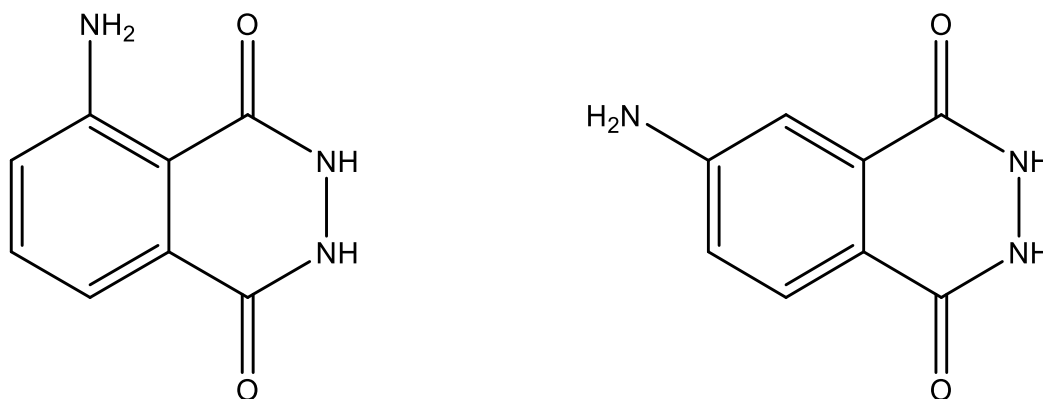


Figure 1.28: Structures of luminol and isoluminol.

Isoluminol is an isomer of luminol where the amine group is found in the 4 position rather than in the 5 position, isoluminol; as expected has a similar chemiluminescence efficiency as luminol but due to the position of the amine group it reduces steric issues and therefore can be used in chemiluminescence labelling, however it is substantially more expensive than luminol.¹³¹

Luminol is commonly used with hydrogen peroxide, where the hydrogen peroxide acts as an oxidising reagent

Figure 1.29 shows the luminol and hydrogen peroxide reaction:

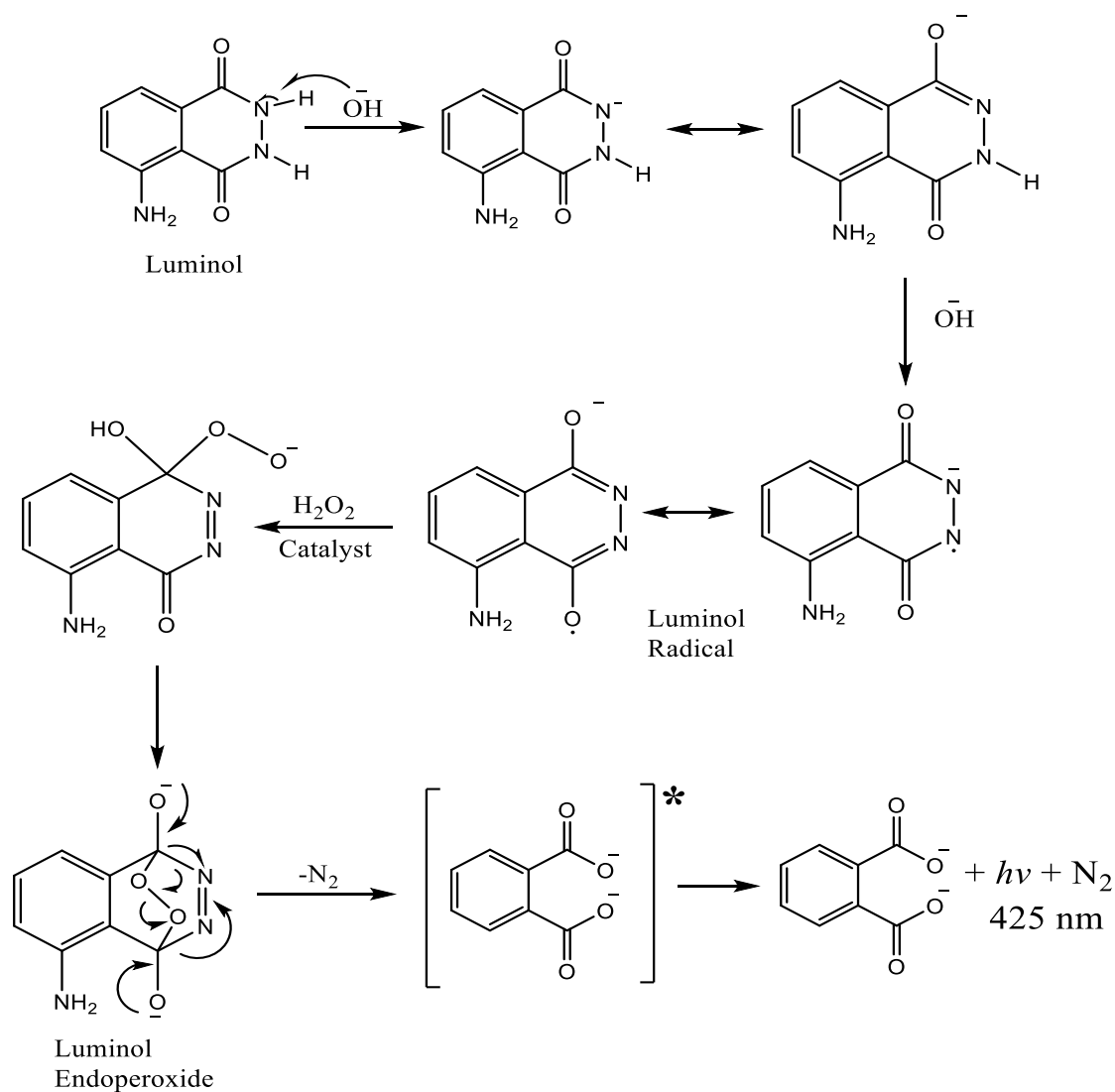


Figure 1.29: Mechanism showing the luminol reaction when in a basic aqueous environment followed by its reaction with hydrogen peroxide which emits light at 425 nm. Adapted from Chemiluminescence and Bioluminescence Past, Present and Future.¹³²

Once luminol is dissolved in a base the acidic protons bound to the nitrogen atoms dissociate forming the anion radical. Upon interaction with hydrogen peroxide and a catalyst the oxygen from the peroxide attacks the positive carbon due to the presence of the ketone. This forms luminol endoperoxide. As the nitrogen cleaves off and leaves the excited state is formed which upon relaxation emits light.

The mechanism outlined is one of the most commonly presented in the literature and is also found in the textbooks.¹³³ There are however other mechanisms presented in the literature that deviate slightly from the one outlined here, Puga Molina *et al.* presents a mechanism that is very similar however they state that when the peroxide attacks the luminol the hydrogen atom remains a part of the peroxide and does not form the hydroxyl group presented above.

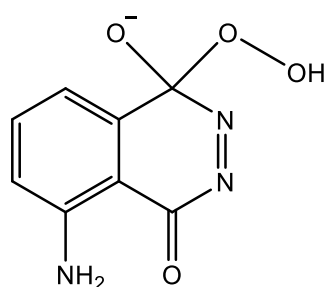


Figure 1.30: the alternative intermediate outline by Puga Molina.¹³⁴

The role of a catalyst is not detailed in the text book mechanism, Chen *et al.* used copper nanoparticles¹³³ as a catalyst while Puga Molina used titanium (III).¹³⁴ While there is agreement with the general process the exact intermediary steps is up for discussion which could well be catalyst dependant.

Luminol itself is not soluble in water, therefore to aid the solubility the luminol is dissolved in a base, the basic environment allows dissolution as well as increasing the intensity of light emitted, due to the base being able to remove the protons on the nitrogen groups, resulting in the luminol becoming more reactive resulting in a larger emission of light, however this does impact the shelf life of the solutions, which needs to be taken into account when designing a system that relies on luminol detection methods.¹³⁵

Cobalt (II) is a well-known chemiluminescence catalyst and quite a lot of work has been carried out where cobalt is detected at sub ppb levels based on its efficient catalysis.¹³⁶

In 1975 Burdo and Seltz proposed a mechanism of how cobalt catalyses this reaction and this shown in figure 1.31:¹³⁵

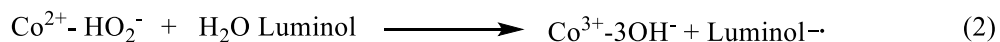


Figure 1.31: Proposed mechanism for the cobalt catalysis of luminol and hydrogen peroxide.

Burdo proposed that for the luminescence to occur cobalt and peroxide react to form a cobalt-peroxide intermediate, step 1 within the figure. Step 2 shows that this intermediate reacts with luminol in aqueous media to form the luminol radical, Burdo claims this is the rate determining step. This radical then reacts with peroxide to release light (step 3). Comparing this to the general mechanism described above (figure 1.29) the mechanism suggested here is different to that presented which again shows there is minimal agreement as to what the mechanism for this reaction is.

Kinetics of the luminol reaction

The reaction of luminol and hydrogen peroxide exhibits fast reaction kinetics, Lind reported that in aqueous solution the luminol and hydrogen peroxide reaction can have a rate constant of $2 \times 10^5 \text{ s}^{-1}$.¹³⁷

From the various molecules that can be used to carry out chemiluminescence reactions, the luminol and hydrogen peroxide reaction will be utilised due to the commercially available HRP; as well as the extensive use of this combination of reagents in the literature.

1.8.2 Chemiluminescence in microfluidic immunoassays

Chemiluminescence as a detection method is heavily utilised in microfluidics as the chemical reaction generates the light that can be measured unlike other spectroscopic techniques that require an external light source.

In recent times there has been an increase in the number of papers published using CL immunoassays in LOC with the need to use smaller and less complicated systems, it has been shown that CL immunoassays can be heavily utilised on chip.¹⁰⁸ A few examples of current applications are discussed:

Fan *et al.* developed a microfluidic CL immunoassay system to quantify the protein α -fetoprotein. This protein is produced typically by the foetal liver and the levels subside after birth and is largely illusive in adults. However if this protein is found in large concentrations this could indicate the early onset of liver cancer. The development of a microfluidic device allows rapid detection of this protein, combining this with chemiluminescence allows the required sensitivities to be reached. In this example a limit of detection of 1.5 ng mL^{-1} was determined in serum. This system was based on using HRP as the CL catalyst with luminol and hydrogen peroxide.¹³⁸

Pires and Dong developed a microfluidic system that uses chemiluminescence immunoassays to monitor waterborne pathogens in this case *Legionella pneumophila*, within this work the HRP based chemiluminescence system was again utilised however they also included the use of gold nanoparticles, these nanoparticles enhanced the CL signal making it more sensitive and allowing 25 times improvement over previous methods.¹³⁹

Due to the sensitivities that can be achieved through CL, as well as the ease and simplicity of the detection method; this method was chosen to take forward and investigate to quantify the concentrations of progesterone and oestriol in saliva. CL is definitely a method that can be used within point-of-care systems.

1.8.3 Chemiluminescence detection

To collect a chemiluminescence emission a dark environment is required to house the detector. Detection is achieved by two main methods, the use of a photomultiplier tube or a charge coupled device (CCD). CCDs are usually used in conjunction with a camera, both of these tools have their advantages and disadvantages and each will be discussed fully. The types of detector chosen have a wide dynamic range, so that they can detect both very low levels of light emitted as well as light that is produced at a higher intensities. The light has to be detected within the region that luminol emits, which is 425 nm in aqueous media so the detector should work within the 400 – 500 nm range.

Photomultiplier tubes

Traditionally photomultiplier tubes have been the most popular photodetector with its high sensitivities, due to its ability to detect a very small number of photons, figure 1.32 shows how a photomultiplier tube operates.

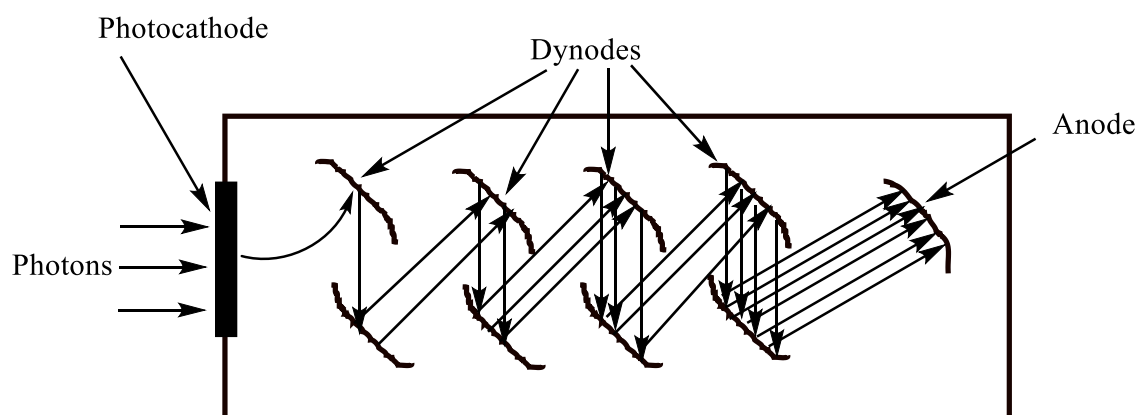


Figure 1.32: A schematic showing the operation of a photomultiplier tube.

Initially the photon interacts with the photocathode, which is commonly made from antimony that is doped with a variety of different group 1 metals.¹⁴⁰ After interaction with the photon a photoelectron is released due to the transfer of light energy to the electron. As these electrons travel through the tube they are amplified *via* a series of dynodes at increasing voltages until the anode is reached; the current that has been generated through the system is then measured.¹¹⁹ Photomultiplier tubes have the benefits of being very sensitive; however carrying out multiplexing is more challenging as the photomultiplier tube would need to be coupled with a monochromator; alongside this the analytes would have to emit light at different wavelengths and then analysed individually. This would lead to a complicated detection system, because of this these detection systems are not utilised within this investigation.

Charge coupled devices (CCD)

Within a CCD there are separate areas; as can be seen from figure 1.28 these separate areas are called pixels these pixels absorb photons which are stored for the duration of the exposure. After this time the pixels are integrated against the time that the image was taken to give an image which can then be analysed. Through the use of a CCD integrated into a camera and a heterogeneous immunoassay we can measure the concentrations of both progesterone and oestriol within one sample. The image provided allows the spatial resolution by having an understanding of what the image is displaying and therefore which antibodies the light signal is coming from.

How does a CCD operate?

CCDs can be integrated into a camera; this can allow the analysis of multiple analytes through analysis of the image that is detected. Figure 1.33 shows how a CCD operates.

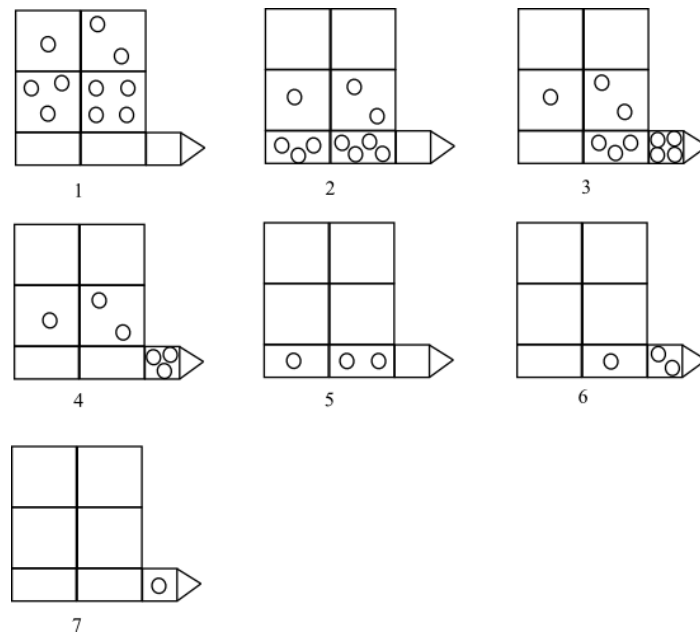


Figure 1.33: Schematic showing how a CCD operates based on a 2 x 2 pixel chip, where the circles represent photoelectrons that are stored within the pixels.¹¹⁹

From figure 1.33, step one represents the end of the exposure. During the exposure as the CCD absorbs the photons of light; the electrons are promoted from the valence to conduction bands and stored within the individual pixels of the camera.

Step 2 shows that the charge stored within each row transfers down one row, this results in the lowest row being transferred to the readout area.

Step 3 the charges within the readout register and then transferred to the charge to voltage convertor (CVC) where the charge is converted to a voltage.

Step 4 shows the last pixel content from the read-out register has been transferred into the CVC.

Step 5 shows the next pixel row being transferred to the lower row.

Steps 6 and 7 represent a repeat of steps 3 and 4 until all the charge has been cleared and the CCD is ready for the next exposure.¹¹⁹

1.9 Electrochemistry

The use of electrochemical measurements are of great benefit due to the high amount of control that can be achieved through these techniques, with that the technique in itself becomes quality control of a redox process simply by looking at the voltammograms and knowing what is on and around the electrode surfaces. Electrochemistry has the benefits of very good sensitivities with respect to immunoassays Liu *et al.* achieved fmol limits of detection.¹⁴¹

What is electrochemistry?

An electrochemical experiment typically involves a solution that contains electrolyte and redox species that is under investigation. When a potential difference is applied across the electrode-solution interface redox species undergo either oxidation or a reduction; this is dependent on the potential applied. Through this applied potential the electrical double layer is formed figure 1.34:

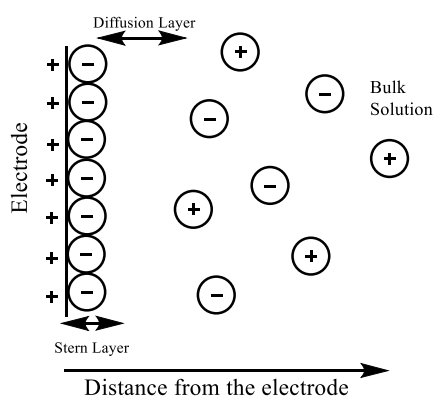


Figure 1.34: Schematic representing the electrical double layer.

1.9.1 Movement of ions towards the electrode

Generally when redox species are being oxidised a positive current is observed and when the species are reduced a negative current is observed. This current is known as Faradaic current and obeys Faraday's Law of electrolysis. Equation 1.12.

$$m = \left(\frac{Q}{F}\right) \left(\frac{M}{z}\right) \quad (1.12)$$

Where m is the mass of the species liberated from the electrode surface (grams), Q is the electrical charge passed through the substance (coulomb), F is Faraday's constant $96485.4 \text{ C mol}^{-1}$, M is the molecular mass of the species (g mol^{-1}) and z is the number of electrons transferred per ion. Where $Q = it$ where i is the current and t is time; showing there is a relationship between the amount of substance and the current passed.

It is necessary that there is constant flux of material to the electrode surface to allow current to be produced. This current is proportional to the concentration of the redox species in solution. The constant flux of material occurs through mass transport.

There are three main ways mass transport can occur and this is through diffusion, migration and convection it is important to note that the current observed is because of all these three reasons.¹⁴²

Diffusion

Diffusion is the migration of molecules from an area of high concentration to an area of low concentrations, as described in section 1.7.4.

The current produced is proportional to the diffusion coefficient as expressed in equation 1.12:

$$i_A = nFAD_A \frac{[A]_{bulk} - [A]_{x=0}}{\delta} \quad (1.13)$$

Where i_A is the current produced (Ampere), n is the number of electrons transferred, F is Faraday's constant ($96485.4 \text{ C mol}^{-1}$), A is the electrode area (cm^2), D_A is the diffusion

coefficient (cm s^{-1}), $[A]$ is the concentration of species A in the bulk solution (M) and at a distance (x) of 0 from the electrode surface and δ is the diffusion layer thickness (cm).¹⁴²

Migration

Migration is the movement of charged species against an electric potential gradient due to the potential that is exerted upon a solution. However due to the diffusional double layer described previously migration is difficult to measure, therefore to compensate for this a huge excess of electrolyte is used, typically in the region of 0.1 M, so all the current that comes from migration is from the background electrolyte and not from the redox species in question. The flux through migration can be calculated by equation 1.14:

$$J_A = DzE[A]F/RT \quad (1.14)$$

Where J_A is the flux of the material, D is the diffusion coefficient (m s^{-1}), z is the charge on the ion, E is the electric field (N C^{-1}), $[A]$ is the concentration (M), F is Faraday's constant ($96485.4 \text{ C mol}^{-1}$), R is the universal gas constant ($8.3142 \text{ J mol}^{-1} \text{ K}^{-1}$) and T is the absolute temperature (K).

Convection

Convection is the mechanical movement of the species in a solution, this occurs either through natural forces or mechanical forces. Natural forces include gravity, temperature affects; surface tension etc. These are difficult to control and model, however these are not significant over short timescales $< 10 \text{ s}$. Mechanical forces occur through human processes such as stirring the solution. The flux through convection is measured by equation 1.15:

$$J_A = V_A[A] \quad (1.15)$$

Where J_A is the flux of the material, v is the solution velocity (m s^{-1}) and $[A]$ is the concentration (M).¹⁴³

Combining all three forms of mass transport equations, (equations 1.2, 1.14 and 1.15) gives the Nernst-Planck equation:

$$J_A = -D_A \frac{\delta[A]}{\delta x} - \frac{D_A z E [A] F}{RT} D_A + v[A] \quad (1.16)$$

Where J_A is the flux of the species, $[A]$ is the concentration (M), x is the distance from the electrode surface (cm), D is the diffusion coefficient (cm s^{-1}), E is the electric field (N C^{-1}), z is the charge of the species, F is Faraday's Constant ($96485.6 \text{ C mol}^{-1}$), R is the universal gas constant ($8.3142 \text{ J mol}^{-1} \text{ K}^{-1}$), T is the absolute temperature (K) and v is velocity (m s^{-1}).

Electrochemistry in microfluidic systems

Incorporating electrodes into microfluidic devices can provide a simple; low cost route to detect and monitor analytes; electrochemical routes have very good sensitivities.^{144, 145} For example Chen *et al.* used gold nanoparticles as an electrochemical route to detect haemoglobin A1c which is a biomarker that can give information on a patients glucose levels, within their work the nanoparticles were tagged to the anti-haemoglobin antibodies. This system operated through a sandwich immunoassay where antibodies were pre-immobilised onto the surface. The detection occurred through the electrochemical response of the nanoparticles with sensitivities of 25 ng mL^{-1} substantially lower than what was required for haemoglobin A1c.¹⁴⁶ Shiohara *et al.* developed an automated microfluidic immunoassay whereby a blood sample was mixed in a solution of colloidal gold which contained a secondary antibody, this was then loaded

onto a pre-prepared chip and inserted into an automated machine which gave an electrochemical readout as the concentration of insulin in the blood.¹⁴⁷

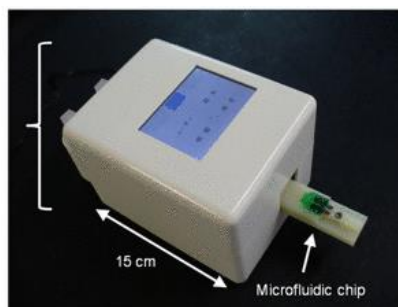


Figure 1.35: Photograph showing the integrated microfluidic, electrochemical immunoassay. (Permission of use granted by Springer Publishing).¹⁴⁷

Electrochemical methods provides a suitable method for investigation as the sensitivities are close to those seen with CL as well as electrochemical process are readily used commercially today e.g. the glucose test that diabetics use.

Electrochemical approaches for POC systems are very promising, due to the sensitivities and control that can be exerted from them. One of the most common and widely used POC systems, the diabetes glucose test operates through an electrochemical approach.

With electrochemistry currently out there as a route to carry out quantitative measurements simply and universally, it would make sense to explore the possibility of exploiting this for the aims of this work.

1.9.2 Electrochemical methods

Electrochemical redox measurements are generally conducted through a three electrode setup where there is a working electrode, a counter electrode also known as the auxiliary electrode and a reference electrode. The working electrode is where the chemistry happens, the counter electrode (auxiliary electrode) is to complete the electrical circuit such that the current flows between the working and counter electrodes and finally the

reference electrode which gives a stable known potential to relate the measured potential against.¹⁴⁸

The role of the reference electrode is key to ensure the working electrode is producing the desired potential. The need for this is two-fold, one is due to charging on the electrode surface as a result of the double layer present a larger voltage maybe required to overcome this and therefore not interact with the species in question at the correct voltage and secondly, due to the solution resistance resulting in the working electrode having to work even harder to overcome that which together results in Ohmic loss. To ensure the correct potential is measured throughout the solution the reference electrode feeds this information back to the potentiostat so the working electrode can alter the potential accordingly. This is the negative feedback loop. Also the use of electrolyte aids conduction within the solution. The impact of Ohmic loss can be minimised by reducing the current in the system, which can be achieved through lower concentrations, slower scan rates and smaller electrode radii, this is due to the current being proportional to each of these variables.^{149, 150}

Cyclic voltammetry

Cyclic voltammetry (CV) works by applying a set potential and then increasing the voltage in the case of an oxidation or decreasing it in the case of a reduction to a second potential and returning to the original potential. Figure 1.36 shows the CV waveform where a scan occurs between V_1 to V_2 and returning to V_1 representing one cycle.

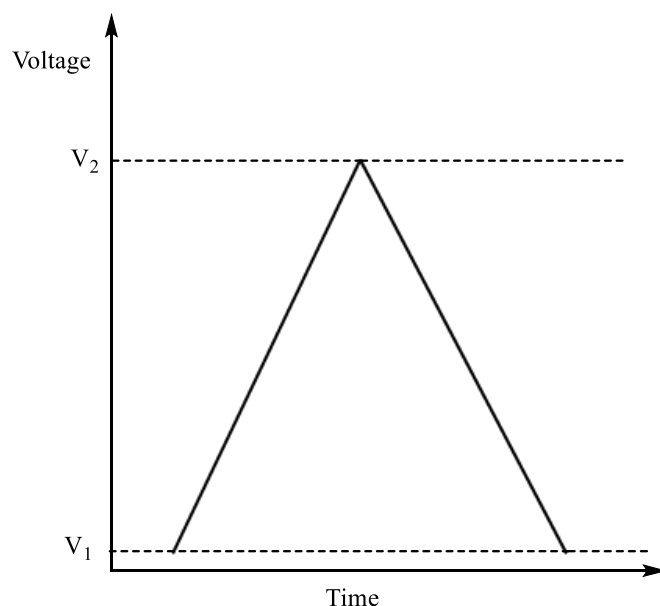


Figure 1.36: A diagram of a cyclic voltammetric waveform.

Cyclic voltammetric experiments are carried out at a set scan rate which is measured in V s^{-1} . Scan rates can vary from being fast or slow depending on the type of experiment being carried out, scan rate investigations allow a strong characterisation of the electrochemical system giving information such as kinetics and diffusion coefficients. When conducting the first sweep there is generally an oxidation followed by a reduction; however this only applies if the reaction is reversible, if the reaction is irreversible then only a single peak is observed either the oxidation or the reduction peak. Figure 1.37 gives an example of a reversible cyclic voltammogram.

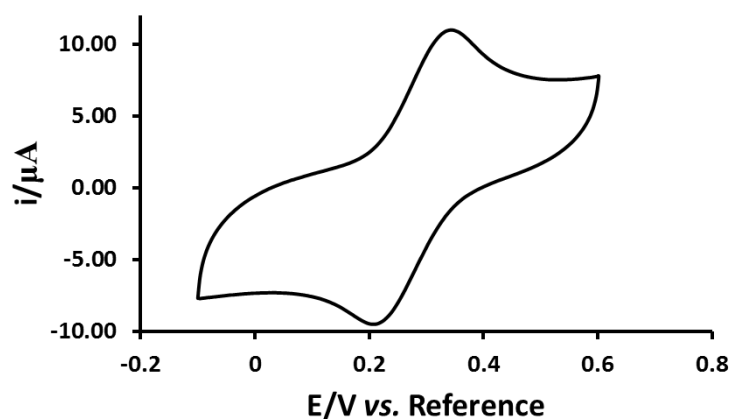


Figure 1.37: Example of a cyclic voltammogram.

From the voltammogram typically the peak current and peak potentials for both the oxidation and reduction peaks are used to carry out the analysis. The use of cyclic voltammetry is a good technique to use to get an understanding of the system that is being investigated. However the techniques inability to differentiate between capacitive and faradaic current limits the sensitivities that can be achieved. Capacitive current is the current observed due to the electrical double layer at the electrode surface and faradaic current is that observed as a result of an electrochemical reaction taking place.

Square wave voltammetry

Square wave voltammetry as a concept was described by Barker and Jenkins¹⁵¹ in 1952, however due to the available instrumentation at the time the application was very limited, however as technology has improved today's potentiostats allows this technique to become more available and is commonly used in analytical studies.¹⁵² This technique has become increasingly popular amongst analytical chemists and the development of medical based systems due to the sensitivities that can be achieved, compared to cyclic voltammetry. The waveform is shown in figure 1.38:

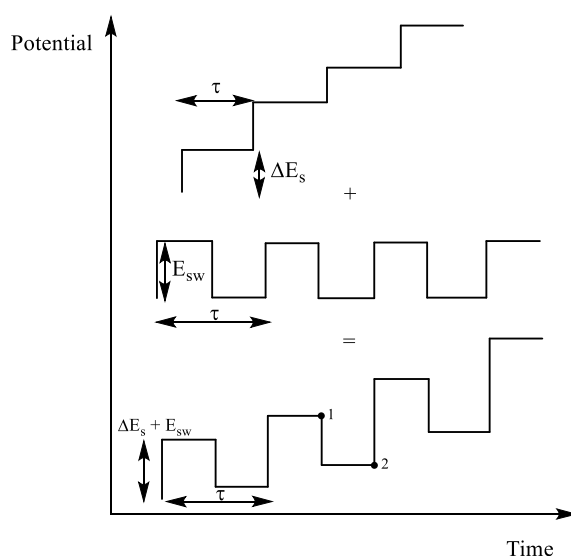


Figure 1.38: Diagram showing the square wave waveform where a staircase waveform and square wave waveform are combined to result in the overall square wave voltammetric waveform, current measurements are taken at points 1 and 2.¹⁵²

A square wave voltammetric waveform consist of staircase waveform superimposed onto a square wave this can be seen in figure 1.38. The square wave signal generated is taken at two points within the waveform, where the current at point 1 and at point 2 are then subtracted from each other (equation 1.17).

$$\Delta I = I_2 - I_1 \quad (1.17)$$

Square wave voltammetry has grew in popularity due to the sensitivities that can be achieved. These sensitivities are the result of the techniques ability to differentiate between capacitive and faradaic current due to the current only being measured at the end of the pulse. The result of this is an increased sensitivity. Unlike CV, SWV is unaffected by oxygen due to the pulsing of the technique, whereas with CV oxygen can have an effect on the measurements.

Square wave voltammetry has the benefits of being very sensitive allowing detection sensitivities towards nM range and within this thesis it will be presented that this technique can be used to detect low levels of progesterone.

1.10 Conclusions

In conclusion to this chapter the methods described in the literature to carry out immunoassays have been reviewed. It is clear that heterogeneous immunoassays are the most sensitive and selective they also enable spatial isolation.

Various different ways to immobilise antibodies onto surfaces have been discussed, glass and plastic surfaces were reviewed both in terms of their suitability for immobilisation as well as their application as substrates for microfluidic devices. Electrode platforms were also investigated as a way to immobilise the antibodies due to the control of the surface that these allow coupled with use of an electrode for electrochemical detection which is

sensitive and minimises the issues that could arise with spectrometric detection.¹⁴¹ Chemiluminescence is likewise a detection method that was investigated for the same reason that the detection method is simple with just a CCD camera and a dark environment necessary and CL is very sensitive.¹³⁸

As a result of the literature survey heterogeneous immunoassays provide better sensitivities and selectivity as well as the option to have spatial isolation of the antibodies, therefore this technique was taken forward. Glass and plastic substrates were looked at as fabrication platforms for the microfluidic system as well as their prominence as antibody immobilisation platforms. Within this system CL and electrochemical detection methods were utilised and compared as to which detection method was the most sensitive.

1.11 Aims and Objectives

The aims of this work was to develop a POC device that can rapidly monitor progesterone and oestriol concentrations in saliva using CL detection. CL allows sensitive detection with simple instrumentation, where a CCD camera could be used. The objective was first to develop a reproducible immobilisation protocol for antibodies on solid surfaces. Having developed a successful immobilisation protocol, CL and electrochemical immunoassays were carried out to determine the sensitivities of the system. The final objective was to then incorporate this system into a flow device.

Chapter 2 Experimental

This chapter outlines the reagents, materials and instrumentation used to carry out immunoassays. This is followed by an in depth explanation as to design of the devices that were investigated throughout.

2.1 Reagents

Within this section the general reagents used throughout this work are presented:

Chemical	Supplier	Purity/Grade
Anti-progesterone	AbCam	N/A
Progesterone-HRP	Randox Life Science Ltd.	N/A
Progesterone	Sigma Aldrich	>99%
Anti-oestriol	AbCam	N/A
Oestriol	Sigma Aldrich	>99%
Potassium Carbonate	Fischer Scientific	98%
HCl	Fischer Scientific	
NaBH ₄	Sigma Aldrich	>98%
Glutaraldehyde	Sigma Aldrich	98%
KCl	Fischer Scientific	99%
Tween-20	Sigma Aldrich	97%
Bovine Serum Albumin (BSA)	Sigma Aldrich	>96 %
Anti-Human-FITC	Sigma Aldrich	N/A
Sulfo-NHS	Sigma Aldrich	98.5%
EDC	Sigma Aldrich	99%
PBS Tablets	Sigma Aldrich	Not Specified
Luminol	Sigma Aldrich	97%
Hydrogen Peroxide	Fischer Scientific	Not specified
(3-aminopropyl)-triethoxysilane (APTES)	Sigma Aldrich	99%
(3-glycidyloxypropyl)-trimethoxysilane (GPTS)	Sigma Aldrich	≥98%

Glacial Acetic Acid	Fischer Scientific	Analytical Reagent Grade
Sodium Hydroxide	Fischer Scientific	Analytical Reagent Grade
Ethanol	Fischer Scientific	Analytical Reagent Grade
Acetone	Fischer Scientific	Analytical Reagent Grade
Tetrabutylammonium perchlorate	Sigma Aldrich	>99 %
4-Nitrobenzenediazonium tetrafluoroborate	Sigma Aldrich	97%
Ferrocenecarboxaldehyde	Sigma Aldrich	98%
Diethyl ether	Fischer Scientific	Analytical Reagent Grade
LiAlH ₄	Sigma Aldrich	98%
Sodium chloride	Fischer Scientific	
Ammonium nitrate	Sigma Aldrich	97%
Potassium Phosphate	Sigma Aldrich	99%
Potassium citrate	Sigma Aldrich	99%
Uric acid sodium salt	Sigma Aldrich	99%
Urea	Sigma Aldrich	98%
Lactic acid sodium salt	Sigma Aldrich	N/A
Bovine submaxillary gland mucin Type I-S	Sigma Aldrich	N/A
Oestradiol	Sigma Aldrich	99%
Oestrone	Sigma Aldrich	99%
Testosterone	Sigma Aldrich	99%
Vitamin D ₃	Alfa Aesar	>98%

2.2 Materials

There are variety of different materials that have been used throughout this work the details of which are given:

B270 glass was used for the microfluidic systems, this glass was purchased with chrome and photoresist pre-deposited on the surface (Telic Co, Valencia, California US). The chromium layer was etched using Microposit[®] Developer (50 % in water) and Chrome

Etch 18 Solution (Rohm-Haas materials supplied by Chestech, Ltd. UK). The glass itself was etched using 1 % HF/5% NH₄F at 65 °C. The photoresist and chromium that remained was removed using Microposit[®] Remover and Chrome Etch 18 Solution respectively.

For the polymer devices the polymer used was supplied by Altuglas International where PMMA granules were purchased with a melting point of 200 °C.

For the electrochemical investigation the gold and glassy carbon working electrodes with 3 mm diameters; the Ag/AgCl reference electrodes were all obtained from Alvatek (UK). Nickle wire counter electrode was obtained commercially details however are unknown. Tin doped indium oxide electrodes (75 x 25 mm) were purchased from Delta Technologies (US).

2.3 Instrumentation

All CL images were taken using a CCD camera used for the chemiluminescence analysis was a QHY6 CCD camera (QHXCCD, US) fitted with an 8 mm high resolution pixel lens (Computar, US) the camera was housed in a light-tight box, the camera was controlled by software provide by QHYCCD. Image analysis was carried out using Image J, whereby the average pixel intensity of the image was determined.

The light-tight box was necessary to minimise background light interferences which had dimensions of 60 cm x 29.5 cm x 24.5 cm. This box was developed for a previous project and had been optimised to carry out chemiluminescence measurements. Within this box the CCD camera was placed.

Fluorescence images were taken using an Axiovert S100 microscope (Zeiss, UK) fitted to an IEEE-1394 CCD camera with HCIImage software, (Hamamatsu, Japan), with a mercury lamp as a light source.

All UV-Visible spectroscopy was carried out using a PerkinElmer, UV-Vis spectrometer Lambda Bio 10 controlled by a UV-Win Lab software.

For all flow based experiments a KDS-200-CE syringe pump (kD Scientific, US) was used to introduce all reagents into the flow devices.

Contact angle measurements were carried out using K1 contact angle goniometer (Kruss, Germany)

All electrochemical experiments were conducted using a combination of an Autolab (UK) PGSTAT101 which was connected to the Nova software designed by Autolab (UK). A μ Autolab Type III in connection with GPES software (Autolab, UK) as well as a Palmsens 3 connected to the Palmsens software (Alvatek, UK).

2.4 Design of the Microfluidic Device

The chemiluminescence method relies on a competitive immunoassay therefore it was necessary that two inlets are present in the device, one for the saliva sample and a second for the progesterone-HRP; these two inlets are also necessary for the luminol and H₂O₂. The device needed to contain channels that allows thorough mixing due to this occurring through diffusion (section 1.7.4) and a channel where the antibodies can be spotted.

Device design

The device had to be designed in a way so that multiple antibodies could be immobilised, i.e. anti-progesterone and anti-oestriol. For the system to be LOC all mixing and detection protocols have to take place within the device itself and therefore the mixing of the reagents needs to be taken into consideration especially as previously outlined has to occur through diffusion.

To meet these two requirements, the mixing element of the device had to be designed properly to enable fair competition as is required for a competitive immunoassay. The use of serpentine allows this to occur efficiently due to the corners that can be fabricated within the device. As well as this the chip needs to be designed so that diffusion occurs over the shortest possible distance (table 1.2). Secondly an area needed designating for the immobilisation of the antibodies, an immobilisation channel was required; this channel would be slightly wider than the serpentine to allow the spotting of the antibodies as well as a larger area for CL to be observed.

The diffusion coefficient of progesterone was $4.75 \times 10^{-10} \text{ m}^2 \text{ s}^{-1}$ as calculated from equation 1.4 at a temperature of 298 K. Taking a typical channel width of 150 μm and the diffusion coefficient calculated; using equation 1.3 the time required to cross the channel is 23.68 seconds which therefore is the minimum amount of time that the reagents need to be flowing prior to entering the immobilisation channel to guarantee sufficient mixing.

Taking a flow rate of 10 $\mu\text{L min}^{-1}$ and a channel width of 150 μm the velocity can be calculated to be 0.94 cm s^{-1} . (Equation 2.2) Which means for a minimum diffusion time of 23.36 seconds the serpentine needed to be at least 25 cm long.

$$\text{Velocity} = 4 \times \text{flow rate} / (\pi \times (\text{width}^2)) \quad (2.2)$$

The microfluidic device designed means that throughout the flow rate has to be a maximum of 10 $\mu\text{L min}^{-1}$ to ensure sufficient mixing of reagents and this is reflected throughout.

The volume of liquid within the serpentine region of the device would be 1.5 μL .

This initial chip design was based on using a chemiluminescence only detection. Having designed the device, fabrication was required and this design was utilised in both glass and PMMA.

For the fabrication of the device an initial design was carried out using autoCAD software. This design was then sent to J .D. Phototools (Oldham UK) to create a mask for fabrication.

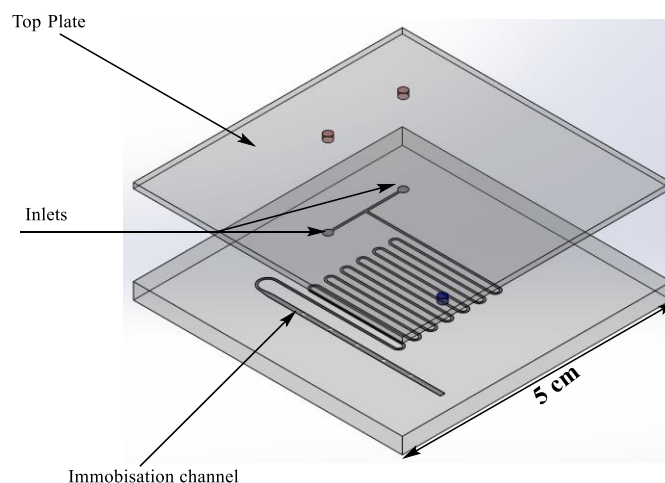


Figure 2.1: Design of microfluidic chip with a 150 μm channel width and a 50 μm depth within the serpentine region and a channel width of 800 μm and a depth of 100 μm in the detection channel serpentine length is 25 cm from the T-junction.

Within this work both a biologically compatible adhesive (to minimise damage to the antibodies) and double sided sellotape were used to bond the top and bottom plates. After the bonding of the device Teflon tubing (1.5 mm diameter) was added to the two inlets and the waste outlet and glued into place with epoxy resin. Thermal bonding was not used as the high temperatures would destroy the antibodies that had been immobilised prior to bonding of the device.

Fabrication in polymer

As discussed in section 1.7.2, polymer chips can be fabricated by using an injection moulder. The initial design was made in aluminium to develop a mould which was then used to fabricate the polymer chips. Heated PMMA was injected into the mould which when cooled formed the shape of the mould giving the microfluidic chip. Figure 2.2 shows the mould along with the polymer chip resulting from it.

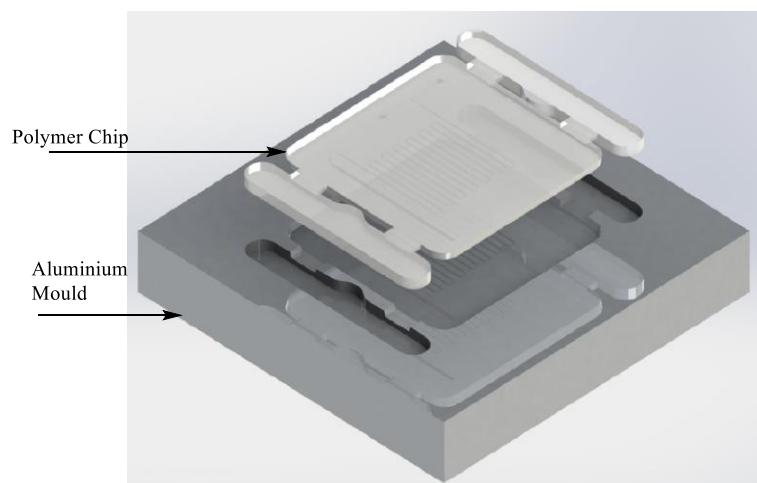


Figure 2.2: Illustration showing the aluminium mould and the resulting polymer chip.

The device shown in figure 2.2 was designed based on that shown in figure 2.1 where there is a detection channel for the analysis where the antibodies were immobilised and a serpentine for reagent mixing. This chip was designed for chemiluminescence detection. Section 2.5 discusses the integrated microfluidic device with an electrode. PMMA was the polymer of choice due to the methacrylate groups on the surface. These groups allowed the surface to be modified resulting in functional groups that allow the antibody to react with forming covalent bonds. In the same way as outlined for the glass microfluidic device the antibodies were spotted in the immobilisation channel with the top and base plate bound using double sided tape. The same tubing was used for the inlets and outlets and glued using epoxy resin.

2.5 Inclusion of Electrodes in Flow Devices

One of the biggest challenges in microfluidics is being able to integrate electrodes on chip due to the need of three electrodes. With this in mind a device was designed that uses the electrochemical immobilisation platform; but uses CL detection removing the need to incorporate two other electrodes. Within this section the designs were based on the reagents being mixed prior to flowing through the device. Initially a macroflow system was designed where the volumes of reagents are typically > 1 mL.

Macrofluidic integrated device

Initial integration revolved around using a macrofluidic device with a flat transparent electrode, this electrode was a tin-doped indium oxide (ITO) electrode. The device is shown in figure 2.3.



Figure 2.3: Macrofluidic device that can be integrated with an electrode.

The device operated by placing the electrode onto the device and gluing into place with wax, the benefit of using wax is that it dries very quickly and is hydrophobic so the use of aqueous media, will not interact with the wax and with no leakages if applied correctly. This device will be discussed fully in section 5.3.3.

Integrated microfluidic device

Due to the delicate nature of the flat ITO electrode it is necessary to have the top and base plate of the device already prepared and therefore to incorporate the electrode is through a slotting the electrode into the device. As shown in figure 2.4.

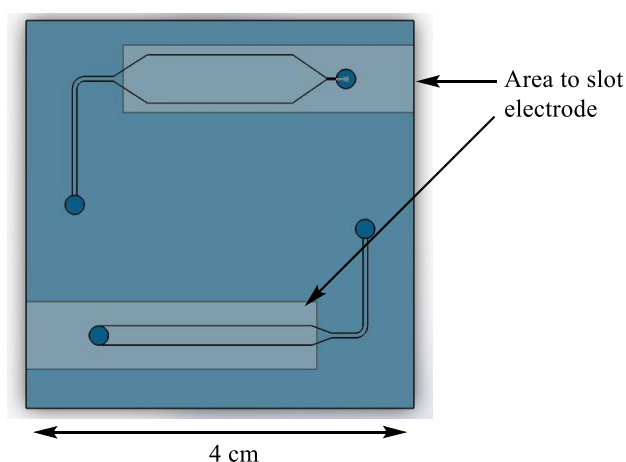


Figure 2.4: Design of the integrated microfluidic device.

Initially the top plate and base plate were bound together by using double sided sellotape and a roller to ensure the two layers are sufficiently bound to minimise the risk of leakage. Whenever required the electrode could be slotted into the device and analysis can take place. The design contained two different detection channels, the difference being is that the wider channel allows a similar comparison to the macroflow device (figure 2.3), while the smaller channel allows a smaller volume of reagents to be used. In the same way as with the macroflow system the antibody immobilisation process was carried out before incorporating the electrode into the device.

2.6 Experimental Setup

Microfluidic investigation

Figure 2.5 shows a schematic of the CL setup for the microfluidic systems:

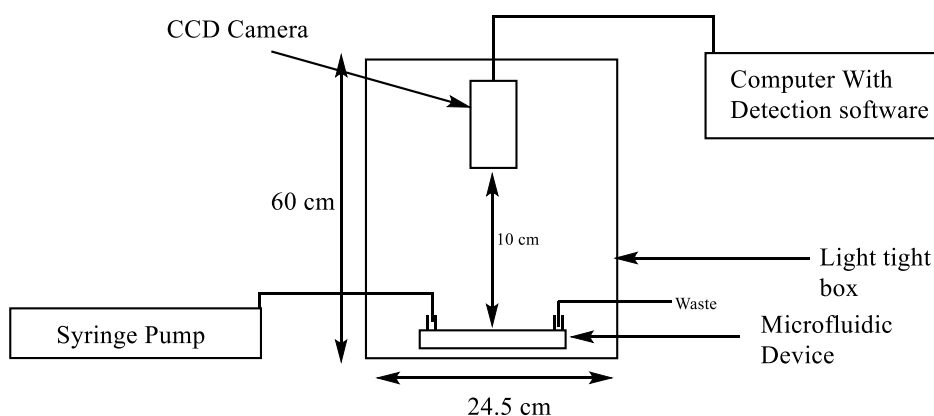


Figure 2.5: schematic showing the general experimental setup for the CL microfluidic system.

The setup consists of a black box which houses the CCD camera, the microfluidic device is placed under it. The two inlets were connected to the tubing between the syringe pump the black box. The syringe pump itself has two areas where the syringes are housed and connected to the tubing. The camera is also connected to the computer where the image is captured. The outlet of the device is connected to a vial to collect waste which was also housed in the box.

Electrochemical setup

The basic electrochemical setup is shown in figure 2.6, the setup consisted of a potentiostat connected to a computer with the appropriate software; with a three electrode setup (a working, counter and reference electrode).

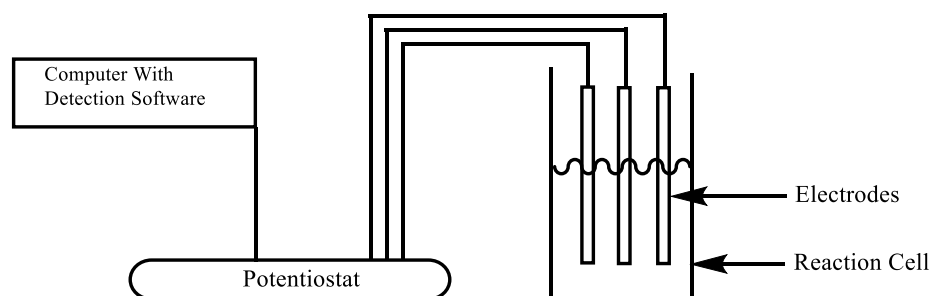


Figure 2.6: Schematic showing the basic electrochemical setup where a potentiostat is connected to a computer and to three electrodes: A working, counter and a reference electrode.

Within this work three different electrode materials were investigated as working electrodes these were gold, glassy carbon and tin-doped indium oxide. Nickel wire was used throughout as a counter electrode as this enabled more versatility with respect to the experimental setup (figure 4.4), the reference electrode was the silver/silver chloride.

2.7 Conclusions

This chapter describes the basic reagents, equipment and procedures used in this thesis. Specific experimental procedures are described in the subsequent chapters.

Chapter 3 Chemical Process for Antibody Immobilisation

3.1 Introduction

This chapter describes the development of a sensitive microfluidic chemiluminescence immunoassay using the chemical immobilisation of antibodies. The route investigated for analysis was through a competitive immunoassay where progesterone (found in a saliva sample) was mixed with progesterone tagged with horseradish peroxidase (HRP), so that both compete to bind to the anti-progesterone antibodies. Immobilising antibodies onto solid substrates can be particularly challenging for the reasons outlined in section 1.5 with the substrate having a bearing on the simplicity and success of the immobilisation process.

The solid supports investigated were glass and plastic, these substrates were chosen due to the ease of fabrication, transparency at 425 nm and the fact they have been well documented in the literature. Conducting a chemiluminescence immunoassay for progesterone analysis is not widely reported, Deboever in 1994 carried out a successful chemiluminescence immunoassay for progesterone in saliva using microtitre plates.¹⁵³ This has not been replicated however and involved large amounts of saliva samples and as yet has not been reproduced on a microfluidic scale. More recently the majority of work reported focuses on progesterone in serum¹⁵⁴⁻¹⁵⁶ with respect to humans and there is a large focus on other animals;¹⁵⁷ the reason for using serum is the higher concentrations found; but as outlined this does not represent a true chemical understand of the patient (section 1.3), in serum the progesterone is both free and protein bound, the protein bound progesterone is chemically inactive. This would elevate the concentrations of progesterone present but not indicate the concentration of the chemically active species.

3.2 Experimental Procedures

3.2.1 Evaluation of the CL detection method

Initial experiments involved determining the concentrations of luminol and hydrogen peroxide that results in the highest CL emission signal. Univariate experiments were carried out initially by using cobalt (II) as a catalyst and varying the concentrations of hydrogen peroxide and luminol between 1 mM and 50 mM. To measure the optimum luminol concentration, hydrogen peroxide was fixed at 10 mM in sodium hydroxide (0.1 M, pH 9) and likewise for luminol when investigating the best concentration for H₂O₂. For all experiments the concentration of cobalt (II) prepared was 1 mM. For each measurement an Eppendorf tube was used within which 500 µL of the luminol, 500 µL of H₂O₂ and 1 µL of the Co²⁺ were added to the tube and was instantly placed under the CCD camera for analysis. After the camera was calibrated the CL reagents were evaluated again but with HRP as the catalyst, the HRP was prepared by diluting by a factor of 1000 the supplied stock with 10 mM PBS. 10 µL of this solution was used for the catalysis again and with 500 µL of luminol and 500 µL of hydrogen peroxide.

3.2.2 Chemical immobilisation on glass slides

To evaluate the two methods selected for immobilisation contact angle measurements were made on the glass slides at different stages throughout the silanisation procedures.

APTES silanisation

Initial experiments were conducted on 1 x 1 cm squares cut from microscope slides, glass surfaces were cleaned by washing with acetone, water and ethanol following a method described by Joung *et al.*¹⁵⁸ The slides were immersed into each solvent for 10 minutes under sonication and subsequently dried in an oven at 80, 120 and 80 °C for each solvent respectively (taking into account the different boiling points of the solvents). This method was selected over the more traditional method of using piranha solution^{159, 160} because

despite the guarantee of having very clean glass chips; the use of concentrated sulfuric acid and hydrogen peroxide is not ideal and if an alternative method is possible, this will be preferential when it comes to the development of a POC device.

Once the cleaned glass chips were dried they were placed in a solution containing APTES 2 % v/v in anhydrous acetone (acetone was dried using molecular sieves) for 1 hour as suggested by Howarter *et al.*¹⁶¹ This was to increase the hydrophobicity of the glass as well as to give rise to amine functional groups. The chips were then left in a Petri dish overnight at 110 °C to cure for a minimum of 15 hours. After this the contact angle was measured on the glass surfaces.

Addition of the linker and antibody

Two different methods of linking the antibody to the APTES surface were investigated, the first linker, glutaraldehyde was selected as one of the most commonly used linkers in the literature, it reacts with the amine on the glass surface as well as the amines present on the antibody. The second linking method utilises a combination of EDC and sulfo-NHS and again is widely reported in the literature as discussed in chapter 1.

For the glutaraldehyde method the slides were placed into a solution containing 5% v/v glutaraldehyde in deionised water for two hours as described by Pui *et al.*¹⁶² The glass slides were then removed from the solution and dried; they were then placed into a holder (figure 3.1) where initially 5 µL of a Fluorescein isothiocyanate (FITC) tagged antibody was spotted onto the slides, the purpose of this was to determine the success of the antibody immobilisation by observing any fluorescence emission. Other slides were spotted with 0.2 µL of anti-progesterone undiluted from the supplier (1 mg mL⁻¹).



Figure 3.1: A 3 x 3 array holder for 1 x 1 cm squared chips.

For the EDC/sulfo-NHS method after APTES silanisation a 50:50 mixture of anti-progesterone (undiluted) and a solution consisting of 11 mg of sulfo-NHS and 4 mg EDC in 1 mL PBS (10 mM) was prepared as described by Vashist.¹⁶³ Again 5 μL of a FITC tagged antibody was also used to determine the success of the protocol through fluorescence. A 0.2 μL aliquot of this solution was then spotted onto the glass slide and left for 18 hours at 4°C.

Fluorescence studies

FITC is a molecule that absorbs blue light and emits green light. After the FITC tagged anti-human antibodies were immobilised, the slides were washed to remove any antibody that was unbound. The slides were placed under a fluorescence microscope with blue light (488 nm) beamed onto the glass with emission measurements made.

CL immunoassay protocol on glass slides

The glass slides were removed from the fridge and were washed with 10 mM PBS to remove any unbound anti-progesterone. Progesterone stock solution was prepared by dissolving 1 mg of progesterone in ethanol, which was then made up to 50 mL with 10 mM PBS to give a solution of 20 $\mu\text{g mL}^{-1}$, from which the standards were prepared in PBS (10 mM). For the immunoassay a 250 μL aliquot of a solution consisting of 125 μL of progesterone-HRP, which was prepared by diluting the concentrate purchased by 1000 as per the supplier's instructions, along with 125 μL of progesterone solution. After this

the glass slides were then left for 1 hour in an automated shaker to allow the progesterone to bind to the antibodies (incubate); they were then washed with PBS (10 mM) to remove any unbound progesterone. To make the CL measurement an initial background measurement was taken before a 1:1 ratio of luminol and hydrogen peroxide was dispensed (125 μL of each, 10 mM luminol pH 9, 10 mM H_2O_2) and added to glass slides which had been placed in the holder (Figure 3.1) and this was then immediately placed under the CCD camera for analysis.

Chemiluminescence immunoassay on a microfluidic device

When the experiment was investigated on the microfluidic device the entire immobilisation procedure was the same with the surface treated with APTES followed by anti-progesterone immobilisation with EDC/sulfo-NHS, the glutaraldehyde linker was not utilised in this study. The antibodies were spotted within the detection channel of the microfluidic device (figure 2.1) and left for 18 hours at 4°C. The device was washed with PBS (10 mM) and then prepared as outlined in section 2.4 to bind the base and top plates together. The device was then placed into the CL box under the CCD camera. Progesterone-HRP and untagged progesterone were then pumped into the microfluidic device and left to incubate for 1 hour. After this time PBS (10 mM) was pumped through to remove any unbound progesterone this was carried out for 15 minutes at a flow rate of 50 $\mu\text{L min}^{-1}$, the higher flow rate can be used here as no mixing is necessary. This was followed by the same concentrations of luminol and hydrogen peroxide (10 mM of each, pH 9). Figure 3.2 shows a photograph of the microfluidic device used for on chip analysis.

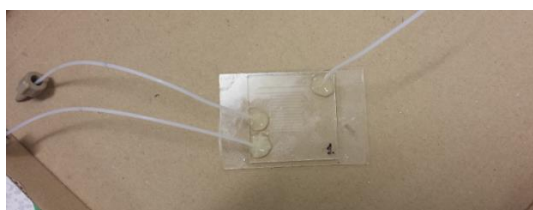


Figure 3.2: Photograph of the microfluidic device.

GPTS silanisation

The glass slides were prepared by the same method as for the APTES method, however the silanisation procedure followed the method reported by Mathias⁶⁴. In this method a solution containing 2 % GPTS and 50 mM glacial acetic acid in ethanol was prepared and the glass slides were placed in the solution for 1 hour. They were then dried under nitrogen and left for a further hour before being spotted with the anti-progesterone (0.2 μL) (the GPTS method does not require the use of a linker unlike the APTES method). After spotting the anti-progesterone, the CL protocol was implemented as described for APTES.

3.2.3 CL immunoassay using a plastic substrate

Standard ELISA procedure for comparison

An ELISA was carried out using a method outlined by Dixit *et al.*⁷³ where the wells from a 96-well microtitre plate were initially washed with 100 μL of ethanol for five minutes at 37 °C, each well was then washed five times with 300 μL of water, after this the wells were incubated for 10 minutes in a 1% w/v KOH at 37 °C, followed by five washes with 300 μL of water. The wells were then treated with 2% v/v APTES in water, 100 μL of this solution was added to each well and left to incubate for 1 hour at 80 °C, the wells were then allowed to equilibrate to room temperature and subsequently washed again with water (five times 300 μL). To each well 100 μL of the antibody solution was added which consisted of 990 μL of 4 $\mu\text{g mL}^{-1}$ anti-progesterone in PBS (10 mM) and 10 μL of EDC (4 mg mL^{-1}) and sulfo-NHS (11 mg mL^{-1}), this mixture was left for 10 minutes prior to addition to the wells. This was left overnight at 37 °C. The wells were washed with 300 μL of PBS (10 mM) 3 times, after which 300 μL of progesterone and progesterone-HRP was added to each well and left to incubate for 1 hour. The wells were then subsequently washed with PBS (10 mM, 5 x 300 μL) and the CL emission signal was instantly

measured with 300 μL of luminol (10 mM, pH 9) and hydrogen peroxide (10 mM). Again after an initial background signal was captured.

CL immunoassay on PMMA

Two methods were compared for immobilisation. Poly (methyl methacrylate) (PMMA) slides were prepared by cutting the plastic into squares of the same dimensions used for the glass slides (10 mm x 10 mm). In the first method the surfaces were functionalised using the method outlined by Goddard *et al.*⁷⁶ The PMMA slides were placed in a solution consisting of 10 M NaOH for 16 hours at 40 °C, this was carried out to hydrolyse the methacrylate group on the surface to the carboxylic acid group. After 16 hours the PMMA slides were washed with copious amounts of water and the contact angles were then measured.

A second method was then investigated as described by Cheng *et al.*⁷⁵ where lithium aluminium hydride was used to reduce the ester groups to the alcohol, this was carried out by preparing a solution consisting of 4 g of LiAlH_4 in 25 mL of diethyl ether. The success of the method was evaluated by measuring the contact angles as Cheng stated this method could be used to monitor the change from a hydrophobic, to a hydrophilic surface.

The structure of PMMA can be seen by figure 1.13.

Once the antibodies were immobilised the procedure was followed as described previously on the glass slides using the same concentration of progesterone-HRP.

3.3 Results and Discussion

3.3.1 Evaluation of the CL detection method

Before proceeding with the CL immunoassays it was vital to ensure that the CL detection method being used in this work was optimised so the variables such as camera exposure time and reagent concentrations result in obtaining the largest signal possible. In all this work the pH for the reaction was set at pH 9 this was due to the use of biological molecules, typically a higher pH gives larger CL signals, however if the pH is too high this can denature the antibodies therefore the pH was kept at 9 throughout.¹⁶⁴⁻¹⁶⁷ Previous workers however found different optimum concentrations of luminol and for this reason this was investigated further. For the initial experiments to optimise the exposure time the catalyst used was Co^{2+} rather than HRP as it is readily available and inexpensive. Changing the catalyst did not affect the selection of the variables as shown in the later optimisation experiments where HRP was used.

Calibrating the CCD camera

The camera used to carry out the detection had to be calibrated in order to determine the best conditions to carry out the CL reactions as well as to determine any limitations of the detector. The exposure time was the length of time an image needed to be exposed to the CCD camera to obtain the highest CL emission signal. This is shown in figure 3.3.

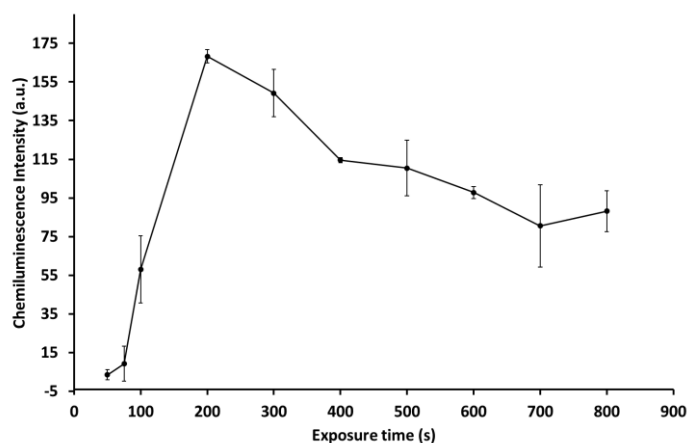


Figure 3.3: Graph showing how the signal intensity changes with the image exposure time (n=3).

The graph shows a sharp increase in intensity of CL emission as the exposure time of the image increases. This increase peaks at 200 seconds where an intensity of 174 a.u. was observed. After this the signal decreases as the exposure time increases and then it begins to level off at 400 s.

This graph reflects the fast kinetics of the luminol and hydrogen peroxide reaction, with a rapid increase in the signal to about 200 s followed by a decline. The camera itself carried on capturing the image which was then averaged out at the end of the exposure. From this system an optimum exposure time of 200 seconds is used.

Optimisation of the luminol concentration

Using the procedure outlined in section 3.2.1 the optimum concentration of luminol was investigated with the concentration ranging 1 – 50 mM.

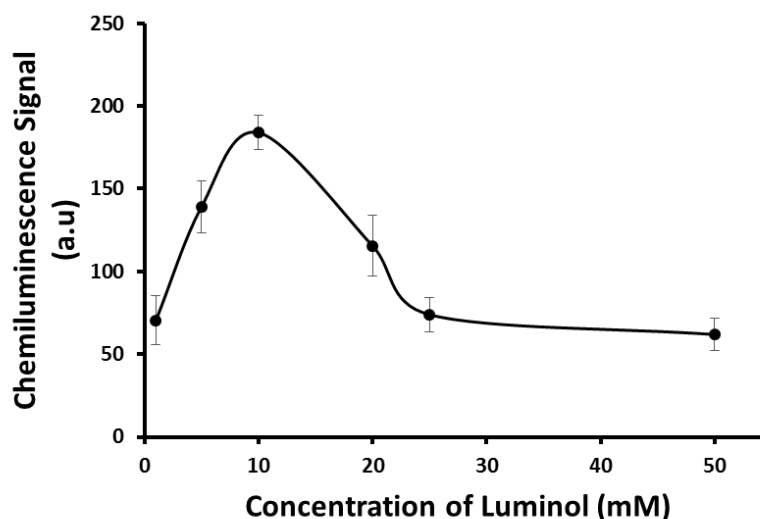


Figure 3.4: A graph showing how the light intensity changes with changing luminol concentration when made in 0.1 M NaOH, with a cobalt (II) chloride concentration of 1 mM and a H₂O₂ concentration of 10 mM. (n=3).

Figure 3.4 shows the change in CL emission signal with an increasing concentration of luminol at pH 9. The CL emission intensity increases, until 10 mM where a signal of 190 a.u. was observed. Between 10 and 25 mM luminol the signal intensity sharply decreases, then after 25 mM the emission intensity levels off. A review by Khan *et al.* discusses the properties of luminol and state that within the literature this trend is commonly observed, with the CL intensity increasing with the concentration of luminol until it reaches an optimum.¹⁶⁴ After which there is a decrease in the CL signal, the reasons this occurs is due to the hydrogen peroxide being used up, an experiment was conducted where the concentrations of luminol and hydrogen peroxide were kept the same. It was found that 25 and 50 mM solutions of luminol (pH 9) and hydrogen peroxide with 1 μ L of 1 mM Co²⁺ resulted in a substantial increase in the CL signal. Both concentrations gave a CL intensity of 254 a.u. which indicated signal saturation. This indicates that the drop in signal observed in figure 3.4 is due to the peroxide being used up. However this large signal means quantification is not possible. What can definitely be concluded is that

luminol is a very sensitive molecule and any alterations in the solution can hugely impact the efficiency of the reaction.¹⁶⁴

From this result a concentration of 10 mM luminol gave the highest CL emission signal and therefore all subsequent experiments within this sub-section will be conducted with a luminol concentration of 10 mM.

Optimisation of hydrogen peroxide concentration

The hydrogen peroxide concentration was optimised by keeping the luminol concentration constant at 10 mM, (pH 9) based on the previous result and the cobalt (II) catalyst at 1 mM. Figure 3.5 shows the result from this investigation.

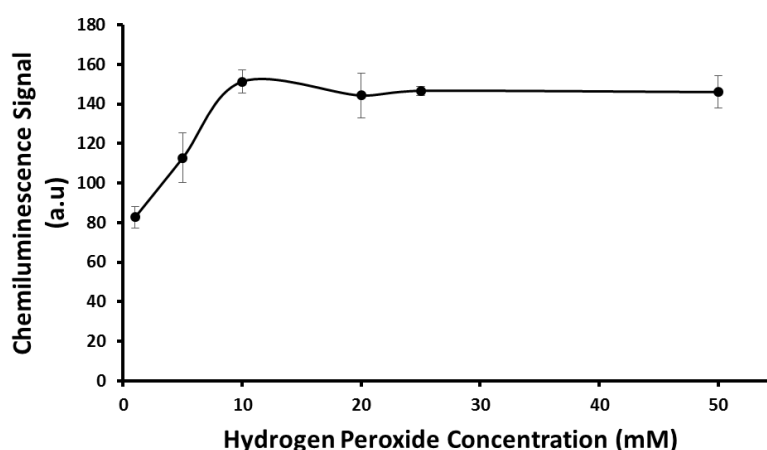


Figure 3.5: A graph showing the effect of hydrogen peroxide concentration on CL intensity where the concentration of luminol was fixed at 10 mM with the concentration of cobalt (II) chloride was 1 mM.

The graph shows that the CL emission signal increased as the concentration of hydrogen peroxide increased until a concentration of 10 mM with an intensity of 160 a.u. At higher concentrations the signal intensity levelled off and remaining approximately constant. For this reason the concentration of hydrogen peroxide was set at 10 mM for future experiments.

However unlike luminol where the light signal decreased the hydrogen peroxide signal plateaus indicating no signal change therefore 10 mM was a suitable concentration to use.

3.3.2 Optimising HRP as a chemiluminescence catalyst

Having determined the optimum camera conditions to carry out the CL analysis the reagents need to be optimised for the CL immunoassay where HRP was used as the catalyst, 10 μL of HRP solution was used instead of the 1 μL of cobalt because when the 1 μL was used the CL signal was too low and using anything higher than 10 μL resulted in the saturation of the signal. Signal saturation is a problem because the signal cannot be quantified.

Following the procedure described in 3.2.1 the best luminol and hydrogen peroxide concentrations were identified using an exposure time of 200 seconds based on the previous results. Figure 3.6 shows how the concentration of luminol effects the light emission when catalysed with HRP.

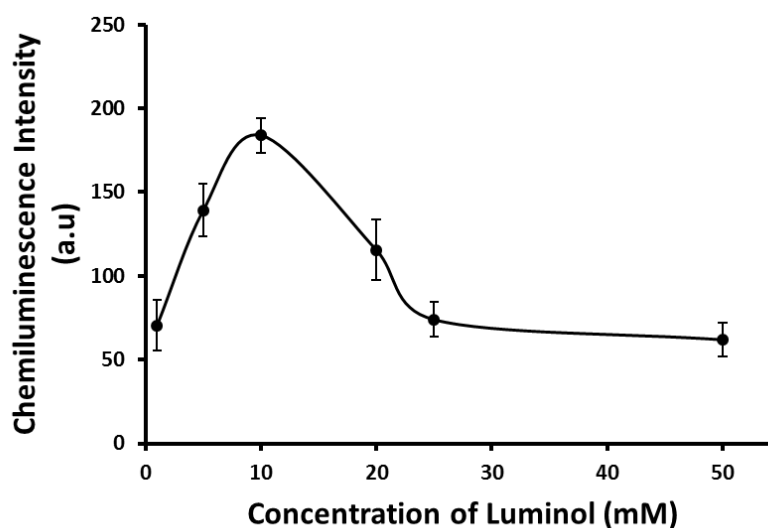


Figure 3.6: Calibration curves showing the effect of luminol concentration when the concentration of hydrogen peroxide was kept constant at 10 mM the system was catalysed using HRP.

The graph shows an increase in signal as the concentration of luminol increases until a concentration of 10 mM where a light emission of 190 a.u was measured. Again between 10 and 25 mM there is a decrease in the light emission, after which the intensity tails off.

This graph is the same as that from the previous section where a light intensity of 190 a.u. was observed with a tailing off between 10 and 25 mM luminol. Figure 3.7 shows the effect of changing the hydrogen peroxide concentration.

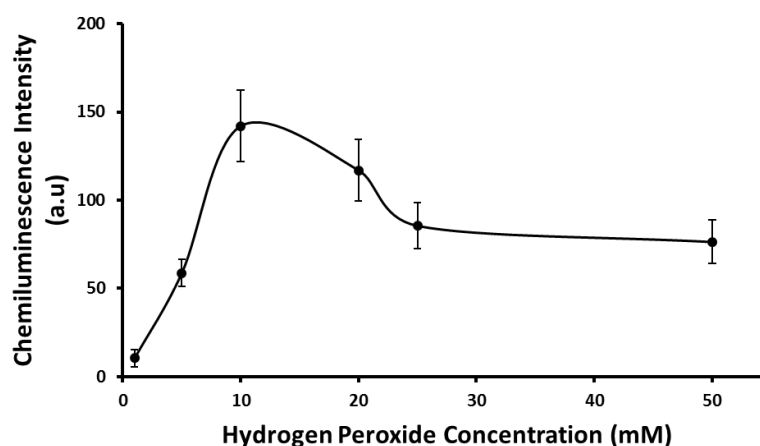


Figure 3.7: Calibration curves showing the effect of hydrogen peroxide concentration when the concentration of luminol was kept constant at 10 mM with the system catalysed by HRP.

The graph shows an increase in the light signal until a peak is reached at a concentration of 10 mM where a signal of 150 a.u. was measured. This plot then decreases between 10 and 25 mM where it finally tails off. Unlike in the previous section where the intensity of light remained constant at concentrations larger than 10 mM, this graph follows the same trend seen for the luminol where the intensity decreases initially before tailing off. However at 10 mM a signal of 150 a.u. is the same as seen in the previous section. With only the catalyst being different with HRP in this case, similar trends should be observed with respect to the luminol and hydrogen peroxide concentrations.¹⁶⁸

Through this section an exposure time of 200 seconds results in the camera capturing the highest intensity of light and concentrations of luminol and hydrogen peroxide giving the largest intensity of light that can be quantified was using 10 mM of each reagent.

There has been work published where the trends that have been observed have been the same however reasons for the decrease in the CL signal at larger concentrations of luminol and H₂O₂ were not reported.^{164, 169, 170} Having determined the best concentrations the immunoassay itself was investigated.

3.3.3 Chemiluminescence immunoassay on glass slides

As described in section 1.5.1 there are many different methods for immobilising antibodies onto glass surfaces, within this investigation APTES and GPTS was investigated. APTES was chosen as it widely used in the literature. GPTS was selected for comparison, as this reagent does not require a linker and is also widely reported in the literature.

Effectiveness of the silanisation process

To test the effectiveness of the silanisation process the contact angle of the glass slides were measured, this was achieved by using Young's equation for wettability¹⁷¹ (equation 3.1) this was to monitor the change in the hydrophilicity of the glass surface.

$$\gamma_{SA} = \gamma_{SL} + \gamma_{LA} \cos \theta \quad (3.1)$$

Where γ_{SA} is the surface tension at the solid air interface, γ_{SL} is the surface tension at the solid liquid interface, γ_{LA} is the surface tension at the liquid air interface and θ is the contact angle. This equation is depicted in figure 3.8:

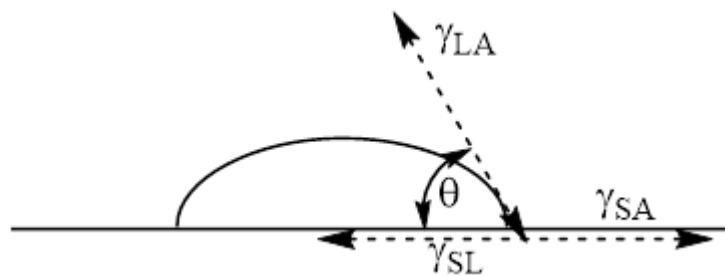


Figure 3.8: Contact angle of a liquid droplet on a solid surface.

Young's equation states that if the contact angle is $< 90^\circ$ the surface is hydrophilic, if the contact angle is $> 90^\circ$ the surface is said to be hydrophobic.¹⁷¹ Contact angle measurements are typically carried out using a contact angle goniometer this was true for this work also.

Figure 3.9 shows the change in contact angle of the glass surface for the APTES method:

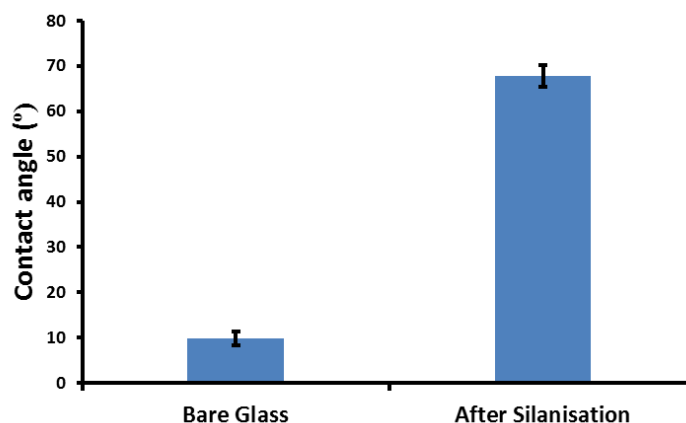


Figure 3.9: Contact angle of the glass chips when the glass is initially prepared and after silanisation with APTES. (n=5).

The bare glass surface had a contact angle of 10° and after silanisation with APTES had risen to 70° , these were based on taking three measurements on each of the glass slides and taking an average of that slide, followed by an overall average over 5 different glass slides.

This result clearly shows that after each step the glass surface becomes more hydrophobic with a contact angle of $>70^\circ$ the anti-progesterone antibodies will therefore form a partial droplet on the glass surface that will not spread easily, which when combining with another antibody at a later date is essential to enable spatial resolution of the two different antibodies. The average value of 70° corresponds to previous reported contact angles for APTES Rajesh *et al.*¹⁷² and Jain *et al.*¹⁷³

Figure 3.10 shows the contact angle analysis of the glass chips functionalised with GPTS:

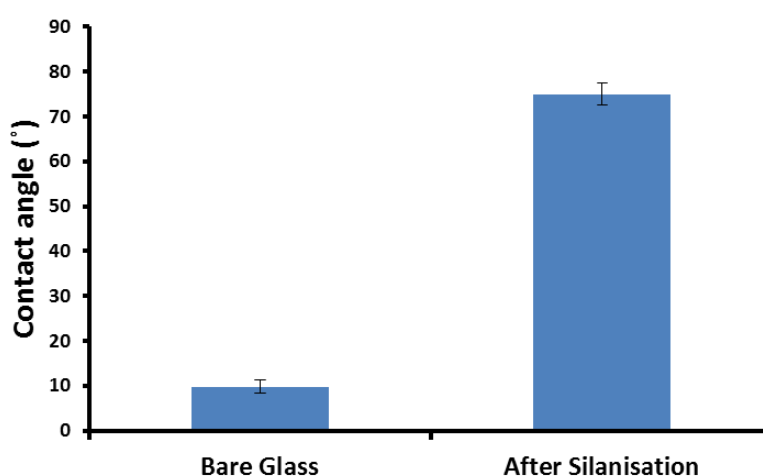


Figure 3.10: Contact angle of the glass chips when the glass is initially prepared and after silanisation with GPTS. (n=5).

Like with the previous silanisation protocol the bare glass has a water contact angle of 10° but after silanisation the contact angle was 75° . Like the previous measurement the contact angle of each individual slide was based on three different areas of that slide, followed by an overall average of 5 slides.

Again the initial glass surface is hydrophilic and after silanisation the contact angle increases. With an average contact angle of 75° the use of GPTS gives rise to a slightly more hydrophobic surface than the APTES this does relate to the literature where values of 72° have been reported.¹⁷⁴

CL immunoassay on the APTES surface with the glutaraldehyde linker

A CL immunoassay of progesterone was carried out following the method described in section 3.2.2 using the glass slides in which glutaraldehyde was used as the linker between the antibody and the APTES surface. No results could be obtained using this method, with no CL emission signal the reasons for this were not clear, this indicated that the antibody potentially had not immobilised onto the glass surface.

Antibody immobilization confirmation

The problem could be with either the CL detection method or the immobilisation procedure so the immobilisation was tested using fluorescence detection. Fluorescein isothiocyanate (FITC) tagged anti-human antibodies were immobilised using the APTES method with the glutaraldehyde linker. After washing with PBS the glass slide was placed under the fluorescence microscope. The glass slide showed little to no fluorescence indicating that the antibody was not immobilising onto the glass surface and was being washed away.

The problems encountered using glutaraldehyde as a cross linker were discussed in the introduction (section 1.5.1.1). Shriver-Lake *et al.* states that glutaraldehyde is known to have batch to batch issues with its ability to self-polymerise affecting reproducibility and reliability.⁶³ On further examination of the literature, Whipple and Ruta state that in aqueous solution glutaraldehyde forms a “cyclic hemihydrate” (figure 3.11) the consequence of this is that the properties will change, affecting the route through which the immobilisation process of anti-progesterone to the amine derivatised surface occurs.¹⁷⁴

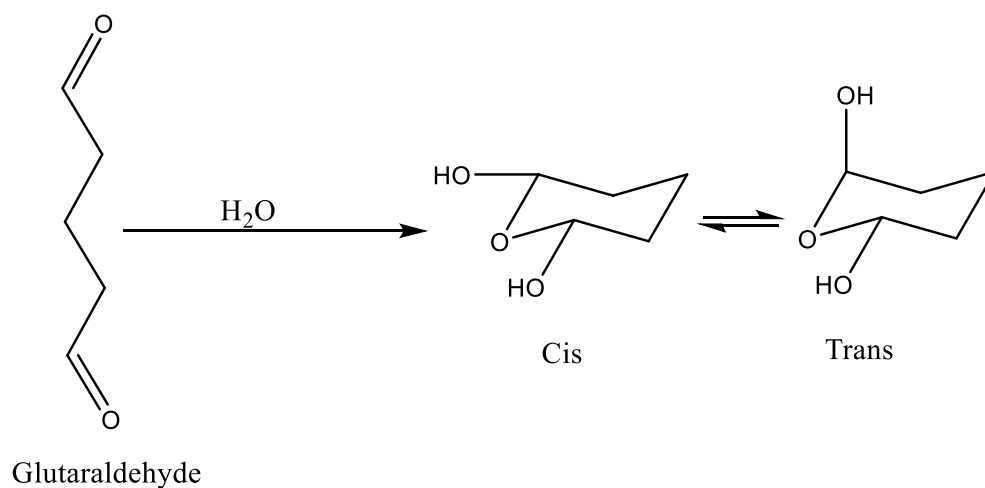


Figure 3.11: Schematic showing the formation of the hemicyclic as stated by Whipple and Ruta when glutaraldehyde is used in water.¹⁷⁴

EDC/sulfo-NHS immobilisation process

This alternative approach for immobilising the antibody on the APTES silanised glass surface was then investigated using the FITC tagged anti-human antibodies. Prior to carrying out the CL analysis. Figure 3.12 shows the fluorescence image of the glass slide with the immobilised antibody.

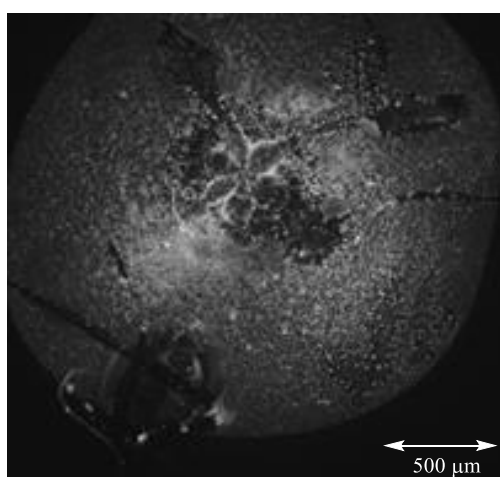


Figure 3.12: Image of FITC tagged anti-human antibodies on an APTES modified glass surface using EDC/sulfo-NHS linker after 5 washes with 300 μ L of PBS (10 mM).

The image shows a fluorescence response which can be attributed to the FITC that is tagged to the antibody. FITC is excited by blue light, and upon relaxation to the ground state emits green light. This image however is not uniform with darker areas which could be attributed to damage during the immobilisation and washing processes.

The results however showed that using the EDC/sulfo-NHS route the antibody was immobilised which is an improvement over the glutaraldehyde linker therefore the EDC/sulfo-NHS combination was used for further investigation of the CL immunoassay.

Fluorescence examination of GPTS functionalised glass slides

Using the same method as described for the APTES functionalised glass slides FITC tagged antibodies were deposited onto the GPTS functionalised glass surface and left to immobilise overnight. Figure 3.13 shows the fluorescence image of the glass slide with the immobilised antibody.

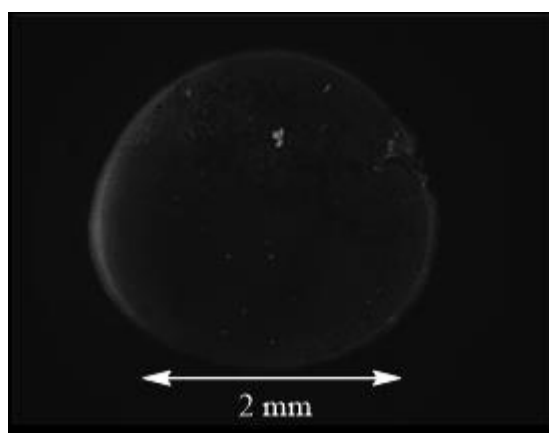


Figure 3.13: Fluorescence image of FITC-tagged anti-human antibodies on a glass surface after 5 washes with 300 μ L of PBS (10 mM).

An image is seen but the clarity is very low compared to figure 3.11 so this method does not appear to give improved results over the previous method.

CL immunoassay on the APTES functionalised glass slides

Clearly the most promising method for antibody immobilisation appears to be using APTES with the EDC/sulfo-NHS linker and therefore this immobilisation method was used to carry out the CL immunoassay. Initially a test was carried out where the immobilised antibodies were incubated with progesterone-HRP only to obtain the highest signal possible. Prior to carrying out the competitive immunoassay. An image of CL emission observed is shown in figure 3.14:

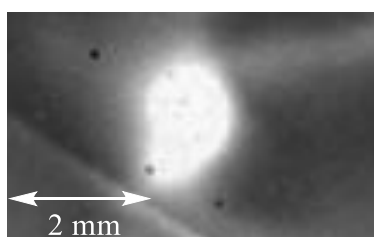


Figure 3.14: CL image of anti-progesterone antibody bound with progesterone-HRP.

The image shows a bright spot where the antibodies are immobilised which is the highest CL emission that will be produced. The image shows that this method of immobilisation is successful and therefore a calibration could be developed.

Competitive CL immunoassay

A set of progesterone standards were prepared ranging from 31.5 pg mL^{-1} up to 3.15 ng mL^{-1} (0.1 nM up to 10 nM) in 10 mM PBS . These are the levels that one would expect in saliva that can give a strong indication of the progesterone levels for both fertility and pregnancy studies.⁸

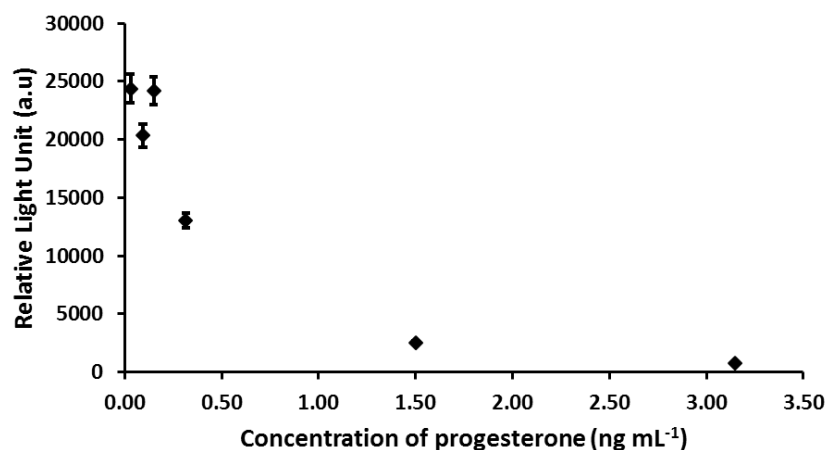


Figure 3.15: Calibration curve for the CL competitive immunoassay of progesterone between the ranges of 31.5 pg mL⁻¹ rising to 3.15 ng mL⁻¹.

Figure 3.15 shows a gradual decrease in the light intensity as the concentration of progesterone increases until it levels off, this is as expected for a competitive immunoassay; whereas, as the untagged progesterone concentration increases the amount of progesterone-HRP bound to the antibody decreases resulting in a reduction in catalytic activity giving a lower signal. Taking this graph and plotting as a logarithmic scale results in a calibration curve as shown in Figure 3.16.

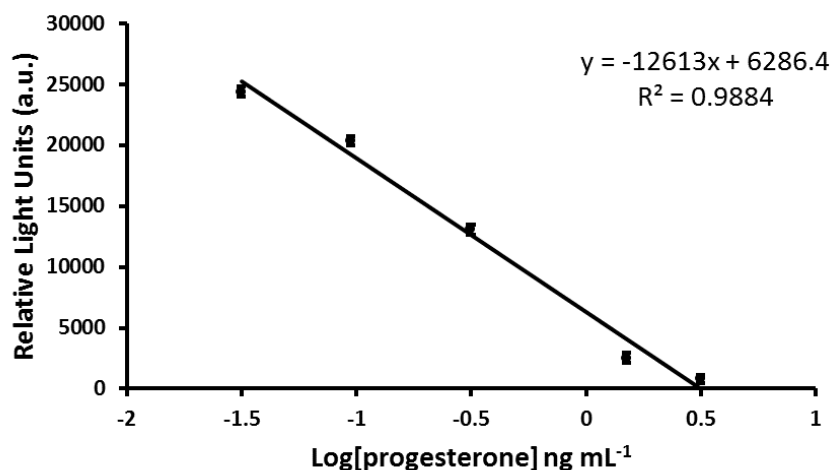


Figure 3.16: Calibration curve showing how the intensity of light emitted changes with the increase in concentration of the untagged progesterone. (n=5).

Taking the logarithmic scale results in a linear trend which is expected when carrying out measurements over a couple of orders of magnitude.

It was useful to plot the change in signal with increasing progesterone concentration as compared to when only progesterone-HRP was present as shown in figure 3.17.

This plot can be used to calculate the LOD.

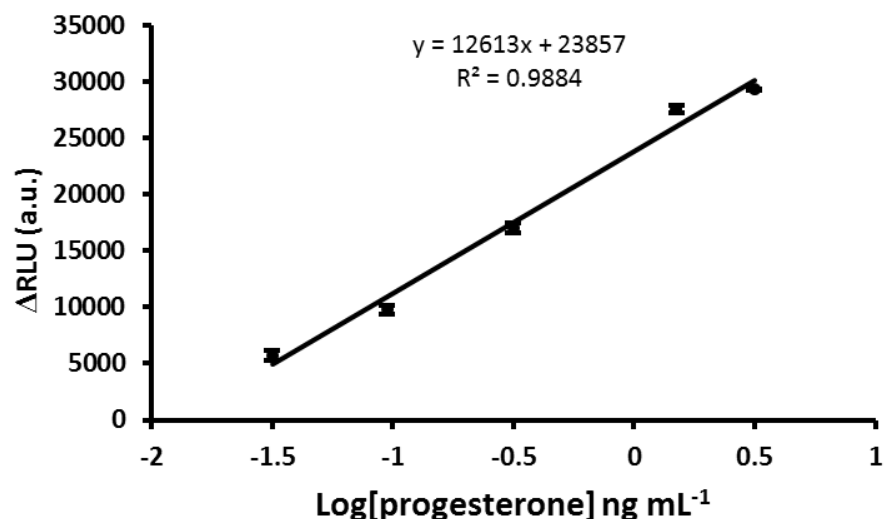


Figure 3.17: Calibration curve of untagged progesterone against the CL signal change where the signal obtained is subtracted from the blank. (n=5).

Using equation 3.2 and figure 3.17 the LOD can be calculated to be: 33 pg mL⁻¹.

$$LOD = y_b + 3s_b \quad (3.2)$$

Where LOD is the limit of detection, y_b is the y-intercept and $3s_b$ is three times the standard deviation of the blank. With a calculated LOD of 33 pg mL⁻¹ the sensitivity of the system falls slightly above the 31 pg mL⁻¹ stated earlier however compared to published work where detection limits of 100 pg mL⁻¹ ¹⁷⁵, 0.08 μg mL⁻¹ ⁷², and 8 nM¹⁵⁴ are reported and compared with the ELISA shown in section 3.3.4; the method is very sensitive and shows promise to be transferred onto a microfluidic chip however this was

achieved with progesterone in 10 mM PBS and not saliva and the system overall was not reproducible and obtaining sufficient results was challenging.

CL on GPTS functionalised glass slides

Although this method did not look promising with the FITC tagged antibodies it was decided to try it with CL detection. The measurements were made in the same way as for APTES with glutaraldehyde where progesterone-HRP was used to obtain the highest possible signal. The results are shown in figure 3.18.

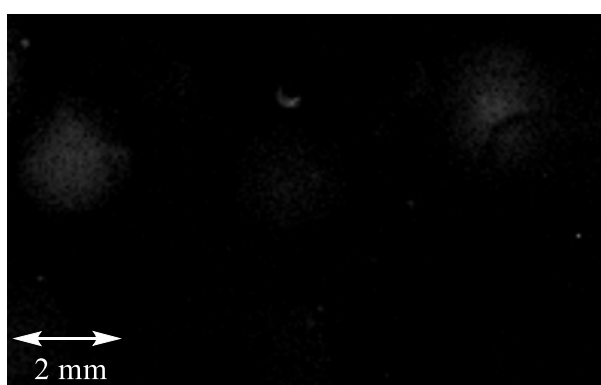


Figure 3.18: CL image of anti-progesterone on GPTS functionalised glass chips with progesterone-HRP.

A **large** CL emission signal was not observed, unlike the image in figure 3.14 which when using HRP-progesterone only a large signal would be expected. The difference in results could be due to the orientation of the antibodies on the surface. With this method epoxy groups are used which bind through the amine groups on the antibody that are found in the Fab region of the antibody. Bonding in this way would result in an undesirable antibody orientation therefore minimising the antibodies interaction with the sample resulting in very little HRP binding. With the amine derivatised glass surface (APTES) the immobilisation occurs through covalent bonds to the acid groups on the antibody which are found primarily at the base of the heavy chains within the fragment crystalline region of the antibody which was maybe more favourable.

Commercial ELISA for progesterone

To be able to make a clear assessment of the CL immunoassay which was being developed it was decided to carry out a commercial ELISA for progesterone Figure 3.19 shows a calibration curve with the light intensity observed against the concentration of progesterone along with the change in light signal against progesterone concentration were plotted with the LOD of the system calculated.

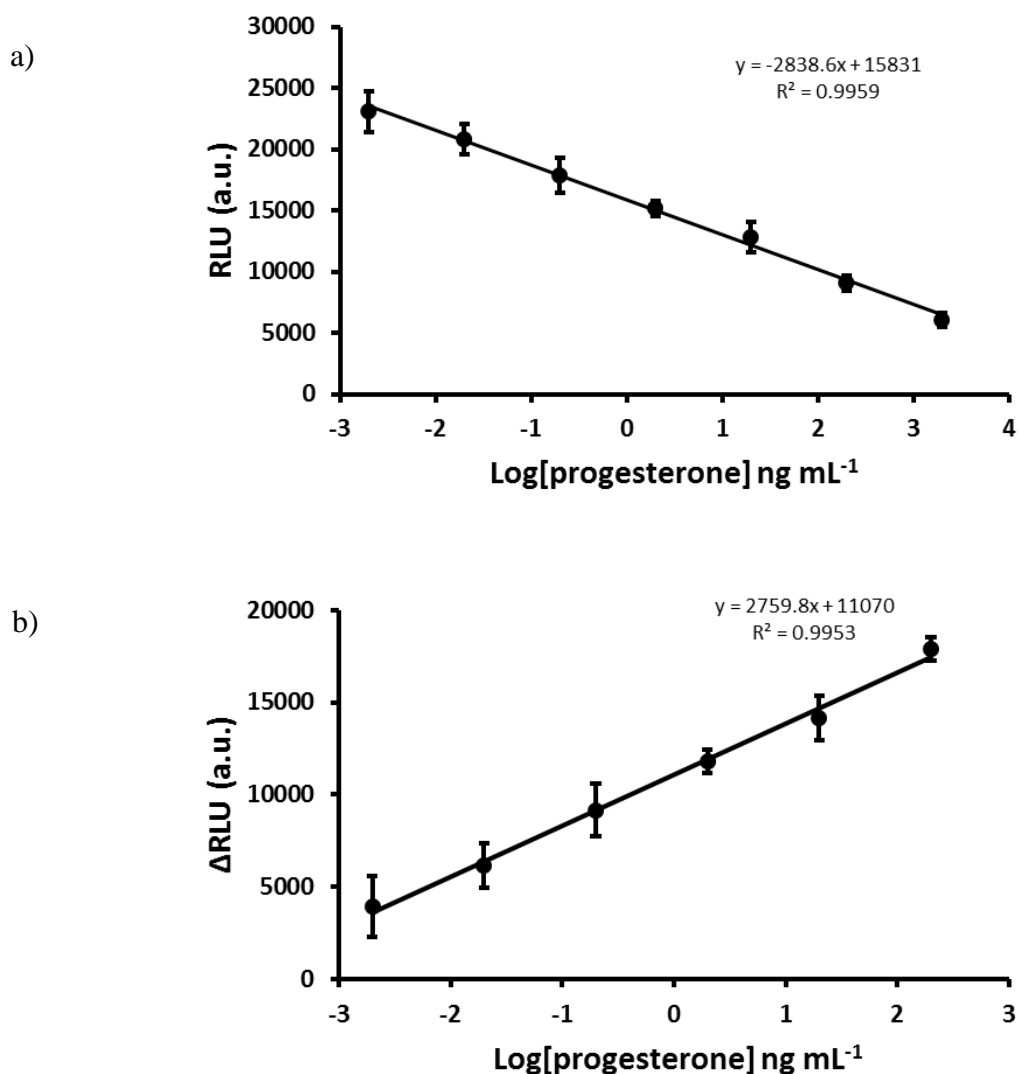


Figure 3.19: a) Calibration curves showing how the light intensity changes as the concentration of untagged progesterone changes and b) the light signal change after subtracting the blank signal from the intensity measured (n=3).

Figure 3.19 a & b) demonstrates a linear correlation which was expected as the concentration of progesterone increases, where more progesterone molecules are competing for the antibody binding sites compared to the progesterone-HRP. The LOD was determined using equation 3.2.

This was calculated to be $26 \pm 5 \text{ pg mL}^{-1}$ which was comparable to the work by Dixet *et al.*⁷³ where a LOD of 39 pg mL^{-1} was determined through this system. Comparing this to the result on the glass slides where a LOD of $33 \pm 3 \text{ pg mL}^{-1}$ was determined, it can be concluded that the LOD from our method was slightly higher than that from the conventional method but it is within the error calculated and is lower than previous published work indicating a sensitive CL immunoassay for progesterone had been developed.

3.3.4 CL immunoassay on a microfluidic device

Optimising the flow rate on the microfluidic device

Having successfully carried out chemical immobilisation on glass slides which was followed up with a successful competitive immunoassay, the system was transferred onto the microfluidic device shown in figure 3.2. As the top and base plates were bonded using doubled sided tape, the device needed to be tested to ensure that the presence of the tape does not reduce the CL emission signal. This test was conducted by measuring the UV-Visible absorption spectrum of the device with the tape in place, this can be seen in figure 3.20:

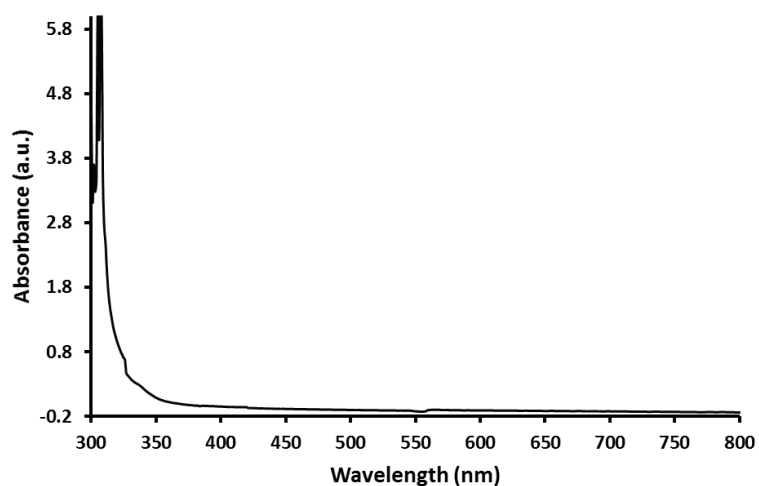


Figure 3.20: UV-Vis spectrum of the microfluidic device.

The absorption rapidly decreased as the wavelength increased and is very low by 350nm. As the CL emission signal is at 425 nm the presence of the tape will not affect the measurement.

Mixing of the in the microfluidic chip

As a starting point a CL immunoassay was directly attempted on the microfluidic device, initially only progesterone-HRP was pumped into the device and left to incubate. After this the CL reagents were added where a flow rate of $1 \mu\text{L min}^{-1}$ was used. This initial result is shown in figure 3.21.

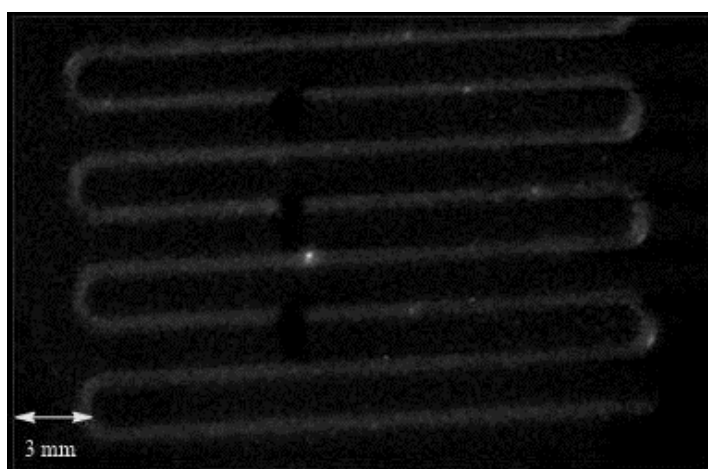


Figure 3.21: CL image showing the initial experiment on the microfluidic device at a flow rate of $1 \mu\text{L min}^{-1}$.

A bright glow can be seen in the serpentine. This shows that not only has mixing occurred too quickly but emphasises what was mentioned in the introduction that the luminol and hydrogen peroxide reaction has very fast reaction kinetics, meaning a faster flow rate would be required to ensure the light only comes from the immobilisation channel and not within the serpentine.

From this result the flow rate was investigated so that the mixing of luminol and hydrogen peroxide does not occur too quickly or too late.

Before carrying out the CL immunoassay the ability of the microfluidic device to rapidly mix the CL reagents was assessed. Red food dye diluted 1:10 with water was used for this experiment. Images of the T-junction and the wider channel at the end where the antibodies would be spotted are shown in figure 3.22:

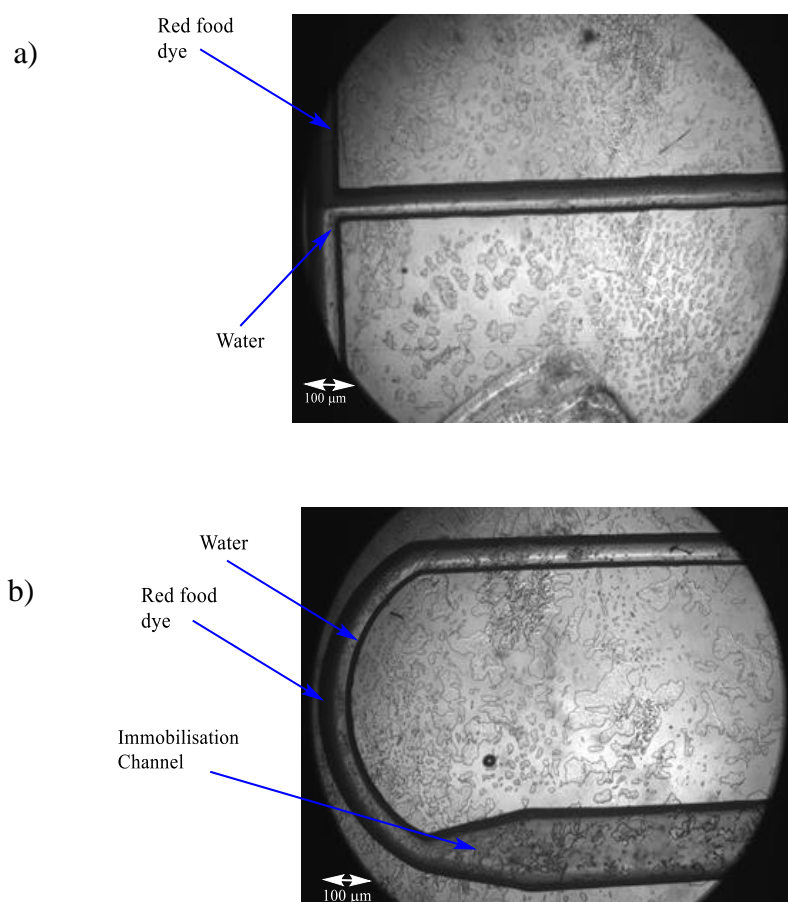


Figure 3.22: Microscopes images showing a) the T-junction of the microfluidic chip and b) the start of the reaction chamber at the end of the chip.

Figure 3.22a shows the T-junction of the microfluidic device, the point at which the mixing of the CL reagents would start. The image shows a clear separation between the food dye (darker colour) and the water (lighter colour). This confirms there is laminar flow as expected with the design (Reynold's number calculated to be of ~ 1 as in section 1.8.4.). Figure 3.22b shows the entrance of the mixing serpentine channel leading to the wider immobilisation channel. In the serpentine it is possible to see a small amount of white where the two liquids have not yet fully mixed. Once the mixture enters the immobilisation channel there is however a universal colouration across the channel showing that the two reagents mixed thoroughly which is vital for good detection. Using Image J software a greyscale profile was obtained across the chamber for different flow rates as shown in figure 3.23:

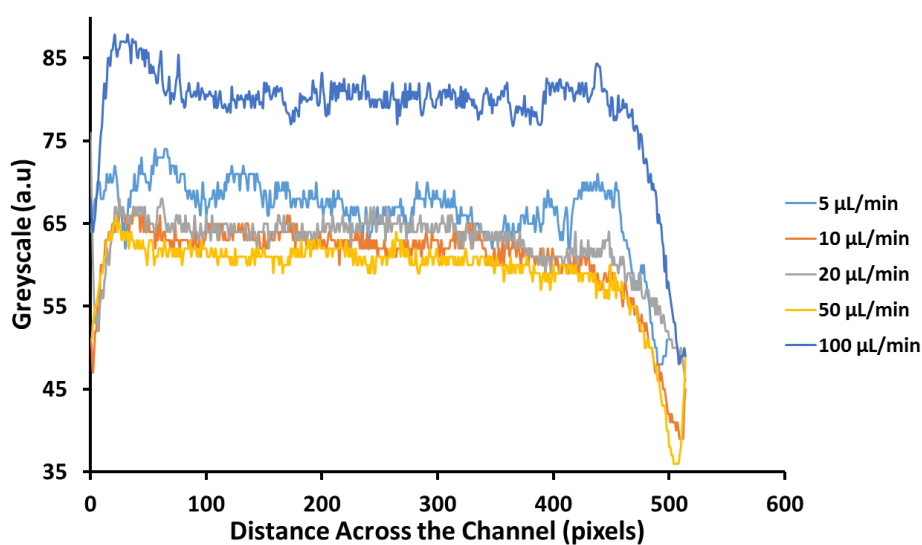


Figure 3.23: Flow profile of the microfluidic reaction chamber showing the greyscale value per pixel at various flow rates.

The graph shows that across the channel the greyscale remains fairly constant for all flow rates except for the $100 \mu\text{L min}^{-1}$ where there is a sharp decrease in the greyscale value around the 400 pixels mark which would be attributed to water and dye having not mixed fully. Therefore for the CL immunoassay on chip a flow rate of 5 mL min^{-1} was used.

Chemiluminescence immunoassay using the microfluidic device

Having obtained a calibration on the glass slides the process was transferred to the microfluidic device which had been prepared in the same way (APTES, EDC/sulfo-NHS, anti-progesterone). After incubation and a wash with 10 mM PBS the CL was measured.

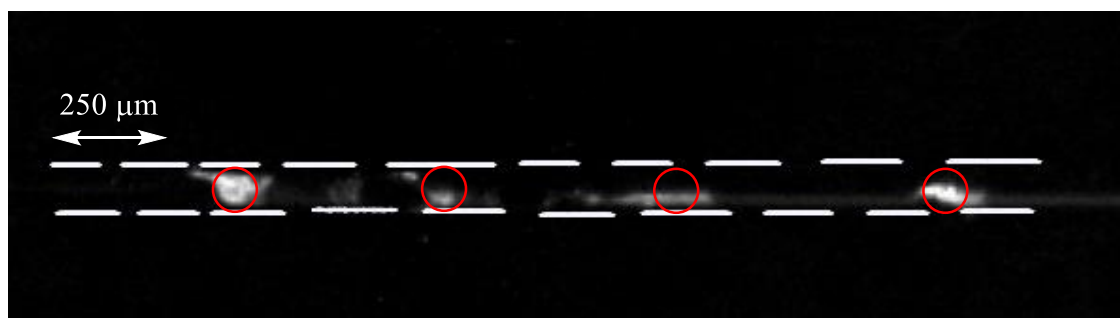


Figure 3.24: CL image of the reaction chamber where the red circles represent the areas where the initial antibody spots were deposited.

Figure 3.24 shows only one clear spot, the other spots spread across the channel this could be due to the antibodies not immobilising effectively under flow conditions or the immobilisation being affected when the two glass plates were bonded.

Many different approaches were taken to try and overcome this problem, including the use of an automated spotter in an attempt to control the volume and positioning of the antibody droplets within the microfluidic device. This also ended without success.

It was clear after these many repeats around ~50+ attempts reliability was clearly an issue.

3.3.5 CL Immunoassay on plastic substrates

As discussed in chapter one plastic substrates are gaining a lot of popularity for point of care microfluidics due to the ease of manufacture on a large scale with low cost (after an initial outlay for the fabrication equipment). Once the equipment is in place and moulds having been fabricated; the microfluidic systems can then be fabricated in batch very quickly and cheaply allowing them to be disposable which is not really possible with glass devices due to the complex and expensive fabrication process.

CL immunoassay on PMMA chips

PMMA was chosen as a substrate to investigate as a platform for a CL immunoassay because of the ester groups present (figure 1.13), these groups can be more easily modified compared to a polymer like cyclic olefin copolymer which has no functional groups; PMMA therefore allows a simpler route for surface modification and therefore antibody immobilisation. PMMA is also biologically compatible.¹⁷⁶

If the CL immunoassay is to be finally carried out in a closed microfluidic device the plastic must not absorb the CL emission therefore a UV-Vis absorption spectrum was obtained as can be seen in figure 3.25:

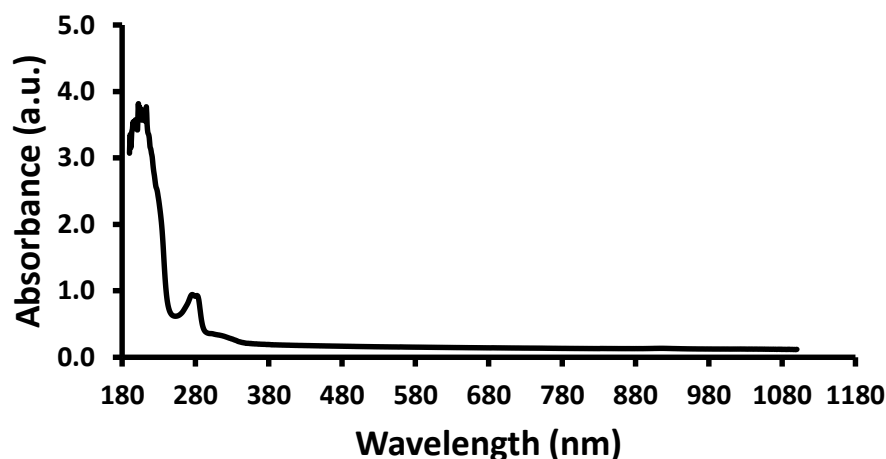


Figure 3.25: UV-Vis spectrum of PMMA.

Figure 3.25 shows that PMMA absorbs at 280 nm which is well within the UV region of the electromagnetic spectrum which from the literature is characteristic for PMMA.^{177, 178}

With the CL reaction of luminol and hydrogen peroxide emitting light at 425 nm the PMMA will not absorb any emitted light and affect the analysis.

The lithium aluminium hydride reduction gave us a better starting point due to the formation of OH groups on the surface. The surface could then be treated with APTES in the same way as described on glass.

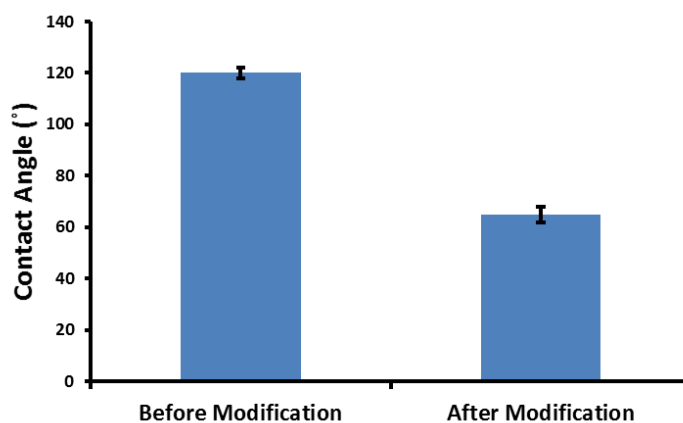


Figure 3.26: Contact angle analysis of PMMA before modification and after modification with LiAlH_4 .

Figure 3.26 shows that the PMMA itself has a contact angle of 120° which is reduced after modification to around 60° , however the plastic was damaged during the surface modification process before the measurements were taken. The surface had become very rough and opaque which would impact the transmission of light. For this reason this method was discarded.

Following this setback base hydrolysis was investigated with 10 M NaOH which results in the corresponding carboxylic acid. Unlike the lithium aluminium hydride reduction where the plastic was damaged, this method resulted in usable chips, figure 3.27 shows contact angle analysis before and after surface modification.

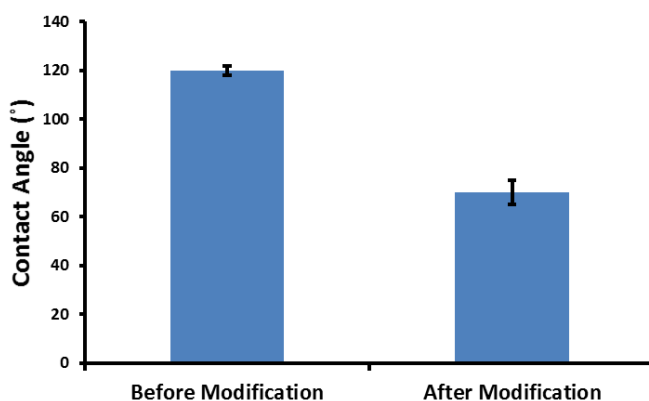


Figure 3.27: Contact angle analysis of PMMA before modification and after modification with 10 M NaOH.

The graph shows that the contact angle was of 120° prior to modification and decreased to 70° after modification. It has been reported in the literature that after base hydrolysis the contact angle can be between 60 and 80°^{179, 180} and that after this the surface can be activated with EDC and sulfo-NHS with the anti-progesterone then being added to the modified PMMA surface. Initially progesterone-HRP (1:1000 dilution) was added to the immobilised anti-progesterone to obtain the maximum CL emission signal followed by the measurement and this is shown in figure 3.28.

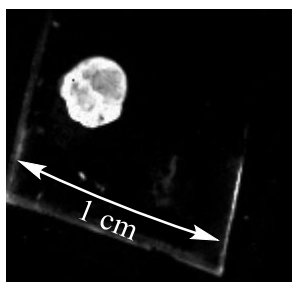


Figure 3.28: Image of the PMMA chip with progesterone-HRP.

The image shows that the progesterone-HRP is binding to the area where the antibodies are immobilised. Following this a range of progesterone standards were prepared as described previously to obtain a calibration.

However this turned out not to be successful as there were too many irreproducible results, for this reason plastic chips were not taken any further as a platform to immobilise the antibodies.

After examining the literature; work by Seitz *et al.*¹⁸¹ it is clear that despite APTES being used extensively on glass and polymer the monolayer formed are not as reproducible and stable as expected, the findings within this paper discusses the interaction of APTES with phosphate buffer (pH 7.4) and found that the use of aqueous media can damage the monolayer with 60% of the layer disappearing after a 2 hour exposure to the buffer. This observation followed previous work by Pasternack *et al.*¹⁸² where the same observation was seen when water was examined on APTES derivatised surfaces and Lapin *et al.*¹⁸³

used APTES to immobilise streptavidin through a biotin linker, they also observed that the stability and reproducibility was compromised observing the behaviour of the biotinylated species was affected. The reasons that this issue is not picked up on more in the literature is not clear, but through the work carried out in this chapter APTES was certainly shown to be a problematic reagent that could not guarantee reproducibility.

3.4 Conclusion to the Chemical Immobilisation Investigation

Within this chapter a CL immunoassay of progesterone was successfully demonstrated on 1 x 1 cm square chips. The detection limit was found to be $33 \pm 3 \text{ pg mL}^{-1}$ which compared well with the commercial ELSIA kit which had a detection limit of 26 pg mL^{-1} . These detection limits were well within the required range for progesterone in saliva samples but the fact that the system was unsuccessfully transferred onto a microfluidic based system was disappointing. Careful reading of the literature about the widely reported use of APTES confirms that there are problems due to the instability of the monolayer. This would become particularly problematic in a flow system which perhaps explains the problems encountered when transferring the off chip systems onto the microfluidic device. A disadvantage is quantifying the concentration of antibodies on the glass surface, any quantification would not necessarily be true after multiple modifications due to the issues outlined. With so many different issues throughout the surface modification and immobilisation process obtaining this information is near on impossible so that it is reproducible. When developing a POC system reliability in the manufacture is key and if an immobilisation protocol was not going to be reproducible a new approach needed to be investigated.

Chapter 4 Electrochemical Process for Antibody Immobilisation

4.1 Introduction

Chemically modification of glass and plastic surfaces was unsuccessful due to the irreproducibility of the modification protocol. It was therefore necessary to develop a reproducible immobilisation process. An electrochemical immobilisation method developed by Dou *et al.*⁵⁴ consisted of tagging ferrocene to an antibody of interest, this was then immobilised onto a modified gold electrode surface. This electrode had been previously modified to contain aniline which was achieved through the deposition of nitrobenzene, followed by an electrochemical reduction to the corresponding amine.

The generation of the amine surface allows the antibody to covalently bind to the electrode surface through the COOH group found at the base of the heavy chain within the Fc region of the antibody, this attachment allows more antibodies to adopt an orientation that is “end on” rather than “side on”.^{54, 184}

An electrochemical immobilisation process following this method allows validation of the modification steps of the process using cyclic voltammetry. The principle of this method is shown in figure 4.1:

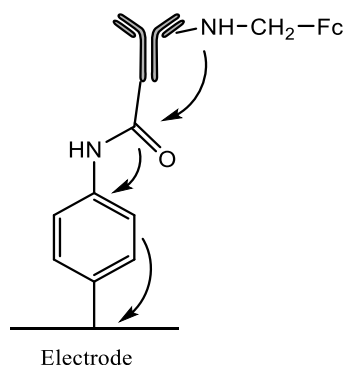


Figure 4.1 Theoretical concept for the electrochemical protocol for antibody immobilisation the arrows are representative of the transfer of an electron through a molecular wire. Fc represents ferrocene.

Forming the amine on the surface allows the COOH terminal of the antibody to react forming an amide linkage. This creates a “molecular wire” between the electrode and the antibody.¹⁸⁵ Having the amide functionality allows resonance between the oxygen and nitrogen atoms; the functional group is also planar improving the electron transfer through the wire. These properties are vital for electron communication to occur between the ferrocene and the electrode surface. Figure 4.2 shows the possible resonance structures as presented by Mujika *et al.*

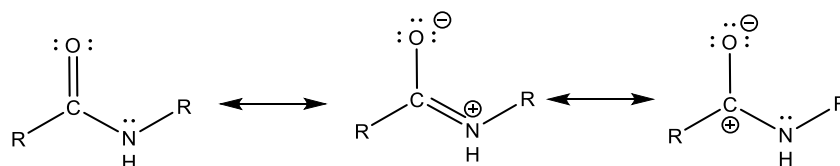


Figure 4.2 Resonance structures for the amide functional group.¹⁸⁶

As shown in figure 4.1 the arrows represent an oxidation process where the ferrocene (Fc) loses an electron to the electrode surface. The wire can operate through the aid of the benzene ring to transport the electron from the antibody to the electrode. The reverse would be true for an electrochemical reduction. As the figure shows the structure is **RIGID** which aids the antibody orientation, for example if the antibody was to orientate upside down the bulky ferrocene groups would be crowded by the benzene rings on the surface which would not be favourable. This should enable reproducible quantitative measurements to be made.

Within this chapter this concept was investigated as a route to develop a reproducible antibody immobilisation protocol; where the protocol in itself can act as a checklist to confirm success and therefore exploit this method to carry out an electrochemical immunoassay, the immunoassay operates through a blocking of the redox ferrocene. When there is no antigen present a large electrochemical signal would be observed, after interaction with the antigen, the antigen blocks the ferrocene resulting in a lower signal.

4.2 Experimental Procedures

4.2.1 Synthesis of ferrocene tagged antibodies

Antibodies alone generally cannot give an electrochemical response that can be affected by the addition of the corresponding antigen, therefore a redox tag is introduced onto the antibody that can give rise to a measurable electrochemical signal, in this case ferrocene was used as the tag using the methodology outlined by Dou *et al.*⁵⁴ where 10 μL of 1 mg mL^{-1} anti-progesterone was added to 190 μL of PBS (10 mM). The pH was then adjusted to ~ 9 with aqueous K_2CO_3 (5% w/v). A solution of ferrocenecarboxaldehyde in dimethylformamide (DMF) (20 mg in 200 μL^{-1}) was also prepared, the anti-progesterone solution was then added to the ferrocenecarboxaldehyde solution to give an antibody to ferrocenecarboxaldehyde mass ratio of 1:500. This mixture was left for 30 minutes to incubate allowing the formation of the imine product Ab-N=CH-Fc (Fc = ferrocene in this context). This was then reduced to Ab-NH-CH₂-Fc by the addition of sodium borohydride (2 mg), this solution was left for 10 minutes. The pH was readjusted to ~ 7 with 0.1 M HCl and again left for 10 minutes. All pH changes were confirmed by spotting a small amount of the mixture onto Whatman[®] universal indicator paper, pH 1-11.

The antibody was purified to remove any excess ferrocene, this was carried out *via* centrifugation (12,000 rpm for 20 min), the resulting supernatant was then transferred into 2 x Vivaspin[®] 500 centrifuge tubes; the solution was then re-centrifuged under the same conditions as described previously except for 8 minutes rather than 20, the waste liquid had then transferred into the collection part of the Vivaspin[®] tube, via the membrane with the purified antibodies remaining within the top vial. The solution was topped up to 100-150 μL with 10 mM PBS and centrifuged for a third time as a washing step, the final solution was made up to 200 μL with PBS (10 mM) within each tube and stored in the fridge at 4 °C until required. Figure 4.3 shows an overall schematic of the protocol.

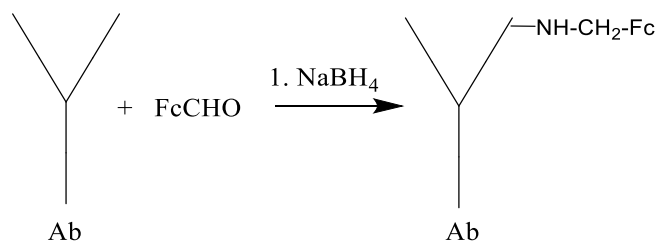


Figure 4.3 Schematic showing how the antibody tagging protocol with ferrocene.

4.2.2 Electrode modification

For the antibody immobilisation to occur the electrode needed to be modified to contain functional groups the antibody could bind through; this was carried out through a nitrobenzenediazonium reduction. Once the nitrobenzene was deposited the nitro functionality was electrochemically reduced to the amine.

The electrode material of choice was important as each substrate has different properties which can affect the immobilisation efficiency, this also had to reflect the cost of the electrode itself and the efficiency at which it could be utilised for this application.

During the electrochemical experimentation three different electrode materials were investigated:

- Gold
- Glassy carbon (GC)
- Tin doped indium oxide (ITO)

All electrochemical experiments were conducted using a standard three electrode setup where the counter electrode was a nickel wire with a Ag/AgCl reference electrode; this was true for all experiments discussed within this chapter.

Electrode modification

The gold and glassy carbon electrodes were used as purchased and were thoroughly polished before each modification process with alumina slurry. The electrode is fabricated with either a gold or glassy carbon rod in a plastic casing allowing the electrode to be placed directly into the solutions with the counter and reference electrodes.

The ITO electrodes were cleaned with isopropanol, copper tape was then connected to one end of the ITO electrode (1 cm on the electrode, 1 cm as a connection point) with three circular adhesive spacers with holes, these enabled the antibodies to be spotted onto the electrode surface, as well as providing the opportunity to measure multiple analytes.

The experiments on the ITO electrode were carried out by initially wrapping the counter electrode around the reference electrode, the reference electrode was then held in place by a clamp and retort stand, which was then be lowered into a (~70 μL) droplet pipetted onto the ITO electrode (This droplet refers to any solution required throughout).

This is depicted in figure 4.4:

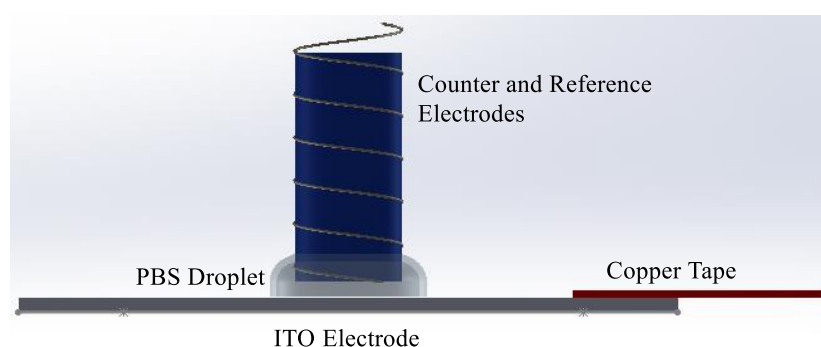


Figure 4.4: Diagram of the ITO electrode, 2 cm of copper tape was used with 1 cm on the electrode itself and 1 cm as a connection point, the centre of the spacers are 4 mm from the end of the electrode then a further 12 mm and a second 12 mm from the centre of the first and second spacers respectively.

Deposition solutions were made up consisting of 2 mM 4-nitrobenzenediazonium tetrafluoroborate and 0.1 M tetrabutylammonium perchlorate (TBAP) in acetonitrile (MeCN) and a second solution containing 0.1M KCl and ethanol with a 90:10 ratio.

The electrodes were then placed into the first solution containing the nitrobenzenediazonium tetrafluoroborate, cyclic voltammetry was used to deposit the nitrobenzene starting at +0.7 V scanning down to -0.4 V and with a return sweep to +0.7 V this was carried out over 3 cycles.

The electrode was washed with acetonitrile and air dried. The electrode was then immersed into the second solution containing the KCl and ethanol where the nitro group was reduced to the amine group again using cyclic voltammetry with the scans starting a +0.4 V with a sweep to -1.2 V and returning to +0.4 V again over 3 cycles.

This reduction gave the required amine group on the electrode surface for the antibodies to covalently bind towards. The values for the starting potential and reverse potential needed adjusting depending on electrode material and reference electrode used. All scans were conducted at a scan rate of 100 mV s^{-1} and all solutions were degassed under nitrogen or argon for 15 minutes prior to voltammetry commencing. The modification process is outlined in figure 4.5.

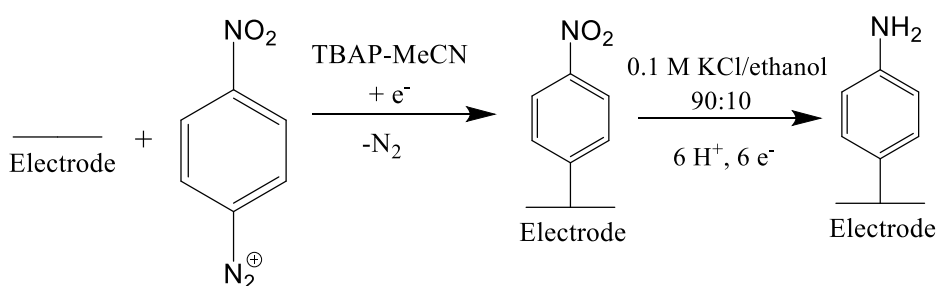


Figure 4.5 Schematic of the electrode modification process.

4.2.3 Antibody immobilisation and electrochemical immunoassay

An activation solution was prepared containing 2 mM EDC and 5 mM sulfo-NHS in PBS (10mM). A 50:50 mixture was then prepared using this solution and the ferrocene-tagged anti-progesterone antibodies (15 μ L of each); this mixture was then left for 15 minutes; this was to activate the acid groups on the antibody. Subsequently 30 μ L of this solution was pipetted onto the electrode surface and left covered in the fridge (~ 4 $^{\circ}$ C) for 18 hours. The activation buffer was prepared fresh every time it was required. Bringing figures 4.3 and 4.5 results in the concept that is shown in figure 4.1.

Conducting the electrochemical immunoassay

Electrodes were removed from the fridge and washed with a Tween-20/PBS solution, (0.1 v/v tween-20 in 10 mM PBS) this was followed by treatment with 30 μ L Bovine Serum Albumin (BSA) blocking buffer (1% BSA, 10 mM PBS) for 30 minutes. The electrodes were re-washed with the Tween-20/PBS solution. All voltammetric experiments were conducted in deoxygenated solutions. When electrodes were not used they were stored in PBS (10 mM).

Cyclic voltammetry was conducted on the antibody coated electrodes with scans starting at 0 V sweeping to + 0.6 V and returning to 0 V in PBS. Immobilised anti-progesterone antibodies were characterised by carrying out cyclic voltammetry at various scan rates, with these scan rates ranging from 10 mV s^{-1} to 1000 mV s^{-1} .

For the immunoassay itself a scan rate of 100 mV s^{-1} was used for cyclic voltammetry over 3 scans in 10 mM PBS. This was followed by square wave voltammetry where the frequency was 25 Hz and an amplitude of 1 mV the scan was conducted between 0 V and +0.5 V.

A stock concentration of progesterone was prepared by dissolving 1 mg of progesterone in 1 mL of ethanol and made up to 50 mL using PBS (10 mM) to give a $20 \mu\text{g mL}^{-1}$ progesterone stock solution, 10 fg mL^{-1} , 100 fg mL^{-1} , 1 pg mL^{-1} , 10 pg mL^{-1} , 100 pg mL^{-1} , 1 ng mL^{-1} , 10 ng mL^{-1} , 100 ng mL^{-1} and $1 \mu\text{g mL}^{-1}$ standards were then prepared using PBS (10 mM).

After each measurement the electrode was washed with 10 mM PBS and the antigen was added. Beginning with the lowest concentration 1 fg mL^{-1} (30 μL) the progesterone was left to incubate for 15 minutes, the electrode was again washed in PBS (10 mM) and the same experiment carried out starting with the cyclic voltammetry and followed by the square wave voltammetry. This procedure was repeated for the other antigen concentrations:

4.2.4 Electrochemical immunoassay in artificial saliva

The stock solution of progesterone was made up in the same way as previous described, however all standards were then prepared in artificial saliva. The artificial saliva was prepared using a recipe outlined by West *et al.*¹⁸⁷ the recipe consisted of sodium chloride (1.954 g L^{-1}), ammonium nitrate (0.328 g L^{-1}), potassium phosphate (0.639 g L^{-1}), potassium chloride (0.202 g L^{-1}), potassium citrate (0.308 g L^{-1}), uric acid sodium salt (0.021 g L^{-1}), urea (0.198 g L^{-1}), lactic acid sodium salt (0.146 g L^{-1}) and bovine submaxillary gland mucin Type I-S (30 g L^{-1}), the solution was made up in deionised water. The immunoassay was repeated as previous using the optimum incubation time determined.

4.3 Results and Discussions

To determine that the electrochemical immobilisation protocol was successful it was necessary to look at each stage individually; tagging the ferrocene to the antibodies, the nitrobenzenediazonium reduction, the subsequent reduction to the amine and the antibody immobilisation. Before carrying out any immobilisation process characterisation of the ferrocene tagged anti-progesterone was needed.

4.3.1 Anti-progesterone labelling with ferrocene

The ferrocene moiety attaches to the antibody through an aldehyde/amine linkage forming a secondary amine. This attachment can occur throughout the antibody structure as amine groups are found all over and the amount depends on the amino acid side chains, however as stated in chapter 1 the heavy chains within the fc region contain acid groups; this means at the other end of the protein chain within the fab region amine groups must exist. Through this attachment ferrocene groups will therefore be found within this region and therefore will have an interaction with an antigen that binds to the antibody indicating a signal change can occur.

The number of ferrocene moieties bound to the antibody was determined by UV-Vis spectrophotometry. Initially a full wavelength spectrum was conducted from 800 – 250 nm to determine the wavelength ferrocene absorbs. Following this the calibration was determined of the ferrocenecarboxaldehyde using a concentration range of 0.01 – 1 mg mL⁻¹, and the ferrocene tagged anti-progesterone using a concentration range between 5x10⁻⁴ - 2x10⁻³ mg mL⁻¹. The wavelength used was 454 nm. Figure 4.6 shows the UV spectra of ferrocenecarboxaldehyde and the ferrocene tagged antibodies.

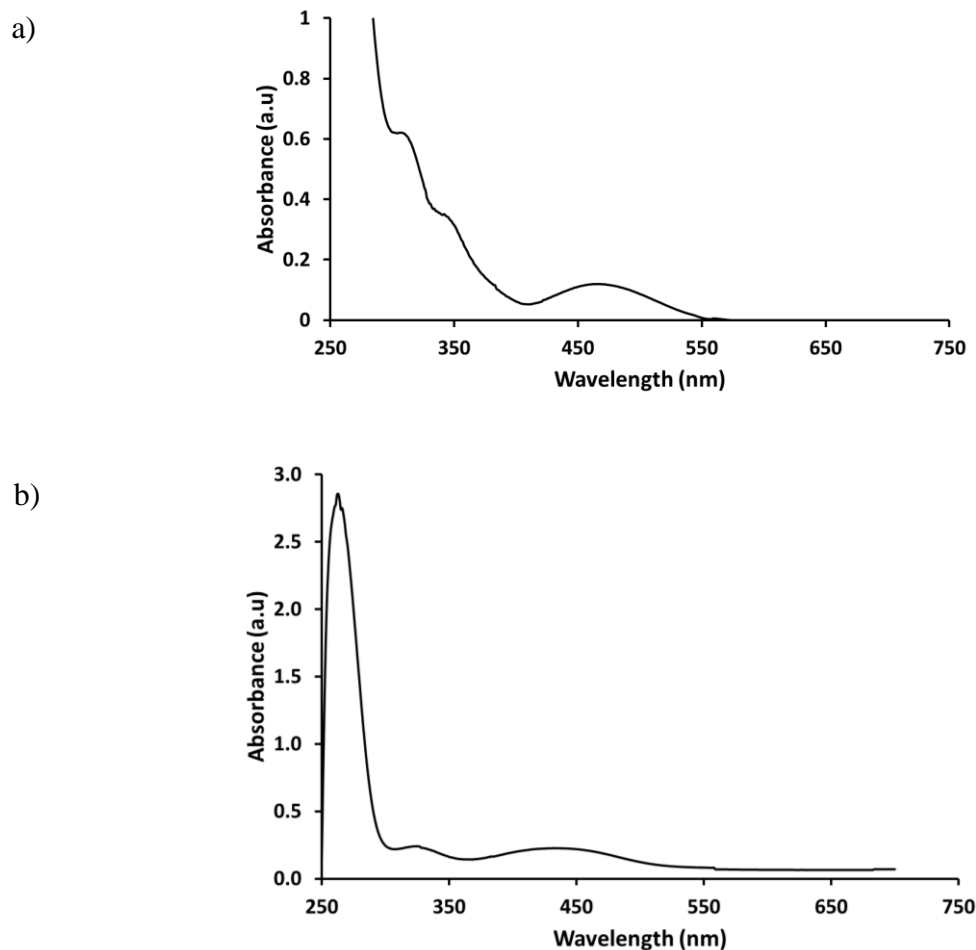


Figure 4.6: UV-Visible spectra of a) ferrocenecarboxaldehyde and b) the ferrocene tagged anti-progesterone antibodies.

It can be seen from spectrum 4.6a there was an absorbance peak at 460 nm and two shoulder peaks at 310 and 350 nm, the peak observed at 460 nm is in agreement with the literature where values of between 440 and 460 nm have been quoted for ferrocenecarboxaldehyde.^{188, 189} The shoulder peaks observed in the UV region of the spectra are weak and from previous work this is expected, and was due to the cyclopentadienyl rings from the ferrocene. Figure 4.6b shows the UV-Vis spectra of the ferrocene tagged anti-progesterone with peaks at 440 nm and at 320 nm and a third sharp peak at 250 nm. The peaks at 440 and 320 nm are due to the ferrocene moieties and with the sharp peak at 250 nm due to protein absorption which is typically observed between 200 and 300 nm. With anti-progesterone specifically absorbing at around 240-255 nm.¹⁹⁰

By carrying out this investigation the success of the antibody tagging was determined. Comparing figure 4.6a and 4.6b there was a slight shift in the peaks observed based on the ferrocene moieties which can be an attribute of the conjugation of the ferrocene to the antibody.¹⁹¹ Using Beer-Lambert Law a calibration of the ferrocene-tagged anti-progesterone and the ferrocenecarboxaldehyde was created. Through taking the ratio of the extinction coefficients of the two systems the average number of tags could be estimated.¹⁹² This assumed all the ferrocene present was tagged to the antibodies, with none present in solution.

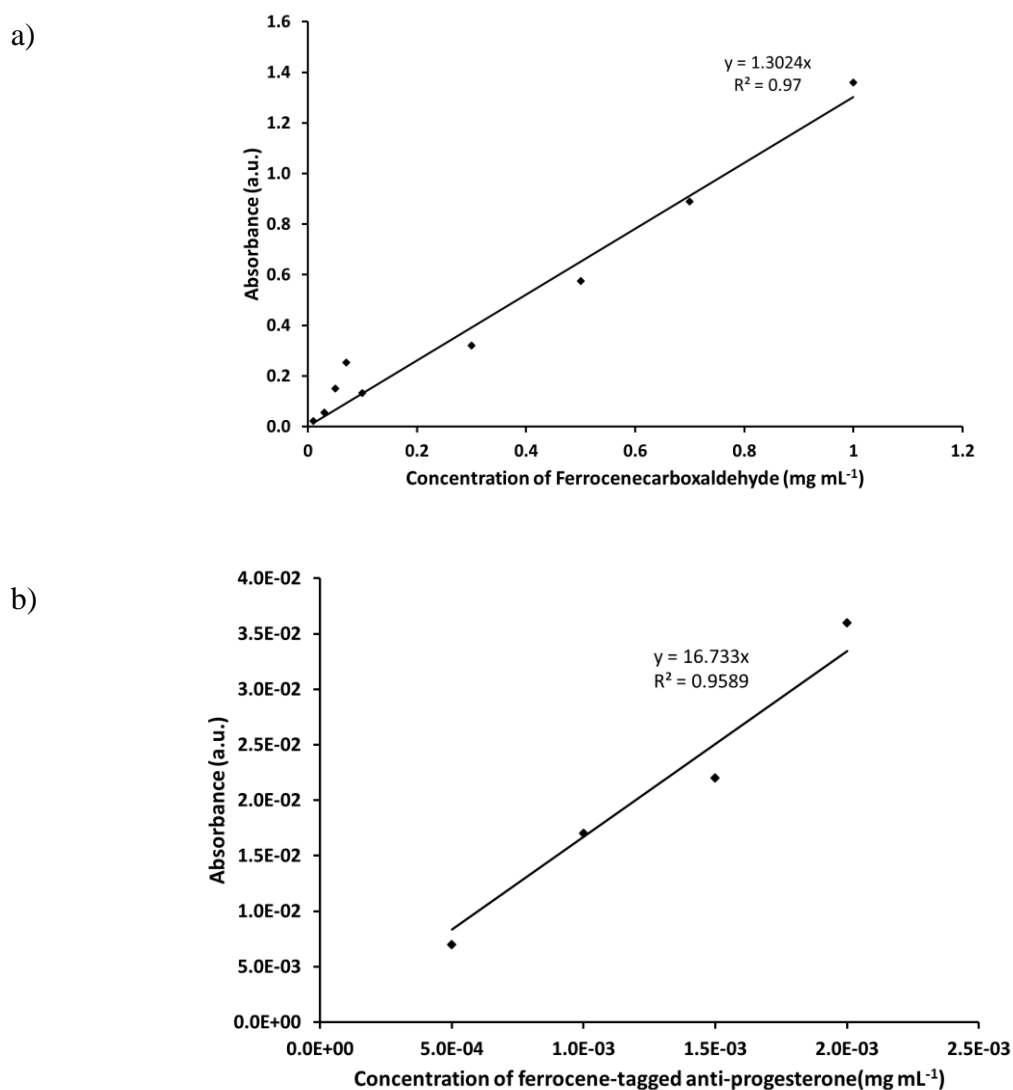


Figure 4.7: Calibration curves of a) ferrocenecarboxaldehyde and b) ferrocene tagged anti-progesterone, with absorption values taken at 454 nm.

Figure 4.7 shows calibration plots of the ferrocene prior to tagging to the anti-progesterone (a) and after tagging to the anti-progesterone (b); both plots show reasonably good correlation ($R^2 > 0.95$). Using Beer-Lambert's law the gradient of the plot represents the extinction coefficient multiplied by the path length. In this case the path length was 1 cm, therefore the extinction coefficient equals the gradient of the calibration plot.

Therefore ϵ was $1.3024 \text{ mL mg}^{-1} \text{ cm}^{-1}$ for the ferrocenecarboxaldehyde and $16.733 \text{ mL mg}^{-1} \text{ cm}^{-1}$ for the ferrocene tagged anti-progesterone.

Through these coefficients the average number of ferrocene tags was determined.

$$\# \text{ of ferrocene tags} = \frac{\epsilon_{\text{ferrocene tagged anti-progesterone}}}{\epsilon_{\text{ferrocenecarboxaldehyde}}} \quad (4.1)$$

$$\# \text{ of ferrocene tags} = \frac{16.733}{1.3024}$$

The number of ferrocene tags therefore equalled ~ 12.8 tags rounded up to ~ 13 tags per antibody. Okochi *et al.* calculated the mean number of ferrocene moieties to be 8, using a similar route where atomic absorption spectroscopy was carried out, with the number of ferrocene moieties calculated through a Beer-Lambert relationship.¹⁹² The reason for this difference is not clear however one possible explanation is the number of free amino groups on the antibody as this will differ between antibodies altering the number of ferrocene moieties observed.

4.3.2 Comparison of electrode materials for the electrochemical immunoassay

4.3.2.1 Electrode modification on different electrode substrates

Nitrobenzenediazonium reduction

Gold electrode

The gold electrode was modified as described in section 4.2.2, with the nitrobenzene deposited onto the surface followed by a reduction to the corresponding aniline.

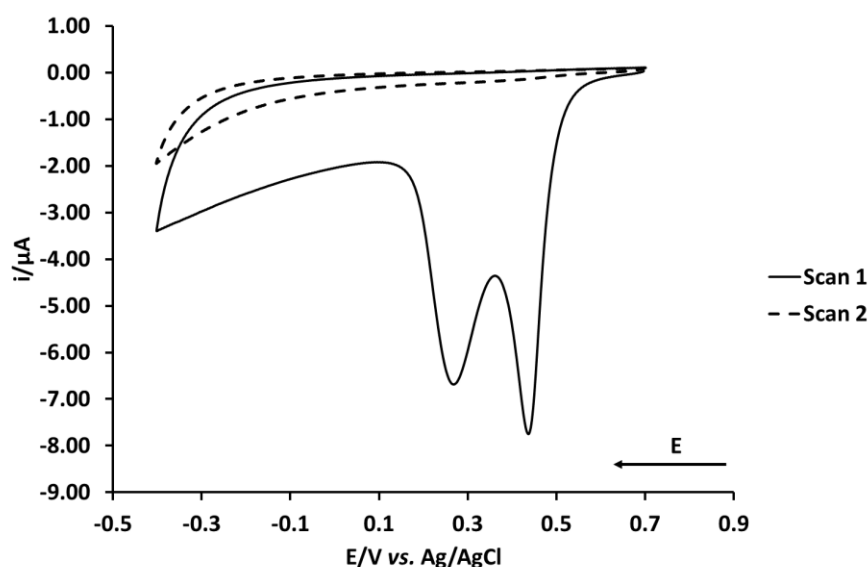


Figure 4.8: Cyclic voltammogram showing the deposition of nitrobenzenediazonium onto a gold electrode surface (2mM in TBAP/MeCN), with two cycles from +0.7 V down to -0.4 V and returning to +0.7 V at 0.1 V s⁻¹.

Figure 4.8 represents the voltammogram of the deposition of nitrobenzene onto a gold electrode surface. From the first scan there are two clear narrow peaks one at +0.45 V and a second at +0.25 V. The second scan shows no peaks. The peaks from scan one represent the nitrobenzene deposition on polycrystalline gold, this was discussed by Benedetto *et al.* whom investigated the double peak phenomenon on gold, obtaining a similar voltammogram as produced here, they attributed this double peak to Au (1 1 1) and Au (1 0 0) facets while they also state that at -0.5 V a broad third peak could be observed due to deposition on other crystallographic facets of gold such as Au (3 1 1) however a third

peak was not observed in this work.¹⁹³ The disappearance of the peaks during the second scan was also seen by Pinson and Podvorica.¹⁹⁴ They attributed these irreversible reduction peaks (from scan 1) to the cleaving of nitrogen and then through scan 2 where the peaks disappear being due to the nitrobenzene layer forming on the electrode surface causing a blocking affect. Laforgue *et al.*¹⁹⁵ stated that after the first scan it is assumed that a monolayer is formed and subsequent scans result in multilayer formation through an addition to the ortho position upon the pre-deposited layer.

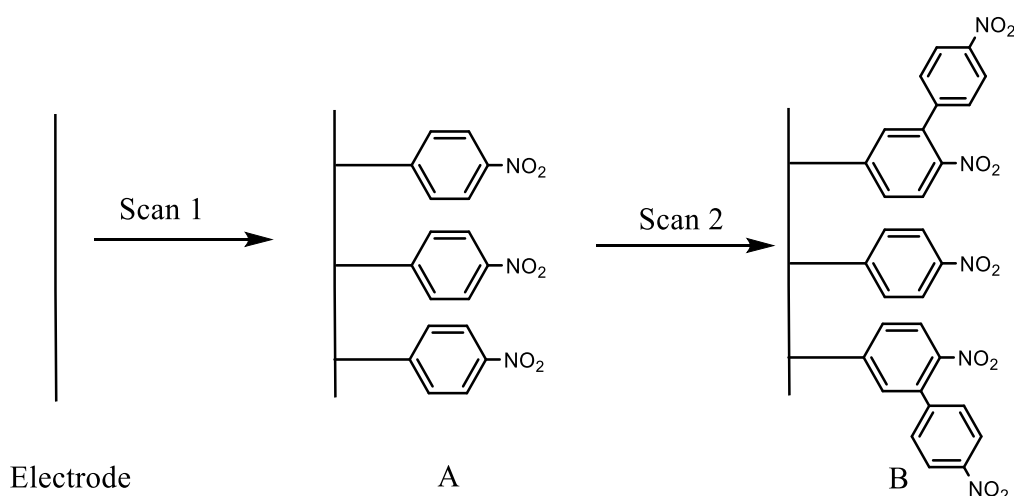


Figure 4.9: Schematic showing the nitrobenzene deposition, where A) a monolayer is formed after the first scan and B) a multilayer after subsequent scans in the ortho position.

Figure 4.9 shows a schematic of the deposition of the nitrobenzene layer during the first scan which is followed by the multilayer formation after scan 2 where the nitrobenzene radical attaches to the ortho position on the benzene ring. Due to the formation of the nitrobenzene radical within the deposition obtaining a monolayer is very difficult to control however this is not an issue because the nitro groups still remain on the surface therefore allowing the subsequent reduction to take place.¹⁹⁶ The mechanism for this deposition was also investigated by Munteanu *et al.*¹⁹⁷ where two possible mechanisms are discussed, one route follows on from work by Zollinger^{198, 199} where there is the formation of a carbocation intermediate (figure 4.10) which is then reduced to the radical.

Munteanu suggested that this mechanism is possible when using solvents of low nucleophilicity such as acetonitrile. The second mechanism is that presented in figure 4.10 where the radical is formed immediately without the carbocation intermediate.

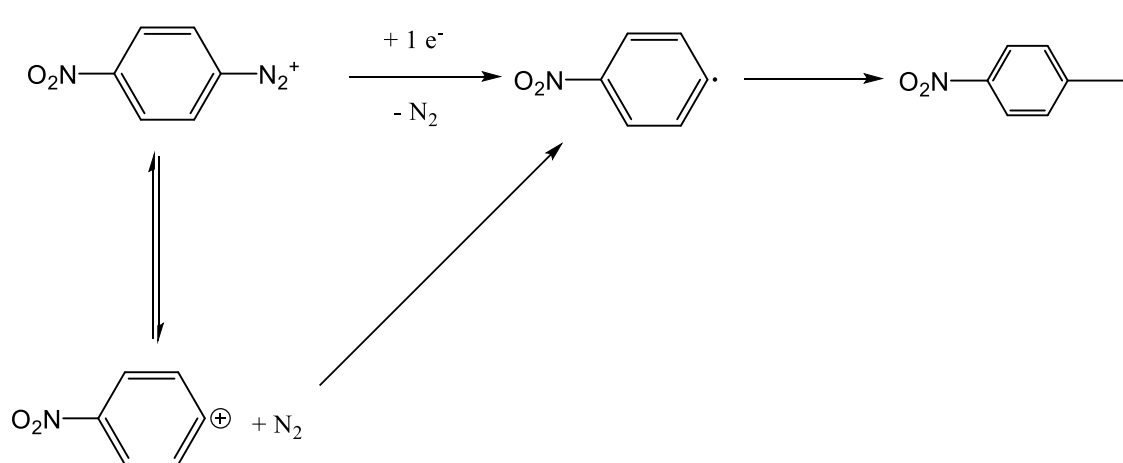


Figure 4.10 schematic showing the potential pathways for nitrobenzenediazonium reduction followed by grafting onto the electrode surface.

Figure 4.10 is a schematic showing the different reaction pathways as outlined by Manteanu. Manteanu does state that the formation of the carbocation intermediate takes in region of 3 hours far longer than electrochemical measurements and therefore conclude that the route is most likely to occur through the formation of the radical (figure 4.9) without any other intermediately steps which is also the generically accepted mechanism. The formation of the radical also explains why multilayers are observed rather than monolayers.

Glassy carbon electrode

Figure 4.11 shows the cyclic voltammogram for the nitrobenzenediazonium reduction on the glassy carbon electrode.

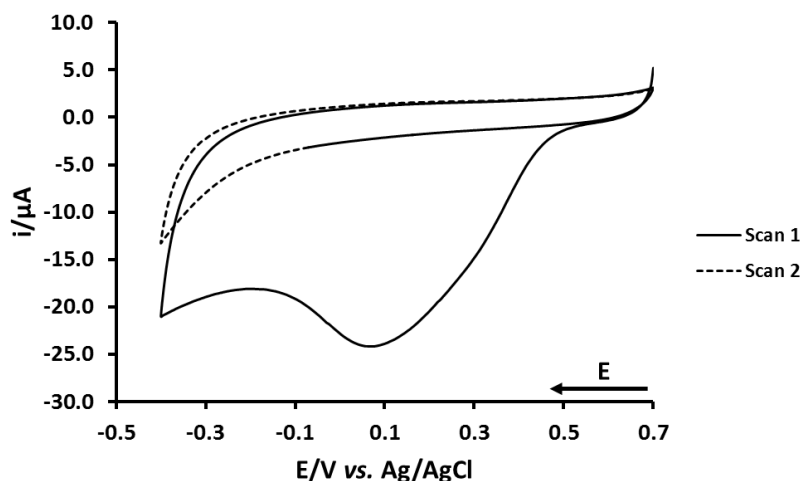


Figure 4.11: Cyclic voltammograms showing the nitrobenzenediazonium deposition onto the GC electrode surface (2mM in TBAP/MeCN), where the solid black line represents the first scan and the dotted line showing the second scan.

The voltammogram shows a broad reduction peak at around +0.05 V through scan 1 with no peak through scan 2. The peak observed through scan 1 is in line with the expected potential for the reduction of the nitrobenzenediazonium salt on a glassy carbon electrode^{194, 200}. This reduction peak disappears through scan 2. Pinson and Podvorica attribute this broad irreversible reduction peak to the cleaving of nitrogen gas from the nitrobenzene. The reason for the peak disappearance in the second scan was the same as that discussed for the gold electrode.¹⁹⁴

ITO electrode

Figure 4.12 shows the cyclic voltammogram for the nitrobenzenediazonium reduction on ITO:

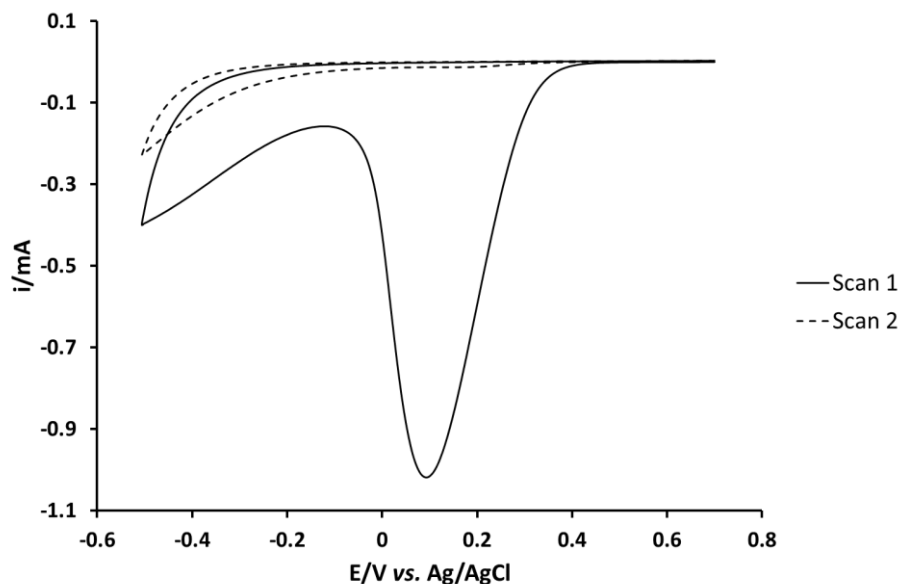


Figure 4.12: Cyclic voltammograms showing the deposition of nitrobenzenediazonium onto an ITO electrode surface (2mM in TBAP/MeCN). Where the solid black line represents the first scan with the dashed line representing the second scan.

From scan 1 a sharp reduction peak was seen at +0.1 V which disappeared through scan 2. The peak observed through scan 1 is similar to those seen on the gold electrode where the peaks were sharp (figure 4.9) rather than broad (glassy carbon, figure 4.11). This single sharp peak indicates that the ITO surface is flat and universal which is unsurprising as the ITO electrodes are fabricated by depositing a thin layer of ITO onto a glass surface.

Comparing the three different substrates, they all gave the expected reduction waves for the nitrobenzene deposition. There are clear differences however in the waves obtained for each of the surfaces and this difference is due to the materials surface properties. The gold and ITO gave rise to sharp reduction peaks whereas the GC with a broad reduction peak.

The difference of the glass carbon and ITO compared to the gold electrode was that the reduction showed one peak instead of two, indicating a more universal crystalline structure across the electrode surface.

Having deposited the nitrobenzene layer onto the electrode surface the nitro group was then reduced to the corresponding amine.

Nitro to amine electrochemical reduction

Gold

The nitro to amine reduction required protons and therefore needed to be carried out in a protic solution, in respect of this process the proton donor was ethanol. Figure 4.13 presents the voltammogram for the nitro reduction on gold:

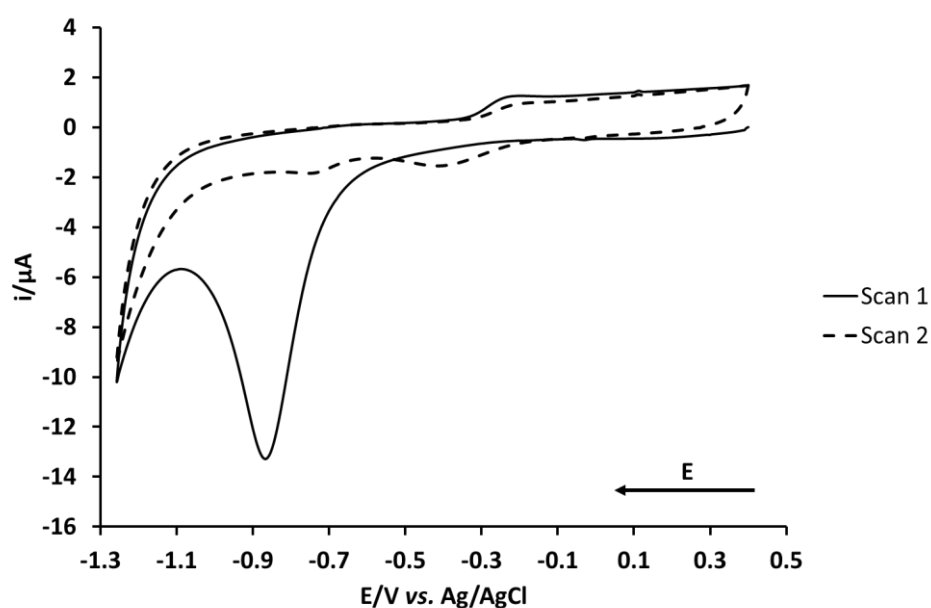


Figure 4.13: Cyclic voltammogram of the reduction of nitrobenzene to aniline on a gold electrode surface, solution consisted of 90:10 0.1 M KCl and ethanol scan rate 0.1 V s^{-1} .

From the first scan a reduction peak at -0.9 V was observed which subsided during scan 2. A reversible system was seen between -0.3 and -0.4 V from the end of the first scan and throughout the second scan. This sharp reduction can be attributed to the six proton, 6 electron reduction of the nitro moiety to the corresponding amine moiety, this peak was in agreement with Gui *et al.* where nitrobenzene deposition and the corresponding reduction to the amine was compared on both gold and glassy carbon electrodes (see next section for glassy carbon). Within their work a sharp reduction peak was seen at -0.9 V.²⁰⁰ Towards the end of the first cycle there was an oxidation peak at -0.3 V which represented the oxidation of phenylhydroxylamine group to nitrosobenzene caused by the formation of nitrosobenzene as an initial intermediate see figure 4.14.

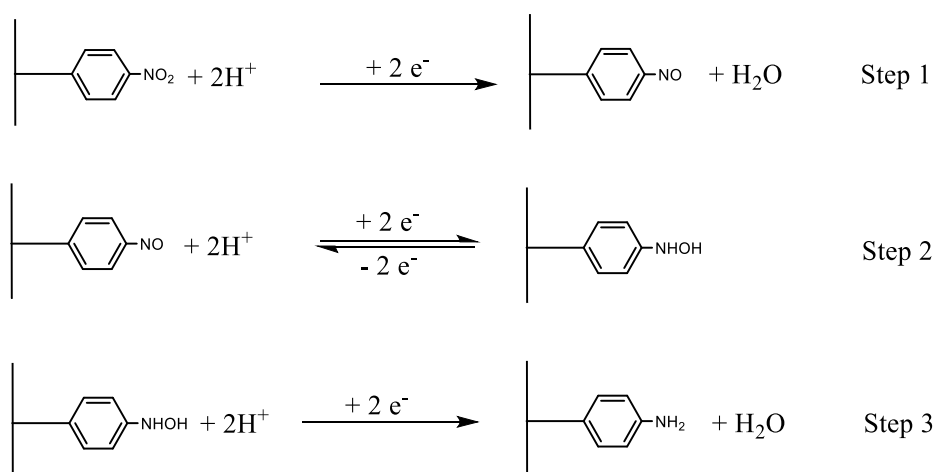


Figure 4.14: Schematic showing the reduction of the nitro group to the corresponding amine through a three step process.

The reaction scheme in figure 4.14 was proposed by Gui *et al.* where in step one there is a two proton, two electron reduction to form the nitroso group and water. In step two this group goes through another two proton, two electron reduction to form the hydroxylamine group which can readily reverse back to form the nitroso group. It is this intermediates reversibility that causes the oxidation and reduction peaks observed in figure 4.6 at -0.3 and -0.4 V. Step three shows a final two proton, two electron reduction to form the amine

group and water. Two moles of water are lost throughout this process which is irreversible.

Glassy carbon

Figure 4.15 shows the cyclic voltammogram for the nitro to amine reduction on glassy carbon:

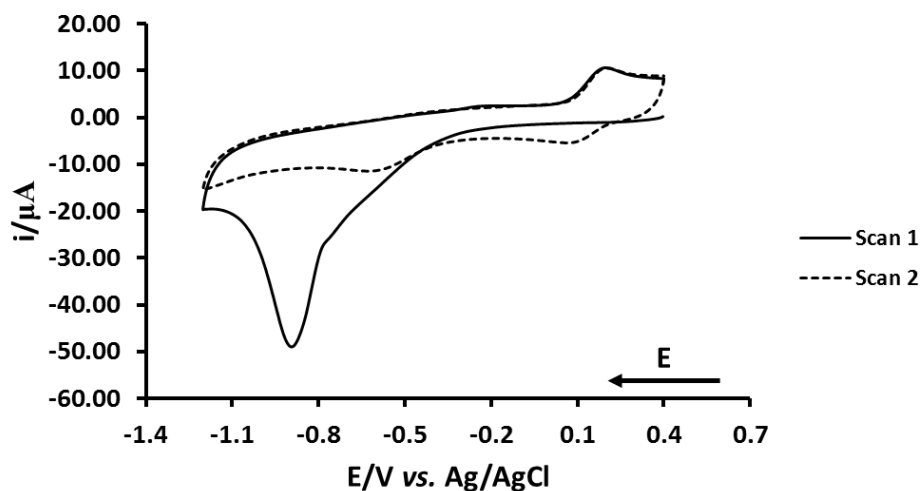


Figure 4.15: Cyclic voltammogram showing the reduction of nitrobenzene to aniline on a GC electrode, where the solid black line represents the first scan and the dotted line showing the second scan, solution consisted of 90:10 0.1 M KCl and ethanol, scan rate 0.1 Vs^{-1} .

The voltammogram shows a sharp reduction peak at -0.9 V followed by an oxidation peak at +0.2 V during scan 1. During scan two there was a reduction peak at +0.1 V. The voltammogram clearly represents all the individual processes that occur during the chemical reaction. The first scan shows a sharp reduction peak at $\sim -0.9 \text{ V}$ indicating the reduction of the nitro group to the amine. Upon completion of the first cycle an anodic peak is observed at +0.3 V with a reduction following at +0.1 V. These peaks represent the oxidation and reduction of the nitroso moieties to the hydroxylamine moieties in the same way as discussed with respect to the gold electrode and shown in figure 4.14.²⁰¹

ITO electrode

Figure 4.16 shows the cyclic voltammogram for the nitro to amine reduction on ITO.

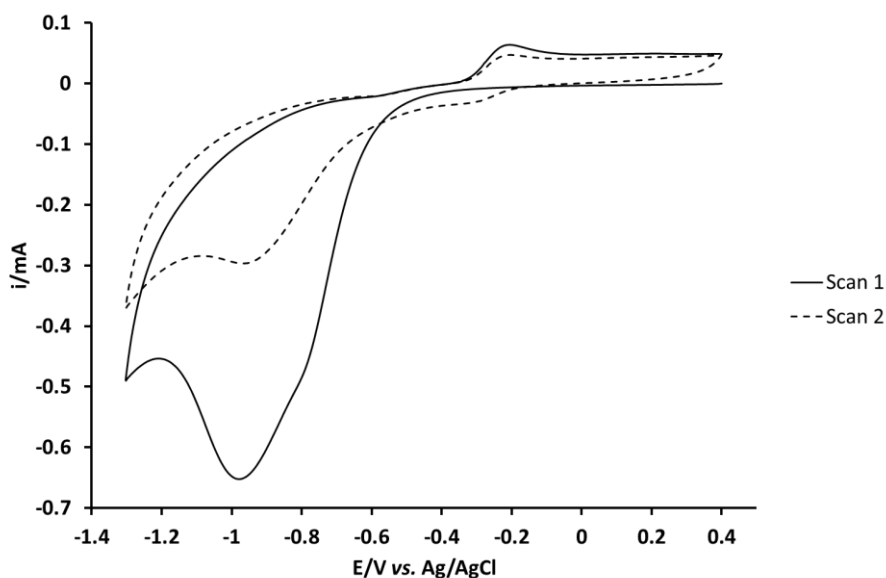


Figure 4.16: Cyclic voltammograms showing the reduction of the nitro moieties to the corresponding amine on an ITO electrode with scan 1 represented by the solid black line and the second scan by the dotted line, solution contained of 90:10 0.1 M KCl and ethanol, scan rate 0.1 V s^{-1} .

For the first scan there is a sharp reduction around -1V followed by an oxidation at -0.2 V. During the second scan reduction peaks are seen at -0.3 V, -0.9 V and an oxidation at -0.2 V. The peak at -1 V is representative of the full reduction of the nitro moieties to the amine through the mechanism presented in figure 4.14. With the oxidation and reduction peaks at -0.2 V and -0.3 V which is step 2 in figure 4.14.

By having the polyaniline layer on the electrode surface electron transfer between the ferrocene and the electrode is enhanced, with the aniline acting as a “molecular wire” (figure 4.1).¹⁸⁵

4.3.2.2 Characterisation of the anti-progesterone immobilised electrode surface

The characterisation of the ferrocene-tagged antibodies on the electrode surface was investigated by using cyclic voltammetry.

Characterisation of ferrocene tagged anti-progesterone immobilised on gold

Figure 4.17 shows the CVs of the antibody modified gold electrode at various scan rates ranging from 10 mV s^{-1} rising to 1000 mV s^{-1} .

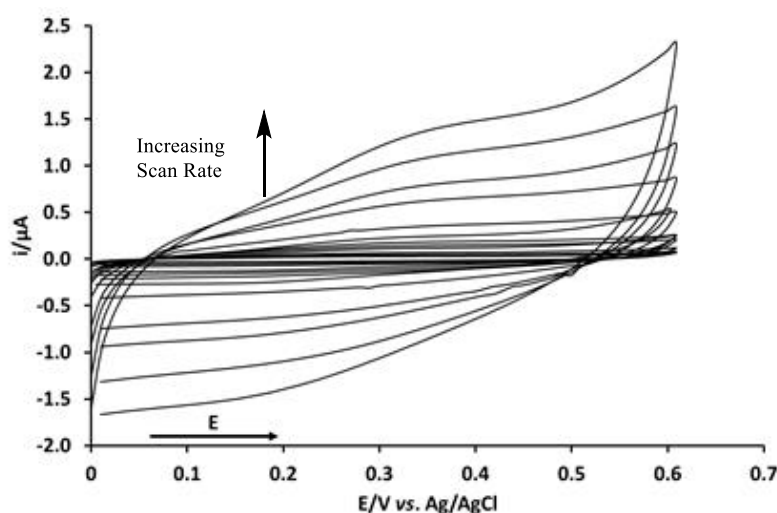


Figure 4.17: Cyclic voltammograms of ferrocene-tagged anti-progesterone on the gold electrode surface with scan rates from 10 mV s^{-1} rising to 1000 mV s^{-1} .

An oxidation peak can be seen at $+0.35 \text{ V}$, which confirms that the ferrocene is on the surface and that the immobilisation process had been successful. The weak redox peak is indicative of large capacitance within the system. To further confirm this a graph was plotted of peak current against scan rate a linear trend would confirm the surface confinement of the redox species.

Equation 4.2 shows the relationship between the peak, the scan rate and the concentration of redox species on the surface. By using this equation it can be confirmed that the ferrocenes are surface confined, by plotting the peak current against the scan rate.

$$i_p = \frac{n^2 F^2 \nu A \Gamma}{RT} \quad (4.2)$$

Where i_p is the peak current (ampere), n is the number of electrons transferred, F is Faraday's constant, A is the area of the electrode surface (m^2), Γ is the surface coverage (mol m^{-2}), ν is the scan rate (V s^{-1}), R is the gas constant and T the absolute temperature (K).²⁰²

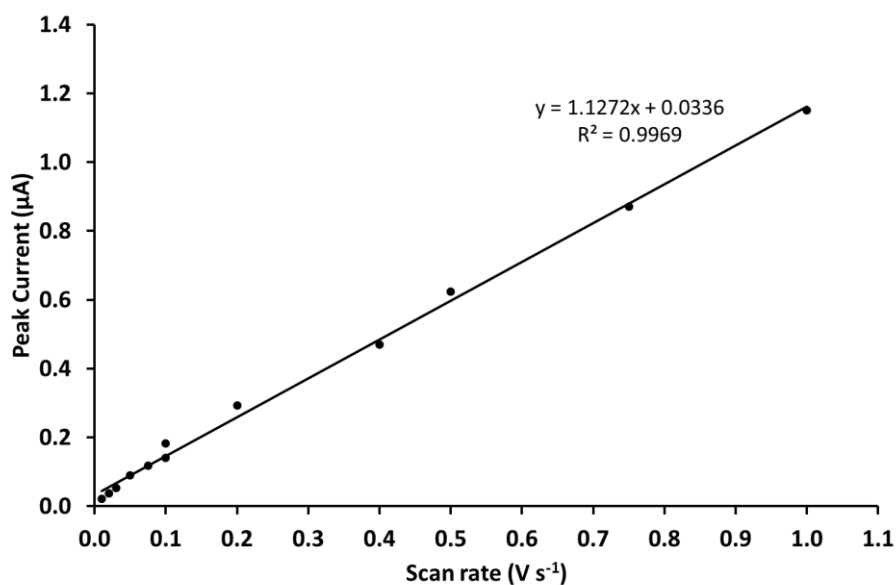


Figure 4.18: Plot showing how the peak current changes with an increase in the scan rate.

Equation 4.2 states that the peak current is proportional to the scan rate confirming that the redox process is confined to the electrode surface and not occurring through diffusion (Randles-Sevcik relationship).²⁰³ Figure 4.18 shows a linear relationship and follows the results reported by Dou *et al.*⁵⁴

This can be further shown by a plot of the $\frac{i_p}{\sqrt{\nu}}$ vs $\sqrt{\nu}$ (figure 4.19):²⁰⁴

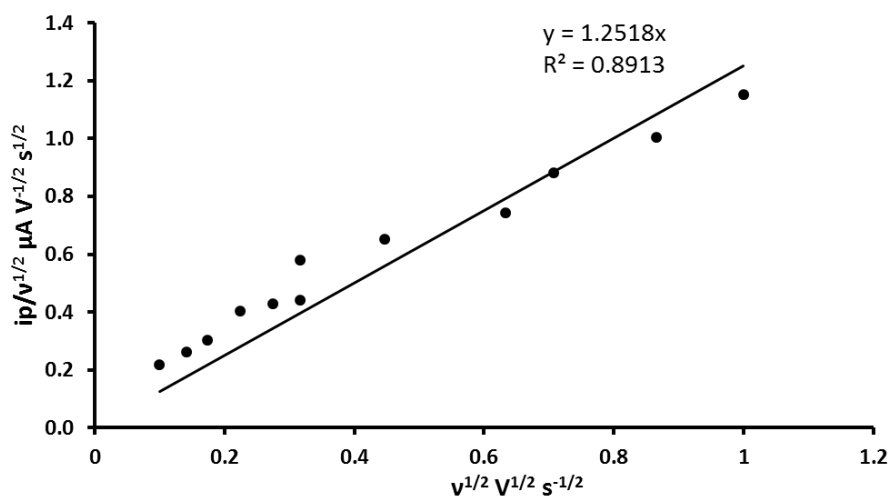


Figure 4.19 plot describing the peak current over the square root of the scan rate versus the square root of the scan rate on a gold electrode.

Figure 4.20 shows a linear relationship between $\frac{i_p}{\sqrt{v}}$ vs \sqrt{v} . As described by Thomasson *et al.* a linear relationship through this plot shows that the peak current is therefore proportional to the square root of the scan rate again confirming the surface confined redox species, this also proves that there is no diffusion occurring at the electrode surface and that the signal is that from the surface confined ferrocenes.²⁰⁴

Cyclic voltammetry of the anti-progesterone modified GC electrode

The applicability of the GC electrode was investigated. Figure 4.20 shows the CVs for a range of scan rates from 10 mV s^{-1} up towards 500 mV s^{-1} .

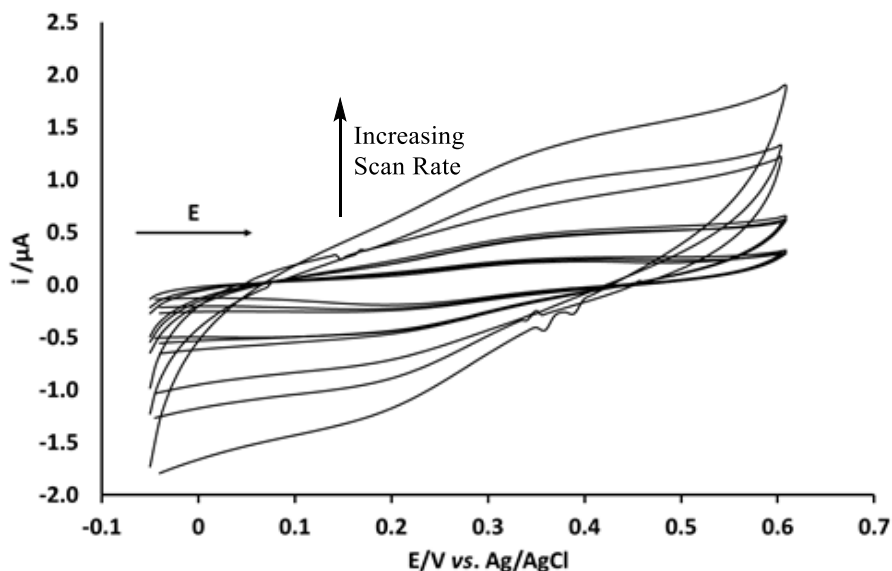


Figure 4.20: CVs of the ferrocene tagged anti-progesterone at various scan rates on a glassy carbon electrode.

It can be seen that at +0.3 V region there is an oxidation wave observed which represents the oxidation of the ferrocene to the ferrocenium cation with a reduction wave being observed at +0.2 V, during the reduction scans grooves can be seen this is a result of noise in the system and external influence on the electrode. The scan rate was plotted against peak current according to equation 4.2 and is shown in figure 4.21:

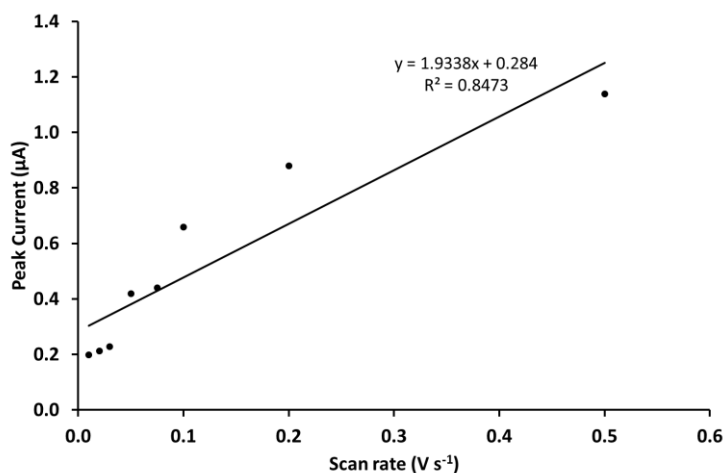


Figure 4.21: A graph showing how the peak current changes with increasing scan rate on glassy carbon.

As the scan rate increases the peak current increases, but would expect a linear relationship between the two (equation 4.2). However as the graph shows a linear relationship was not observed.

Unlike the gold electrode where scan rates up to 1000 mV s⁻¹ were investigated, above 500 mV s⁻¹ the glassy carbon electrode gave voltammograms where an oxidation peak was not clearly visible. With the correlation coefficient being only 0.89, despite the surface confinement of the ferrocene, the reliability and sensitivity of the system could be an issue. A plot of $\frac{i_p}{\sqrt{v}}$ vs \sqrt{v} gave no useful results.

CV of ferrocene tagged anti-progesterone on ITO

The ferrocene tagged antibodies on the ITO electrode surface was then investigated to gage the electrodes suitability, the success of this electrode surface could allow a translation from electrochemical detection to chemiluminescence detection as the surface is transparent.

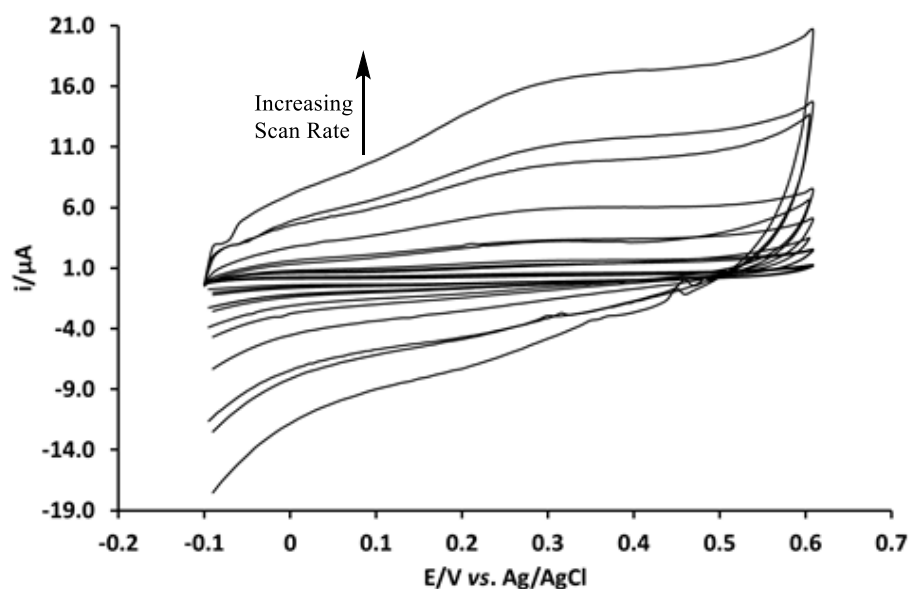


Figure 4.22: CVs of ferrocene tagged anti-progesterone on the ITO surface at various scan rates, ranging from 10 mV s^{-1} to 1000 mV s^{-1} .

Figure 4.22 shows the ferrocene tagged anti-progesterone antibodies on the ITO surface, there is a clear oxidation peak at $+0.275 \text{ V}$ even at the higher scan rates. The figure follows the same trend as that observed for the GC and Au electrodes. The oxidation peak observed at $+0.275 \text{ V}$ represents the oxidation of ferrocene to the ferrocenium cation; with the corresponding reduction seen at $+0.25 \text{ V}$ particularly at the higher scan rates being observed. This reduction was not however as prominent in relation to the oxidation peak.

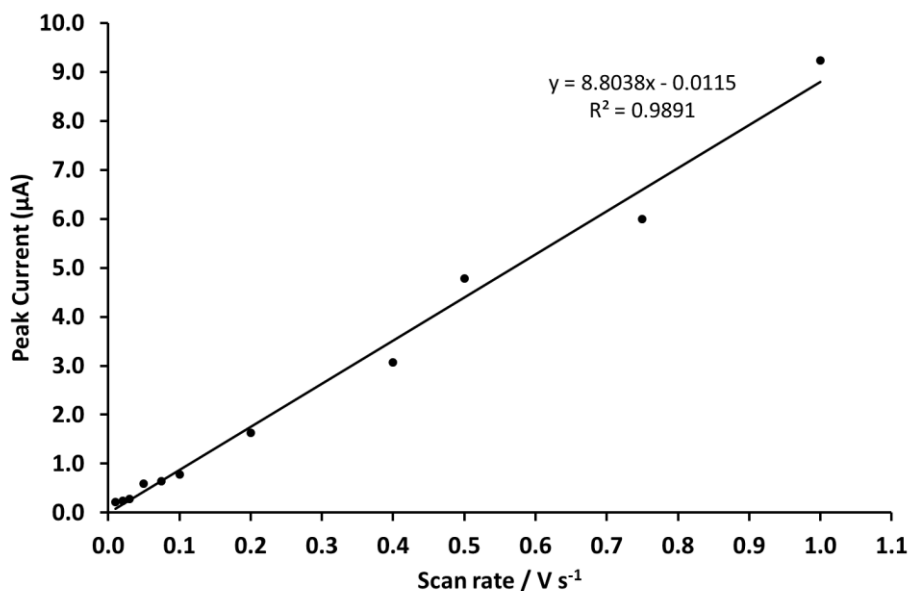


Figure 4.23: Graph showing how the peak current observed changes with the scan rate on ITO.

For this system as shown in figure 4.23 a linear correlation was observed where the peak current increased with the scan rate. The correlation coefficient of 0.98, indicated that the system would be suitable for investigating electrochemical immunoassays.

Similarly as shown for the gold electrode this can be further confirmed though the plot of

$\frac{i_p}{\sqrt{v}}$ vs \sqrt{v} (figure 4.24):

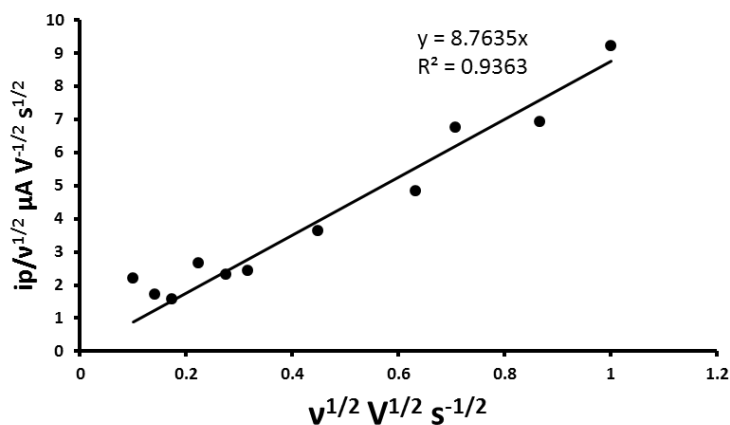


Figure 4.24 plot describing the peak current over the square root of the scan rate *versus* the square root of the scan rate on an ITO electrode.

Figure 4.24 shows a linear relationship with a stronger correlation to that observed on gold further enhancing the surfaces ability to act as a suitable antibody immobilisation platform for carrying out immunoassays. Comparing the three electrode materials the gold and the ITO electrode provide the best substrate for immobilisation of antibodies.

The reasoning for the difference between the three electrode surfaces stems from the electron transfer involved in the deposition process. Lehr *et al.* investigated the nitrobenzene grafting on a glassy carbon electrode, they concluded that the thickness of the nitrobenzene layer is largely affected by the amount of time the electrode is immersed in the solution, indicating a long period of time is required to obtain the nitrobenzene films²⁰⁵. The result of this grafting would impact the concentration of antibodies on the surface impacting the efficiency of the electrode surface to carry out the immunoassay.

4.3.2.3 Electrochemical immunoassay on each electrode surface

Having characterised the antibody immobilisation protocol on the various electrode substrates, an electrochemical immunoassay was carried out. This immunoassay was different to the competitive and non-competitive immunoassays described in section 1.4.2.2. In this method the sample of interest was incubated for 15 minutes with the antibody. As explained in the introduction to this chapter (section 4.1) if no antigen is present there will be a large electrochemical signal produced. After incubation the antigen binds to the antibody blocking the ferrocenes resulting in a lower signal. For all measurements the CV was run at 0.1 V s^{-1} , this was chosen to allow the electrochemical reaction to occur which can be a problem at faster scan rates due to the electrode kinetics and slower scan rates result in a slow analysis time, the same is true for the SWV.

Electrochemical immunoassay on gold

Having determined that the ferrocene-tagged anti-progesterone immobilised onto the gold electrode surface is present and suitable for carrying out an electrochemical immunoassay various concentrations of progesterone were incubated for 15 minutes on the electrode surface according to the procedure outlined in section 4.2.3. Cyclic voltammetry and square wave voltammetry was then carried out on the system before and after incubation.

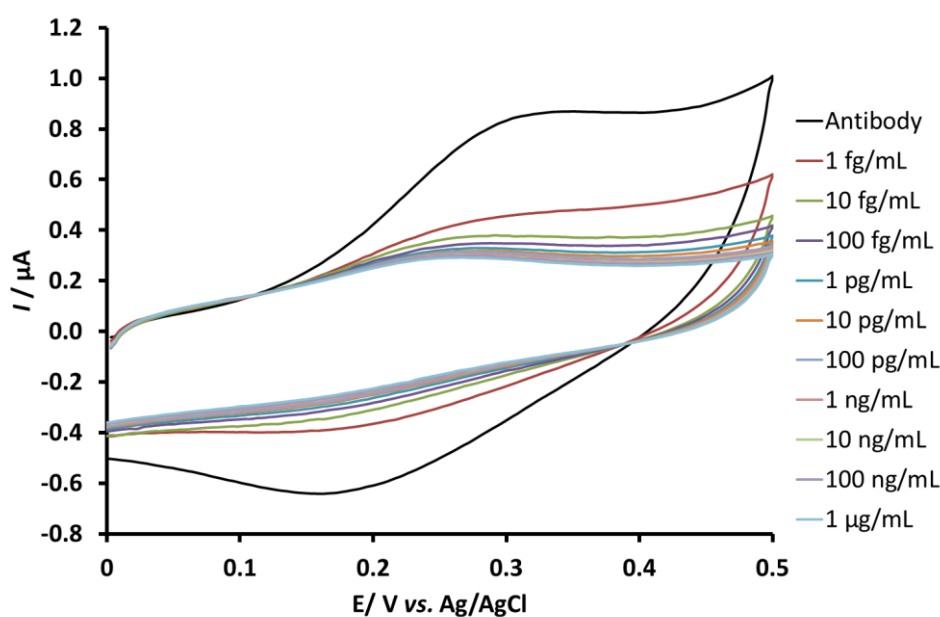


Figure 4.25: Cyclic voltammograms showing the ferrocene-tagged anti-progesterone as the system is incubated with an increasing concentration of progesterone, varying from 1 fg mL^{-1} rising to $1 \mu\text{g mL}^{-1}$ for 15 minutes, the black line represents the antibody before any progesterone addition scan rate 0.1 V s^{-1} . Measurements were carried out in 10 mM PBS .

The legend within figure 4.25 applied directly for all other voltammograms within this section. The black line represents the anti-progesterone without any addition of progesterone, which clearly shows an oxidation and reduction peak at +0.3 V and +0.2 V respectively. After the first addition of progesterone there is a substantial decrease in the observed current for both the oxidation and reduction peaks and this continues as the concentration of progesterone increases. The CV gives a good indication as to how the system responds upon addition of progesterone however, to use this technique for

analytical quantification, square wave offers increased sensitivity. For the reasons outlined in chapter 2.

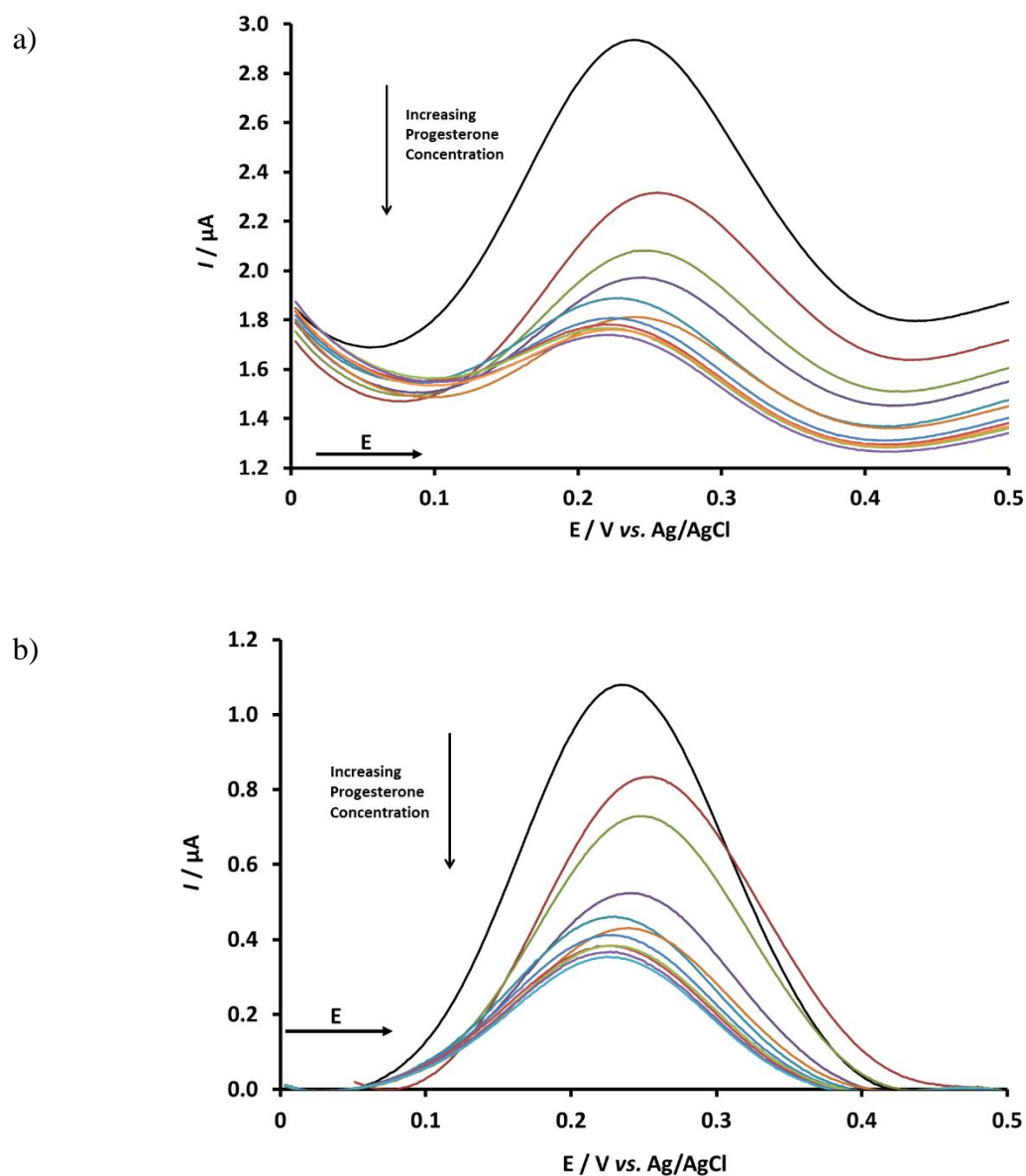


Figure 4.26: Square wave voltammograms showing the change in signal as the concentration of progesterone added increased from 1 fg mL^{-1} rising to $1 \text{ } \mu\text{g mL}^{-1}$ on a gold electrode. The black lines represents the anti-progesterone prior to the addition of progesterone. A) Without baseline correction and b) with baseline corrections, frequency 25 Hz, amplitude 1 mV. Measurements were carried out in 10 mM PBS.

Figure 4.26a shows the square wave voltammograms obtained as the concentration of progesterone incubated on the electrode surface increased. With b) showing the same voltammograms but with a baseline correction to show the trend more clearly. It can clearly be seen that there is a clear drop in the current observed as the concentration of progesterone increases.

This signal change shows that there was an affect from the antigen in this case progesterone and the ferrocene tagged onto the antibody, as found by Dou *et al.*⁵⁴

Using this signal change a calibration was obtained to measure the systems applicability to monitoring the concentrations of progesterone

The change in peak current was calculated by using $\Delta i = i_{Ab} - i_{Ag}$ where i_{Ab} represents the current prior to the addition of antigen and i_{Ag} represents the current after the addition of the antigen.

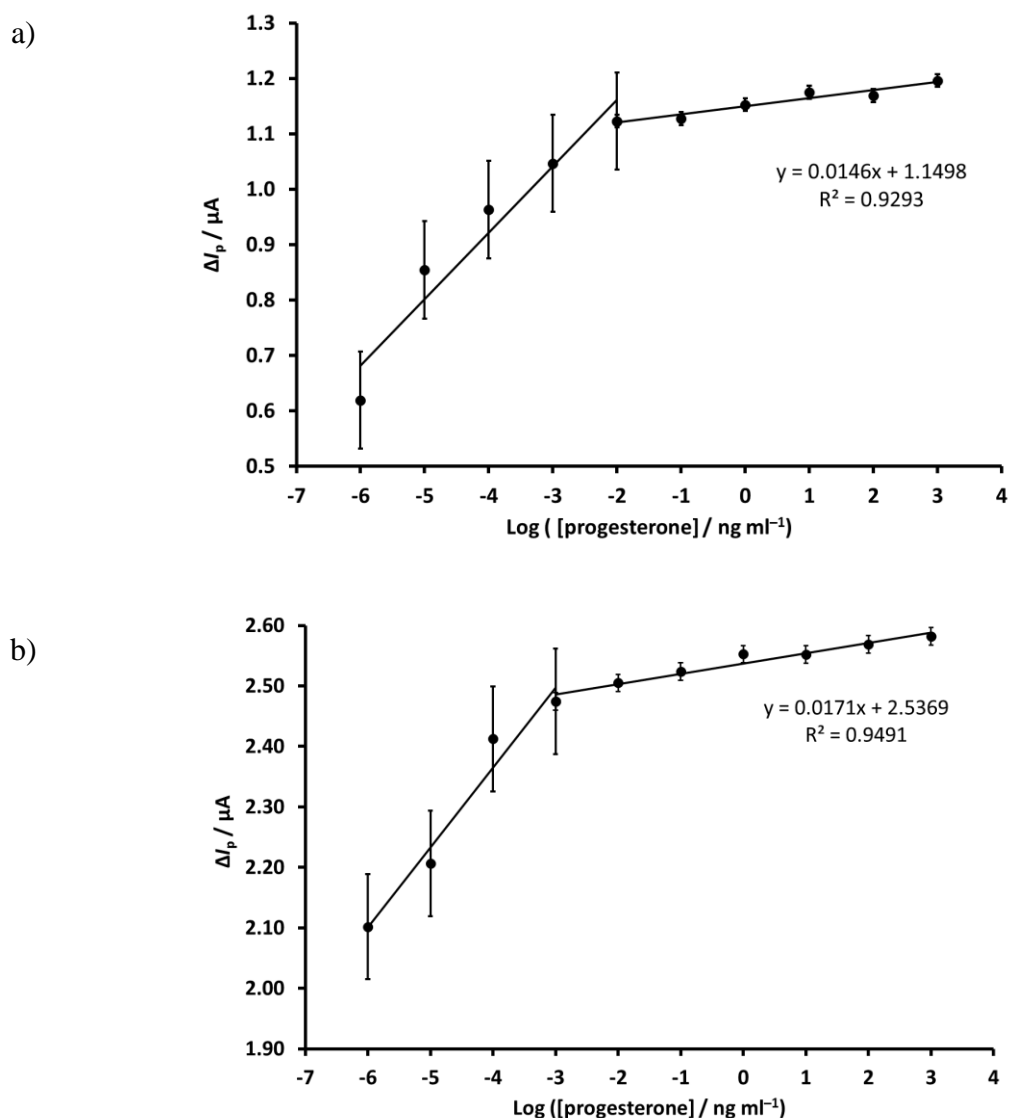


Figure 4.27: a) Calibration curves with a plot of the change in peak current against the concentration of progesterone added within the range of 1×10^{-6} ng mL $^{-1}$ rising to 1×10^{-3} ng mL $^{-1}$ from the experimentally determined square waves; b) calibration plot of the same concentration range from the baseline corrected square wave voltammograms on a gold electrode (n=3) .

Figure 4.27 shows the calibration plots from a) the experimentally determined square wave measurements and b) the baseline corrected ones. The first plot shows a clear linear range with minimal error between 1×10^{-2} ng mL $^{-1}$ and 1×10^3 ng mL $^{-1}$; which is in accordance to the work by Dou *et al.* where a LOD of 23 pg mL $^{-1}$ was determined.⁵⁴

By using the baseline corrected results the linear range increased (1×10^{-3} – 1×10^3 ng mL $^{-1}$). Using these results the correlation coefficient also improved (0.9491).

Electrochemical immunoassay on glassy carbon

Although the glassy carbon was inferior to the other electrodes investigated for this application it was decided to just checkout its applicability.

Figure 4.28 shows the CVs of the ferrocene tagged antibody as the concentration of progesterone added increases for the glassy carbon electrode, with concentrations ranging from 1 fg mL^{-1} to $1 \text{ } \mu\text{g mL}^{-1}$.

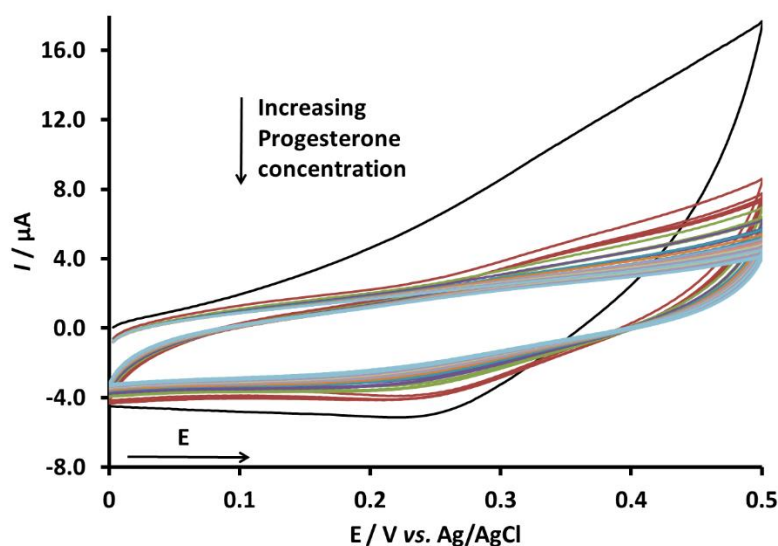


Figure 4.28: Cyclic voltammograms of the ferrocene tagged anti-progesterone upon addition of various concentrations of progesterone ranging from 1 fg mL^{-1} rising to $1 \text{ } \mu\text{g mL}^{-1}$ for an incubation period of 15 minutes with the black line representing the ferrocene tagged anti-progesterone prior to progesterone addition, scan rate 0.1 V s^{-1} . Measurements were carried out in 10 mM PBS .

The black line represents the ferrocene tagged anti-progesterone prior to the addition of progesterone. As before the voltammograms do not show a clear oxidation peak, however a reduction peak can be seen at $+0.27 \text{ V}$, the current produced during the reduction decreases as the concentration of progesterone increases.

The CVs of the ferrocene tagged antibodies are in agreement with the work carried out on the gold electrode, where larger progesterone concentrations resulted in a decreased in

the current measured in both the oxidative and reduction peaks. Figure 4.29 shows the SWV voltammograms.

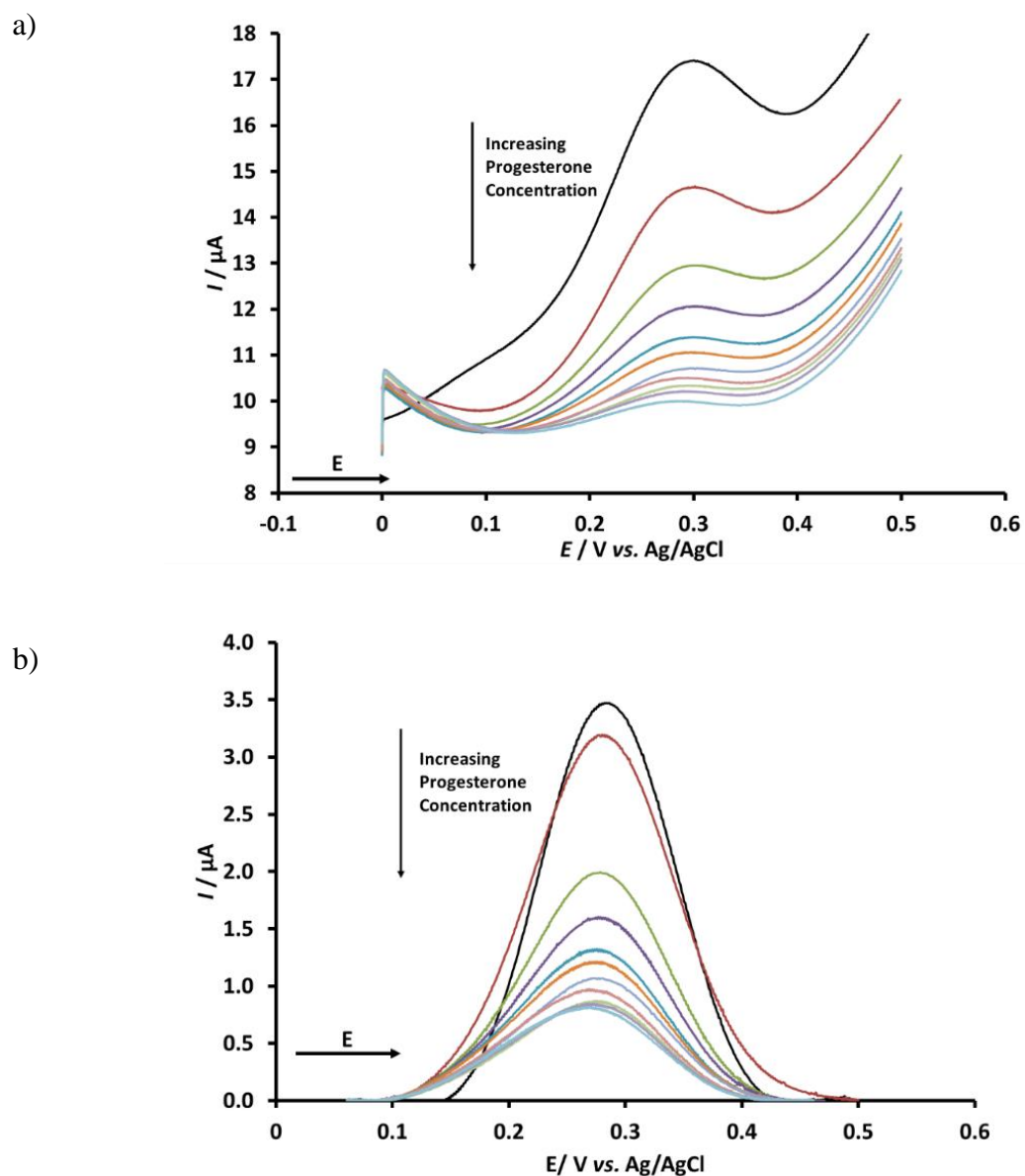


Figure 4.29: Square wave voltammograms of ferrocene-tagged anti-progesterone, where the black line represents the antibody alone, with subsequent voltammograms representing various concentrations of progesterone ranging from 1 fg mL^{-1} up to $1 \text{ } \mu\text{g mL}^{-1}$, where a) is without and b) is with a baseline correction with all measurements an incubation period of 15 minutes was used, frequency was 25 Hz and an amplitude of 1 mV. Measurements were carried out in 10 mM PBS.

Figure 4.29 shows the SWV voltammograms with a) showing the measured voltammograms with b) the baseline corrected voltammograms. Both diagrams clearly show a peak at +0.3 V, with the peak current reducing as the concentration of progesterone increased.

As observed on the gold electrode, the signal change is clearer with square wave voltammetry compared to the cyclic voltammetry; a calibration curve was plotted by taking the signal change before and after progesterone incubation from the square wave measurements:

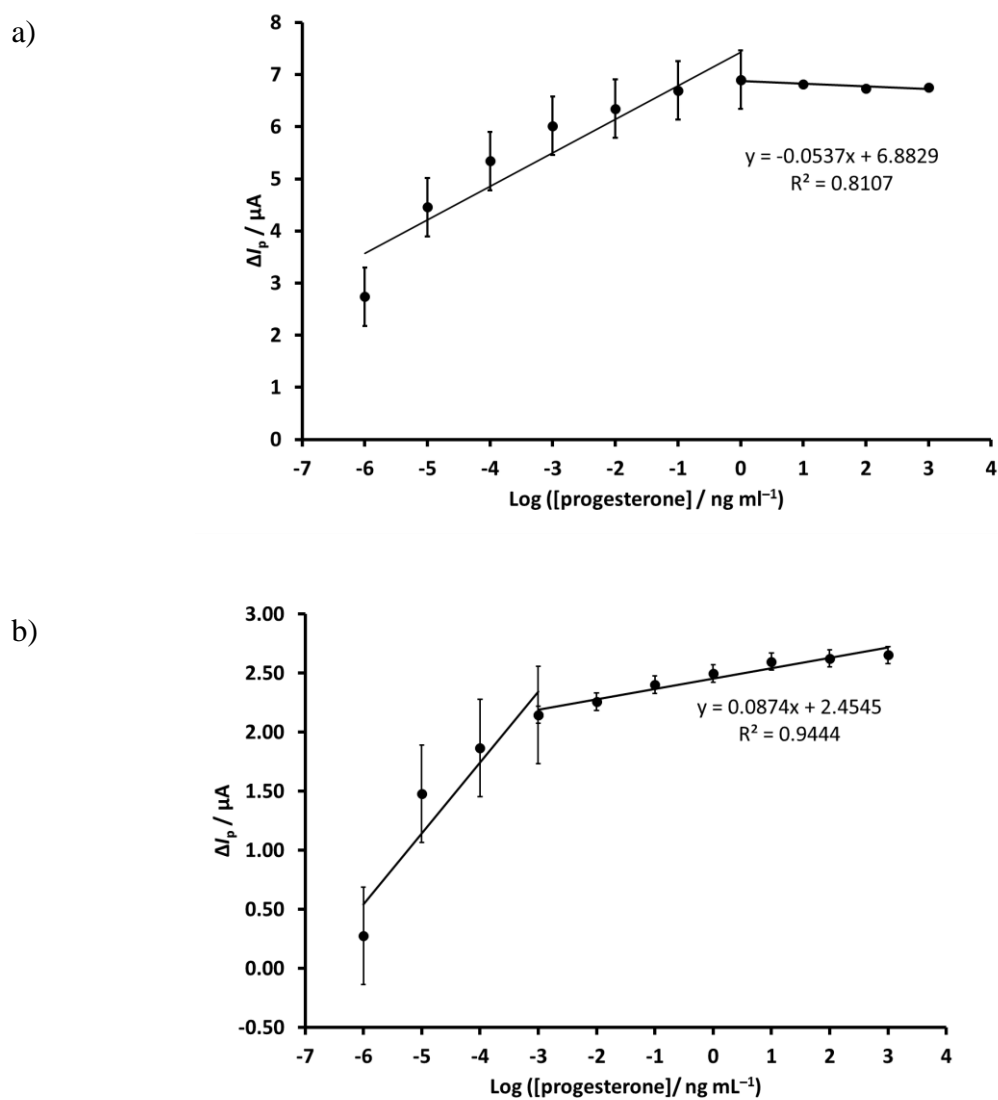


Figure 4.30: Calibration curves representing the change in peak current against the concentration of progesterone within the range of 1×10^{-6} ng mL⁻¹ rising to 1×10^{-3} ng mL⁻¹ where a) is without and b) is with a baseline subtraction on a glassy carbon electrode (n=3).

Figure 4.30a shows the calibration curve taken from the experimentally measured square wave voltammograms unfortunately a linear relationship within the required clinical range for progesterone was not obtained due to the difficulty in interpreting the voltammograms. The baseline corrected square waves figure 4.29b the voltammograms can be interpreted which gives the calibration curve shown in figure 4.30b where a linear correlation can be observed within the required clinical range for progesterone. The use of a glassy carbon electrode for an electrochemical immunoassay for the detection and quantification of progesterone in saliva samples was possible, the gold electrode gave clearer cyclic and square wave voltammograms; which allowed interpretation of the results to be carried out more accurately; increasing the reliability of the system.

Electrochemical immunoassay on ITO

The same concentration range that was investigated on the other electrode surfaces was repeated for ITO, again with the corresponding CVs and SWVs measured with concentrations ranging from 1 fg mL^{-1} to $1 \text{ } \mu\text{g mL}^{-1}$.

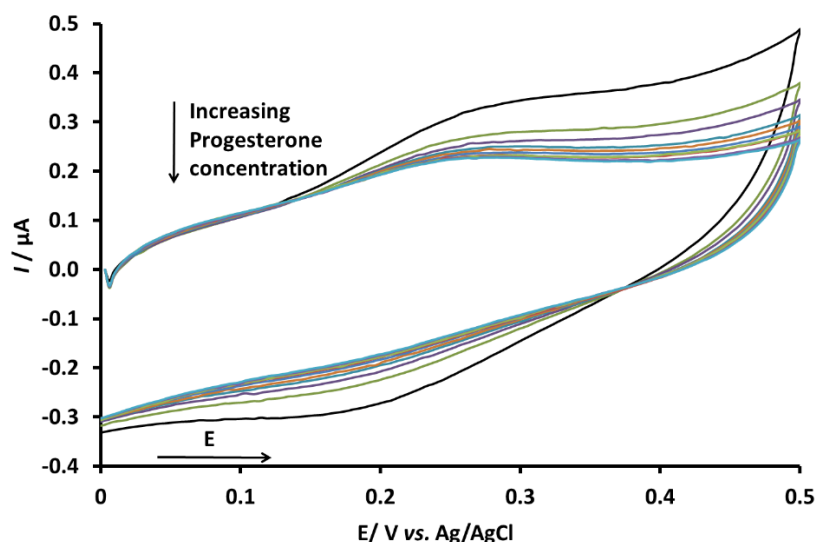


Figure 4.31: CVs of ferrocene tagged anti-progesterone on an ITO electrode surface, where the black line represents the ferrocene tagged anti-progesterone prior to any incubation with progesterone. The coloured voltammograms represents each concentration of progesterone ranging from 1 fg mL^{-1} increasing to $1 \text{ } \mu\text{g mL}^{-1}$, scan rate of 0.1 V s^{-1} . Measurements were carried out in 10 mM PBS .

Figure 4.31 shows how the cyclic voltammetric measurement changed with addition of progesterone. The CV for the ferrocene tagged anti-progesterone shows a clear oxidation peak at around +0.25 V and a reduction peak at around +0.2 V with the same trend that was observed on the other electrode materials; where the peak current decreases with an increase in progesterone concentration.

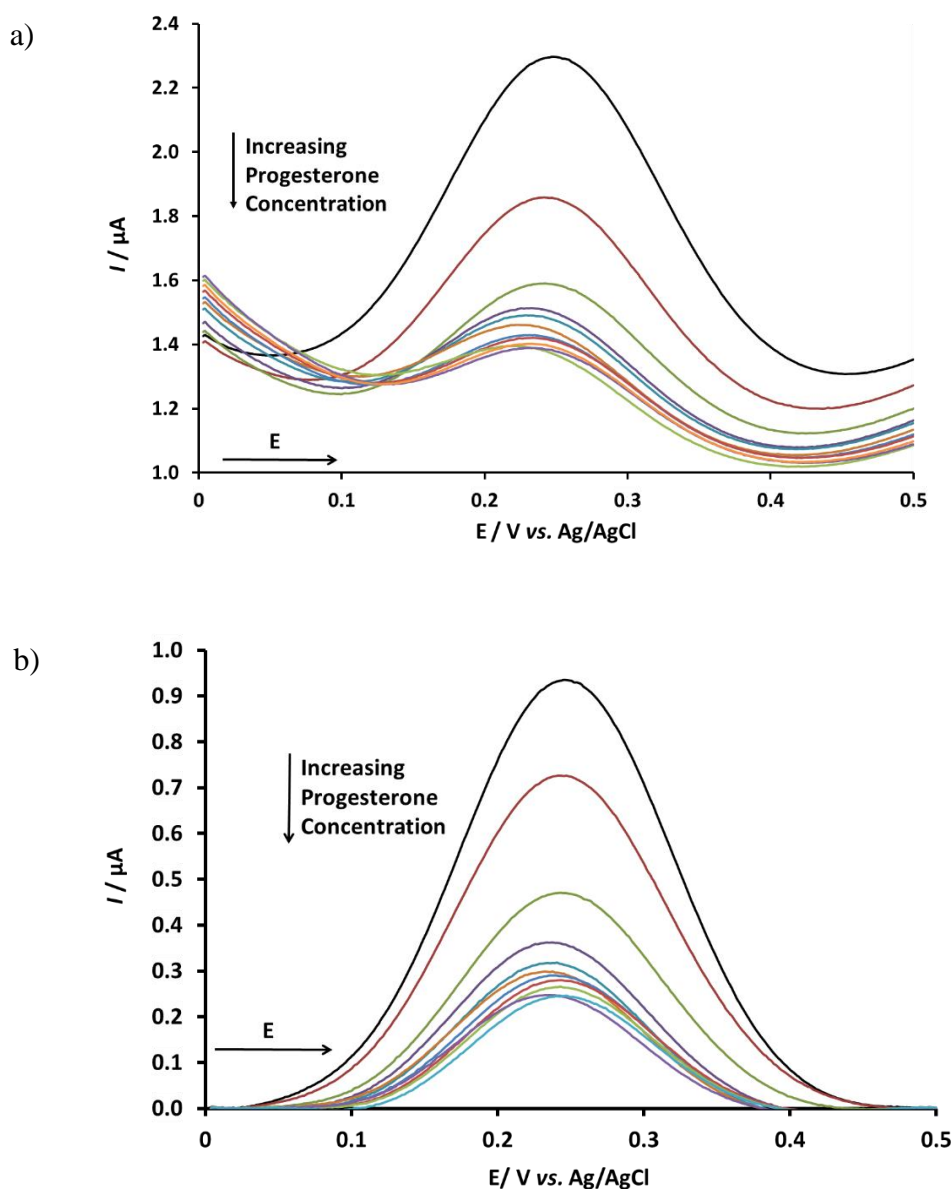


Figure 4.32: a) Square wave voltammograms of the ferrocene tagged anti-progesterone, where the black line represents the anti-progesterone prior to any progesterone addition. The concentrations studied were between 1 fg mL^{-1} and $1 \text{ } \mu\text{g mL}^{-1}$. Where b) represents the same voltammograms however with a baseline correction, frequency of 25 Hz and amplitude of 1 mV. Measurements were carried out in 10 mM PBS.

Figure 4.32 shows the square wave measurements with changing concentration of progesterone, in the same way as shown with the CVs the peak current decreases as the concentration increases and like the other electrodes the square wave voltammograms were easier to interpret compared to the CVs. Figure 4.33 shows the calibration plots from these measurements. Again the calibration was plotted by subtracting the initial signal from the signal observed after incubation with the progesterone in PBS.

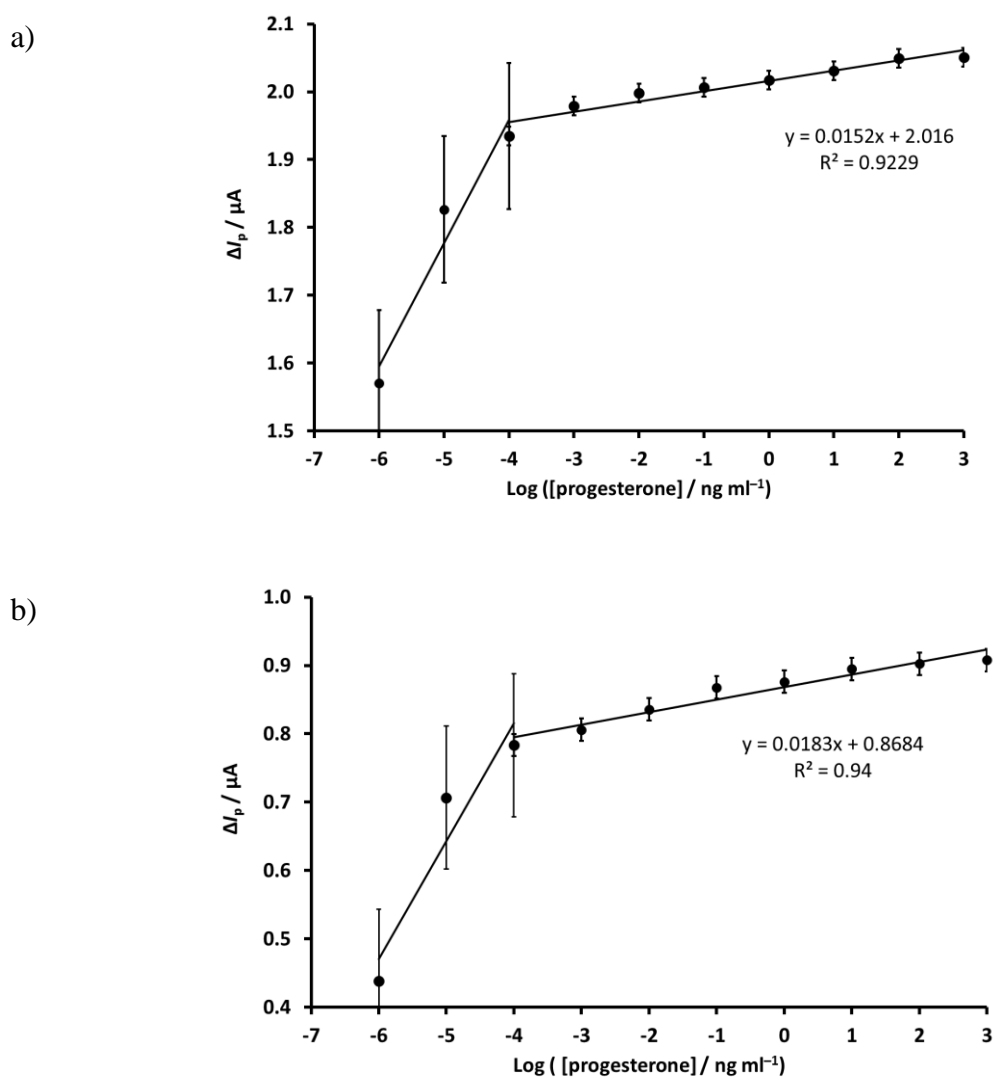


Figure 4.33: Calibration curves showing the change in peak current against the concentration of progesterone. Where a) represents the experimental square waves and b) the baseline corrected square waves (n=5).

Figure 4.34 shows a linear correlation between the change in peak current and the change in the progesterone concentration. This linear trend can be seen for the both the measured square waves and those that had a baseline correction.

Observing figure 4.33 instantly the sensitive on the ITO surface has increased in comparison to that seen on the other surfaces, from the calibration the linear region is from $1 \times 10^{-4} \text{ ng mL}^{-1}$ (0.1 pg mL^{-1}) rising to $1 \text{ } \mu\text{g mL}^{-1}$, which is an order of magnitude more sensitive than that observed on the gold and carbon electrodes.

Conclusion to electrode material investigation

In conclusion all three electrode materials investigated could be used to carry out an electrochemical immunoassay to quantify progesterone within the clinical range for progesterone found in saliva.

	Au	GC	ITO
Successful Surface Characterisation	Successful	Somewhat Successful	Successful
Sensitivity	$1 \text{ pg mL}^{-1} \rightarrow 1 \text{ } \mu\text{g mL}^{-1}$	$1 \text{ pg mL}^{-1} \rightarrow 1 \text{ } \mu\text{g mL}^{-1}$	$0.1 \text{ pg mL}^{-1} \rightarrow 1 \text{ } \mu\text{g mL}^{-1}$
Within Required Range	Yes	Yes	Yes
Reproducibility of antibody immobilisation.	Very 56 out of 60 attempts.	Somewhat 50 out of 65 attempts.	Very 60 out of 62 attempts and still on going.

Table 4.1: Comparison of the various electrode materials investigated.

Table 4.1 shows that the most sensitive electrode substrate was the ITO electrode where a progesterone concentrations of 0.1 pg mL^{-1} were observed, an order of magnitude lower than that for the other two electrode materials however all three were within the required range for progesterone in saliva. Au and ITO were the easiest to analyse. The glassy carbon electrode performed the worst. The key differences of these results is the electrode surfaces, gold and glassy carbon have non-uniform surface whereas ITO is flat with a

fractal dimension tending to 2.²⁰⁶ With ITO being transparent, the most sensitive and flat this was selected for further studies.

4.3.3 Optimising the ITO electrode for progesterone analysis in saliva

Having concluded that the ITO electrode was the most efficient at carrying out antibody immobilisation as well as the subsequent immunoassay, the system was evaluated further with the aim of incorporating the system into a flow device (chapter 5).

Firstly within this investigation the system in its entirety needs investigating, having concluded the electrode material the immunoassay protocol itself needs optimising this was achieved by an incubation time study. The incubation times looked at were 15, 30 and 60 minutes, these time frames were chosen to maintain a reasonable time frame for a POC measurement.

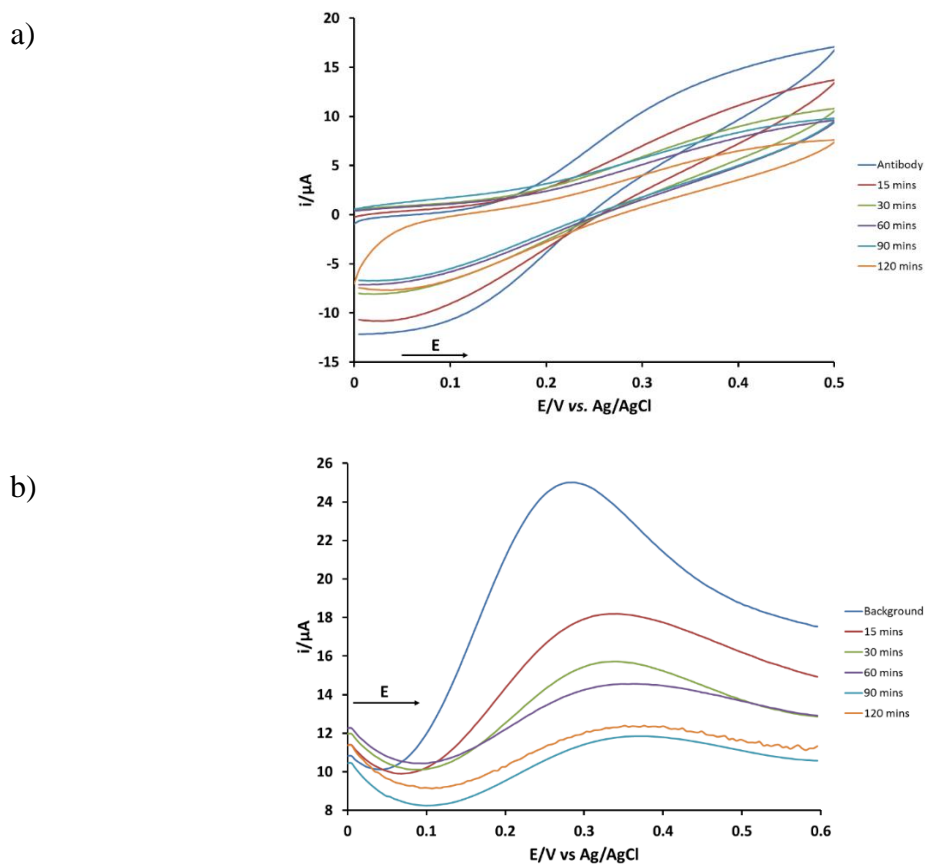


Figure 4.34: a) CVs of the ferrocene tagged anti-progesterone, before and after incubation with 100 pg mL^{-1} progesterone at various incubation times, scan rate of 0.1 V s^{-1} and b) the square wave voltammograms representing the same incubation times frequency 25 Hz , amplitude 1 mV . Measurements were carried out in 10 mM PBS .

Within this experiment the oxidation and reduction peaks from the CVs are not clear as shown in figure 4.34a, however oxidation and reduction waves can be interpreted at +0.3 V and +0.1 V respectively. The square wave voltammograms which are much clearer than the CVs. A peak can be seen after each measurement between +0.25 V and +0.3 V. For both figures 4.34a and 4.34b there was a decrease in signal as the incubation time increases.

From the CV measurements, figure 4.35 shows the peak current changes for the oxidation and reduction peaks as the progesterone/anti-progesterone incubation time increases.

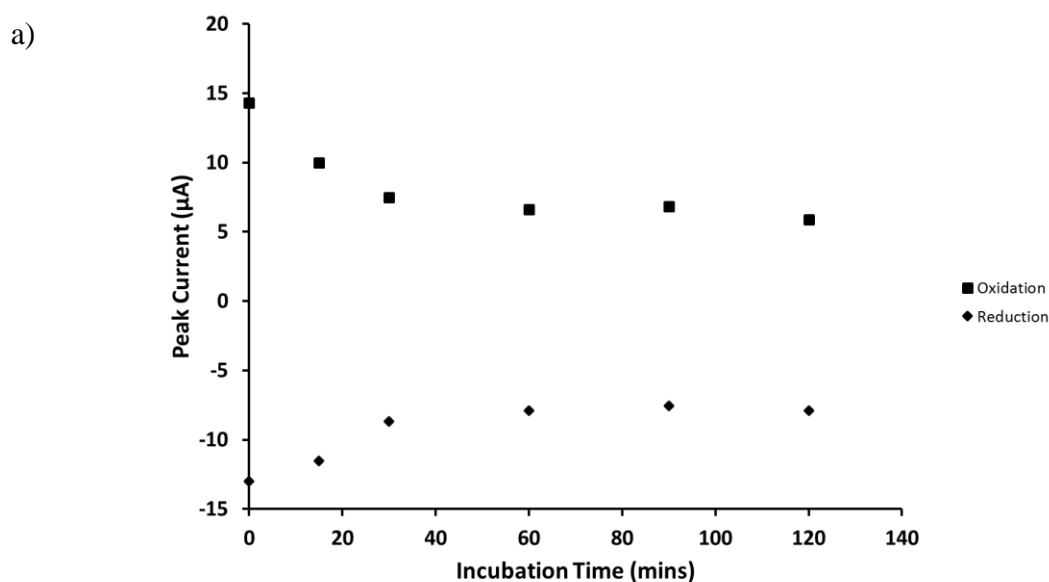


Figure 4.35: a) Graph showing how the peak oxidation and reduction currents change with incubation of 100 pg mL⁻¹ progesterone at various times from the CV measurements.

A current drop is observed after progesterone addition as expected up until the 30 minute incubation period for both the oxidation and reduction processes. After which the current produced stays constant; this indicates that equilibrium has been met where the antigen absorption and desorption is equal.⁵⁴ Through the plot we can see the system is Langmuir-looking, within this area of work it is common to use the Langmuir Isotherm as a route to quantify adsorption of this nature. Latour *et al.* talks about using this model to investigate

protein absorption. This model is used primarily due to the simplicity of the model allowing quantification of the adsorption process between the antigen and the surface.²⁰⁷ However it must be stressed that the use of this model does rely on a number of assumptions, these include all binding sites are homogeneous, each binding site binds with one molecule, no interaction that can affect the binding behaviour and equilibrium is met within the experiment.

This model is widely used however as a way of quantifying the adsorption and provides a route to potentially take forward and investigate further. For these reasons this model will be used throughout.

This observation was also found when analysing the SWV voltammetry.

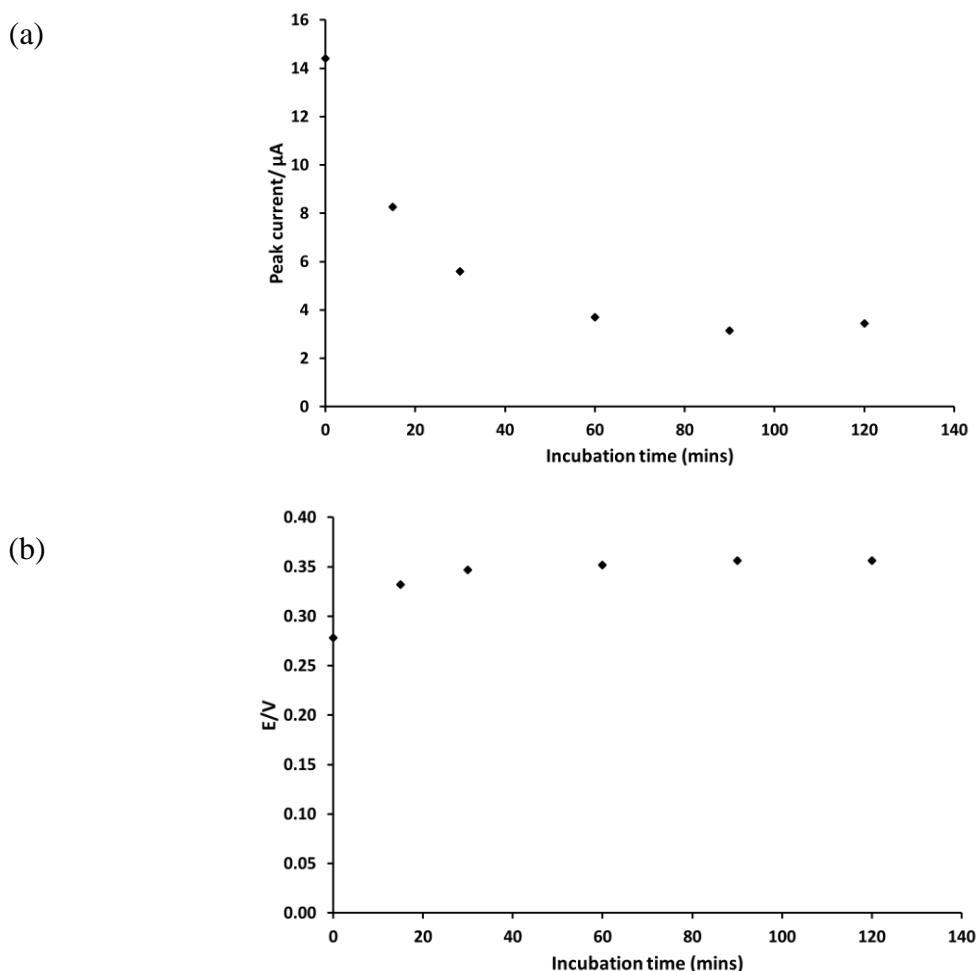


Figure 4.36: a & b) Graphs showing how the peak current and peak potentials for the oxidation of ferrocene tagged anti-progesterone change with incubation time, through measurement using square wave voltammetry.

Figure 4.36a shows the same trend that was observed from the cyclic voltammetry measurements where a peak current drop occurred after 15 and 30 minute incubation times, until the current plateaued after which a constant peak current was observed.

From this investigation therefore the optimum incubation time was 30 minutes, this incubation time was used when carrying out the electrochemical immunoassay in saliva.

Resistivity measurements

In this work measuring more than one antibody is essential it would therefore be useful to have spatial resolution this was achieved by separating the electrode into three areas with circular adhesives. However this affects the resistance across the electrode, because of this each individual area had the resistance measured, this was measured over 4 different electrodes with an average taken this affect can be seen in table 4.2:

	Area 1 (kΩ)	Area 2 (kΩ)	Area 3 (kΩ)
Electrode 1	0.77	0.60	0.34
Electrode 2	0.76	0.56	0.30
Electrode 3	0.83	0.57	0.33
Electrode 4	0.72	0.55	0.34
Average	0.77	0.57	0.33

Table 4.2: Resistivity measurements across the ITO electrode, where area 1 is 3.6 cm away from the copper tape, area 2 is 2.4 cm away from the copper tape and area 3 being 1.2 cm away from the copper tape.

From the table it is clear that the having the spacers on the electrode does have a minor effect on the resistance however this is not large enough to impact the immobilisation process, this will only affect the area in itself; overall across the electrode there has been no significant impact to the results obtained. Having determined this it was possible to look at the concentration of antibodies on the electrode surface.

Number of antibodies on the electrode surface

Having determined the peak current for the ferrocene tagged anti-progesterone using cyclic voltammetry in figure 4.29 which was 15 μA and the number of ferrocene tags per antibody which was calculated to be 13 on average (section 4.3.1), the number of antibodies on the surface could be determined using equation 4.3:

$$i_p^\circ = \frac{1}{4} \left(\frac{F}{RT} \right) SFv \cdot \Gamma_{tot} \gamma \quad (4.3)$$

Where:

i_p° is the peak current of the pure ferrocene tagged to the antibody in the absence of antigen (15.21 μA).

F is Faradays constant (96484.6 C mol^{-1}).

RT is the amount of thermal energy in the system and is the product of the molar gas constant (8.314 $\text{J mol}^{-1} \text{K}^{-1}$) and the absolute temperature (298 K).

S represents the area of the electrode ($0.28 \times 10^{-4} \text{ m}^2$).

v is the scan rate 0.1 V s^{-1} .

Γ_{tot} is the number of antibodies per unit area.

γ is the number of ferrocene moieties on each antibody (13).

Rearranging the equation and putting the values in gives:

$$\Gamma_{tot} = \left(\frac{1.521 \times 10^{-5}}{0.25 \cdot \left(\frac{96484.6}{8.314 \cdot 298} \right) \cdot 96484.6 \cdot 0.28 \times 10^{-4} \cdot 0.1} \right) / 13$$

Solving this equation gave the number of antibodies on the electrode surface as $4.46 \times 10^{-7} \text{ mol m}^{-2}$ or $4.46 \times 10^{-11} \text{ mol cm}^{-2}$. This concentration calculated per unit area was expected for this type of system with a pre-deposited film on the electrode, where values of $10^{-6} \text{ mol m}^{-2}$ have been reported.²⁰⁸ It must be noted however the concentration of antibodies will change slightly across the electrode because of the resistivity changes discussed previously.

4.3.4 Electrochemical immunoassay of progesterone in artificial saliva.

Having successfully determined that this system can be used to carry out an electrochemical immunoassay, it was necessary to investigate the system in a biologically relevant matrix, which with respect to the aims of this work was saliva. As described in section 1.3.

The artificial saliva was prepared using the recipe outlined in section 4.4.4 and was spiked with progesterone using a 30 minute incubation period.

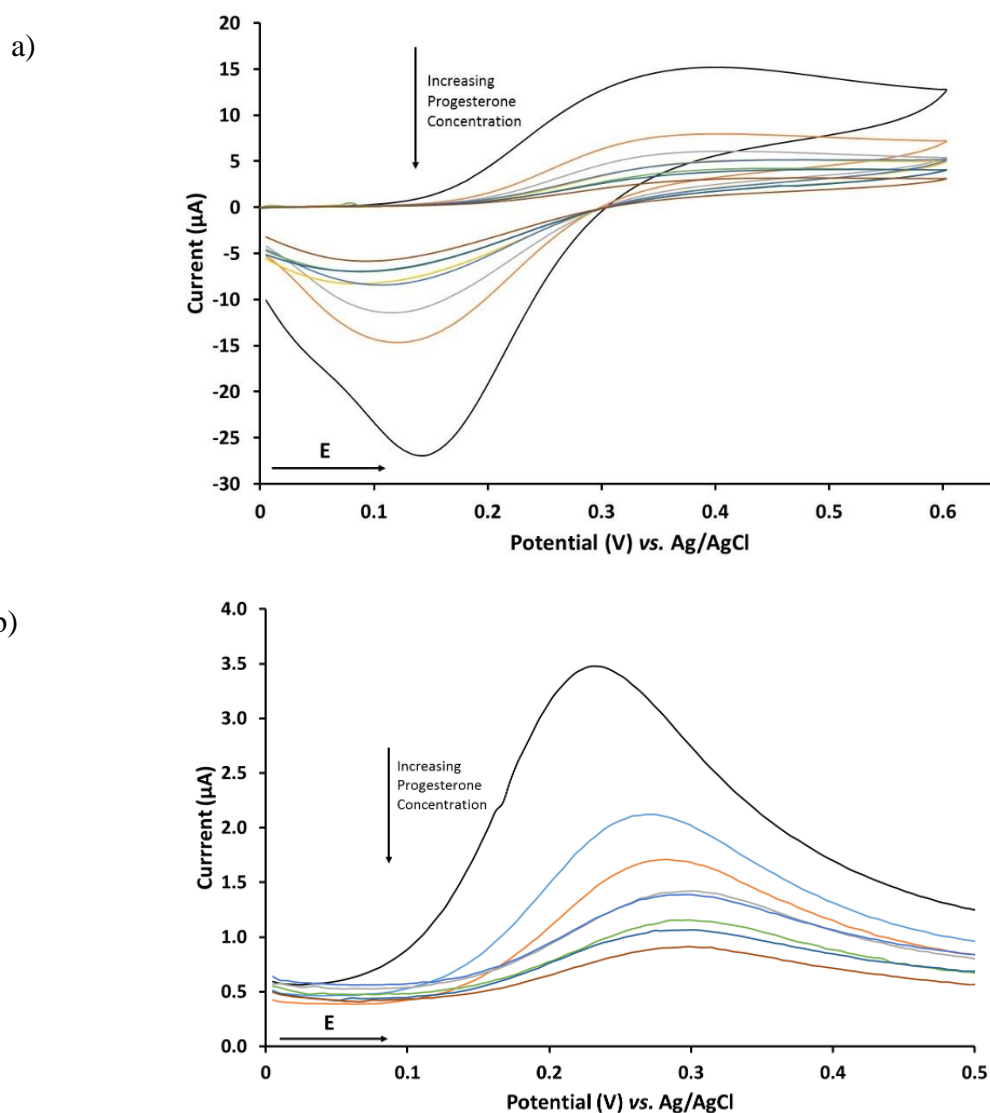


Figure 4.37: a) Cyclic voltammograms showing the signal change as the concentration of progesterone increases, where a concentration range of 1pg ml^{-1} to $1\text{ }\mu\text{g mL}^{-1}$. B) SWV voltammograms from the same concentration ranges, where the black voltammograms represents the ferrocene-tagged anti-progesterone prior to any progesterone addition.

Figure 4.37 shows a) the CVs and b) the SWVs illustrating the change in signal as the concentration of progesterone increased in saliva.

The CVs show an oxidation at $+0.3\text{ V}$ and a sharp reduction at $+0.1\text{ V}$ which is a shift from that observed in the buffer, the reason for this shift is probably due to the matrix being used, despite this the same trend is observed that the signal observed decreases as the concentration of progesterone added increases, this can be clearly seen through the

SWV voltammograms. From these voltammograms the calibration was plotted as change in peak current against the log of the progesterone concentration:

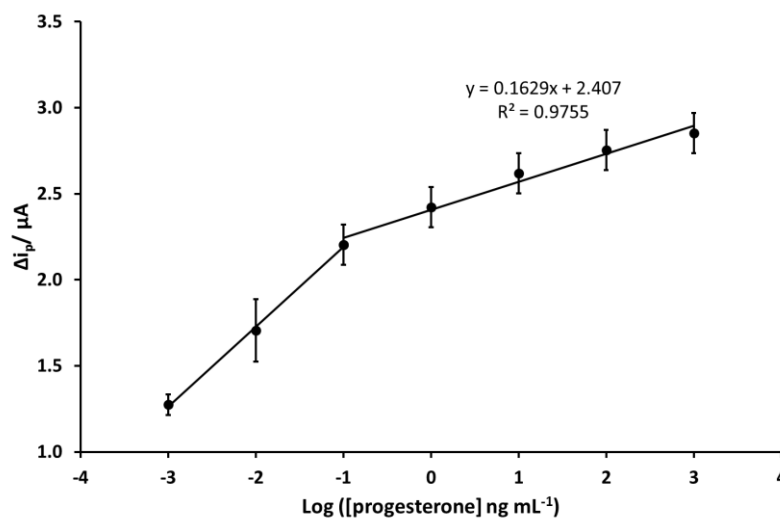


Figure 4.38: Calibration curve of progesterone in artificial saliva between the ranges of 1 pg mL⁻¹ and 1 μg mL⁻¹ (n=3).

The calibration plot shows a linear correlation within the required clinical range for progesterone in saliva, with a LOD equalling 1.7 pg mL⁻¹. This was calculated by: LOD = average signal of the blank + 3 times the standard deviation of the blank. This LOD is an order of magnitude higher than that seen on the ITO when the buffer was used, this change is probably due to the matrix used however this LOD is significantly better than that obtained using the glass slides (chapter 3) where an LOD of 33 pg mL⁻¹ was calculated which was using buffer and not saliva meaning this method is significantly more sensitive. This is probably due to the improvement in the immobilisation process, resulting in more antibodies being orientated in the desired manner.

4.4 Conclusion to the Electrochemical Immunoassay Investigation

In this chapter a successful electrochemical immunoassay system has been developed that can be used to quantify the concentration of progesterone within a sample of saliva. Various electrode materials were investigated and although all three electrode surfaces (Au, GC and ITO) could be used for an electrochemical immunoassay for progesterone with the required clinical sensitivity for progesterone in saliva, ITO was demonstrated to provide the best performance, which is due to the flat ITO layer deposited onto the glass. The uniform layer enabled a uniform layer of nitrobenzene to be deposited which potentially resulted in a uniform layer of antibodies. The use of gold was also successful, this was expected seeing as SPR systems use gold chips to carry out immunoassays in the laboratory. Glassy carbon gave the poorest results due to surface characteristics. A longer emersion time for the nitrobenzene deposition is required which means a large number of cycles are required.

Having determined the optimum electrode material the incubation time was optimised which came out to be 30 minutes; this incubation time was acceptable for POC as a result can be determined within 35 minutes. However as can be seen from the electrode material investigation (section 4.3.2.3) the required sensitivity for our analysis can be achieved in 15 minutes. The system was also selected to test with a matrix of artificial saliva, showing the system would work with respect to real biological matrix. With a LOD of 1.7 pg mL^{-1} proving that the method is extremely sensitive especially in comparison to the work described in chapter 3 where a LOD of 33 pg mL^{-1} was determined which primarily is due to the improved orientation of the antibody on the surface. Bearing in mind the LOD in chapter 3 was in 10 mM PBS and the value quoted above was in saliva.

The system was fully characterised, through the use of UV-Visible spectroscopy and the average number of ferrocene tags on the antibody was found to be ~13; with the concentration of antibodies on the surface of $7.69 \times 10^{-10} \text{ mol cm}^{-2}$. This quantification is a **HUGE** benefit of the electrochemical system as every step was quantifiable and controllable allowing strong reproducibility that would not be possible using the methods outlined in chapter 3.

One problem with the use of this ITO method as an electrochemical sensor is that the resistivity was not uniform across the electrode with the spot closest to the copper tape having a lower resistance than furthest away, so while the immobilisation process is successful another detection system needed to be looked at where this does not become such a huge issue. Incorporating the protocol into a flow system, where CL detection would take place would limit these affects. This issue itself could be solved however by having individual connections to each spatial area (figure 4.39).

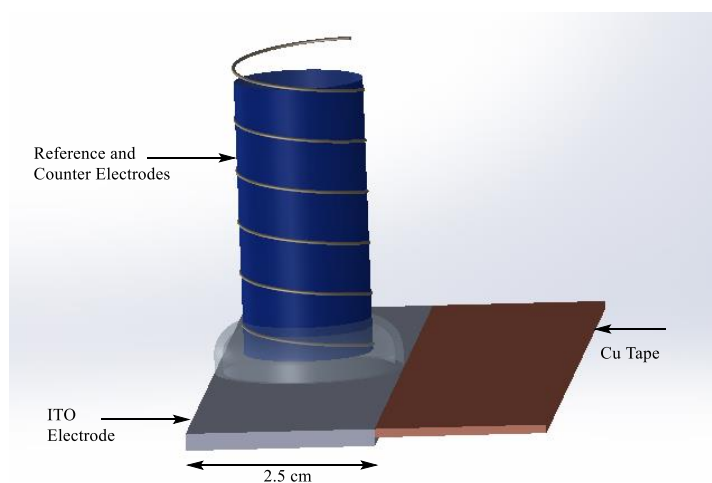


Figure 4.39: Illustration showing a potential fresh electrode design to enable a continuous connection across the ITO electrode.

Figure 4.39 shows that placing the copper tape across the electrode surface, there is a universal connection across the entire electrode allowing the reactions that occurs within the different areas to occur uniformly.

ITO as an electrochemical immobilisation platform can therefore be utilised by slotting the modified electrode into a microfluidic device and investigate the use of CL as a detection method, as this will then eliminate the need for counter and reference electrodes.

This investigation has developed a robust immobilisation protocol that is reproducible which is essential for our aims, which was due to the rigid orientation of the antibody on the surface resulting in the ideal orientation.

Chapter 5 Development of a Chemiluminescence Immunoassay for Progesterone and Oestriol with an Electrochemical Immobilisation Protocol

5.1 Introduction

Having demonstrated that the electrochemical immobilisation procedure was successful on the transparent ITO, giving reproducible reliable results with electrochemical detection the method was then adapted for CL detection. This was investigated because CL detection gives high sensitivity with simple instrumental requirements, with no need to incorporate electrodes for the detection and is therefore idea for a point of care systems.

In chapter 3 HRP was investigated as a catalyst for the luminol and hydrogen peroxide reaction, HRP contains an iron centre which carries out the catalysis for the hydrogen peroxide/luminol reaction. Like HRP ferrocene contains iron and therefore it was a possibility that the ferrocene attached to the antibody for the electrochemical detection could be used as the reaction catalyst. In fact Schiffrin and Wilson used oxidised ferrocene to catalyse the luminol/H₂O₂ reactions.²⁰⁹ It was therefore decided to try CL detection just using the ferrocene tagged antibody omitting the expensive HRP reagent. Figure 5.1 presents a schematic of the concept for the CL immunoassay.

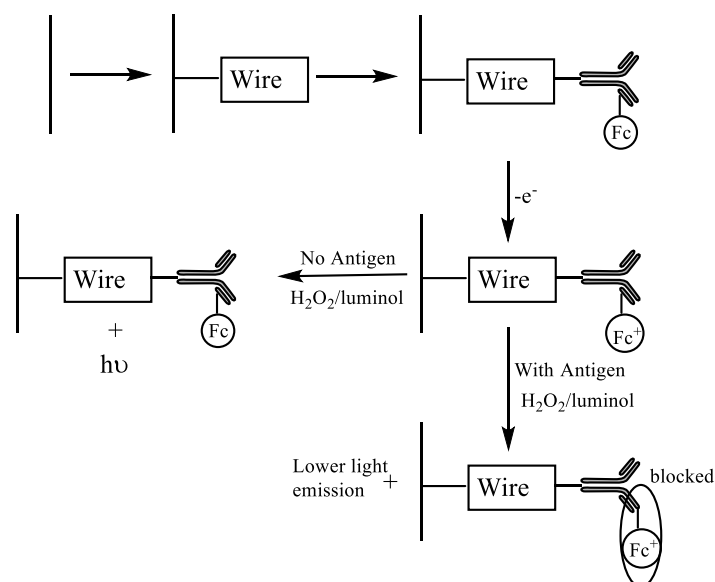


Figure 5.1: Schematical concept showing how a CL immunoassay would work using ferrocene tagged antibodies, the wire represents the aniline group as discussed in chapter 4.

In this approach oxidised ferrocene tagged to the antibody without the presence of an antigen would generate the largest CL emission signal as the oxidised ferrocene is reduced and the luminol is oxidised generating the light. If a sample was introduced binding would occur between the antigen and antibody blocking the ferrocene moieties (as with the electrochemical detection). This would affect the electron transfer at the surface which would result in a reduction in the light signal observed.

The plan would be to prepare the ITO electrodes with the immobilised and oxidised ferrocene tagged antibody. This could then be slotted into a POC device as and when required.

5.2 Experimental Procedures

5.2.1 Immobilisation of ferrocene tagged anti-progesterone onto an ITO electrode

Antibody immobilisation onto the ITO

Anti-progesterone and anti-oestriol antibodies were tagged with the ferrocene redox species using the same protocol that was described within section 4.2.1. With the electrode surface modification and immobilisation following that explained in section 4.2.2. Two spots were isolated on the electrode by using adhesive stickers with holes punched out. Anti-progesterone was spotted on one of these areas and anti-oestriol on the other enabling spatial isolation.

Preparation of the electrode to carry out CL immunoassay

In the same way as before the electrode surface was blocked with 1% BSA in PBS, for 30 minutes, after the wash with PBS (10 mM) an electrochemical oxidation of the ferrocene moieties was carried out, using CV where a scan was undertaken from 0V to +0.6 V with the same parameters outlined in section 4.2.2 however a scan rate of 10 mV s⁻¹ was utilised for this process. This was to enable more time at a set potential which would kinetically favour the ferrocene oxidation. The system was stopped after viewing the oxidation peak of the ferrocene. This was carried out in a PBS solution using the same three electrode setup as previous (section 4.2).

5.2.2 Procedure for carrying out the CL immunoassay

For the first experiments the immunoassay was carried out as static experiment on the modified electrode. The oxidised electrode was placed under the CCD camera where a background image was taken. Subsequently an image was taken where 70 μL of luminol and hydrogen peroxide (10 mM of each) had been added to each individual spot. This volume was chosen as volumes $<40 \mu\text{L}$ gave no signal and would not cover the entire spot, volumes $>70 \mu\text{L}$ over-flowed the spatial area with volumes in between resulting in a larger signal as the volume increased.

Preliminary signal change observations

A preliminary experiment was conducted to determine whether a signal change would be observed after incubation. 10 ng mL^{-1} of progesterone was incubated for 1 hour this was to give the greatest chance for interaction between the antigen and antibody to such an extent any signal change would be observed. The stability of the oxidised ferrocene was investigated by making CL measurements immediately after oxidation, 1 hour after oxidation and 1 day after oxidation and comparing the results. The electrode was stored in PBS between measurements.

Optimisation of the CL reagents

Various concentrations of luminol and hydrogen peroxide were investigated to obtain the optimum conditions for this particular CL immunoassay. The concentrations again ranged from 1 mM to 50 mM for both luminol and hydrogen peroxide. For the reasons presented in chapter 3 the pH was maintained at pH 9 throughout. The exposure time was also optimised in the same way as described in section 3.3.1.

Developing a calibration curve

Calibration curves were obtained by making measurements for a range of standards solutions (0.01, 0.1, 1, 10 and 100 ng mL⁻¹) for both analytes (progesterone and oestriol) within the artificial saliva matrix section 4.2.4). 30 µL aliquots of each concentration of progesterone and oestriol were pipetted onto the corresponding spot and left to incubate. Various incubation times were also investigated, 15, 30 and 60 minutes.

After the sample was left to incubate the electrode was washed with PBS and placed back under the camera where again another background image was taken. 70 µL of luminol/H₂O₂ (10 mM of each) was added and an image captured.

Interference studies

To investigate any potential interference oestradiol, oestrone, testosterone and vitamin D₃ were investigated with a standard of 20 ng mL⁻¹. This concentration was selected as it is greater than the upper concentration of each molecule to be found naturally within females.^{15, 210, 211}

5.2.3 CL immunoassay within a flow cell

For the flow cell (figure 2.3) the copper tape was removed from the ITO electrode with the oxidised antibodies as copper can catalyse the luminol and hydrogen peroxide reaction.²¹² The electrode was then placed face down onto the macroflow cell and was fitted into place with wax (see section 2.5). The flow rate was then optimised using flow rates ranging from 0.1 mL min⁻¹ to 2.5 mL⁻¹. The concentration of reagents was kept the same as for the static method.

For the immunoassay within the flow cell a mixture of luminol and hydrogen peroxide was pumped through the cell and an initial CL image was taken, the cell was flushed with PBS (10 mM) to remove the luminol and hydrogen peroxide, and then each standard was pumped into the cell incubate over the same time frames (15, 30 and 60 minutes), followed by a further wash with PBS (10 mM). Luminol and hydrogen peroxide were again flushed into the chip and the CL image taken before washing the cell out again.

5.2.4 CL immunoassay in the microfluidic device

The microfluidic device presented in figure 2.4 was utilised to carry out the CL immunoassay on a microfluidic system. The device contained two chambers one with a larger channel and another with a thinner channel. These were incorporated with the larger channel being similar to the macroflow with the smaller channel more representative of a microfluidic channel. The oxidised ITO electrode was slotted into the device where a CL reaction was carried out where the hydrogen peroxide and luminol were flowed into the device and a CL image taken.

5.3 Results and Discussion

Chapter 4 demonstrated an electrochemical approach to immobilisation that resulted in a reproducible protocol for antibody immobilisation. Wilson and Schiffrin demonstrated the chemiluminescence reaction of hydrogen peroxide and luminol where ferrocene in its oxidised form undergoing the catalysis.²⁰⁹ This chapter utilises this finding as a route to carry out a CL immunoassay.

The voltammetry showing the oxidation of the ferrocene-tagged antibodies to the ferrocenium cation is shown in figure 5.2.

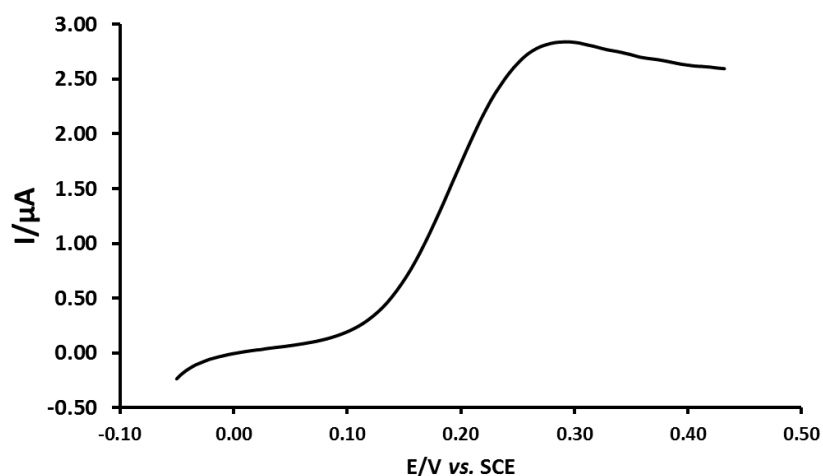


Figure 5.2: Cyclic voltammogram showing the oxidation of the ferrocene-tagged antibodies, at a scan rate of 10 mV s^{-1} .

The ferrocene oxidation occurs at around $+0.25 \text{ V}$, which is in line with the voltammetry observed in the previous chapter. Only half of the CV was carried out to form the ferrocenium cation and prevent the subsequent reduction.

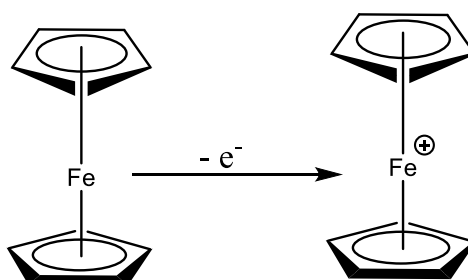


Figure 5.3: Reaction Scheme showing the oxidation of ferrocene to the ferrocenium cation.

Ferrocenium Cation Stability

For this system to be used for POC the electrochemical oxidation needs to occur only once, therefore to test this stability a CL image was taken prior to ferrocene oxidation, immediately after ferrocene oxidation, 1 hour after the oxidation and 1 day after ferrocene oxidation this can be seen in figure 5.4:

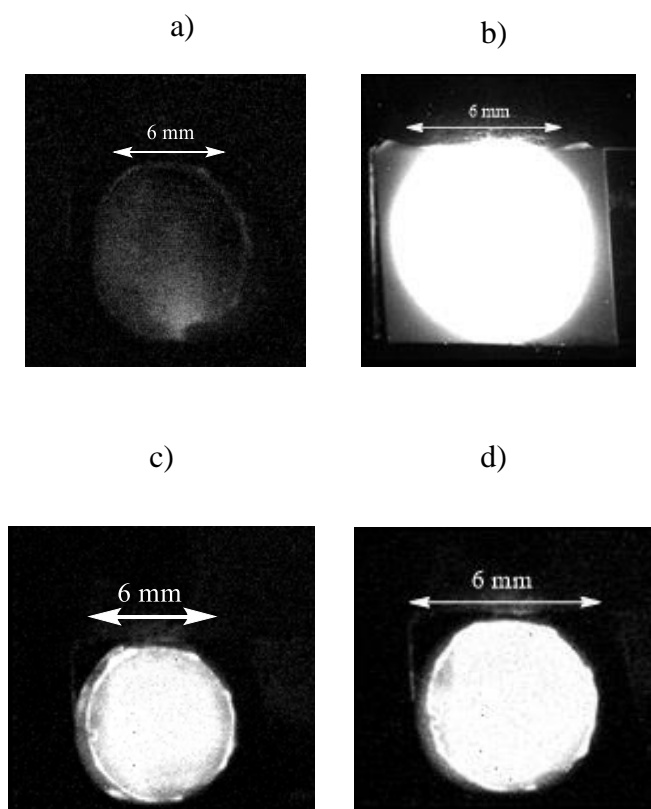


Figure 5.4: CL images of ferrocene-tagged anti-progesterone, where a) represents the ferrocene molecule before oxidation, b) immediately after ferrocene oxidation, c) 1 hour after ferrocene oxidation and d) 1 day after oxidation 10 mM luminol (pH 9) and 10 mM H₂O₂.

For a system that will be used for POC the system needs to be simple with minimal reaction steps, therefore a system where ferrocene oxidation is needed before every CL measurement would not be favourable, thankfully as shown in figure 5.3 where no oxidation has occurred no signal was seen this confirms that ferrocene in its neutral state does not catalyse the hydrogen peroxide/luminol reaction 5.4a, 5.4b after oxidation the light signal increases showing that in the oxidised state the catalysis occurs with 5.4c showing the oxidised ferrocene after one hour storage in PBS and 5.4d after one day storage in PBS. Showing the system is stable and therefore can be utilised as a route to carry out a CL immunoassay that can be incorporated into a POC system. It has been reported that ferrocene can be stable in aqueous solutions.²¹³ This stability in large could be down to the presence of phosphate ions within the buffer stabilising the cation.

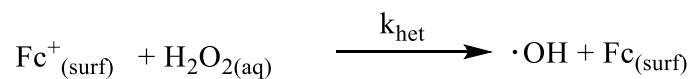


Figure 5.5: mechanism of the catalytic effect of the ferrocene.

Figure 5.5 presents the reaction pathway for the ferrocenium catalysis of luminol and hydrogen peroxide by breaking down the hydrogen peroxide forming hydroxide radical which then reacts with luminol in a similar way as presented in figure 1.31.

5.3.1 CL immunoassay for progesterone on the ITO electrode

A preliminary experiment was carried out to see if a CL signal would be observed before and after incubation with progesterone. Figure 5.6 shows this change with 10 ng mL^{-1} progesterone. With 10 ng mL^{-1} being chosen as a high concentration for the simple reason of giving a clear signal change.

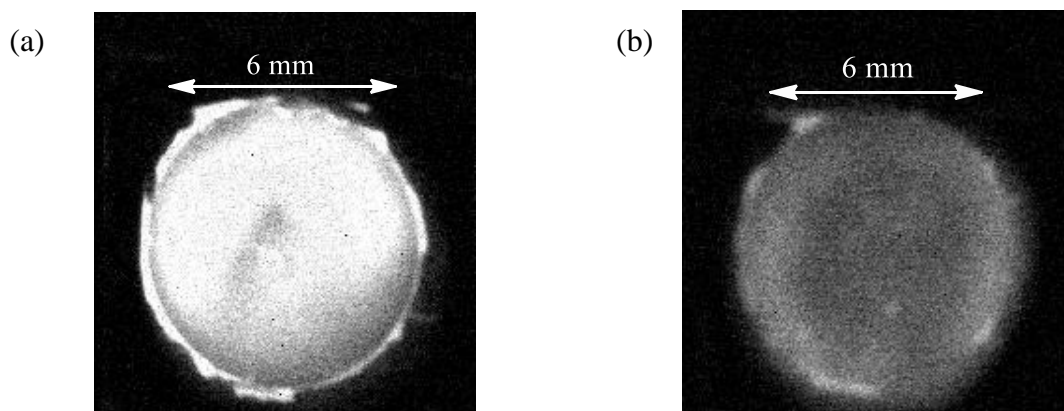


Figure 5.6: CL images of anti-progesterone antibody on the ITO surface before (a) and after (b) incubation with 10 ng mL^{-1} of progesterone.

Figure 5.6 shows two images of the oxidised ferrocene tagged anti-progesterone, each image represents a 30 μL spot of hydrogen peroxide and luminol before incubation with progesterone and after a 60 minute incubation with 30 μL of 10 ng mL^{-1} progesterone the 60 minute incubation was chosen simply to give a sufficient amount of time for any reaction to occur and to generate a large signal change with the concentration being towards the higher end of interest and would generate a clear signal change.

When the ferrocene moieties bind to the antibodies through an amide linkage this relies on the aldehyde group from the ferrocene carboxyaldehyde reacting with free amine groups on the antibody, these groups can be found all over the antibody however are richly found within the fab region of the antibody where the paratope is located.¹⁹² For this reason when a target antigen binds to the antibody, there is also an interaction with the ferrocene molecules. This results in a blocking affect that decreases the catalytic efficiency resulting in a reduction in the CL signal observed. This theory is in conjunction with that described within the previous chapter and the paper by Dou *et al.*⁵⁴

What brings about the change in signal?

Block the interaction of the solution with the surface confined catalyst, results in a lowering of the rate constant (k_{het} , figure 5.5) and therefore a reduction in the catalytic effect of the oxidised ferrocene, resulting in a lower intensity of light.

Optimisation of CL reagents

Concentrations of luminol and hydrogen peroxide were once again optimised to consider the use of a different method and catalyst. The same concentration ranges were investigated with the pH of luminol kept at pH 9.

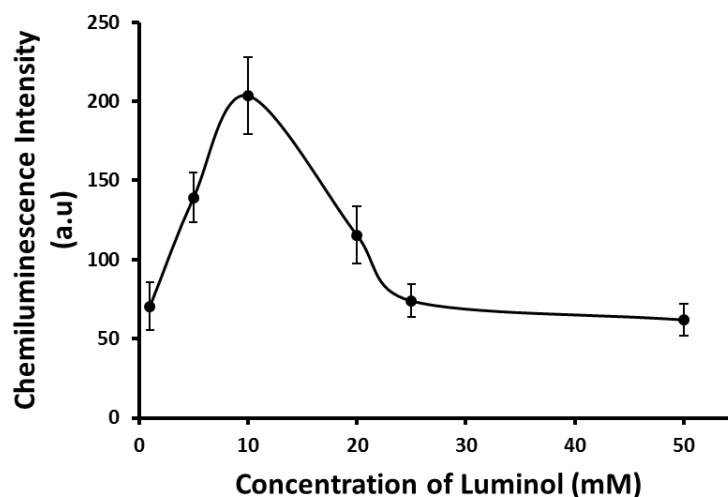


Figure 5.7: Calibration curves showing the effect of luminol concentration when the concentration of hydrogen peroxide was kept constant at 10 mM the system was catalysed using oxidised ferrocene (pH 9).

Figure 5.7 shows how the CL intensity changes with the concentration of luminol, there is an increase in the CL intensity as the concentration increases between 1 and 10 mM. Between 10 and 25 mM the luminol concentration decreases after which the intensity levels out. This observation is the same as that observed in section 3.3.1 and 3.3.2, where 10 mM was found to be the optimum concentration of luminol and the same trend was observed, where there was an increase in the CL signal until an optimum was observed followed by a decrease in intensity.

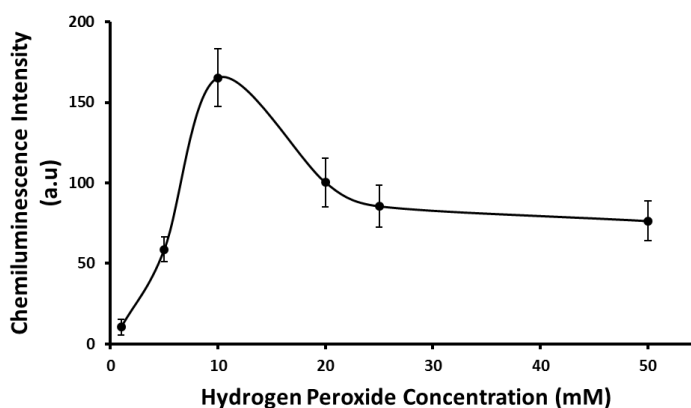


Figure 5.8: Calibration curves showing the effect of hydrogen peroxide concentration when the concentration of luminol was kept constant at 10 mM (pH 9) with the system catalysed by oxidised ferrocene.

Figure 5.8 shows how the CL intensity changes with the concentration of H_2O_2 it can be seen that as the concentration of H_2O_2 increases between 1 and 10 mM the CL signal increases. Between 10 and 25 mM the CL intensity decreases before levelling out between 25 and 50 mM. This trend is the same as that observed for luminol (figure 5.8) and the hydrogen peroxide optimisation in section 3.3.2. The reasons for these trends were outlined in chapter 3 where the reagents were being used up causing the signal to decrease. Comparing these to the optimisation conditions within chapter 3 the same concentrations have been found with slight differences in the actual intensity observed. Taking the luminol concentration when cobalt (II) was the catalyst (figure 3.4) and HRP (figure 3.6), both of these catalyst gave a CL intensity of 185 a.u. the oxidised ferrocene however resulted in a CL intensity of 200 a.u. further enhancing the oxidised ferrocene as an efficient CL catalyst.

Optimisation of the exposure time

It was necessary to determine the amount of time an image is taken to get the largest CL signal, therefore the CL was measured over various exposure times ranging from 50 seconds to 800 seconds. Figure 5.9 shows the difference in the CL signal observed as the exposure time changes.

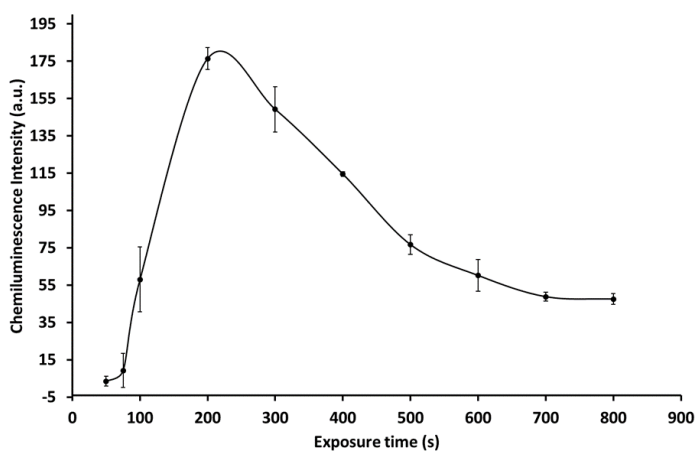


Figure 5.9: Graph showing the optimisation of exposure time where a mixture of 10 mM luminol and 10 mM H_2O_2 was measured, whereby 200 seconds was found to be the optimum exposure time.

From figure 5.9 an exposure time of 200 seconds was viewed to give the highest light intensity, which was an ideal time frame for our aims, with the development of a point-of-care device where the analysis needed to be as quick as possible. After the 200 second time period the light signal decreases this is due to the chemical reaction having taken place and concluded while an image is still being taken. All experiments therefore used a 200 second exposure time.

5.3.2 CL immunoassay of progesterone and oestriol on the ITO electrode

Progesterone concentrations varying from 0.1 ng mL^{-1} up to 10 ng mL^{-1} were investigated; as these cover the required calibration range for a sample of saliva (section 1.3.1). Each concentration was incubated at incubation times of 15 minutes, 30 minutes and 60 minutes to determine the optimum incubation time. The detection was subsequently analysed by taking the fraction of the surface that has been blocked as presented in section 4.4.3. This was interpreted to measure the fractional surface blockage (equation 5.1).²⁰⁷

$$\theta = 1 - \frac{S_{after}}{S_{Before}} \quad (5.1)$$

Where: θ = the fraction of the surface blocked.

S_{before} = the CL signal produced without antigen present (a.u.).

S_{after} = the amount of light that could be produced if the surface was not blocked by the antigen (a.u.).

The equation operates by determining the vacant adsorption sites therefore if no antigen has adsorbed to the surface then $S_{\text{before}} = S_{\text{after}}$. Which would equal 1. Subtract this value from 1 can allow us to see the fraction of those vacant sites that have been filled by the antigen. If all sites were filled then the signal after incubation would be 0 and therefore theta would be 1. Figure 5.10a shows this measurement as a function of the incubation time. With figure 5.10b showing the same graph plotted as a calibration as a function of the concentration.

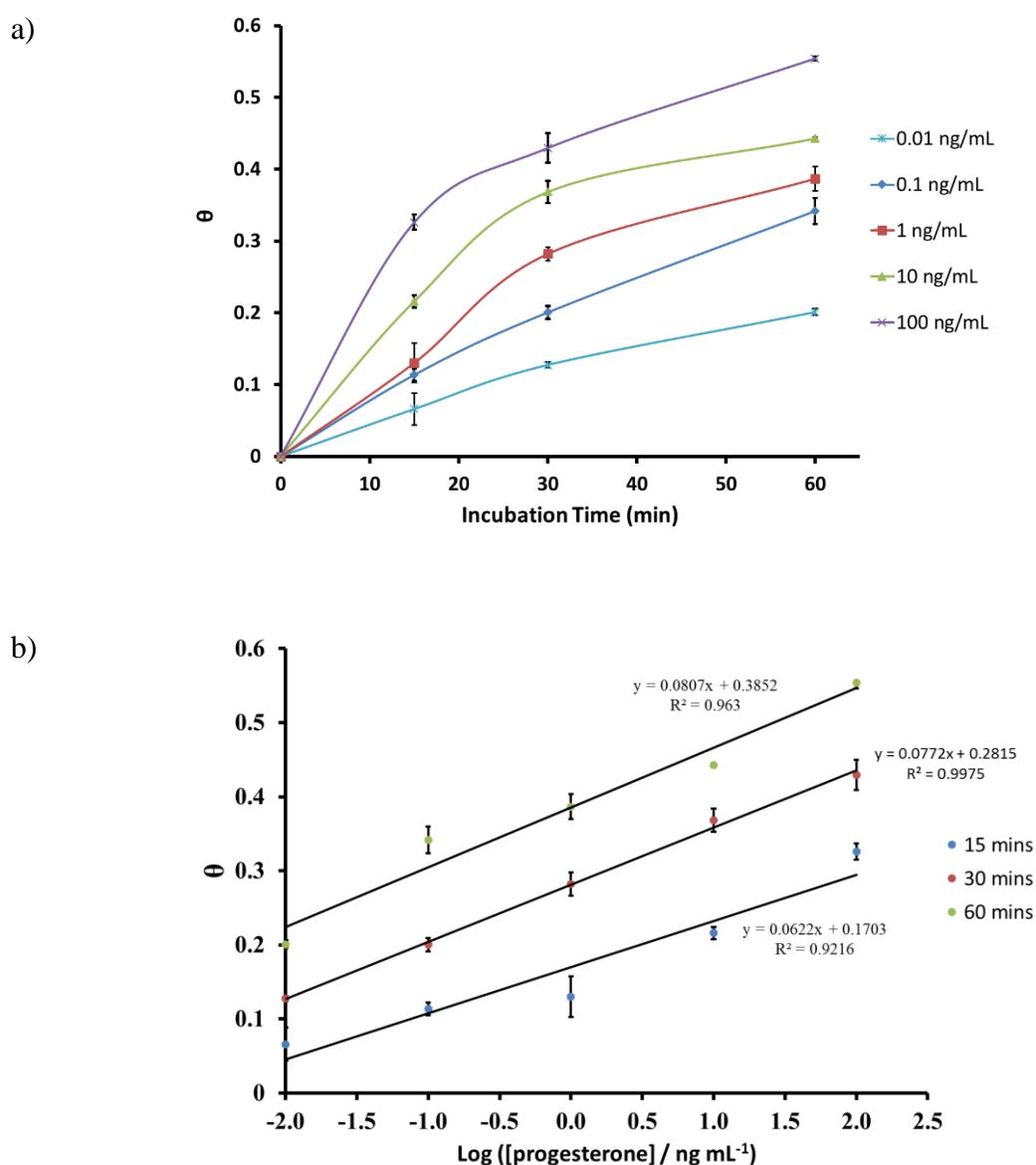


Figure 5.10: (a) How the antigen surface coverage (θ) changes based on various incubation times and for various concentrations of progesterone. (b) Calibration curves of surface coverage of progesterone at various incubation times. (n=5).

The error bars were calculated by taking the standard deviations of the θ values obtained across the five repeats. Figure 5.10a shows the Langmuir-looking plot seen in the previous chapter, with an initial sharp increase in θ until a point where the value tails off. With the 1 and 10 ng mL⁻¹ standards giving a clear indication that after 30 minutes incubation the system is approaching equilibrium. However for all concentrations after a minute or two there is a sharp rise in θ . This is not unexpected if you consider that the binding equilibrium constant for progesterone ($K_{\text{association}}$) is $4 \times 10^9 \text{ L mol}^{-1}$ (value obtained from the data sheet supplied by AbCam) resulting in a $K_{\text{dissociation}}$ of $2.5 \times 10^{-10} \text{ mol L}^{-1}$ this is the inverse of the association constant. The equilibrium strongly favours the anti-progesterone : progesterone complex rather than the progesterone and anti-progesterone separately; which explains the initial sharp rise in theta. However as only a limited amount of sample was used there will be a point where the majority of progesterone within the sample has bound to the antibody and equilibrium is met. Resulting in the theta value stabilising over an increased incubation time.

To show this further figure 5.10b shows a calibration where the surface coverage (θ) is plotted as a function of the concentration and after a 30 minute incubation period. A good correlation of data ($R^2=0.9975$) is observed, taking this plot, the LOD is determined to be 2.35 pg mL⁻¹ which was calculated by taking three times the standard deviation of the blank signal across the antibody immobilisation on three different electrodes added to average of these signals, ($3S_b + \text{average background signal}$).²¹⁴ Having successfully developed a reproducible method for progesterone quantification oestriol was now investigated in an attempt to develop the overall system to meet the aims of this thesis.

Figure 5.11 shows the same calibration plot but for oestriol.

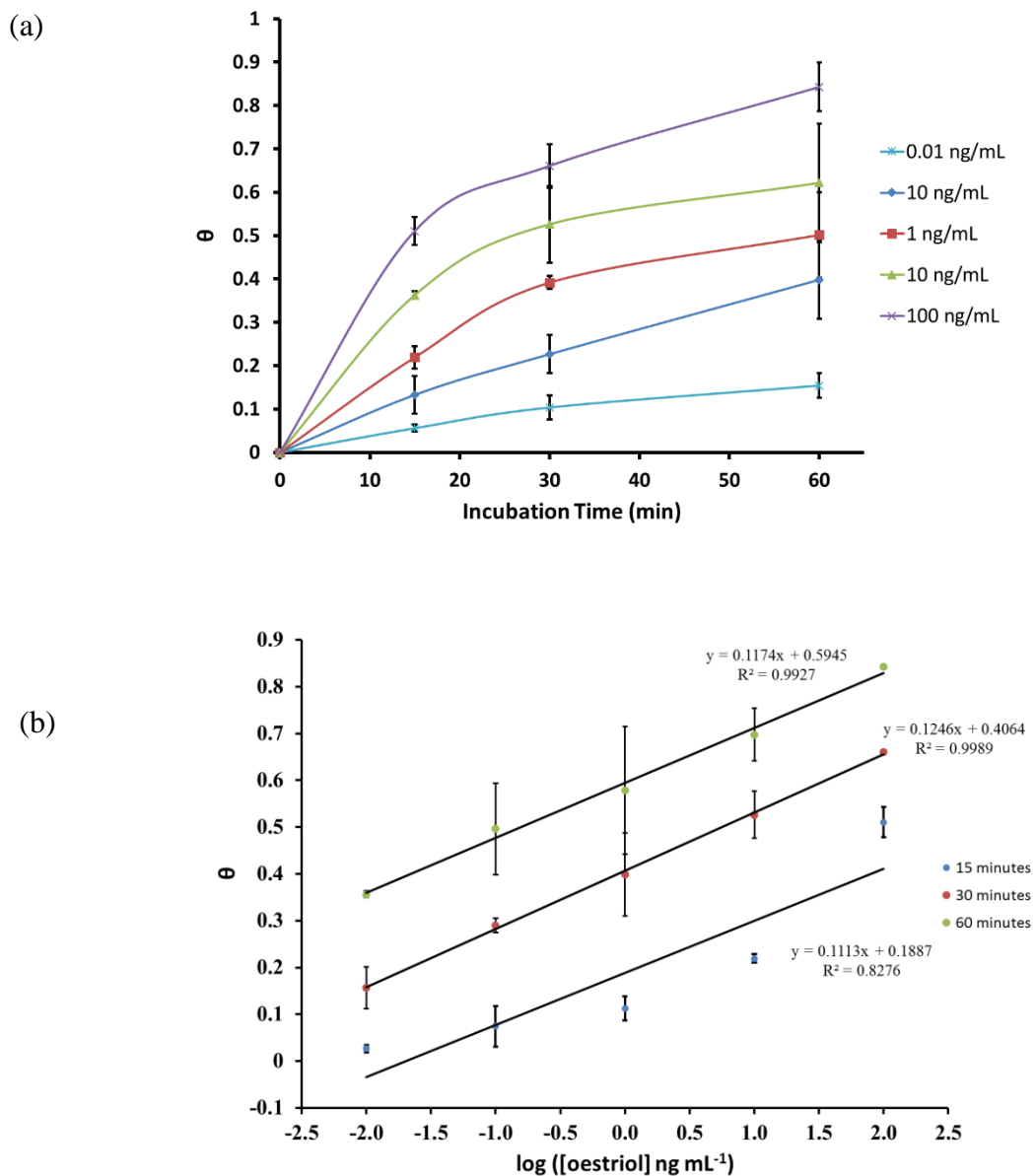


Figure 5.11: (a) How the surface coverage (θ) changes based on various incubation times and for various concentrations of oestriol. (b) Calibration curves of surface coverage of oestriol at various incubation times. ($n=5$).

Figure 5.11a shows the same diagram as in figure 5.10a where the surface coverage is plotted as a function of the incubation time. In the same fashion as observed in figure 5.10a where there is an initial sharp increase in theta as the oestriol binds to the antibody until a point where equilibrium is met and theta therefore tails off. Through a calibration plot the LOD can be calculated as well as coming to a conclusion as to the optimum incubation time to give reliable results for oestriol.

Taking the incubation of 30 minutes where there was the strongest correlation of data ($R^2=0.9989$), the LOD can be calculated to be 2.54 pg mL^{-1} .

From figures 5.10b and 5.11b a 30 minute incubation time gives a good reproducible correlation of data, with a time frame that is ideal for a POC device giving a total analysis time of 45 minutes from giving the sample to obtaining a final result; well within the required concentration ranges of both hormones as well.

The optimum incubation time of 30 minutes was not unexpected as this was the same as the electrochemical immunoassay. Like the electrochemical approach 15 minute incubations could be used for progesterone, however as figure 5.10b shows after 15 minutes the trend was not linear for oestriol and therefore it would not be appropriate to use this time scale.

Interference studies

An interference study was carried out to identify whether any compounds found in saliva may interfere with the analysis. This is a result of some molecules having similar structures and therefore could interact with the antibodies in a similar fashion.⁴²

Oestradiol and Oestrone are the two other key hormones within the oestrogen group and was analysed as a potential interference to anti-oestriol, testosterone and vitamin D3 as potential anti-progesterone interferences. Typical levels found in women do not exceed 20 ng mL⁻¹, with levels typically found <0.5 ng mL⁻¹ the concentrations may rise with some medical conditions.^{15, 210, 211} Table 5.1 shows the structure of each molecule.

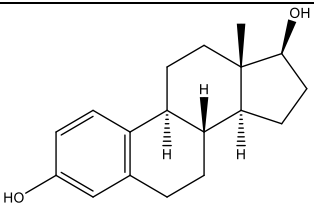
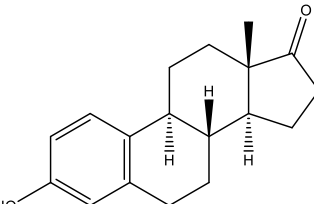
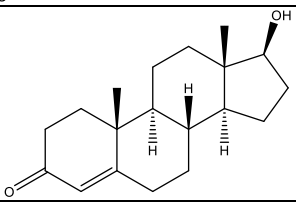
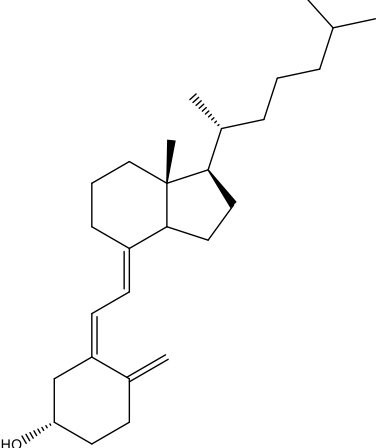
Molecule	Structure
Oestradiol	 <chem>O=C1CC[C@H]2[C@@H]3[C@H]([C@@H]1CC[C@@H]2O)CCC4=CC(=C)C=C4O</chem>
Oestrone	 <chem>O=C1CC[C@H]2[C@@H]3[C@H]([C@@H]1CC[C@@H]2O)CCC4=CC(=C)C=C4O</chem>
Testosterone	 <chem>CC12CCC3=C(C(=O)CC4=CC=CC=C4O)C[C@H]3[C@H]([C@@H]1CC[C@@H]2O)C</chem>
Vitamin D3	 <chem>CC(C)CCCC[C@H]1CC[C@@H]2[C@@]1(CC[C@H]3[C@H]2CC=C4[C@@]3(CC[C@@H](C4)O)C)C</chem>

Table 5.1: structures of the different potential interference molecules.

For each interfering molecule a 30 minute incubation time was used to coincide with the optimum conditions for progesterone and oestriol monitoring.

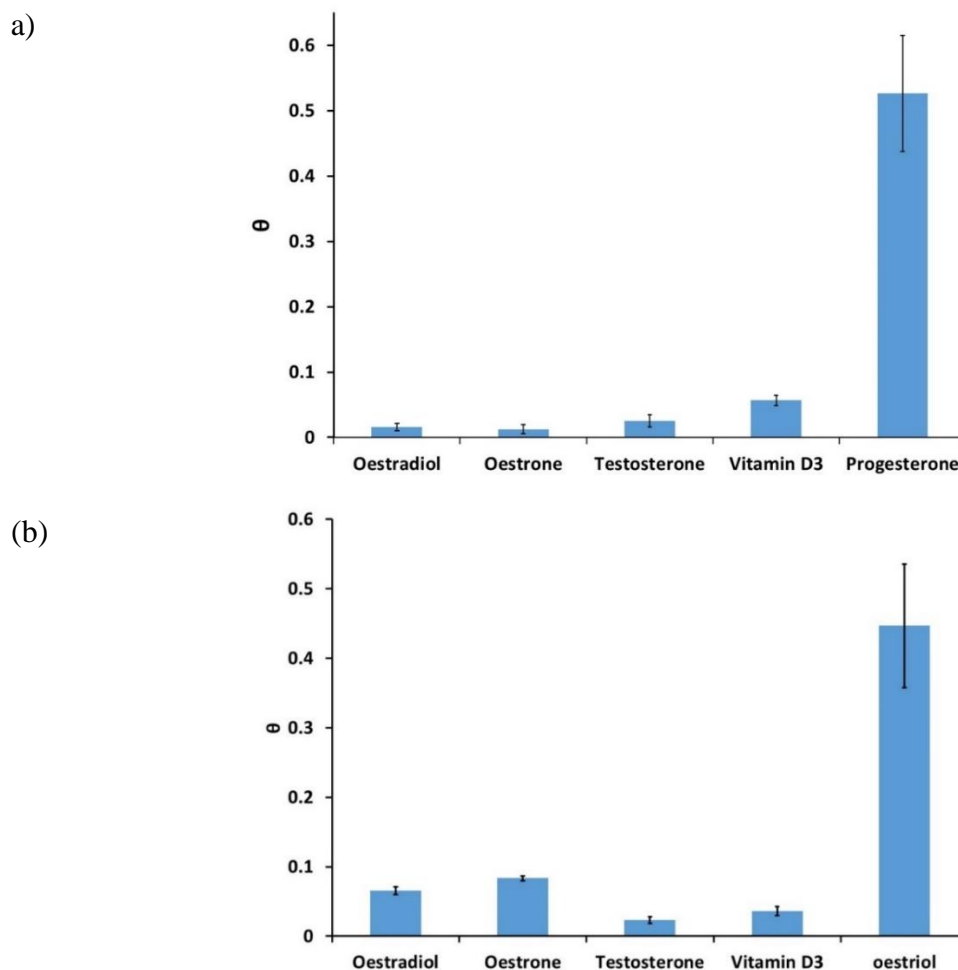


Figure 5.12: Specificity of ferrocene-tagged antibody CL immunoassay the results are based on a 30 minute incubation time and a 20 ng mL^{-1} concentration; where a) represents interference with respect to anti-progesterone antibodies and b) anti-oestriol antibodies.

Figure 5.12a shows in interaction of the different molecules with the anti-progesterone antibodies, the oestradiol, oestrone and testosterone have very little interference ($\theta \sim 0.02$ - 0.05) with the measurements. Vitamin D3 however does have a minor interaction with the antibody ($\theta = 0.08$), vitamin D3 does have a similar structure except the backbone seen with steroidal molecules is not closed this interaction however is very small and would not hugely impact on any analysis.

Figure 5.12b shows the interaction of these molecules with anti-oestriol, as expected the testosterone and the vitamin had very little interaction with the antibodies ($\theta=0.02 - 0.05$), the oestradiol and oestrone had a larger affect ($\theta =0.06$ and 0.09). These two molecules are part of the oestrogen group and therefore have very similar structures to oestriol, with oestradiol containing a second alcohol group and oestrone containing a ketone, therefore these molecules will interact with their corresponding antibody in a similar as oestriol does resulting in the interference. Like with the anti-progesterone this interference is not huge and would not drastically impact on any results. Remember these are based on a concentration of 20 ng mL^{-1} which would represent a substantial increase in the concentrations found naturally the system therefore shows good selectivity towards the target analyte this allows accurate determination for clinicians without the risk of false results due to interferences.

5.3.3 Progesterone and oestriol immunoassay using the macroflow device

Optimisation of the macroflow system

Figure 5.13 shows an image within the macroflow device itself of the spots, the antibodies was prepared in the same manner as previously described. The flow cell had a total volume of $549 \mu\text{L}$.

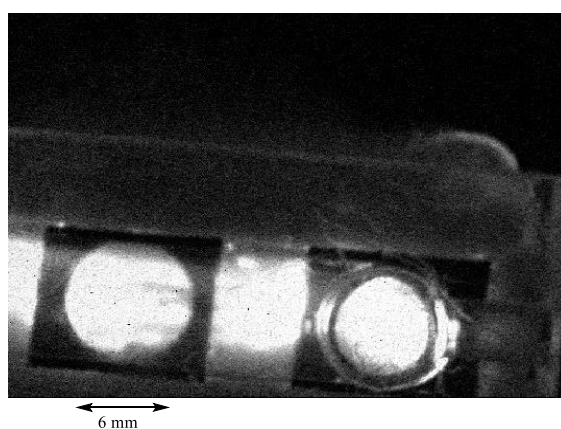


Figure 5.13: Photograph showing the CL emission from the macroflow system, where a flow rate of 1 mL min^{-1} was used and a hydrogen peroxide (10 mM) and luminol (10 mM, pH 10) with the left-hand spot representing anti-oestriol and the right-hand spot representing anti-progesterone.

Figure 5.13 shows the CL response from the integrated macroflow device, from the image the flow is from right to left. Upon contact with the first spot a bright light was observed which transferred across to the second spot, where the emission continues, this could be due to an emission tail that can be seen through a flow system, this is a consequence of the excited species relaxing while flow is continuing.²¹⁵ This is a problem ensuring the light emission is isolated to the spots themselves and not elsewhere. This tail could be controlled by the flow rate as well as by separating the spots further apart so that the emission from the first spot does not interfere with the second.

The intensity of light for each individual area was similar (190 ± 10 a.u and 185 ± 13 a.u), this means that the resistivity issues across the electrode as discussed in chapter 4 does not affect the CL signals observed. The optimum flow rate was investigated for the two spots individually and the CL measured. The exposure time was 200 seconds and the luminol and hydrogen peroxide concentrations were 10 mM each as used previously.

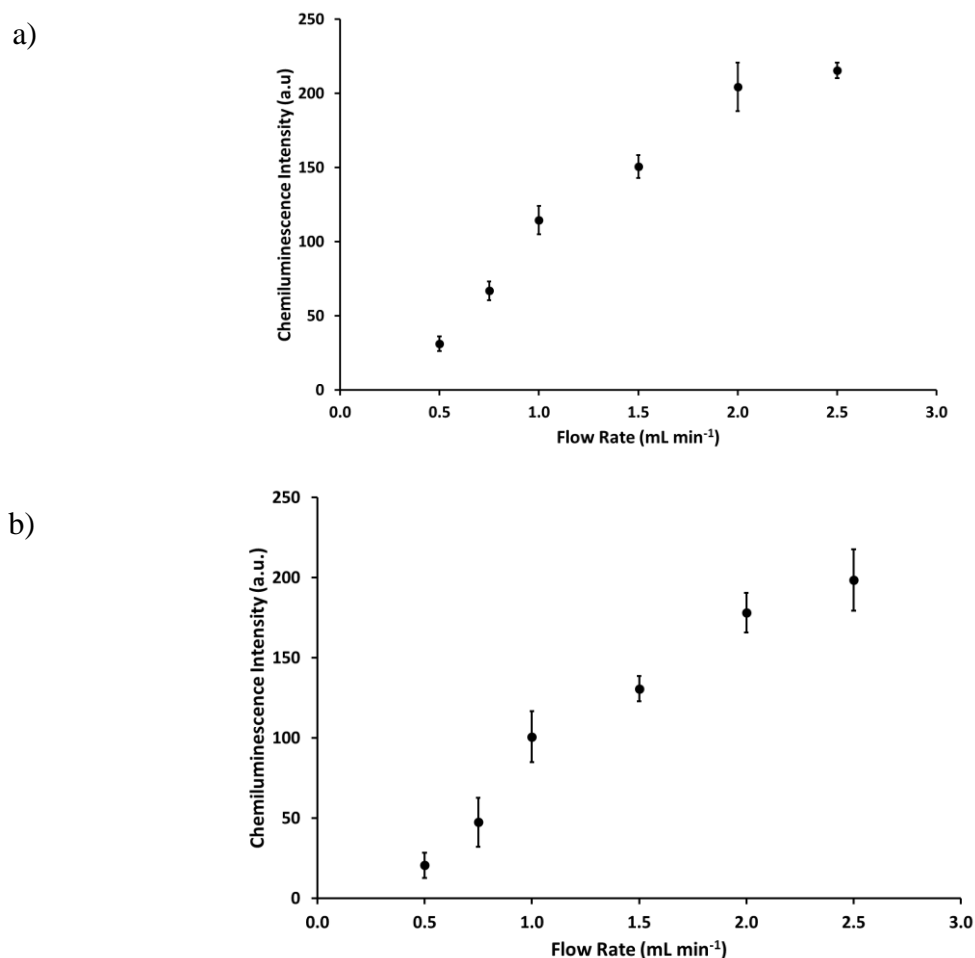


Figure 5.14: Effect of flow rate on the chemiluminescence intensity for a) spot 1 and b) spot 2.

Figures 5.14a and b shows how the flow rate affects the CL intensity observed for both spots on the ITO surface. As the flow increases the CL intensity increases.

As expected the CL intensity increases with flow rate in the same way observed by Marle and Greenway,²¹⁶ where the CL signal increased with flow rate, however due to the risk of an emission tail which was previously observed the flow rate was kept at 2 mL min⁻¹. An emission tail was seen at the 2.5 mL min⁻¹ flow rate which explains the large error bar at this flow rate within figure 5.14 b. Therefore all further experiments are carried out at 2 mL min⁻¹ this is due to the fast kinetics of the luminol and hydrogen peroxide reaction described in section 1.8.

CL immunoassay within the flow cell

Using the optimum parameters an immunoassay for the detection of progesterone and oestriol was conducted where the standard solution in saliva was pumped into the cell until the cell was full and left to incubate for various time periods as for the static system (section 5.3.2).

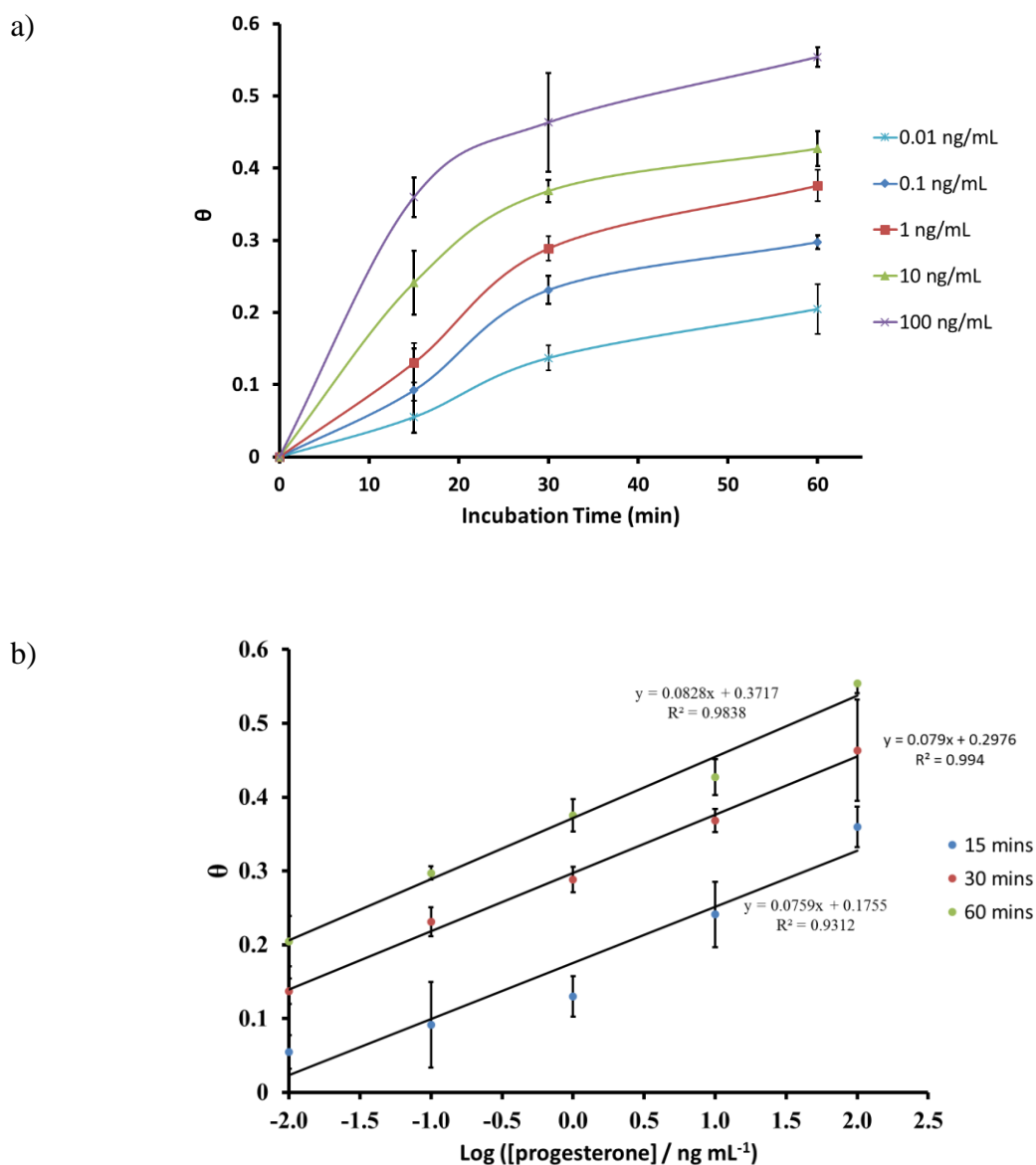


Figure 5.15: (a) How the antigen surface coverage changes based on various incubation times and for various concentrations of progesterone. (b) Calibration curves of surface coverage of progesterone at various incubation times. (n=5).

Figure 5.15 (a) represents the surface coverage of progesterone on the electrode surface from the figure there is a sharp increase in theta as the time increases, the theta value then levels out as the incubation time increases up until a point where it begins to tail off. (b) illustrates a calibration curve at each incubation time showing how theta changes with concentration.

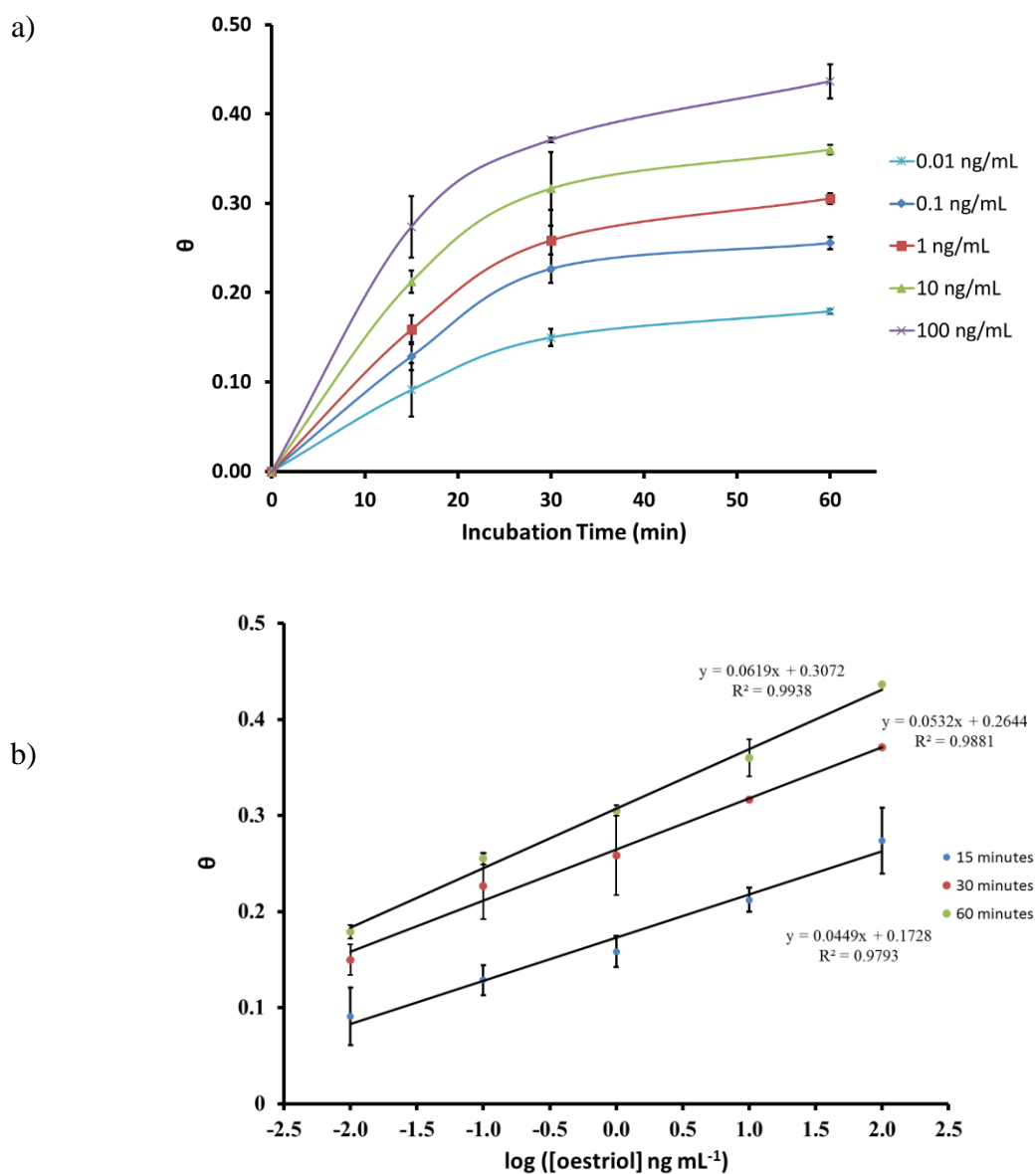


Figure 5.16: (a) How the surface coverage changes based on various incubation times and for various concentrations of oestriol. (b) Calibration curves of surface coverage of oestriol at various incubation times. (n=5).

Figure 5.16 presents the same Langmuir-looking relationship for oestriol with 5.16a showing an increase in theta as the incubation time increases for the various concentrations of oestriol, through plotting this as a calibration curve (figure 5.16b) a clear linear trend was observed at each incubation period.

From the calibration curves, a 30 minute incubation gave the optimum results for both analytes from the results reducing the incubation time would not be possible due to the poor linear trend observed after 15 minutes for progesterone. 30 minutes was found to be the optimum incubation time using this flow system as well as with the static system. The LODs for progesterone and oestriol were calculated to be: 56.6 pg mL^{-1} and 26.9 pg mL^{-1} for progesterone and oestriol respectively. These LODs are an order of magnitude larger than those from the static system, the reason for this could be due to the volume of sample within the cell which is significantly larger than the volumes used on the static system. These results are comparable to those obtained in chapter 3 for progesterone where a LOD of 33 pg mL^{-1} was determined.

5.3.4 Integrated microfluidic device

Having obtained decent results using the larger flow cell a device needed designing that consisted of smaller volumes in an attempt to improve the sensitivity. With this in mind a device was designed with the capability to simply slot the modified ITO electrode, into the device (figure 2.4). The initial device designed consisted of two channels of different widths to try and determine if volume was the reason that the sensitivity suffered previously. Although ideally the system would be automated and the CL reagents would be mixed on chip, it has been proven in figure 3.21 and figure 3.24 that it is possible to get the light on the device. Having shown this all that was required to start with was a proof that CL can occur from the antibodies themselves therefore the CL reagents were premixed and pumped into the device. The tubing was then glued into place with luminol and hydrogen peroxide mixture flowed through the system at $100 \text{ } \mu\text{L min}^{-1}$, once the

reaction chamber was full with luminol and hydrogen peroxide a CL image was taken. Initially no signal was observed, this was investigated further.

Comparing CL signal off and on chip

Prior to slotting the electrode into the device a CL image was taken, this was a control to enable us to see whether the reaction would work. After this the electrode was slotted into the device and the CL image repeated using the same flow parameters. The electrode was then removed and another CL image taken. Figure 5.17 shows these CL images:

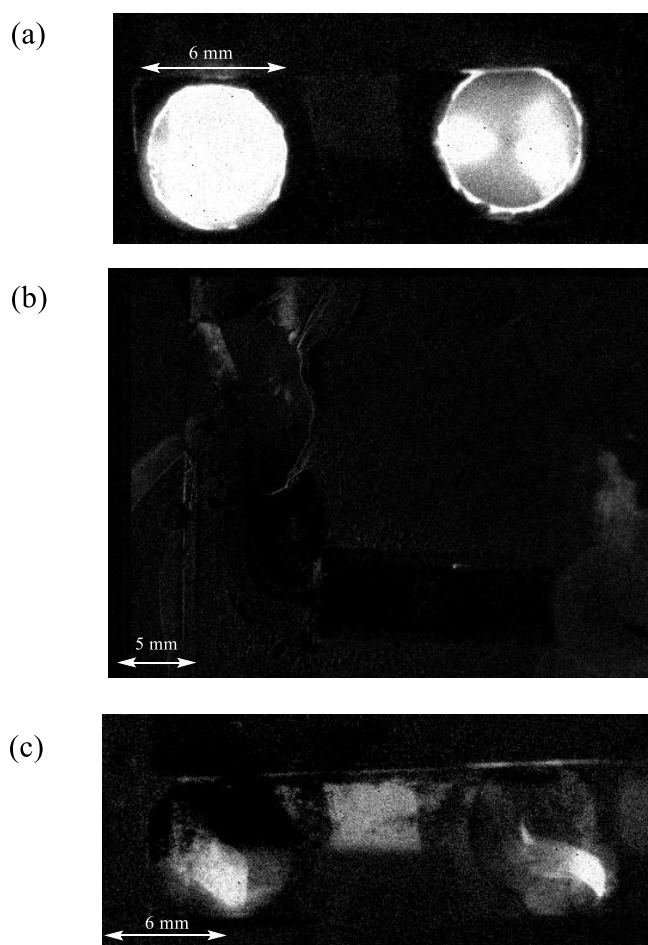


Figure 5.17: CL images of a) ITO electrode before slotting into the chip, b) inside the microfluidic device and c) after removing from the microfluidic device after expose to H₂O₂ and luminol.

Figure 5.17a shows the ITO electrode straight after ferrocene oxidation and two signals can be seen from the individual areas. Figure 5.17b is the ITO modified electrode slotted into the microfluidic device, no CL signal was seen after excessive exposure to luminol and hydrogen peroxide. Figure 3.17c is the same ITO electrode removed from the microfluidic device with a repeat CL measurement.

From the figure there was clearly an issue when slotting the electrode into the microfluidic device. It can be seen from the final image because the signal observed is substantially lower than prior to insertion into the microfluidic chip. This investigation was conducted in the larger of the two chambers of the device shown in figure 2.4.

This issue could be attributed to the fact the top and base plates of the chip are bound together through double-sided sellotape resulting in some of the tape leaching into the area where the electrode is placed. Causing difficulty in the insertion and damaging the surface of the electrode.

This was repeated, however with the area where the electrode is inserted and the tape cut away. Unfortunately this resulted in the same outcome.

5.4 Conclusion to CL Investigation on an Electrochemical Immobilisation Platform

Having developed a robust protocol for antibody immobilisation through an electrochemical approach, where the antibodies are orientated in the ideal way and quantified on the ITO surface, this chapter focused on translating this into a POC system.

The use of the static ferrocene moieties tagged to the antibodies immobilised on the ITO electrode was investigated as a route to carry out CL analysis. A CL immunoassay was successfully developed by this method. LODs of 2.35 pg mL^{-1} for progesterone and 2.54 pg mL^{-1} for oestriol were obtained this is well below the lower limit necessary for progesterone in saliva which is 31 pg mL^{-1} and oestriol which is between 0 and 5 ng mL^{-1} .

¹. The LOD for progesterone was comparable to that obtained using the electrochemical method (chapter 4) where a LOD of 1.7 pg mL^{-1} was calculated and significantly better than that obtained in chapter 3 where a LOD of 33 pg mL^{-1} was calculated.

Potential interferences were looked at and from the results the process developed was selective to the required analyte, with a slight interference from oestradiol and oestrone with the anti-oestriol antibodies which was not surprising as they are very similar molecules.

Following the success of the static method the electrode was incorporated into a macrofluidic device. This device unfortunately required larger amounts of reagents; despite this the device was a success with reasonable LODs which were an order of magnitude larger than that seen on the ITO itself. The reasons for this discrepancy could be due to the measurements under flow conditions and the volumes within the cell. To try and solve this a microfluidic device was designed where the electrode could simply be slotted into.

Slotting the electrode into a device would be ideal for clinicians as they can carry out analysis quickly and easily. Unfortunately however transferring this onto a microfluidic based system was not successful, having looked at the ITO electrode before and after analysis on the device there was clearly an issue. This could be due to damage during the slotting process which is an area that would have been investigated except time restraints did not allow this.

However the static system worked very well and would still be very simple as a POC device, it was not automated but simply pipetting reagents onto electrode and placed under a camera a result can be obtained quickly and accurately for both progesterone and oestriol while requiring minimal volumes of reagents.

Chapter 6 Conclusions & Future Work

This thesis describes the development of novel heterogeneous immunoassays as a route to quantify the concentrations of progesterone and oestriol in saliva samples the concentration range for progesterone is $<31 \text{ pg mL}^{-1}$ to $>100 \text{ pg mL}^{-1}$, for oestriol the concentration ranges from $0 - 5 \text{ ng mL}^{-1}$.^{8, 15, 31} This was achieved using CL and electrochemical detection methods.

Clinicians require a simple, automated, rapid and cost effective system to carry out medical diagnoses, with this in mind POC devices are ideal to meet these requirements. To monitor progesterone and oestriol in saliva the methods needed to be sensitive. Chapter 1 describes the various ways this could be achieved. Immunoassays were selected due to the strong antibody/antigen interaction, this would enable the sensitivities and selectivity to be reached. Heterogeneous immunoassays relies on the antibody being immobilised onto a solid surface, this technique provides the ability to spatially isolate individual antibodies as well as improving the sensitivity and selectivity of the system.

For a successful immunoassay protocol the detection method of choice was of great importance, different methods will result in different LODs and instrumental requirements. For POC this needed to be sensitive with simple instrumentation. Therefore chemiluminescence was chosen as the primary detection method due to the sensitivities that can be achieved as well as the simple instrumentation where only a camera and a dark environment is required. Electrochemical detection was also investigated due to the sensitivities that can also be achieved and the robustness of the antibody immobilisation protocol.

For a heterogeneous immunoassay the solid substrate of choice is important, in chapter 1 various different solid substrates were compared as well as the chemical processes required to immobilise the antibodies onto the surfaces. CL detection requires this surface needs to be transparent so that the light can be detected and analysed, concluding that glass and plastic were the ideal substrates to take forward for CL detection, these substrates also had the benefit of being widely utilised and investigated with different possible immobilisation routes.

Chapter 2 described the way in which a POC device can be engineered, initially a design was created based on microfluidic properties outlined in chapter 1; within this design channels were included that allowed sufficient mixing of reagents, as well as a channel to spot the antibodies, this design was fabricated in glass and plastic.

Subsequent designs then involved the incorporation of a transparent ITO electrode into a microfluidic device, this was achieved by slotting the electrode into the device after the electrochemical processes had taken place removing the need of other electrode materials.

Direct CL detection through the use of glass and plastic devices

Chapter 3 described a direct microfluidic approach with CL detection; where anti-progesterone antibodies were immobilised onto glass and plastic surfaces. Two glass surface modification methods were studied where the surface was silanised with APTES and GPTS. The GPTS approach did not work despite being reported as a route for immobilising antibodies onto glass surfaces; this was likely due to the orientation of the antibody. The epoxide group binds through the amine found primarily on the paratope this would inhibit the interaction of the antibody with a sample. APTES gave better results and was used in combination with two different linker's glutaraldehyde and EDC/sulfo-NHS. The glutaraldehyde proved to be unsuccessful giving irreproducible results. The

problem has been reported in the literature where batch to batch differences and the molecules ability to self-polymerise affecting its performance. The use of EDC/sulfo-NHS as a linker did prove successful for the immobilisation of anti-progesterone onto glass slides. Through this approach a LOD of $33 \pm 3 \text{ pg mL}^{-1}$ was determined which was better than or comparable to methods quoted in the literature for progesterone quantification. This value also represents the lowest concentration found in saliva samples within error.

The antibody immobilisation process used on the glass slides was then transferred onto the microfluidic device. It however proved difficult to generate positive and reproducible data; this could be due to a number of reasons for example the requirement to bond the two plates together after immobilisation. Polymer microfluidic devices were then investigated as an alternative.

The use of plastic substrates enable the development of systems that are disposable, cheap and easily fabricated in bulk which would not be possible with the glass devices. PMMA was the plastic of choice due to the presence of the methacrylate groups which can be modified to form other functional groups. 2 alternative methods were investigated as routes to modify the polymer surface. The first method was to use LiAlH_4 to reduce the ester groups to the alcohol groups this route was attempted to prove a similar immobilisation route as the one used on glass. This however resulted in a damaging of the surface in a way that the plastic was no longer transparent. A second method was therefore attempted which involved hydrolysing the ester groups to the carboxylic acid. This was somewhat successful however serious reproducibility problems resulted in no useful measurements being obtained.

Overall a CL immunoassay for progesterone on glass slides had been carried out, however reproducibility issues and the inability to quantify the concentration of the antibody on the surface resulted in the need to develop a fresh immobilisation protocol.

Electrochemical immunoassay of progesterone

To overcome the problems encountered through the direct immobilisation and CL detection on glass and plastic substrates; a previously successful electrochemical immobilisation and detection platform⁵⁴ was investigated as a route for progesterone quantification. Three different electrode materials were investigated; gold which has been used previously, glassy carbon and ITO due to its transparent properties indicating it could be incorporated with CL. Carrying out an electrochemical immobilisation protocol enabled the possibility to quantify the antibody concentration on the surface.

The electrode surfaces were modified through the reduction of nitrobenzenediazonium tetrafluoroborate. With nitrobenzene immobilised on the surface the nitro moieties were then reduced to the corresponding amine. As well as this the anti-progesterone antibodies were modified to contain ferrocene tags which are redox active. Through UV-Vis spectroscopy the average number of ferrocene tags per antibody was determined to be ~ 13 from this the concentration of antibodies on the surface was calculated and this was found to be $4.46 \times 10^{-7} \text{ mol m}^{-2}$. The antibodies were immobilised onto the surface through the use of EDC and sulfo-NHS.

The electrode surfaces were characterised to confirm the surface confinement of the ferrocene-tagged anti-progesterone which was carried out using cyclic voltammetry at various scan rates, with the peak current plotted as a function of the scan rate. All three systems showed a linear response confirming the redox species is surface confined.

Although the Au and ITO were hardly affected by the scan rate, the GC electrode was affected by higher scan rates indicating the electrode kinetics on the GC was slower than on the other surfaces.

The progesterone immunoassay was carried out on all three electrode surfaces resulting in calibration ranges within the required clinical range for progesterone, with ITO an order of magnitude more sensitive than the other substrates. ITO gave a linear range between 100 fg mL^{-1} rising to $1 \text{ } \mu\text{g mL}^{-1}$, whereas the Au and GC electrodes had a linear range between 1 pg mL^{-1} and $1 \text{ } \mu\text{g mL}^{-1}$. ITO resulted as the optimum material to carry out a progesterone immunoassay. The improved sensitivity compared to the work in chapter 3 was due to the rigid structure the ferrocene tagged antibodies have when immobilised on the surface this was due to the ferrocenes being primarily found at the paratope of the antibody, resulting in a better orientation therefore improving the sensitivity. The success of the ITO compared to the other electrode materials also was due to the surface being flat with a fractal dimension tending to 2.

Having concluded that ITO was the optimum substrate; the system as a whole was investigated further. With the aim of developing a POC device the incubation time needed optimising so that the system works within the shortest possible time frame. Various incubation times were investigated 15, 30, 60, 90 and 120 minutes. After 15 minutes a clear signal change was observed and therefore this time frame could be used however 30 minutes was the optimum, at this time the antibody/antigen interaction approached equilibrium.

A calibration was then obtained in a saliva matrix using the optimum conditions to carry out the immunoassay. Using the saliva matrix a LOD of 1.7 pg mL^{-1} was calculated this was an order of magnitude larger than the 100 fg mL^{-1} observed when the progesterone was in PBS. The saliva matrix itself was the reason for this variation. The LOD was

however still well below the required clinical limit for progesterone; this sensitivity was also an order of magnitude lower than the 33 pg mL^{-1} obtained on glass.

Within this work a reproducible immobilisation protocol has been developed where the number of antibodies on the surface had been quantified. Tagging ferrocene to the anti-progesterone enabled a rigid structure on the surface after immobilisation, this structure was such that the antibody was in the desired orientation to have complete interaction with a sample this aids the sensitivity as antibody binding sites are not lost due to undesirable antibody orientation.

Chemiluminescence immunoassay using an integrated functional device

Although the electrochemical immunoassay was successfully developed, translating this onto a microfluidic system would be difficult due to the need to incorporate a reference, a counter electrode and the ITO electrode. With this in mind and not wanting to lose the successful immobilisation protocol, the use of ferrocene to catalyse the luminol and hydrogen peroxide reaction had been previously reported.²⁰⁹ This allowed the development of a system where only the ITO needed incorporating into the device. The use of ferrocene as a catalyst for a CL immunoassay is novel and is substantially cheaper than the more commonly used HRP. On the ITO surface circular adhesives with holes were used to enable the isolation of ferrocene tagged anti-progesterone and ferrocene tagged anti-oestriol antibodies. The ferrocene tagged antibodies were immobilised onto the ITO electrode using the same electrochemical procedure as previously described. A calibration on the ITO surface with artificial saliva for both progesterone and oestriol was obtained, this also involved an investigation into the required incubation time. Within an optimum 30 minute time frame, LODs of 2.35 pg mL^{-1} for progesterone and 2.54 pg mL^{-1} for oestriol were obtained well below the required clinical limits. These LODs were comparable to those obtained in chapter 4 when using the electrochemical detection

where a LOD of 1.7 pg mL^{-1} was obtained for progesterone in saliva and an order of magnitude lower than the CL study outlined in chapter 3. This method removes the need for a potentiostat and multiple electrodes. Also proving a new novel CL immunoassay.

Having shown that progesterone and oestriol could both be monitored in a static system using a CL immunoassay, the development of an integrated flow system began with the design of a macroflow based system. The flow cell was to enable greater autonomy when carrying out the analysis. The modified electrode was incorporated into the device where the experiments were repeated. Through this route again a sensitive calibration for progesterone and oestriol in saliva was determined within 30 minutes, with LODs of 56.6 pg mL^{-1} and 26.9 pg mL^{-1} for progesterone and oestriol respectively. These were an order of magnitude larger than those obtained using the static system which could have been due to the volumes inside the flow cell. Despite this it gave great promise as a route to incorporate onto a microfluidic based system.

A microfluidic device that can incorporate an ITO electrode had been designed, the electrode that had been pre-prepared could be slotted straight into the device enabling easy use for clinicians. Experimentally however this proved to be very difficult for many different reasons, some of which are not necessarily clear, it was observed that an electrode that had resulted in a CL signal immediately before being integrated into the microfluidic device was unable to replicate this. There was a possibility that the electrode was damaged as it was slotted into to the microfluidic device. This was concluded based on the CL images that were taken after the electrode had been removed from the microfluidic device, the CL intensity was substantially lower than prior to insertion into the microfluidic device. Unfortunately due to time restraints further investigation was not possible however there was scope to take the system further with fresh designs.

Through this work the successful development of a robust immobilisation protocol has been developed. This protocol is very reliable and reproducible due to the ferrocenes on the antibody aiding the orientation as these are situated on the paratope region of the antibody. An electrochemical method has been developed which quantifies progesterone concentrations in a saliva sample within the clinical range in 20 minutes. This was followed on where the ferrocene in its oxidised state was used as a catalyst for the CL reaction of luminol and hydrogen peroxide. The static system gave LODs that are substantially lower than the requirement for progesterone and oestriol in saliva. The electrode was then incorporated into a flow device where LODs were an order of magnitude higher than the static system, both systems provided results within the clinical range within 40 minutes.

The development of this CL method is new and novel and removes the need to use the expensive HRP catalyst and a complicated device. All the systems operate within a short time frame where the electrochemical sensor can operate within 20 minutes and the CL systems within 40 minutes. The static ITO system could be utilised as a POC device as the system is simple where only adding reagents to the individual areas was required. This method would therefore allow patients to obtain rapid results at a doctor's surgery or hospital. Fertility and pregnancy biomarkers were looked at in this thesis, however this method could be extended to any process where antibodies could be used.

Future work

Future work would consist of developing more appropriate designs for microfluidic devices that could incorporate the ITO electrode as well as giving the CL signal desired.

One such design is shown in figure 6.1:

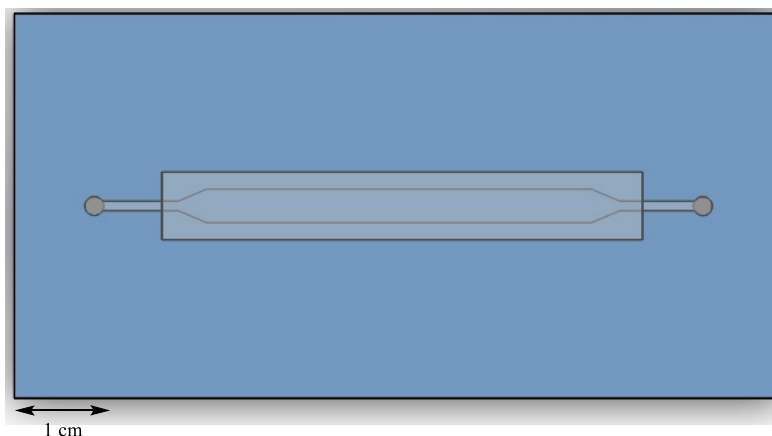


Figure 6.1: Potential design for an integrated microfluidic device.

The device would operate by placing the modified electrode into a central chamber after which the plate with the channels would need to be sealed. With a long and linear channel this could replicate the design of the macroflow device but reducing the volume of the device.

Further work would then continue to look at incorporating a calibration channel to give a comparison of the light signals more accurately and potentially increase the sensitivity of the system as a whole.

Chapter 7 References

1. A. Heyland, J. Hodin and A. M. Reitzel, *BioEssays*, 2005, **27**, 64-75.
2. A. Radu, C. Pichon, P. Camparo, M. Antoine, Y. Allory, A. Couvelard, G. Fromont, M. T. V. Hai and N. Ghinea, *New England Journal of Medicine*, 2010, **363**, 1621-1630.
3. L. C. T. Impey, *Obstetrics & gynaecology*, Wiley-Blackwell, 2012.
4. S. G. Hillier, *Human Reproduction*, 1994, **9**, 188-191.
5. S. Xu, K. Linher-Melville, B. B. Yang, D. Wu and J. Li, *Endocrinology*, 2011, **152**, 3941-3951.
6. S. Chandran, M. T. Cairns, M. O'Brien and T. J. Smith, *Molecular and Cellular Endocrinology*, 2014, **393**, 16-23.
7. M. Hsieh, D. Lee, S. Panigone, K. Horner, R. Chen, A. Theologis, D. C. Lee, D. W. Threadgill and M. Conti, *Molecular and Cellular Biology*, 2007, **27**, 1914-1924.
8. R. F. Walker, G. F. Read and D. Riad-Fahmy, *Clinical Chemistry*, 1979, **25**, 2030-2033.
9. M. Tsampalas, V. Gridelet, S. Berndt, J.-M. Foidart, V. Geenen and S. P. d'Hauterive, *Journal of Reproductive Immunology*, 2010, **85**, 93-98.
10. C. Ticconi, A. Zicari, A. Belmonte, M. Realacci, C. V. Rao and E. Piccione, *Placenta*, 2007, **28**, **Supplement**, S137-S143.
11. A. I. Csapo, M. O. Pulkkinen and W. G. Wiest, *American Journal of Obstetrics & Gynecology*, **115**, 759-765.
12. T. M. Goodwin, *American Journal of Obstetrics and Gynecology*, 1999, **180**, S208-S213.
13. M. A. Kirschner, N. Wiquist and E. Diczfalusy, *Acta Endocrinologica*, 1966, **53**, 584-597.
14. P. Kumar and N. Magon, *Nigerian Medical Journal*, 2012, **53**, 179-183.
15. J. Darne, H. H. G. McGarrigle and G. C. L. Lachelin, *BJOG: An International Journal of Obstetrics & Gynaecology*, 1987, **94**, 227-235.
16. B. Priya, M. D. Mustafa, K. Guleria, N. B. Vaid, B. D. Banerjee and R. S. Ahmed, *BJOG: An International Journal of Obstetrics & Gynaecology*, 2013, **120**, 1003-1011.
17. L. G. Nardo and H. N. Sallam, *Reproductive BioMedicine Online*, 2006, **13**, 47-57.
18. H. Schweigmann, A. Sánchez-Guijo, B. Ugele, K. Hartmann, M. F. Hartmann, M. Bergmann, C. Pfarrer, B. Döring, S. A. Wudy, E. Petzinger, J. Geyer and G. Grosser, *The Journal of Steroid Biochemistry and Molecular Biology*, 2014, **143**, 259-265.
19. X. Huang, D. C. Spink, E. Schneider, H. Ling, A. J. Rai, T. G. Rosano, B. Chen and Z. Cao, *Clinical Chemistry*, 2014, **60**, 260-268.
20. J. A. McGregor, G. M. Jackson, G. C. L. Lachelin, T. M. Goodwin, R. Artal, C. Hastings and V. Dullien, *American Journal of Obstetrics and Gynecology*, 1995, **173**, 1337-1342.
21. R. Smith, J. I. Smith, X. Shen, P. J. Engel, M. E. Bowman, S. A. McGrath, A. M. Bisits, P. McElduff, W. B. Giles and D. W. Smith, *The Journal of Clinical Endocrinology & Metabolism*, 2009, **94**, 2066-2074.
22. N. Choices, Infertility Diagnosis, <http://www.nhs.uk/Conditions/Infertility/Pages/Diagnosis.aspx>, (accessed 13th October, 2014).
23. T. R. Yeko, M. J. Gorrill, L. H. Hughes, I. A. Rodi, J. E. Buster and M. V. Sauer, *Fertility and sterility*, 1987, **48**, 1048-1050.
24. B. Weisz, P. Pandya, L. Chitty, P. Jones, W. Huttly and C. Rodeck, *BJOG: An International Journal of Obstetrics & Gynaecology*, 2007, **114**, 493-497.
25. C. K. Konopka, E. N. Morais, D. Naidon, A. M. Pereira, M. A. Rubin, J. F. Oliveira and C. F. Mello, *Brazilian Journal of Medical and Biological Research*, 2013, **46**, 91-97.
26. S. Yang, D. Zhang, Y. Xu, X. Wang, X. Liu, S. Wang, J. Wang, M. Wu, Z. He, J. Zhao and H. Yuan, *Steroids*, 2013, **78**, 297-303.
27. S. Koka, T. J. Beebe, S. P. Merry, R. S. DeJesus, L. D. Berlanga, A. L. Weaver, V. M. Montori and D. T. Wong, *The Journal of the American Dental Association*, 2008, **139**, 735-740.

28. Z. Chen, S. Feng, E. H. N. Pow, O. L. T. Lam, S. Mai and H. Wang, *Clinica Chimica Acta*, 2015, **438**, 231-235.
29. I. I. Bolaji, *International Journal of Gynecology & Obstetrics*, 1994, **45**, 125-131.
30. W. Schramm, R. H. Smith, P. A. Craig, S. H. Paek and H. H. Kuo, *Clinical Chemistry*, 1990, **36**, 1488-1493.
31. J. Darne, H. H. G. McGarrigle and G. C. L. Lachelin, *British Medical Journal (Clinical Research Edition)*, 1987, **294**, 270-272.
32. H. L. Hedriana, C. J. Munro, E. M. Eby-Wilkens and B. L. Lasley, *American Journal of Obstetrics and Gynecology*, 2001, **184**, 123-130.
33. J. J. Evans, A. R. Wilkinson and D. R. Aickin, *Clinical Chemistry*, 1984, **30**, 120-121.
34. D. J. Aframian, T. Davidowitz and R. Benoliel, *Oral Diseases*, 2006, **12**, 420-423.
35. J. Griffen, *Immunology and Haematology*, Elsevier, Mosby, Second Edition edn., 2003.
36. J. P. Gosling, *Immunoassays*, Oxford University Press, 2000.
37. P. J. Delves, S. J. Martin, D. R. Burton and I. M. Roitt, *Roitt's Essential Immunology*, Wiley-Blackwell, 12 edn., 2011.
38. W. Wang, S. Singh, D. L. Zeng, K. King and S. Nema, *Journal of Pharmaceutical Sciences*, 2007, **96**, 1-26.
39. A. H. Ng, U. Uddayasankar and A. R. Wheeler, *Anal Bioanal Chem*, 2010, **397**, 991-1007.
40. H. Akhavan-Tafti, D. G. Binger, J. J. Blackwood, Y. Chen, R. S. Creager, R. de Silva, R. A. Eickholt, J. E. Gaibor, R. S. Handley, K. P. Kapsner, S. K. Lopac, M. E. Mazelis, T. L. McLernon, J. D. Mendoza, B. H. Odegaard, S. G. Reddy, M. Salvati, B. A. Schoenfelner, N. Shapir, K. R. Shelly, J. C. Todtleben, G. Wang and W. Xie, *Journal of the American Chemical Society*, 2013, **135**, 4191-4194.
41. L. Chen, X. Zhang, G. Zhou, X. Xiang, X. Ji, Z. Zheng, Z. He and H. Wang, *Analytical Chemistry*, 2012, **84**, 3200-3207.
42. A. Saitman, H.-D. Park and R. L. Fitzgerald, *Journal of Analytical Toxicology*, 2014.
43. A. I. Barbosa, A. P. Castanheira, A. D. Edwards and N. M. Reis, *Lab on a Chip*, 2014, **14**, 2918-2928.
44. D. W. Chan, *Immunoassay: A Practical Guide*, American Press Inc., 1987.
45. A. Bange, H. B. Halsall and W. R. Heineman, *Biosensors and Bioelectronics*, 2005, **20**, 2488-2503.
46. W. Qian, D. Yao, F. Yu, B. Xu, R. Zhou, X. Bao and Z. Lu, *Clinical Chemistry*, 2000, **46**, 1456-1463.
47. P. Wood, *Understanding Immunology*, Pearson Education Limited, Prentice Hall, Third edn., 2011.
48. E. G. Lee, K. M. Park, J. Y. Jeong, S. H. Lee, J. E. Baek, H. W. Lee, J. K. Jung and B. H. Chung, *Analytical Biochemistry*, 2011, **408**, 206-211.
49. J. Martinez-Perdiguero, A. Retolaza, L. Bujanda and S. Merino, *Talanta*, 2014, **119**, 492-497.
50. J. S. Daniels and N. Pourmand, *Electroanalysis*, 2007, **19**, 1239-1257.
51. N. J. Russell, S. Foster, P. Clark, I. D. Robertson, D. Lewis and P. J. Irwin, *Australian Veterinary Journal*, 2007, **85**, 487-494.
52. T. Kreisig, R. Hoffmann and T. Zuchner, *Analytical Chemistry*, 2011, **83**, 4281-4287.
53. Y.-K. Wang, Y.-X. Yan, W.-H. Ji, H.-a. Wang, Q. Zou and J.-H. Sun, *Journal of Agricultural and Food Chemistry*, 2013, **61**, 4250-4256.
54. Y. H. Dou, S. J. Haswell, J. Greenman and J. Wadhawan, *Electroanalysis*, 2012, **24**, 264-272.
55. G. Lai, C. Yin, X. Tan, H. Zhang and A. Yu, *Analytical Methods*, 2014, **6**, 2080-2085.
56. G. Kohler and C. Milstein, *Nature*, 1975, **256**, 495-497.
57. R. Wacker, H. Schröder and C. M. Niemeyer, *Analytical Biochemistry*, 2004, **330**, 281-287.

58. C. Zheng, J. Wang, Y. Pang, J. Wang, W. Li, Z. Ge and Y. Huang, *Lab on a Chip*, 2012, **12**, 2487-2490.
59. J. J. Cras, C. A. Rowe-Taitt, D. A. Nivens and F. S. Ligler, *Biosensors and Bioelectronics*, 1999, **14**, 683-688.
60. A. Akkoyun and U. Bilitewski, *Biosensors and Bioelectronics*, 2002, **17**, 655-664.
61. L. G. Mendoz, P. McQuary, A. Mongan, R. Gangadharan, S. Brignac and M. Eggers, *BioTechniques*, 1999, **27**, 778-788.
62. N. R. Glass, R. Tjeung, P. Chan, L. Y. Yeo and J. R. Friend, *Biomicrofluidics*, 2011, **5**.
63. L. C. Shriver-Lake, W. B. Gammeter, S. S. Bang and M. Pazirandeh, *Analytica Chimica Acta*, 2002, **470**, 71-78.
64. P. C. Mathias, N. Ganesh and B. T. Cunningham, *Analytical Chemistry*, 2008, **80**, 9013-9020.
65. J. P. Gering, L. Quaroni and G. Chumanov, *Journal of Colloid and Interface Science*, 2002, **252**, 50-56.
66. W. Kusnezow, A. Jacob, A. Walijew, F. Diehl and J. D. Hoheisel, *PROTEOMICS*, 2003, **3**, 254-264.
67. H.-J. Jang, I.-H. Cho, H.-S. Kim, J.-W. Jeon, S.-Y. Hwang and S.-H. Paek, *Sensors and Actuators B: Chemical*, 2011, **155**, 598-605.
68. G. T. Hermanson, *Bioconjugate Techniques*, Academic Press Inc, 2 edn., 2008.
69. N. Yoon Lee, Y. Yang, Y. S. Kim and S. Park, *Bulletin of the Korean Chemical Society*, 2006, **27**, 479-483.
70. V. Lates, C. Yang, I. Popescu and J.-L. Marty, *Analytical and Bioanalytical Chemistry*, 2012, **402**, 2861-2870.
71. R. A. W. Scott, *The Protein Protocols Handbook*, Springer, Humana Press Inc., 2nd edn., 2002.
72. S.-Q. Ren, W. Xu, B.-J. Tang, G.-M. Hu, Z.-J. Li, G.-N. Chen and J.-M. Lin, *Chinese Journal of Analytical Chemistry*, 2008, **36**, 729-734.
73. C. K. Dixit, S. K. Vashist, F. T. O'Neill, B. O'Reilly, B. D. MacCraith and R. O'Kennedy, *Analytical Chemistry*, 2010, **82**, 7049-7052.
74. E. W. K. Young, E. Berthier and D. J. Beebe, *Analytical Chemistry*, 2012, **85**, 44-49.
75. J.-Y. Cheng, C.-W. Wei, K.-H. Hsu and T.-H. Young, *Sensors and Actuators B: Chemical*, 2004, **99**, 186-196.
76. J. M. Goddard and J. H. Hotchkiss, *Progress in Polymer Science*, 2007, **32**, 698-725.
77. Z. Yang, Y. Chevolut, Y. Ataman-Önal, G. Choquet-Kastylevsky, E. Souteyrand and E. Laurenceau, *Sensors and Actuators B: Chemical*, 2012, **175**, 22-28.
78. L. Brown, T. Koerner, J. H. Horton and R. D. Oleschuk, *Lab on a Chip*, 2006, **6**, 66-73.
79. T. B. Stachowiak, D. A. Mair, T. G. Holden, L. J. Lee, F. Svec and J. M. J. Fréchet, *Journal of Separation Science*, 2007, **30**, 1088-1093.
80. G. A. Diaz-Quijada, R. Peytavi, A. Nantel, E. Roy, M. G. Bergeron, M. M. Dumoulin and T. Veres, *Lab on a Chip*, 2007, **7**, 856-862.
81. J. Raj, G. Herzog, M. Manning, C. Volcke, B. D. MacCraith, S. Ballantyne, M. Thompson and D. W. M. Arrigan, *Biosensors and Bioelectronics*, 2009, **24**, 2654-2658.
82. A. A. Karyakin, G. V. Presnova, M. Y. Rubtsova and A. M. Egorov, *Analytical Chemistry*, 2000, **72**, 3805-3811.
83. S. K. Vashist, *Diagnostics*, 2012, **2**, 23-33.
84. J. Yakovleva, R. Davidsson, A. Lobanova, M. Bengtsson, S. Eremin, T. Laurell and J. Emnéus, *Analytical Chemistry*, 2002, **74**, 2994-3004.
85. Y. Zhang, S. Ge, S. Wang, M. Yan, J. Yu, X. Song and W. Liu, *Analyst*, 2012, **137**, 2176-2182.
86. C.-W. Yen, H. de Puig, J. O. Tam, J. Gomez-Marquez, I. Bosch, K. Hamad-Schifferli and L. Gehrke, *Lab on a Chip*, 2015, **15**, 1638-1641.
87. W. Liu, C. L. Cassano, X. Xu and Z. H. Fan, *Analytical Chemistry*, 2013, **85**, 10270-10276.

88. X. Mu, L. Zhang, S. Chang, W. Cui and Z. Zheng, *Analytical Chemistry*, 2014, **86**, 5338-5344.
89. T. S. Park, W. Li, K. E. McCracken and J.-Y. Yoon, *Lab on a Chip*, 2013, **13**, 4832-4840.
90. A. K. Yetisen, M. S. Akram and C. R. Lowe, *Lab on a Chip*, 2013, **13**, 2210-2251.
91. J. H. Nichols, *Clinics in Laboratory Medicine*, 2007, **27**, 893-908.
92. D. Mark, S. Haeberle, G. Roth, F. von Stetten and R. Zengerle, *Chemical Society Reviews*, 2010, **39**, 1153-1182.
93. G. M. Whitesides, *Nature*, 2006, **442**, 368-373.
94. D. R. Reyes, D. Iossifidis, P.-A. Auroux and A. Manz, *Analytical Chemistry*, 2002, **74**, 2623-2636.
95. P. C. H. Li, *Microfluidic Lab-on-a-Chip for Chemical and Biological Analysis and Discovery*, Taylor & Francis Group, 2006.
96. T. McCreeedy, *TrAC Trends in Analytical Chemistry*, 2000, **19**, 396-401.
97. C. Iliescu, H. Taylor, M. Avram, J. Miao and S. Franssila, *Biomicrofluidics*, 2012, **6**, 016505-016505-016516.
98. O. Rötting, W. Röpke, H. Becker and C. Gärtner, *Microsystem Technologies*, 2002, **8**, 32-36.
99. U. Attia, S. Marson and J. Alcock, *Microfluidics and Nanofluidics*, 2009, **7**, 1-28.
100. D. S. Kim, S. H. Lee, C. H. Ahn, J. Y. Lee and T. H. Kwon, *Lab on a Chip*, 2006, **6**, 794-802.
101. R. Folgado, P. Peças and E. Henriques, *International Journal of Production Economics*, 2010, **128**, 368-378.
102. S. C. Terry, J. H. Jerman and J. B. Angell, *Electron Devices, IEEE Transactions on*, 1979, **26**, 1880-1886.
103. S. J. Haswell, *Analyst*, 1997, **122**, 1R-10R.
104. L. Chia-Yen, C. Chin-Lung, W. Yao-Nan and F. Lung-Ming, *International Journal of Molecular Science*, 2011, **12**, 3263-3287.
105. S. J. Trietsch, T. Hankemeier and H. J. van der Linden, *Chemometrics and Intelligent Laboratory Systems*, 2011, **108**, 64-75.
106. T. M. Squires and S. R. Quake, *Reviews of Modern Physics*, 2005, **77**, 977-1026.
107. P. Atkins and J. de Paula, *Elements of Physical Chemistry*, Oxford University Press, 4th edn., 2005.
108. M. Mirasoli, M. Guardigli, E. Micheleni and A. Roda, *Journal of Pharmaceutical and Biomedical Analysis*, 2014, **87**, 36-52.
109. R. Hood, C. Shao, D. Omiatek, W. Vreeland and D. DeVoe, *Pharmaceutical Research*, 2013, **30**, 1597-1607.
110. J. Pan, Z. Chen, M. Yao, X. Li, Y. Li, D. Sun and Y. Yu, *Luminescence*, 2014, **29**, 427-432.
111. E. K. Sackmann, A. L. Fulton and D. J. Beebe, *Nature*, 2014, **507**, 181-189.
112. A. J. Mach, O. B. Adeyiga and D. Di Carlo, *Lab on a Chip*, 2013, **13**, 1011-1026.
113. P. Yáñez-Sedeño, L. Aguí, R. Villalonga and J. M. Pingarrón, *Analytica Chimica Acta*, 2014, **823**, 1-19.
114. M. A. Schwarz and P. C. Hauser, *Lab on a Chip*, 2001, **1**, 1-6.
115. L.-M. Fu, W.-J. Ju, C.-C. Liu, R.-J. Yang and Y.-N. Wang, *Chemical Engineering Journal*, 2014, **243**, 421-427.
116. A. M. Nicolini, C. F. Fronczek and J.-Y. Yoon, *Biosensors and Bioelectronics*, 2015, **67**, 560-569.
117. D. C. Harris, *Quantitative Chemical analysis*, W.H. Freeman and Company, Seventh edn., 2007.
118. T. K. Kim, S. W. Oh, Y. J. Mok and E. Y. Choi, *Journal of Clinical Laboratory Analysis*, 2014, **28**, 294-300.
119. A. Roda, *Chemiluminescence and Bioluminescence Past, Present and Future*, RSC Publishing, 1 edn., 2011.
120. P. Atkins, T. Overton, J. Rourke, M. Weller and F. Armstrong, *Inorganic Chemistry*, Oxford University Press, Fourth edn., 2006.

121. W. F. Libby, *The Journal of Physical Chemistry*, 1952, **56**, 863-868.
122. R. A. Marcus, *The Journal of Chemical Physics*, 1965, **43**, 679-701.
123. G. Zomer, *Chemiluminescence and Bioluminescence*, RSC Publishing, 2011.
124. R. A. Marcus, *The Journal of Chemical Physics*, 1956, **24**, 979.
125. R. A. Marcus, *The Journal of Chemical Physics*, 1956, **24**, 966-978.
126. R. A. Marcus, *The Journal of Chemical Physics*, 1965, **43**, 2654-2657.
127. D. M. Hercules, *Accounts of Chemical Research*, 1969, **2**, 301-307.
128. I. Weeks, I. Beheshti, F. McCapra, A. K. Campbell and J. S. Woodhead, *Clinical Chemistry*, 1983, **29**, 1474-1479.
129. A. Rodríguez, A. Tjärnlund, J. Ivanji, M. Singh, I. García, A. Williams, P. D. Marsh, M. Troye-Blomberg and C. Fernández, *Vaccine*, 2005, **23**, 2565-2572.
130. H. O. Albrecht, *Zeitschrift für Physikalische Chemie*, 1928, **136**.
131. A. M. Garcia-Campana, W. R. G. Baeyens, L. Cuadros-Rodríguez, F. Barrero, J. M. Bosque-Sendra and L. Gamiz-Gracia, *Current Organic Chemistry*, 2002, **6**, 1-20.
132. *Chemiluminescence and Bioluminescence Past, Present and Future*, RSC Publishing, 1 edn., 2011.
133. W. Chen, L. Hong, A.-L. Liu, J.-Q. Liu, X.-H. Lin and X.-H. Xia, *Talanta*, 2012, **99**, 643-648.
134. L. d. C. Puga Molina and S. V. Verstraeten, *Journal of Luminescence*, 2013, **137**, 191-197.
135. T. G. Burdo and W. R. Seitz, *Analytical Chemistry*, 1975, **47**, 1639-1643.
136. C. M. Sakamoto-Arnold and K. S. Johnson, *Analytical Chemistry*, 1987, **59**, 1789-1794.
137. J. Lind, *The chemiluminescence of luminol in aqueous solutions, a pulse radiolytic study*, Royal Inst. of Technology, Stockholm (Sweden). Dept. of Nuclear Chemistry, 1980.
138. F. Fan, H. Shen, G. Zhang, X. Jiang and X. Kang, *Clinica Chimica Acta*, 2014, **431**, 113-117.
139. N. M. M. Pires, T. Dong, U. Hanke and N. Hoivik, *Sensors (Basel, Switzerland)*, 2014, **14**, 15458-15479.
140. J. Xie, M. Demarteau, R. Wagner, E. May, J. Zhang, M. Ruiz-Oses, X. Liang, I. Ben-Zvi, K. Attenkofer, S. Schubert, J. Smedley, J. Wong and H. Padmore, 2013.
141. G. Liu, J. Wang, J. Kim, M. R. Jan and G. E. Collins, *Analytical Chemistry*, 2004, **76**, 7126-7130.
142. D. R. Crow, *Principles of Electrochemistry*, Taylor & Francis Group, 4 edn., 1994.
143. P. H. Reiger, *Electrochemistry*, Springer, 2 edn., 1994.
144. J. Wang, *Talanta*, 2002, **56**, 223-231.
145. J. Wang, *TrAC Trends in Analytical Chemistry*, 2002, **21**, 226-232.
146. S.-P. Chen, X.-D. Yu, J.-J. Xu and H.-Y. Chen, *Biosensors and Bioelectronics*, 2011, **26**, 4779-4784.
147. S. Shiohara, M. Chikae, Y. Ukita, H. Ushijima, Y. Fukumura, T. Takamura and Y. Takamura, *Microsystem Technologies*, 2014, **20**, 273-279.
148. C. Hamann, A. Hamnett and W. Vielstich, *Electrochemistry*, Wiley-VCH, 1998.
149. D. O. Wipf and R. M. Wightman, *Analytical Chemistry*, 1990, **62**, 98-102.
150. K. B. Oldham, *Analytical Chemistry*, 1969, **41**, 1904-1905.
151. G. C. Barker and I. L. Jenkins, *Analyst*, 1952, **77**, 685-696.
152. R. G. Compton and C. E. Banks, *Understanding Voltammetry*, Imperial College Press, 2 edn., 2011.
153. J. G. Deboever, G. Martens and F. Kohen, *Analytica Chimica Acta*, 1994, **290**, 233-238.
154. F. Ye, J. Liu, Y. Huang, S. Li and S. Zhao, *Journal of Chromatography B*, 2013, **936**, 74-79.
155. H. Lee, C. J. Park and G. Lee, *Analytical and Bioanalytical Chemistry*, 2010, **396**, 1713-1719.
156. X. H. Lv and D. Z. Shi, *Experimental Animals*, 2010, **59**, 231-237.
157. M. Z. Tahir, S. Thoumire, M. Raffaelli, B. Grimard, K. Reynaud and S. Chastant-Maillard, *Domestic Animal Endocrinology*, 2013, **45**, 141-144.

158. C.-K. Joung, H.-N. Kim, H.-C. Im, H.-Y. Kim, M.-H. Oh and Y.-R. Kim, *Sensors and Actuators B: Chemical*, 2012, **161**, 824-831.
159. D. Han, K. B. Kim, Y.-R. Kim, S. Kim, H. C. Kim, J. Lee, J. Kim and T. D. Chung, *Electrochimica Acta*, 2013, **110**, 164-171.
160. H.-I. Peng, C. M. Strohsahl and B. L. Miller, *Lab on a Chip*, 2012, **12**, 1089-1093.
161. J. A. Howarter and J. P. Youngblood, *Langmuir*, 2006, **22**, 11142-11147.
162. T.-S. Pui, A. Agarwal, F. Ye, Y. Huang and P. Chen, *Biosensors and Bioelectronics*, 2011, **26**, 2746-2750.
163. S. K. Vashist, *Biosensors and Bioelectronics*, 2013, **40**, 297-302.
164. P. Khan, D. Idrees, M. A. Moxley, J. A. Corbett, F. Ahmad, G. von Figura, W. S. Sly, A. Waheed and M. I. Hassan, *Applied biochemistry and biotechnology*, 2014, **173**, 333-355.
165. R. Wilson, J. Kremeskötter, D. J. Schiffrin and J. S. Wilkinson, *Biosensors and Bioelectronics*, 1996, **11**, 805-810.
166. G. H. Thorpe, L. J. Kricka, S. B. Moseley and T. P. Whitehead, *Clinical chemistry*, 1985, **31**, 1335-1341.
167. L. Wang, P. Yang, Y. Li, H. Chen, M. Li and F. Luo, *Talanta*, 2007, **72**, 1066-1072.
168. C. Marquette and L. Blum, *Analytical and Bioanalytical Chemistry*, 2006, **385**, 546-554.
169. P. Duan, F. Cai, Y. Luo, Y. Chen and S. Zou, *Luminescence*, 2014, n/a-n/a.
170. S. Xu, W. Liu, B. Hu, W. Cao and Z. Liu, *Journal of Photochemistry and Photobiology A: Chemistry*, 2012, **227**, 32-37.
171. T. S. Chow, *Journal of Physics: Condensed Matter*, 1998, **10**, L445.
172. T. Ahuja, Rajesh, D. Kumar, V. K. Tanwar, V. Sharma, N. Singh and A. M. Biradar, *Thin Solid Films*, 2010, **519**, 1128-1134.
173. S. C. Jain, V. K. Tanwar, V. Dixit, S. P. Verma and S. B. Samanta, *Applied Surface Science*, 2001, **182**, 350-356.
174. E. B. Whipple and M. Ruta, *The Journal of Organic Chemistry*, 1974, **39**, 1666-1668.
175. K. M. Tripp, J. P. Versteegen, C. J. Deutsch, R. K. Bonde, M. Rodriguez, B. Morales, D. L. Schmitt and K. E. Harr, *Theriogenology*, 2008, **70**, 1030-1040.
176. H. W. Park and I. Lee, *Applied Surface Science*, 2014, **308**, 311-315.
177. Y. Zhang, X. Wang, Y. Liu, S. Song and D. Liu, *Journal of Materials Chemistry*, 2012, **22**, 11971-11977.
178. A. Ayes, *Chinese Journal of Polymer Science*, 2010, **28**, 537-546.
179. Y. Zhang, J. Cheng and Z.-r. Yang, *Applied Surface Science*, 2014, **315**, 163-168.
180. M. Suzuki, K. Ikeda, M. Yamaguchi, S. N. Kudoh, K. Yokoyama, R. Satoh, D. Ito, M. Nagayama, T. Uchida and K. Gohara, *Biomaterials*, 2013, **34**, 5210-5217.
181. O. Seitz, P. G. Fernandes, R. Tian, N. Karnik, H.-C. Wen, H. Stiegler, R. A. Chapman, E. M. Vogel and Y. J. Chabal, *Journal of Materials Chemistry*, 2011, **21**, 4384-4392.
182. R. M. Pasternack, S. Rivillon Amy and Y. J. Chabal, *Langmuir*, 2008, **24**, 12963-12971.
183. N. A. Lapin and Y. J. Chabal, *The Journal of Physical Chemistry B*, 2009, **113**, 8776-8783.
184. S. Chen, L. Liu, J. Zhou and S. Jiang, *Langmuir*, 2003, **19**, 2859-2864.
185. S. J. Choi and S. M. Park, *Advanced Materials*, 2000, **12**, 1547-1549.
186. J. I. Mujika, J. M. Matxain, L. A. Eriksson and X. Lopez, *Chemistry – A European Journal*, 2006, **12**, 7215-7224.
187. C. E. West, J. L. Hardcastle and R. G. Compton, *Electroanalysis*, 2002, **14**, 1470-1478.
188. D. R. Scott and R. S. Becker, *Journal of Chemical Physics*, 1961, **35**, 516-531.
189. E. A. Kassab, M. I. Marzouk and M. El-Hashash, *Journal of the Serbian Chemical Society*, 2002, **67**, 593-603.
190. F. Kohen, M. Pazzagli, J. B. Kim, H. R. Lindner and R. C. Boguslaski, *FEBS Letters*, 1979, **104**, 201-205.
191. W.-J. Liu, G.-X. Xiong and W.-P. Wang, *Applied Organometallic Chemistry*, 2007, **21**, 83-88.

192. M. Okochi, H. Ohta, T. Tanaka and T. Matsunaga, *Biotechnology and Bioengineering*, 2005, **90**, 14-19.
193. A. Benedetto, M. Balog, P. Viel, F. Le Derf, M. Sallé and S. Palacin, *Electrochimica Acta*, 2008, **53**, 7117-7122.
194. J. Pinson and F. Podvorica, *Chemical Society Reviews*, 2005, **34**, 429-439.
195. A. Laforgue, T. Addou and D. Bélanger, *Langmuir*, 2005, **21**, 6855-6865.
196. J. Ghilane, M. Delamar, M. Guilloux-Viry, C. Lagrost, C. Mangeney and P. Hapiot, *Langmuir*, 2005, **21**, 6422-6429.
197. S. Munteanu, J. P. Roger, Y. Fedala, F. Amiot, C. Combellas, G. Tessier and F. Kanoufi, *Faraday Discussions*, 2013, **164**, 241-258.
198. H. Zollinger, *Angewandte Chemie International Edition in English*, 1978, **17**, 141-150.
199. I. Szele and H. Zollinger, *Helvetica Chimica Acta*, 1978, **61**, 1721-1729.
200. A. L. Gui, G. Liu, M. Chockalingam, G. Le Saux, E. Luais, J. B. Harper and J. J. Gooding, *Electroanalysis*, 2010, **22**, 1824-1830.
201. Y.-P. Li, H.-B. Cao, C.-M. Liu and Y. Zhang, *Journal of Hazardous Materials*, 2007, **148**, 158-163.
202. F. A. Armstrong, H. A. Heering and J. Hirst, *Chemical Society Reviews*, 1997, **26**, 169-179.
203. W. A. Hayes and C. Shannon, *Langmuir*, 1996, **12**, 3688-3694.
204. M. J. Thomasson, D. J. Baldwin, A. Diego-Taboada, S. L. Atkin, G. Mackenzie and J. D. Wadhawan, *Electrochemistry Communications*, 2010, **12**, 1428-1431.
205. J. Lehr, B. E. Williamson and A. J. Downard, *The Journal of Physical Chemistry C*, 2011, **115**, 6629-6634.
206. D. Raoufi, A. Kiasatpour, H. R. Fallah and A. S. H. Rozatian, *Applied Surface Science*, 2007, **253**, 9085-9090.
207. R. A. Latour, *Journal of Biomedical Materials Research Part A*, 2015, **103**, 949-958.
208. C. B. Walsh, X. Wen and E. I. Franses, *Journal of Colloid and Interface Science*, 2001, **233**, 295-305.
209. R. Wilson and D. J. Schiffrin, *Journal of Electroanalytical Chemistry*, 1998, **448**, 125-130.
210. Y.-c. Lu, G. R. Bentley, P. H. Gann, K. R. Hodges and R. T. Chatterton, *Fertility and Sterility*, 1999, **71**, 863-868.
211. F. S. Khan-Dawood, J. K. Choe and M. Y. Dawood, *American Journal of Obstetrics and Gynecology*, 1984, **148**, 442-445.
212. A. Khataee, M. Iranifam, M. Fathinia and M. Nikraves, *Spectrochimica Acta Part A: Molecular and Biomolecular Spectroscopy*, 2015, **134**, 210-217.
213. G. Tabbì, C. Cassino, G. Cavigliolo, D. Colangelo, A. Ghiglia, I. Viano and D. Osella, *Journal of Medicinal Chemistry*, 2002, **45**, 5786-5796.
214. M.-B. Gholivand, A. R. Jalalvand, G. Paimard, H. C. Goicoechea, T. Skov, R. Farhadi, S. Ghobadi, N. Moradi and V. Nasirian, *International Journal of Biological Macromolecules*, 2014, **70**, 596-605.
215. B. J. Cheek, A. B. Steel, M. P. Torres, Y.-Y. Yu and H. Yang, *Analytical Chemistry*, 2001, **73**, 5777-5783.
216. P. A. Greenwood and G. M. Greenway, *TrAC Trends in Analytical Chemistry*, 2002, **21**, 726-740.

Presentations

K. Wright, G. Kipling, G. Benazzi, N. Brown, S. Haswell, J. Wadhawan, G. Greenway, “Bioanalysis of Fertility Biomarkers Using Electron Transfer Systems”, Oral Presentation, Analytical Research Forum 2014, Burlington House, London, UK.

K. Wright, G. Kipling, G. Benazzi, N. Brown, S. Haswell, J. Wadhawan, G. Greenway, “Chemiluminescence Immunoassay for Pregnancy Monitoring on a Microfluidic Device”, Poster Presentation, Biosensors 2014, Melbourne, Australia.

K. Wright, G. Benazzi, K. Shaw, J. Wadhawan, S. Haswell and G. Greenway, “Fertility Investigation Using Microfluidics”, Poster Presentation, Analytical Research Forum, 2012, Durham University, UK.